UNIVERSIDADE FEDERAL DE SANTA CATARINA
CENTRO TECNOLÓGICO
PROGRAMA DE PÓS-GRADUAÇÃO EM ENGENHARIA ELÉTRICA

Gabriel Santos Bolacell

ASSESSING TRANSMISSION NETWORK FLEXIBILITY: SCIENTIFIC AND TECHNOLOGICAL CONTRIBUTIONS FOR POWER SYSTEM

Florianópolis
2021

Gabriel Santos Bolacell

ASSESSING TRANSMISSION NETWORK FLEXIBILITY: SCIENTIFIC AND TECHNOLOGICAL CONTRIBUTIONS FOR POWER SYSTEM

Tese submetida ao Programa de Pós-Graduação em Engenharia Elétrica da Universidade Federal de Santa Catarina para a obtenção do título de Doutor em Engenharia Elétrica.
Orientador: Prof. Mauro Augusto da Rosa, Ph.D.

Florianópolis
2021

Ficha de identificação da obra elaborada pelo autor,
através do Programa de Geração Automática da Biblioteca Universitária da UFSC.

Bolacell, Gabriel Santos
Assessing transmission network flexibility : scientific and technological contributions for power system / Gabriel Santos Bolacell ; orientador, Mauro Augusto da Rosa, 2021.
191 p.

Tese (doutorado) - Universidade Federal de Santa Catarina, Centro Tecnológico, Programa de Pós-Graduação em Engenharia Elétrica, Florianópolis, 2021.

Inclui referências.

1. Engenharia Elétrica. 2. Dynamic Line Rating. 3. Planejamento de Sistemas Elétricos. 4. Contribuições Científicas e Tecnológicas. 5. Confiabilidade. I. Rosa, Mauro Augusto da. II. Universidade Federal de Santa Catarina. Programa de Pós-Graduação em Engenharia Elétrica. III. Título.

Gabriel Santos Bolacell

ASSESSING TRANSMISSION NETWORK FLEXIBILITY: SCIENTIFIC AND TECHNOLOGICAL CONTRIBUTIONS FOR POWER SYSTEM

O presente trabalho em nível de Doutorado foi avaliado e aprovado por banca examinadora composta pelos seguintes membros:

Prof. Patrik Hilber, Ph.D.
Royal Institute of Technology (KTH)

Prof. Walmir Freitas, Ph.D.
Universidade Estadual de Campinas (Unicamp)

Prof. Leonardo Elizeire Bremermann, Ph.D.
Universidade Federal de Santa Catarina (UFSC)

Prof. Mauricio Valencia Ferreira da Luz, Dr.
Universidade Federal de Santa Catarina (UFSC)

Certificamos que esta é a **versão original e final** do trabalho de conclusão que foi julgado adequado para obtenção do título de Doutor em Engenharia Elétrica.

ICP-Edu
Documento assinado digitalmente
Telles Brunelli Lazzarin
Data: 25/11/2021 10:15:20-0300
CPF: 023.400.719-25
Verifique as assinaturas em https://v.ufsc.br

Prof. Telles Brunelli Lazzarin, Dr.
Coordenador do Programa

ICP-Edu
Documento assinado digitalmente
Mauro Augusto da Rosa
Data: 24/11/2021 14:57:05-0300
CPF: 630.652.400-25
Verifique as assinaturas em https://v.ufsc.br

Prof. Mauro Augusto da Rosa, Ph.D.
Orientador

Florianópolis, 2021.

This work was supported in part by the Brazilian National Council for Scientific and Technological Development (CNPq), and part by the Institute of Systems and Computer Engineering, Research and Development of Brazil (INESC P&D Brasil). The work was developed in Project TECCON II with Transmissoras Brasileiras de Energia (TBE), under the framework of the Research and Development (R&D) Program regulated by Agência Nacional de Energia Elétrica (ANEEL), code PD-2615-0011-2015.

This Ph.D. thesis is dedicated to my dear parents Julio and Viviane, my sister Júlia, and my wife Carolina.

ACKNOWLEDGMENTS

I want to express my sincere gratitude to my advisor, Prof. Mauro Augusto da Rosa, for the amazing support during my Ph.D. period, providing all necessary conditions to me developing a wonderful thesis, not measuring efforts to aid me to experience memorable moments, both professional and social.

Also, I want to acknowledge my colleagues from the TECCON II research project, especially the integration team: Prof. Milton José Cinelli, Daniel Ayoub, Julia Nunes, and Clayrton Henrique, who have provided incredible support to my work and were essential for my developments. We have worked plenty of hours together for 24 months. Also, I want to thank other colleagues from the multidisciplinary team of the TECCON II research project: Leonardo Lira, Ilan Sousa, Gian Chesini, Hugo Freitas, Eduardo Cardoso, Samir Fernandes, and Laura Eduarda Marques.

Still under the TECCON II research project framework, I would like to thank also the colleagues and friends from *Transmissoras Brasileiras de Energia* (TBE) that I have the lucky to meet with during this trajectory: Mario Paulo de Miranda, Francisco Paulino da Silva, Erivan Moraes dos Reis, Geovane Matias, Marciley Veira dos Santos, Cláudio Souza Gaspar, Oneziano Francisco da Conceição, Victor Alexander Mizael Ortega, Israel Vitorino, Tiago Machado da Silva, Fernando Cesar da Cruz, Antonio Fernando de Souza, and Eden Luiz Junior. They have provided always great support, having patience and attention with me and my team during the works developed in Lages substation and on tower 23/1 of Lages - Abdon Batista 230 kV transmission line.

Some professors connected with INESC P&D Brasil also have provided remarkable support to my thesis, which I can cite in name of all: Prof. Diego Issicaba (UFSC), Prof. Mauricio Luz (UFSC), Prof. José Pissolato (Unicamp), and Prof. Tarso Vilela (UFS). In addition, I need to mention my acknowledgment for the colleagues from LabPlan (UFSC): Rodrigo Vaz, Lucas Fritzen Venturini, Pedro Vieira, Érika Pequeno, and Sandy Tondolo.

During the time I have spent in Porto, Portugal, I met wonderful people that have provided the necessary supporting. I want to say thank you to the friends from the Centre for Power and Energy Systems (CPES) and Centre for Applied Photonics (CAP) of INESC TEC, especially to: Leonel Carvalho, Prof. Pedro Jorge, Paulo Santos, Paula Castro, Luísa Mendonça, and Igor Rezende.

Finally, but not the least important, I want to say thanks to my family, that has been supporting me since the beginning of my life: Julio, Viviane, and Júlia, and to my wife, Carolina, for all the love, motivation, and patience during my Ph.D. period.

“Have the courage to follow your heart and intuition.
They somehow already know what you truly want to become.”
(Steve Jobs)

ABSTRACT

During the last decades, the models used to estimate transmission systems performance have been evolving devising to accommodate a technological transformation which the electric sector has been experiencing since deregulation. The energy transition, mainly driven by the integration of variable renewable energy sources (e.g., solar and wind power), direct current links, power electronic interfaces, battery energy storage systems, as well as power system components automation, is promoting a new power system with hybrid characteristics, where the increasing of the asynchronous and synchronous subsystems are presenting new challenges to operation and planning phases. In this sense, transmission lines performance analyses are being realized under the actual technological perspective, seeking to improve models considering new technological developments. In order to contribute to this new performance evaluation paradigm, this thesis is divided into three distinct exploratory segments. Segment I presents a discussion over the state of the art, highlighting new challenges and opportunities in power systems related to technologies, models, and methodologies of analysis. Segment II describes the optical monitoring system prototype installation in a high voltage transmission line (operating environment), enabling models implementation for assessments of functions such as Dynamic Line Rating (DLR), and making possible operative measures linked to transmission line flexibility. This segment II also highlights the technological developments achieved during the research. Segment III presents contributions related to assessing the capacity of the transmission systems ability to respond to sudden changes in the power system point of operation, representing operational parameters of generating units and variable capacity of transmission lines. This segment highlights contributions in the power systems analysis scope, enabling explore the results achieved in segment II. Numerical results have shown that the proposed DLR-based technology method can be safely included in the list of possible alternatives to reinforce transmission systems. A high voltage transmission line of the Brazilian Interconnected System, IEEE reliability test systems, and the Iberian Peninsula power system, which is composed of Portugal and Spain, are used as study cases.

Keywords: Dynamic Line Rating. Reliability. Scientific Contributions. Technological Contributions. Transmission System Flexibility.

RESUMO

Durante as últimas décadas, os modelos utilizados para estimar o desempenho de sistemas de transmissão têm evoluído visando acomodar uma transformação tecnológica pela qual o setor elétrico está passando desde a sua desregulamentação. A transição energética, impulsionada principalmente pela integração de fontes de energia renováveis variáveis (e.g., energia solar e eólica), elos de corrente contínua, interfaces de eletrônica de potência, sistemas de armazenamento de energia, bem como a automação de componentes de potência, está promovendo um novo sistema elétrico com características híbridas, onde o crescimento de subsistemas síncronos e assíncronos vem apresentando novos desafios para as fases de operação e planejamento da expansão. Nesse sentido, as análises de desempenho de linhas de transmissão estão sendo realizadas sob a perspectiva tecnológica atual, buscando aprimorar modelos considerando novos desenvolvimentos tecnológicos. Com o objetivo de contribuir com este novo paradigma de avaliação de desempenho, esta tese está dividida em três segmentos exploratórios distintos. O segmento I apresenta uma discussão sobre o estado da arte, destacando novos desafios e oportunidades em sistemas de energia relacionados a tecnologias, modelos e metodologias de análise. O segmento II descreve a instalação de um protótipo de sistema de monitoramento óptico em uma linha de transmissão de alta tensão (ambiente operacional), permitindo a implementação de modelos para a avaliação de funções como *Dynamic Line Rating*, e possibilitando medidas operativas ligadas a flexibilidade da linha de transmissão. Este segmento II destaca os desenvolvimentos tecnológicos alcançados no decorrer da pesquisa. O segmento III apresenta as contribuições que estão relacionadas com a avaliação da capacidade do sistema de transmissão em responder a mudanças repentinas no ponto de operação do sistema elétrico, representando parâmetros operacionais de unidades geradoras e capacidade variável de linhas de transmissão. Este segmento destaca contribuições no campo da análise dos sistemas elétricos, possibilitando explorar os resultados alcançados no segmento II. Resultados numéricos mostraram que o método tecnológico probabilístico baseado em DLR pode ser incluído como uma alternativa de planejamento para reforçar o sistema de transmissão. Para ilustrar os resultados, uma linha de transmissão de alta tensão do Sistema Interligado Nacional, sistemas teste do IEEE e o sistema elétrico da Península Ibérica, o qual é composto por Portugal e Espanha, são utilizados como estudos de caso.

Palavras-chave: Confiabilidade. Contribuições Científicas. Contribuições Tecnológicas. *Dynamic Line Rating*. Flexibilidade do Sistema de Transmissão.

RESUMO EXPANDIDO

Introdução

Desde o primeiro sistema de energia elétrica, no final do século XIX, os sistemas de potência vêm evoluindo, prestando um serviço eficiente aos consumidores e lidando continuamente com o *trade-off* entre economia e confiabilidade. Nos últimos anos, o paradigma do sistema de potência vem mudando devido às profundas transformações experimentadas nos aspectos regulatórios e na forma de geração, transmissão e monitoramento de energia. A transição energética conduzida principalmente pela integração de unidades geradoras renováveis variáveis conectadas por inversores exige melhorias nos critérios de flexibilidade do sistema, a fim de manter os pontos operacionais dentro das faixas de limites estáticos e dinâmicos. Nesse sentido, o sistema de transmissão, por sua vez, desempenha um papel importante no sistema elétrico, pois proporciona condições para o transporte de energia desde as usinas de geração até os pontos de consumo. Do ponto de vista do planejamento da expansão, novos métodos precisam ser considerados na escolha da alternativa de planejamento mais econômica para resolver problemas técnicos futuros, tendo em vista as incertezas e os desafios da transição energética em curso, garantindo a operação confiável do sistema.

Objetivos

Os objetivos dessa tese de doutorado podem ser classificados em três segmentos distintos. O segmento I visa apresentar uma discussão sobre a evolução de tecnologias, modelos e metodologias de análise, destacando novos desafios e oportunidades associados à transformação do sistema elétrico. O segmento II busca discutir detalhes da instalação de um protótipo para monitorar a condição de linhas de transmissão de alta tensão, onde os resultados são relacionados ao desenvolvimento do projeto de pesquisa TECCON II e amparados no conceito do *Technology Readiness Level* (TRL). A pesquisa foi elevada ao TRL 7, apoiada por estudos desenvolvidos nesta tese de doutorado, demandando a migração do protótipo do ambiente de laboratório para a demonstração no ambiente operacional. A elevação do TRL do protótipo do sistema de monitoramento é discutida apresentando, por exemplo, as especificações necessárias de novos componentes, modificações no circuito óptico e testes de calibração necessários para viabilizar a instalação em campo. O segmento III, por sua vez, apresenta as abordagens científicas relacionadas à variação da capacidade de transmissão através da estimativa do *Dynamic Line Rating* (DLR). Um método probabilístico baseado na tecnologia DLR é proposto para fornecer flexibilidade ao sistema de transmissão. O objetivo é medir o impacto de considerar limites de ampacidade variáveis, proporcionando flexibilidade ao sistema de transmissão. As linhas de transmissão irão operar com limites variáveis, seguindo séries horárias de direção e velocidade do vento, irradiância solar e temperatura ambiente, por meio de dados históricos.

Metodologia

As contribuições tecnológicas estão conectadas com o desenvolvimento do projeto de pesquisa TECCON II, no qual o autor participou e contribuiu em distintas áreas

de estudo. Para evidenciar os avanços tecnológicos, uma escala de maturidade (TRL) é utilizada para identificar os principais resultados do projeto de pesquisa e as contribuições do autor para elevação do TRL. Com relação as contribuições científicas, a adição de novas tecnologias no sistema elétrico requer a utilização de novos modelos para estimação da performance do sistema. Logo, a proliferação de tecnologias que estimam, em tempo real, a ampacidade de linhas de transmissão está exigindo que novas representações sejam agregadas à análises de planejamento do sistema de potência. Nesse sentido, propõe-se uma metodologia para o cálculo da ampacidade em tempo real de linhas de transmissão baseado no modelo térmico dinâmico do condutor e um framework probabilístico, baseado na tecnologia DLR, para avaliar a confiabilidade de sistemas elétricos, tendo como objetivo analisar a viabilidade de considerar a tecnologia DLR como uma alternativa de planejamento. Na abordagem proposta, a modelagem da linha de transmissão é composta por dois aspectos distintos: (a) modelo estocástico do ciclo falha/reparo; e (b) modelo dinâmico da ampacidade em tempo real baseada em fatores climáticos. Portanto, séries horárias históricas para velocidade e direção do vento, irradiância e temperatura ambiente são utilizadas para estimar a ampacidade do condutor da linha de transmissão.

Resultados e Discussão

Os resultados ligados às contribuições tecnológicas apresentam detalhes referente a instalação de um protótipo de monitoramento em tempo real em uma linha de transmissão de 230 kV do Sistema Interligado Nacional, promovendo a operação de uma solução com maturidade tecnológica nível 7. Adicionalmente, margens de carregamento disponíveis na linha de transmissão são estimadas levando em conta o limite estático e dinâmico do condutor. Os resultados alcançados com o sistema de monitoramento em tempo real possibilitam a aplicação do DLR. Na perspectiva científica, as contribuições estão ligadas a estimação de índices de confiabilidade, os quais são usados para quantificar o risco do sistema em não suprir a carga com base no uso do DLR probabilístico como alternativa de planejamento, avaliando o impacto da tecnologia no planejamento de redes elétricas. Os resultados indicam que em geral o DLR proporciona vantagens ao sistema, reduzindo o número de eventos associados a falta de limite de capacidade do sistema de transmissão. Como o limite térmico de uma linha de transmissão depende de sua temperatura máxima de projeto e a temperatura do condutor aéreo varia em função da corrente da linha e das condições meteorológicas, a capacidade da linha de transmissão irá variar de acordo com essas variáveis. Assim, o método probabilístico DLR é capaz de alterar o desempenho do sistema dependendo do ambiente onde a linha de transmissão está localizada. Dessa forma, os resultados numéricos baseados na tecnologia DLR proposto como alternativa de planejamento de transmissão explora a ideia de que o limite de capacidade da linha de transmissão pode ser variável e dinâmico, dependendo das condições climáticas reais.

Considerações Finais

À medida que o potencial energético renovável aumenta em todo o mundo, impulsionado principalmente por fontes de energia solar e eólica, há uma necessidade de maximizar as capacidades da rede de transmissão a fim de escoar a geração de eletricidade para as grandes cidades. Embora a localização e a construção de plantas

de geração solar e eólica são relativamente fáceis, está se tornando cada vez mais difícil construir novas linhas de transmissão. Portanto, autoridades de energia elétrica em todo o mundo estão procurando novas maneiras de maximizar a capacidade das linhas de transmissão. Nesse contexto, a tecnologia DLR surge como uma solução de planejamento incremental que pode ser incluída com segurança na lista de possíveis alternativas para maximizar ou reforçar a capacidade da rede de transmissão, sendo uma opção para conectar novas usinas de geração e atender cargas futuras de forma segura, proporcionando flexibilidade para implementação de estratégias operativas de escoamento da geração de energia elétrica para os grandes centros. No âmbito das contribuições tecnológicas, a infraestrutura TECCON alcançou o nível 7 de maturidade tecnológica (TRL) e, portanto, surge como uma nova opção de sistema de monitoramento em tempo real, possibilitando a implementação de metodologias para o cálculo da ampacidade estática e dinâmica (DLR) e outras aplicações.

Palavras-chave: Contribuições Científicas. Contribuições Tecnológicas. *Dynamic Line Rating*. Flexibilidade do Sistema de Transmissão. Planejamento de Sistemas de Energia Elétrica.

LIST OF FIGURES

LIST OF TABLES

LIST OF ABBREVIATIONS AND ACRONYMS

AC	Alternating Current
ACSR	Aluminum Conductor Steel Reinforced
AMC	Asset Management Center
ANEEL	*Agência Nacional de Energia Elétrica*
API	Application Programming Interface
CBM	Condition-Based Monitoring
CEMIG	*Companhia Energética de Minas Gerais*
CH	Channel
CLT	Central Limit Theorem
CM	Condition Monitoring
CNPq	*Conselho Nacional de Desenvolvimento Científico e Tecnológico*
CPST	*Contrato de Prestação de Serviços de Transmissão*
CWDM	Coarse Wavelength-Division Multiplexing
DC	Direct Current
DLR	Dynamic Line Rating
DOR	Down Operating Reserve
DR	Dynamic Rating
DWDM	Dense Wavelength-Division Multiplexing
EDFA	Erbium Doped Fiber Amplifier
EMI	Electromagnetic Interference
EMO	Easy Monitoring Overhead Transmission
FACTS	Flexible AC Transmission Systems
FBG	Fiber Bragg Grating
FFT	Fast Fourier Transform
FODP	Fiber Optical Distribution Panel
FOR	Forced Outage Rate
GPS	Global Positioning System
HL	Hierarchical Level
HVDC	High Voltage Direct Current
HVL	High Voltage Laboratory
ICT	Information and Communication Technologies
IEC	International Electrotechnical Commission
iid	independent identically distributed
IoT	Internet of Things
IP	International Protection Marking
LabPlan	*Laboratório de Planejamento de Sistemas de Energia Elétrica*
LPG	Long Period Grating
MC	Monte Carlo

MCS	Monte Carlo Simulation
MinDT	Minimum Down Time
MinUT	Minimum Up Time
MPPT	Maximum Power Point Tracking
MR	Must Run
MTTF	Mean Time to Failure
MTTR	Mean Time to Repair
NASA	National Aeronautics and Space Administration
NERC	North American Electric Reliability Council
OCS	Optical Current Sensor
OESPU	Opto-Electronic Signals Processing Unit
OFS	Optical Fiber Sensors
ONS	*Operador Nacional do Sistema Elétrico*
OPF	Optimal Power Flow
OPGW	Optical Ground Wire
OSA	Optical Spectrum Analyzer
PBS	Polarizing Beam Splitter
PCB	Printed Circuit Board
PD	Photodetector
PF	Power Flow
POW	point-on-wave
PVA	*Parcela Variável por Atraso na Entrada em Operação*
PVI	*Parcela Variável por Indisponibilidade*
PVRO	*Parcela Variável por Restrição Operativa*
REN	Redes Energéticas Nacionais
RIG	Rare-earth Iron Garnet
RMS	Root Mean Square
SAGSEC	Sags and Tensions in Multi-span Tension Section
SCADA	Supervisory Control and Data Acquisition
SLR	Static Line Rating
SMCS	Sequential Monte Carlo Simulation
SV	Sampled Values
TBE	*Transmissoras Brasileiras de Energia*
TECCON	Technology in Optical Fiber Sensors for Supervision, Protection and Control of Electrical Energy Systems
TECCON MS	TECCON Monitoring System
TRL	Technology Readiness Level
TSO	Transmission System Operators
UFMA	*Universidade Federal do Maranhão*

UFSC	*Universidade Federal de Santa Catarina*
Unicamp	*Universidade Estadual de Campinas*
UOR	Up Operating Reserve
vRES	Variable Renewable Energy Sources

CONTENTS

1 INTRODUCTION

Since the first electric power system, at the end of 19th century, power systems have been evolving, providing an efficient service for customers, and ongoing dealing with the trade-off between economy and reliability (MALIK, 2013). During the last years, the power system paradigm has been changing due to deep transformations experienced in regulatory aspects and in the way of generating, transmitting, and monitoring energy. Figure 1.1 presents a framework with the main characteristics related to the power system's traditional and transitioning models, dividing them into three distinct perspectives.

Figure 1.1 – Energy transition in generation, transmission and automation perspectives.

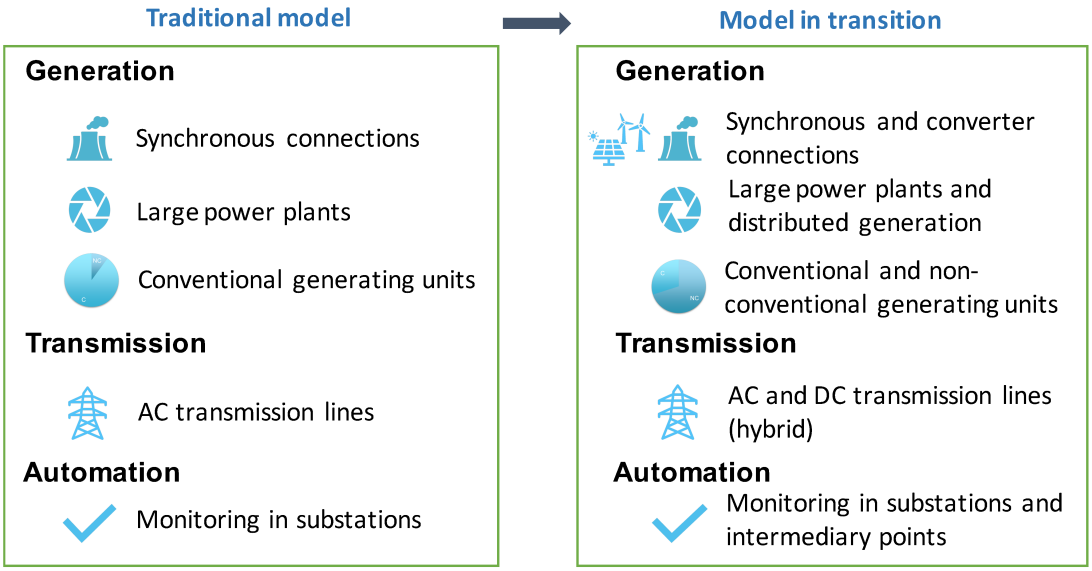

Source: own.

The energy transition, mainly conducted by the integration of variable and renewable inverter-based generating units, High Voltage Direct Current (HVDC) transmission lines, and new monitoring devices (as shown in Figure 1.1), demands improvements in the system flexibility criteria in order to maintain operative points inside the limits ranges for steady state and dynamic conditions (HATZIARGYRIOU et al., 2021; LUMBRERAS et al., 2021).

Furthermore, Figure 1.2 shows in a timeline some of the main power system transformations. Namely, electric sector deregulation and restructuring accelerated market agreements and interchanges of distinct power systems, whereas the problems related to massive use of thermal generating units provoked changes on the way electricity is produced. The renewable sources generation has been increasing since 90's, when the need for green power generation was discussed. On the beginning of 21st century, the power system has needed to find out new operational conditions in order to identify the best way to operate systems with vRES, since they are not able to provide

inertial response. In this sense, smart grid concept has emerged aiming to discuss about the presence of distributed generation, energy storage, new technologies, and other new devices in the power systems (CESPEDES et al., 2010).

Figure 1.2 – Timeline indicating power system changes and evolution during the end of 20th century and beginning of 21st century.

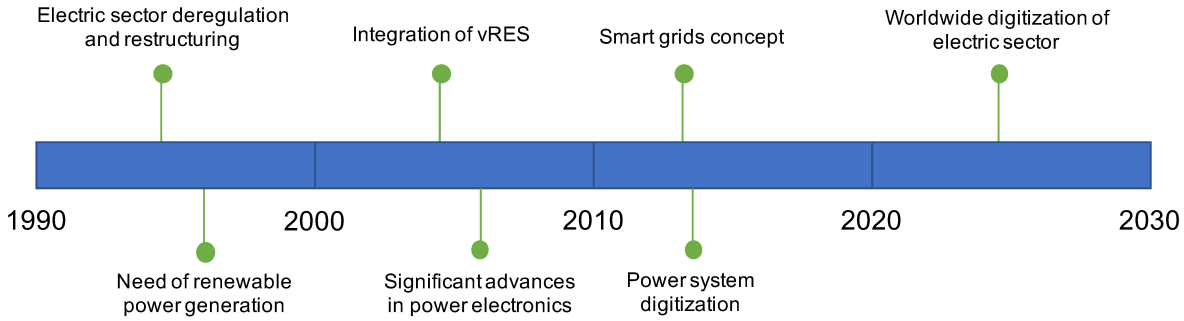

Source: own.

The installation of intelligent monitoring devices, since the second decade of this century (Figure 1.2), can be cited as an alternative able to provide real-time information about the equipment condition and thus improving power system observability. The real-time Condition Monitoring (CM) of high voltage equipment (e.g. cables, insulators, transformers, switchgear) is of interest to prevent component unexpected physical failures and to reduce not only outage times, but also save operational costs (AGGARWAL et al., 2000; FLORKOWSKI; LI, 2020). A CM system identifies significant component changes and trends which are indicative of a possible failure and it can be considered a major element of predictive maintenance technique or Condition-Based Monitoring (CBM).

Regarding sensing solutions used to CM functions, Optical Fiber Sensors (OFS) have been gradually replacing the electronic sensors on transmission line applications (BOHNERT et al., 2003). They can be manufactured using dielectric materials, as so their function is not affected by high electromagnetic interferences. Hence, it is possible to place them near the conductor of the transmission lines to perform the CM functions. Furthermore, OFS provide conditions for incorporation of point-on-wave (POW) concept in monitoring systems, having information in high-resolution (waveform sampling) and time-synchronized (NASPI, 2020).

The transmission network, in its turn, plays an important role in the power system as it provides conditions to convey energy from the generation plants until the bulk consumption points. From the perspective of expansion planning, new methods need to be considered to meet the choice of the most economical planning alternative to solve future technical problems in view of uncertainties and challenges of the ongoing energy transition, ensuring system reliable operation. According to US Canada Power System Outage Task Force (2004), North American Electric Reliability Council (NERC)

indicates that reliable designs need to cover four major objectives: (1) achieve system balance; (2) system resiliency; (3) system stability; and (4) thermal balance. However, this thesis proposes a revision in this definition suggesting an additional objective: (5) system flexibility.

The idea is to consider the thermal balance monitoring of power systems equipment as a basis to cover the other four objectives. Figure 1.3 shows the proposed idea for planning reliable bulk power systems. As a matter of fact, the scope of reliable designs needs to be enlarged to guarantee system flexibility under the perspective of converter interfaced generation technologies, loads and transmission devices (ULBIG, 2014; EPRI, 2016).

Figure 1.3 – Five major aspects to consider for planning reliable power systems.

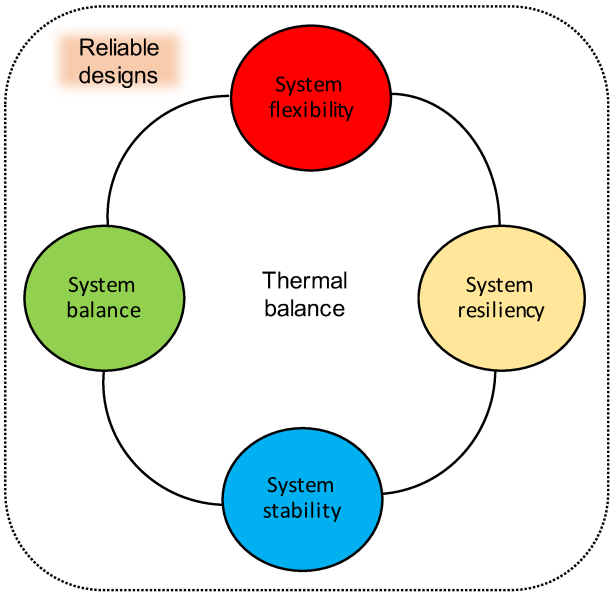

Source: adapted from US Canada Power System Outage Task Force (2004) and Teh (2016).

1.1 BACKGROUND AND MOTIVATION

In Brazil, the field of scientific and technological research is fomented by the Brazilian National Council for Scientific and Technological Development, *Conselho Nacional de Desenvolvimento Científico e Tecnológico* (CNPq), that suggests a classification of the development activities into two distinct groups:

a) Scientific Research Production;

b) Technological Development and Innovative Extension Production.

The first one is intended for regular scientific production, which has research paper as main results. The second one considers researchers who have a clear participation in technological development and innovative extension activities, associated with

a regular and adequate practice of scientific publication. However, the main results are patent registrations (innovation with products), which in general, require less research papers publication to keep the research results protected.

Therefore, the main results of this Ph.D dissertation are positioned into those two groups. The first set of contributions are connected with the technological development and those are called as Technological Contributions. In this research field, the author has performed development activities in the area of OFS for transmission lines CM. Under this perspective, this thesis shows the path to conduct an innovative product from laboratory tests to real applications in a high voltage transmission line of the Brazilian Interconnected System, where the real-time monitoring system installed provides several dimensions of application.

The second perspective, which is a result of the first one and is associated with scientific production, is classified as the Scientific Contributions. It is concerned with representing the application of technological devices to improve power system performance, where Dynamic Line Rating (DLR) technology is investigated in order to be considered as an incremental planning alternative to reinforce transmission network, looking for more optimized and economical ways of using the transmission line.

1.2 OBJECTIVES

This document has been divided into three distinct exploratory segments: (a) Segment I outlines the state of the art related to power system performance evaluation; (b) Segment II presents technological approaches (contributions); and (c) Segment III describes scientific approaches (contributions).

1.2.1 General objectives

Segment I presents a discussion over the evolution of technologies, models, and methodologies of analysis, highlighting new challenges and opportunities associated with power system transformation.

Segment II introduces the Technology Readiness Level (TRL) concept, presenting a prototype to monitor the transmission line condition, where the results are related to Technology in Optical Fiber Sensors for Supervision, Protection and Control of Electrical Energy Systems (TECCON) II research project developments. The research has been elevated to TRL 7 supported by studies developed on this thesis framework. It has required the prototype migration from the laboratory environment to the demonstration in the operational environment. The monitoring system provides information that can be used in a DLR application, as an example of the utilization of the outcomes provided by TECCON II research project. Also, segment II details author contributions associated with conducting the prototype to an application environment (high voltage transmission

line). The monitoring system prototype migration from the laboratory to the operational environment is discussed. Necessary specifications of components, modifications in the optical circuit, and calibration tests required to make feasible the field installation are presented and discussed.

Segment III presents the scientific approaches related to the variation of transmission capacity through DLR estimation. A probabilistic DLR-based technology method is proposed to provide transmission system flexibility. The goal is to measure the impact of having variable ampacity limits providing system flexibility. Transmission lines will operate with variable limits, following hourly series of wind direction, wind speed, solar irradiance, and ambient temperature, by means of historical data. A share of the scientific approaches is connected with the functionality of the technological product addressed in segment II.

Also, complementing the reliability assessment, aspects related to vRES are considered using the operational reserve flexibility concept. Power system reliability evaluations are performed considering three distinct representations and the generation system capacity is analyzed according to three different perspectives: static reserve, operational reserve, and operational reserve with flexibility.

1.2.2 Specific objectives

Segment I - discussion of state of the art, new challenges and opportunities in power systems planning and operation:

- To describe the technologies, models, and methodologies of 20th century;
- To present current technologies, models, and methodologies to deal with the ongoing energetic transition of power systems in the 21st century.

Segment II - technological approaches:

- To present the specific contributions of the author to improve the TRL of the TECCON infrastructure;
- To present the updates and actual status of the TECCON infrastructure technology;
- To show the TECCON infrastructure application as a DLR system.

Segment III - scientific approaches:

- To propose a probabilistic DLR-based technology method;
- To assess the impact of generation and transmission system flexibility in the power system reliability;

- To estimate reliability measures to quantify the risk of loss of load in composite and multi-area systems, using the DLR as a planning alternative.

1.3 THESIS OUTLINE

The remaining of this thesis is organized as follows.

Chapter 2: it is presented a state of the art revision about the technologies, models and methodologies of analysis related to power systems. Following topics are discussed: optical fiber sensors, DLR technology, Brazilian regulatory aspects for transmission lines remuneration, and models and methodologies for power system performance assessments;

Chapter 3: addresses the TECCON MS prototype demonstration in three distinct environments: laboratory, relevant and operational. TRL concept is utilized to affirm this technological approach. This chapter presents practical results for a 230 kV transmission line. Also, it exhibits real-time measurements obtained from the operational environment;

Chapter 4: presents the methodology for power system assessment considering operational flexibility, detailing the real-time ampacity implementation (DLR), and the algorithm for the probabilistic DLR-based technology method;

Chapter 5: addresses the scientific approaches results. It shows data and details of test systems and real power systems used for performance analyses. The DLR method is validated based on CIGRE standard, and power system reliability simulations are performed to provide insights about the impact of the DLR in system performance;

Chapter 6: presents the final remarks and future works for technological and scientific contributions.

2 TECHNOLOGIES, MODELS AND METHODOLOGIES OF ANALYSIS

Over the 20th century, until the 90's, the generation capacity has been predominantly hydro and thermal, whereas the transmission system has been operating with Alternating Current (AC) technology and fixed power capacities (in general, conservative values). The models and methodologies necessary to represent, operate and plan the power system had distinct characteristics from that Transmission System Operators (TSO) are facing nowadays in view of the energetic transition.

First commercial insulators, using porcelain technology, have emerged in the United Kingdom from the year 1840. Over the last twenty years of the 20th century, glass insulators have been predominantly installed on high-voltage electrical power systems. The development of digital computer technology has significantly improved the performance of hardware and software for power system analysis. Also, the applications of HVDC and Flexible AC Transmission Systems (FACTS) have added new control measures to electrical power systems, and have increased power transmission capacity, enhanced control capability, and improved operating characteristics. Besides, at the end of the 20th century, the rapid development of communication technology has enabled the online monitoring of electrical power systems.

In this chapter, it is presented a state of the art covering technologies, models, and methodologies related to power system energy transition. First three sections address the optical fiber sensors and dynamic line rating technologies, and the opportunities in regulatory aspects for transmission lines remuneration, respectively. Following those sections, the models and methodologies used to cope with reliability assessments under energetic transition conditions are presented.

2.1 OPTICAL FIBER SENSORS

Optical fiber has appeared in 1970 with the application, firstly, by telecom companies to overcome the old saturated copper telephone network. In the next decade, the 1980's, due to the optoelectronic industry growth, great dissemination, and optical fiber significant features, optical fiber technology exploitation has been expanded to many applications fields, in particular, to the electric power industry. In this area, the operators need to measure and monitor some important physical parameters, that include, for instance: strain ($\mu\epsilon$), vibration of structures and machines, electric current (from A to kA), voltage (from mV to MV), impedance ($\mu\Omega$), the leakage current of insulators (μA to mA), pollution of insulators, temperature, pressure, gas concentration, and distance between stationary and rotating or moving parts. Therefore, optical fiber technology applied to sensor elements has provided a vast dimension of utilization in the electric power industry (WERNECK et al., 2013).

Conventionally, in the electric power industry, these parameters are measured

using electronic sensors, however, they have two main problems: high voltage presence and presence of high Electromagnetic Interference (EMI) can cause a collapse on the electronic sensor unit. Indeed, in some situations, there is the necessity to measure physical conditions under electrically aggressive ambient. The best option to circumvent those difficulties, which can take the system to erroneous measures taking into account the high interferences of the medium, is the optical fiber sensors because the fiber is made of dielectric material (WERNECK et al., 2013), therefore, it is possible to place them very close or even over a high potential conductor and they do not necessarily need electrical power at the sensor location which is another problem that conventional sensors are subjected.

Some specific characteristics of optical fiber, that are well exploited by sensors based on this technology, can be highlighted (NASCIMENTO, 2016):

- Lightweight and compactness.
- High immunity to EMI.
- Local electrical power not required (they are passive sensors).
- High sensitivity.
- Several sensors can be multiplexed on the same fiber.
- Chemically inert even against corrosion.
- Electrical insulation.
- Work over long distances.

2.1.1 Electric current optical sensors

The Optical Current Sensor (OCS) operation is, in general, based on the Faraday effect, which is a magneto-optic effect, however, another linear effect that can measure the magnetic field in optical sensors is the magnetic force (or Lorentz force). Faraday effect is a magnetic-optic phenomenon discovered in 1845, in which a polarization plane of a light wave linearly polarized (the orthogonal electric field components have the same amplitude and a relative phase that is zero or multiple of π) that propagates through a medium (sensor) is changed (rotated) at magnetic field presence. Thus, there is a rotation at light plane polarization proportional to magnetic field intensity (JORGE, 2001). The angle rotation (θ_f) is explained mathematically by (2.1):

$$\theta_f = \int_L V\vec{B} \cdot \vec{dl} \tag{2.1}$$

where, V is the material Verdet constant (rad/Tm), which depends of the optical source wavelength and temperature; $\vec{B}$ is the magnetic flux density vector (T); and $\vec{dl}$ is the

differential vector along the direction of propagation (m). The main parameter of (2.1) is the Verdet constant, because it is the proportionality factor that determines the material magnetic field sensitivity. This constant is related to the medium variables through (2.2):

$$V \approx -\frac{\pi\gamma}{\lambda\eta} \tag{2.2}$$

where γ is a material constant called magnetogiration; λ is the wavelength of the radiation; and η is the refraction index of the medium (JORGE, 2001). As can be noted, the Verdet constant presents an inverse dependence on wavelength. Also, through the other parameters, V has a temperature dependence (WILLIAMS et al., 1991; DAY; DEETER; ROSE, 1991). Figure 2.1 illustrates the polarization rotation due to a parallel external magnetic field on a magneto-optic material, such as, glass (SILVA et al., 2012).

Figure 2.1 – Faraday effect in the plane rotation of a light polarized in the presence of a magnetic field.

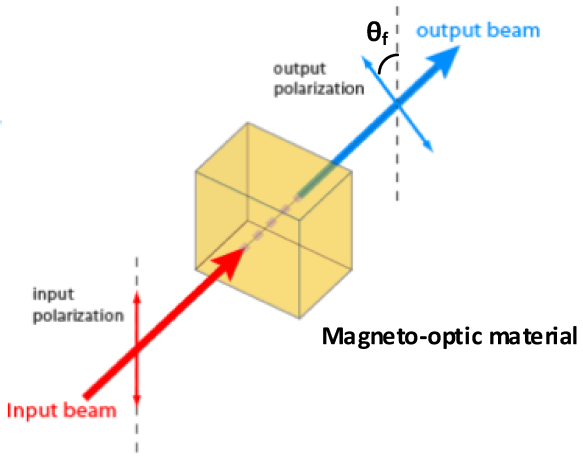

Source: adapted from Medeiros (2016).

On the other hand, the magnetic force sensors measure the force applied by the magnetic field on the sensing element (SILVA et al., 2012). Regarding electrical current measurements in high voltage locals (transmission lines, for example), solutions based on fiber optic have experimented a considerable development in the last thirty years. Thereby, there are some electrical current measurements alternatives based on fiber optic sensors, since they are defined as equipment through which, one physical, chemical, biological measuring interacts with light guided by a fiber optic (intrinsic sensor) or guided to an interaction region (extrinsic sensor) by a fiber optic (where the optical signal leaves the cable and is modulated in another medium), producing an optical signal related to a parameter of interest (RIBEIRO et al., 2005).

Optical sensors are expected to interact with one or more light characteristics (polarization, intensity, phase, wavelength) since, in the end, light modulation must be processed in an optical signal at the receiver, which performs conversion into an

electrical signal. Considering the sensing mechanism employed and the materials used, OCS can be organized in four main groups (SILVA et al., 2012):

a) All-fiber sensor: the fiber itself actuates as the transductor mechanism. The magneto-optic effect is utilized to induce rotation angle at the light propagation polarization plane on fiber, which is proportional to the magnetic field. Usually, the fiber is coiled around the electrical conductor, making the measurement immune to external currents and magnetic fields. Typically, standard silica fibers have a low Verdet constant when compared with glass prisms, nevertheless, many studies have been developed to increase fiber Verdet constant;

b) Bulk optic sensor: this type of sensor uses a piece of glass or crystal with a high Verdet constant as a transductor, which is positioned close (or around) of the electrical conductor. The magnetic field is also measured by the magneto-optic effect. These sensors are generally cheap, robust, and more sensible. They are based on a piece of glass (or crystal) as a sensor element, utilizing fiber optics to couple luminous signal until the sensible element and get the resultant signal to take it until detection state (interrogation);

c) Magnetic force sensors (or Lorentz force): in an analogous process to the piezoelectric elements, when a magnetic field is applied to a magnetostrictive element it induces mechanical changes in the material. These changes can be measured by attaching a Fiber Bragg Grating (FBG) to the magnetostrictive element. Magnetostrictive fiber optic sensors explore the magnetostriction effect, which produces a mechanical deformation in a ferromagnetic material when it is subjected to an external magnetic field;

d) Hybrid sensors: these sensors employ some of the standard electromagnetic technology already existent and some of the optical technology. In this case, the current transducer is done with conventional electromagnetic technology (for instance, a Rogowski coil) but its interrogation and information transportation are done by an optical fiber system (Power Over Fiber – POF concept) (ROSOLEM, 2017). These sensors aim to build an interrogation system that takes advantage of the high level of electrical isolation provided by optical fibers and avoids difficulties associated with birefringence.

Linear birefringence (β) is a characteristic present in some crystalline substances, which have an anisotropic atomic distribution causing different optical properties in distinct directions, i.e., the two orthogonal directions have different refractive indices where light propagates with different velocities (NASCIMENTO, 2016). The all-fiber and bulk sensors, to measure electric current, are addressed in detail following.

2.1.1.1 All-fiber optical sensor

This type of current sensor uses very simple configurations because the fiber can be simply coiled around the electric conductor to be measured by the Faraday effect. A key aspect of this sensor is that the optical fiber acts both as the sensing element and communication channel (simple solutions), which reduces the losses in the fiber connections. Also, the sensor sensitivity can be changed by merely changing the number of turns of the optical fiber around the conductor (JORGE, 2001). Unlike bulk optic sensors, immunity to external currents or magnetic fields, as well as, tunable sensitivity can be easily achieved.

Since all-fiber sensors usually use several meters of fiber, the sensors are more vulnerable to pressure and temperature gradients, mechanical vibrations, and other environmental noises than smaller devices (such as bulk-optic sensors). Some studies have been done to increase the low Verdet constant of standard silica fibers, namely, application of flint fibers, new optical glass for optical fibers with high refractive index and a terbium-doped-core phosphate optical fiber (SILVA et al., 2012; HOTATE; THAI; SAIDA, 1998). There are some fibers produced in the scope of the research project, which can improve the Verdet constant, providing desirable high circular birefringence (CHESINI, 2018).

As the detection scheme for the all-fiber optical sensor, generally, forms a closed circuit around the electrical conductor, it will not be sensitive to external magnetic fields produced by the other electrical conductors of a three-phase system (SILVA et al., 2012). Conversely, a problem of using the fiber as the transducer is the effect of linear birefringence that is induced by mechanical stress, thermal stress, manufacturing imperfections, and other effects. It reduces significantly the sensor sensitivity due to the polarization state degeneration. The light polarization plane rotation is computed using (2.3):

$$\theta_f = \mu_0 V N I \tag{2.3}$$

where μ_0 is the air permeability, N is the fiber number of turns and I is the electrical current.

2.1.1.2 Bulk optic sensor

The bulk optic current sensor is a broadly industrially implemented technology. When compared to all-fiber devices, bulk optic sensors present some advantages: these are usually smaller devices and mechanically stiffer, their Verdet constants are typically two times higher than the ones found in optical fibers, intrinsic linear birefringence is very small which allows sensors with high sensitivities, they are more robust, being more protected against mechanical and thermal gradients, vibrations and other noises.

Another advantage is that this sensor allows easy installation without the need of interrupting the current in the conductor.

The main disadvantages of these sensors are related to the fact that reflections (light interaction with the magnetic field) need to occur inside the bulk optic material and the immunity to external currents/magnetic fields is harder to obtain. Therefore, the rotation angle will be dependent on plenty of factors, for instance, the refractive index of the crystal and outside surrounding medium (such as air), these relations can be explained by (2.4):

$$\theta_f = \frac{\mu_0 V I}{\pi} \arctan\left[\frac{L}{2r}\right] \tag{2.4}$$

where L is the sensor length and r is the distance between the sensor and the conductor.

To solve the optical external factors interference, some solutions have been developed, such as the use of double reflections in each corner of the bulk optic material making a closed optical path (Figure 2.2).

Figure 2.2 – Bulk optic sensor with double reflection.

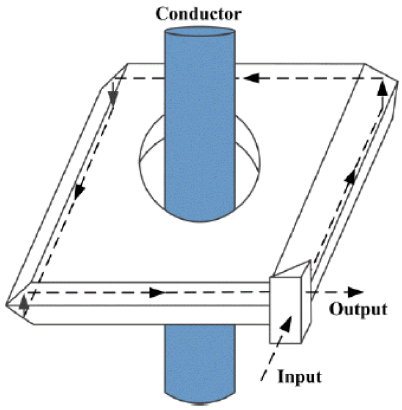

Source: adapted from Medeiros (2016).

However, this idea still presents a problem: the polarization state between the first and second reflections is elliptical, and the signal will be non-linearly affected by the magnetic field to be measured, mainly when this sensor is measuring current in three-phase systems. Several schemes have been proposed to further increase the sensitivities of these sensors, including field concentrators and extending the optical path inside the crystal. Also, one needs to be alert with the light source wavelength as it impacts on Verdet constant and with the compensation of the linear birefringence, however, it is generally small (SILVA et al., 2012).

Due to the temperature dependency of the Verdet constant, it is common to first calibrate the current sensor without the temperature sensor effect and after that, it is carried out a calibration measuring the temperature and compensating its effect by

introducing a correction factor that depends on the temperature, both for all-fiber and bulk sensors (SILVA et al., 2012).

2.1.1.3 Methods to reduce magnetic crosstalk in optical current sensors

According to Niewczas et al. (2001), to solve the problem of magnetic crosstalk caused by other energized conductors, a unique compensation method, which solves, in real-time, a set of linear equations, each representing the instantaneous output signal from one phase current sensor can be applied. The Faraday rotation is induced only if the magnetic field is parallel to the direction of light propagation within the sensing element. Some results exposed showed that the separation distance between the conductors must be very large in order to meet the specified accuracy requirements, i.e., the measurements have acceptable interferences.

Therefore, magnetic crosstalk can be minimized using flat conductors fixed in one plane and separated from each other at the highest possible distance. The results for the conventional optical architecture that they studied in Niewczas et al. (2001) demonstrate that the separation between conductors should be greater than 1.5 m to reduce the crosstalk as necessary for metering application.

Another study demonstrates that the errors associated with bulk optical current sensors working in three-phase electrical systems may be minimized by properly designing the geometry of the system (PERCIANTE; FERRARI, 2008). Through simulation and experiments, the authors demonstrate the relation between magnetic crosstalk and the distance between two electrical conductors ($1/d^3$). It is presented also a new geometric configuration for optical current sensors based on the idea that the optical path inside the magneto-optic materials is parallel to electrical current conductors, except in a small loop around the sensor heads. It can decrease the minimum distance between parallel conductors to 20 cm with a radius of 1 cm and no compensation method is needed, only properly designing geometric configuration.

However, in some practical situations, it is impossible to do a small loop with the electrical conductor around the sensor or to let the conductors only in a parallel plane distanced by 1.5 m or more, as in transmission power lines, which have plenty of different geometric configurations.

2.1.2 Mechanical strain and temperature optical sensors

The most popular optical technique used to measure temperature and strain in most adverse situations is the FBG sensor. Historically, the formation of permanent gratings in optical fiber and the first indications of photosensitivity observations have been first studied in 1978 in Canada (HILL; MELTZ, 1997), (HILL; FUJII, et al., 1978). An FBG consists of a periodical and longitudinal perturbation on fiber refraction index (see

Figure 2.3) which is formed by exposure of the core to an intense optical interference pattern (HILL; MELTZ, 1997).

Figure 2.3 – FBG principle in an optical fiber.

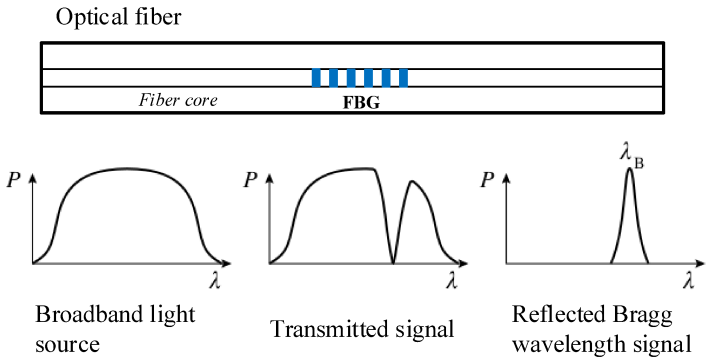

Source: adapted from Hill and Meltz (1997).

The fiber perturbation causes a selective reflection of a light narrow band (some hundreds of picometers), centered on a specific wavelength called Bragg wavelength (λ_B in nm), which is determined by (2.5):

$$\lambda_B = 2\Lambda n_{eff} \tag{2.5}$$

where Λ is the network period or the spacing between the gratings (in nm) and n_{eff} is the effective refraction index of the grating fundamental mode. An FBG can be considered as a set of partial mirrors that transmit light except for the particular wavelength that is reflected. It is noted, from (2.5), that the Bragg wavelength only depends on the distance between gratings (Λ) and the effective index of refraction (η_{eff}).

FBGs may present different reflectivity and wavelength. Both characteristics change with the amount of Ultraviolet (UV) energy (irradiation time or the number of shots) (KERSEY et al., 1997). The relation of the n_{eff} with temperature and deformation is known through thermo- and elastic-optical coefficients, whereas Λ can be modified by silica thermal expansion (dilatation) coefficient or through the displacement itself (increasing the pitch of the grating) applied to the fiber. Temperature changes and longitudinal deformations result in Bragg wavelength variations that might be detected both on transmitted spectrum and on reflected (Figure 2.4) (WERNECK et al., 2013; NASCIMENTO, 2016).

Essentially, besides of temperature and strain dependency of the Bragg wavelength, any external agent that is capable of changing the grating period will displace the reflected spectrum. Therefore, instead of a Fiber Bragg Grating (FBG) be a traditional way to measure temperature and strain, other factors can be measured: vibration, pressure, electric voltage, displacement, etc. Strain effects will modify the geometric properties of the grating, which will lead to a wavelength shift of the Bragg wavelength. Additionally, temperature changes also affect the wavelength shift, and as so must be

Figure 2.4 – Characteristics of an FBG etched in an optical fiber.

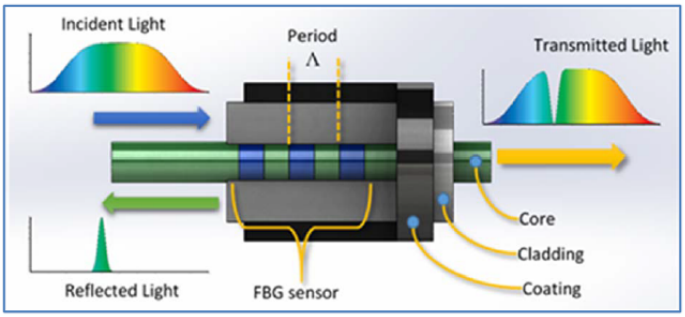

Source: adapted from Nascimento (2016).

accounted for. By differentiating (2.5) with respect to these parameters, as a function of strain (ϵ) and temperature (T), the spectral analysis of the reflected light allows to monitor axial strain or temperature changes, as follows (LUYCKX et al., 2007):

$$\frac{\Delta\lambda_B}{\lambda_B} = (1 - P)\Delta\epsilon + \beta\Delta T \tag{2.6}$$

Basic interferometers and phase mask methods can produce the interference pattern required or, in other words, to inscribe FBGs in optical fibers (NASCIMENTO, 2016; HILL; FUJII, et al., 1978). Although, the main challenge of this type of sensor is to demodulate the information required, i.e., to identify the variation of Bragg wavelength with the parameter intended to measure. The easiest way to demodulate the signal is using an Optical Spectrum Analyzer (OSA), however, it is heavy, very expensive, and not practical for field applications. A second interrogation technique, formed by an interferometric Fabry-Perot tunable filter which is a consolidated technology, but still presents a moderate cost, uses the filter to transmit a signal which is proportional to the convolution between the signal power (reflected light centered on Bragg wavelength) and the filter response. Instead of a Fabry-Perot filter, it is possible to use another FBG or an Long Period Grating (LPG) as a filter (CARVALHO, J. et al., 2012). It is a very simple and low-cost setup implementation.

Aiming to measure electromagnetic quantities (voltage and current) one utilizes, normally, a combination of FBGs with magnetostrictive materials, the FBG is embedded or fixed on magnetostrictive material which is used to measure magnetic field intensity (NASCIMENTO; BAPTISTA, et al., 2015). The Terfenol-D, material composed of an alloy that presents the highest magnetostriction and for this reason it is the most common material at these applications, induces a longitudinal deformation at FBG proportional to the magnetic field, which in turn is proportional to electrical current (FRACAROLLI et al., 2016). To measure the voltage can be utilized the piezoelectric effect, where the electric field application on material causes a deformation. So, the voltage is inferred by electric field measurement (ALLIL; WERNECK, 2011). The choice of FBG as an optical transducer is related to the nature of the spectral response, which confers to this type

of sensor an intrinsic capacity of multiplexing by wavelength.

2.2 DYNAMIC LINE RATING

Conductors of transmission lines are expected to operate, under static conditions of functioning, near to 65℃, depending on transmission line characteristics and grid regulations (MOROZOVSKA; NAIM, et al., 2020). In conventional power systems planning studies, electric energy transmission systems have fixed capacities which are traditionally determined by steady-state thermal limit analysis based on the worst scenario of meteorological conditions (low wind speed and high ambient temperature) or ambient-adjusted, that is, a limit used for the summer and other for the winter (MOROZOVSKA; HILBER, 2017). Namely, the Brazilian National Electric System Operator, *Operador Nacional do Sistema Elétrico* (ONS), operates some transmission lines with a specific power limit for the day and another for the night. However, it is well-known that the weather conditions vary instantaneously and therefore the conductor has its thermal limit rating changing constantly. The conductor thermal behavior methodology is detailed in Appendix A.

In this regard, the Dynamic Rating (DR) topic has attracted attention in the last years as a promising smart grid application, which allows varying the system capacity by monitoring its conditions in real-time (e.g. transformers and transmission lines) (ROCHA et al., 2020; SEPPA, 2002). Transmission lines applications, for instance, may monitor the dynamic conductor state using real-time weather and/or line data such as conductor temperature, mechanical tension, sag, clearance, vibration, and electromagnetic field (FERNANDEZ et al., 2016; FERNANDES, 2018; MOROZOVSKA; HILBER, 2017). In fact, monitoring the conductor thermal behavior enables the DLR technique implementation, also offering a vast dimension of applications towards an optimal transmission system expansion (ROCHA et al., 2020).

The assessment of the impact of DLR on power systems performance has been an object of interest recently (PINTO; GARCIA, 2019; HAJEFOROSH; BOLLEN; ABRAHAMSSON, 2019; TEH; COTTON, 2016). The Information and Communication Technologies (ICT) play an important role in monitoring, controlling, and protecting the power system operation, in particular, Cruzat and Kopsidas (2019) evaluates the impact of ICT coupled to time-varying line rating on network reliability. In Teh (2016), a complete analysis of dynamic thermal rating for transmission lines is presented. The author demonstrates the economic benefits in considering the DLR instead of Static Line Rating (SLR) (fixed ratings) on power system operation by determining the electricity costs for both situations using a 4-bus example network.

DLR is an emerging measure to improve the efficiency of line utilization (WALLNERSTRÖM et al., 2014) and can be determined by two approaches: direct or indirect. Direct methods are based on monitoring line characteristics, such as conductor tem-

perature, line sag, mechanical tension through the line, and clearance to the ground. Indirect DLR estimation is a prediction-based method using local weather data or generating the data by using numerical weather modeling (HAJEFOROSH; BOLLEN; ABRAHAMSSON, 2019).

A transmission line consists of multiple spans or line sections. Each line section has a specific rating which depends on the distinct weather conditions. The line ampacity (I_{line}) problem needs to determine the current rating by selecting the minimum rating among the monitoring line sections. Therefore, the line current flows through the transmission line without surpassing any rating limits of all line sections. This process can be explained mathematically by (2.7), considering an arbitrary transmission line.

$$I_{line} = min(I_1, I_2, \ldots, I_n) \tag{2.7}$$

where n is the number of line sections and I represents the current rating calculated for each line section considering the weather conditions and conductor physical properties.

The impact of real-time thermal rating on power network reliability has been investigated in Greenwood and Taylor (2014). The simulation has been conducted considering the generation system perfectly reliable and the line ratings have been approximated with a normal distribution as a proportion of static rating. In this case, the DLR application has reduced the LOLE expectation by 67%. DLR can increase the transmission line rating by 10% to 30% over 90% of the time, with an improvement of 50% being possible in windy areas (TEH; COTTON, 2016).

Some countries have been tested DLR application on their transmission lines. In Latvia, for instance, the TSO introduced a DLR implementation to prove that the theoretical approach of the IEEE 738 Standard (IEEE, 2013) gives similar results with real measurements and the conclusion was positive (MUTULE et al., 2016). The Markov chain models have been used to simulate nearly close weather conditions based on 10-year statistical data. Furthermore, mechanical analyzes may present the most important positions for DLR equipment building to get maximum observability of monitoring results and avoid line outages. The general form of DLR benefit is shown in Figure 2.5.

In order to calculate the DLR is needed to solve the following two problems:

1. Determination of the thermal current limit for a particular span which may involve different measurements and different calculation techniques.

2. Determination of the weakest span, i.e., the span which represents a limit for the whole power line. Furthermore, the weakest span may vary in consequence of different atmospheric conditions and span characteristics (tension, clearance margin, etc.).

The main factors that influence a typical transmission line corridor are depicted in Figure 2.6, which shows the complexity associated with assessing DLR. It is noted that

Figure 2.5 – Comparison of static and dynamic current limits.

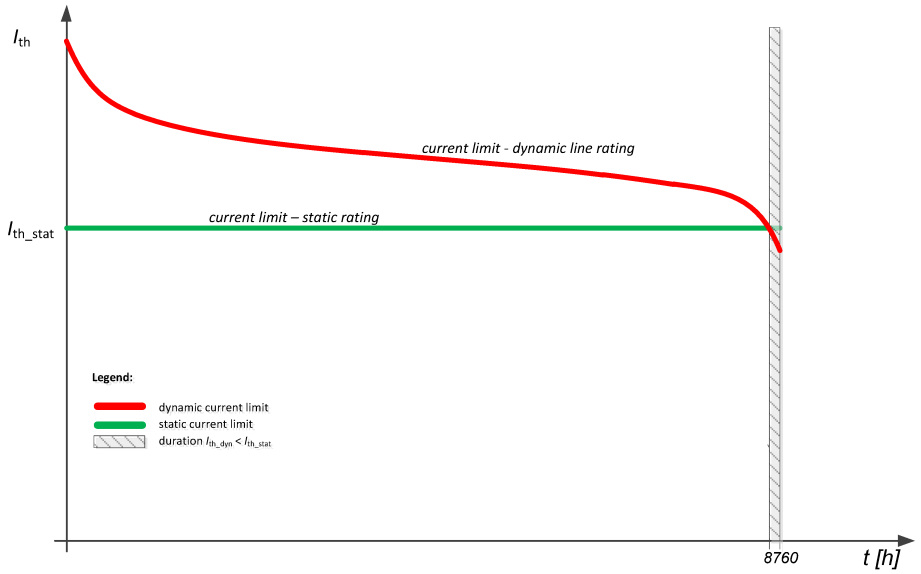

Source: adapted from ENTSO-E (2015).

the current along the line is almost the same, however, the current-carrying capacity of a span varies according to the atmospheric conditions. Ideally, the DLR determination should measure atmospheric conditions and geographical information for every span.

The DLR study can be divided into long- and short-term horizons as presented as follows. In addition, at the end of this section, an overview of existing monitoring systems, which provide conditions for DLR exploration, is exposed.

Long-term studies refer to investment (planning) and design of line corridors. The main objective is the extension or expansions of the present transmission networks. The classical approach on transmission system planning studies is to establish a constant line capacity based on the worst weather conditions (SLR), avoiding the conductor surpasses its thermal limit. Some system operators determine seasonal ratings, aiming to increase, in some situations, the ratings compared with the worst case scenario. On the other hand, DLR enables the utility or TSO to postpone expansion through revealing the hidden current capacity.

The DLR calculation for the short-term operation includes a wide range of issues, ranging from system real-time operation to hourly, daily, and weekly operating decisions. It can support maintenance scheduling of overhead lines from a week perspective or increase the rating of the loaded lines if the weather conditions allow it. To update the thermal limit of critical lines is the main purpose of short-term studies. Different techniques handle the uncertainties associated with DLR calculation: probabilistic, fuzzy- and interval-based are the common ones (SOROUDI; AMRAEE, 2013).

Figure 2.6 – The variability of influencing factors on transmission line rating.

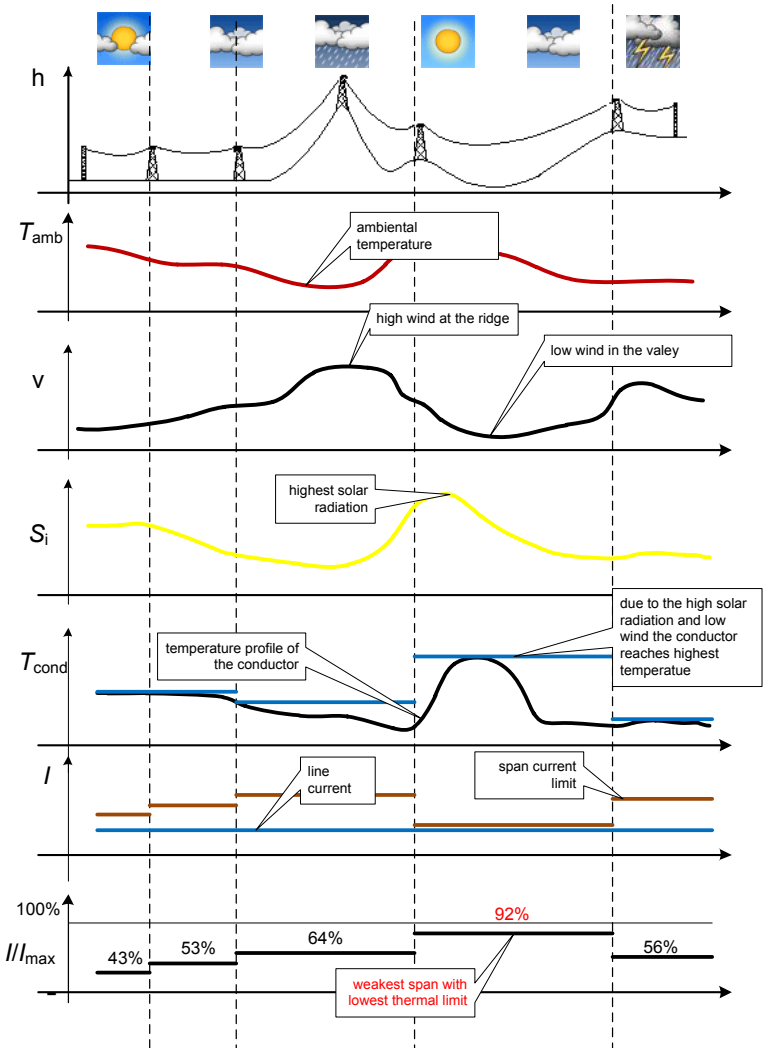

Source: adapted from ENTSO-E (2015).

2.2.1 Monitoring systems

A study about existing monitoring systems for DLR has been done in Morozovska and Hilber (2017). Several DLR systems are available in the market, differing from each other by the required measurements and proposed approaches for ampacity calculations. Different companies produce different equipment for DR data collection. Some of them, for instance, are used to measure the conductor temperature or monitor mechanical tension in the conductor (FERNANDEZ et al., 2012; SEPPA, 1993). Therefore, there is a wide variety of DLR systems, each one with its specific characteristics, limitations, applications, and merits.

The CAT-1^{TM} Dynamic Line Rating System has a weather forecast, conductor temperature evaluation and mechanical tension monitoring (USI, 2019a). It measures the mechanical tension of an overhead transmission line conductor in the anchorage insulator using load cells and relates this value to the conductor temperature that is

used in the real-time ampacity calculation in the system computational tool. The current system is the fourth generation and over 500 systems have been installed worldwide. Figure 2.7 illustrates the CAT-1™ system.

Figure 2.7 – CAT-1™ System.

(a) Load cells. (b) Net Radiation Sensors.

Source: adapted from USi (2019a).

Power Donut® Line Monitor is installed directly at the conductor, the latest generation is completely self-contained and self-powered (USI, 2019b). It measures Root Mean Square (RMS) current, RMS voltage, reactive and active power, and conductor temperature, vibration, and sag angle. Some studies are reporting the Power Donut utilization in monitoring systems for transmission lines, as exposed in Nascimento, Brito, et al. (2004). Figure 2.8 depicts the monitoring system equipment.

Figure 2.8 – Power Donut 3 System.

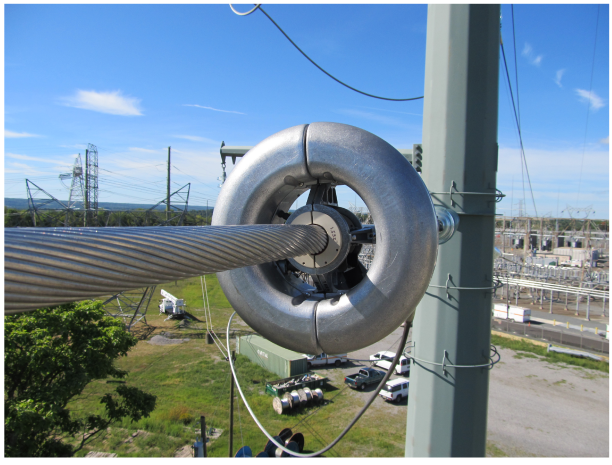

Source: adapted from USi (2019b).

Sonar System measures directly the distance conductor-ground through sound waves. It measures the time taken for a sound pulse to propagate from a sensor head to a target and back (BLACK; CHISHOLM, 2015). Besides, it has a temperature sensor for eventual adjusts in the measurements due to sound speed variations. Figure 2.9 shows

the SONAR sensor installed in a *Companhia Energética de Minas Gerais* (CEMIG) transmission line.

Figure 2.9 – SONAR XPS-40 System.

Source: adapted from Nascimento, Giudice, et al. (2001).

The Easy Monitoring Overhead Transmission (EMO) system enables the acquisition of power cable temperature at an economical low-cost (FERNANDEZ et al., 2012). Figure 2.10 shows the EMO being clipped on the line. It has communication via wireless with a reach limitation of 60 m (sensor/base station). A battery pack is used as an energy supply.

Figure 2.10 – EMO system live-line installation.

Source: adapted from micca (2019).

Another existing DLR system is the TLM Conductor Monitor, which provides a complete picture of conductor behavior. The TLM measures the clearance-to-ground, conductor temperature, vibration, and electric current. It is installed directly on the conductor (Figure 2.11), being a self-powered solution for system voltages up to 765 kV (LINDSEY MANUFACTURING CO., 2019).

The TLM conductor monitor provides the continuous data on conductor behavior required for facility rating, regulatory compliance, and DLR. The system uses satellite communication and according to the manufacturer the computational program developed utilized together with the TLM provides ampacity forecasting for a period up to 48 h.

Figure 2.11 – TLM Lindsey.

Source: adapted from Lindsey Manufacturing Co. (2019).

Ampacimon is installed on the conductor directly (Figure 2.12), measuring its sag based on the vibration frequency spectrum (AMPACIMON, 2019). The acquired data by the sensors are sent via GSM-GPRS to an Ampacimon server directly linked with the operator.

Figure 2.12 – Ampacimon clipped on the line.

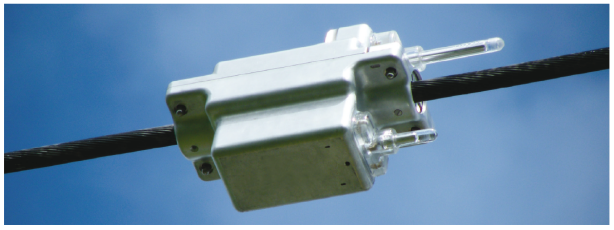

Source: adapted from Ampacimon (2019).

The system is self-powered and allows live-line installation. The originality is in the vibration frequency analysis allowing the sag monitoring at critical spans without any calibration or additional parameters set.

Sagometer is also available in the market (EPRI, 2001). It performs measurements of horizontal and vertical variations of the conductor catenary using a camera installed in the tower and a small reflexive target. The Sagometer utilizes digital imaging to determine the clearance-to-ground of overhead conductors and then communicates the information to system operators. Figure 2.13 displays a second-generation Sagometer being installed on a transmission line.

As the last example, Sags and Tensions in Multi-span Tension Section (SAGSEC) is an apparatus related to automatic, real-time measurement of the actual position of an overhead line conductor (line sag measurement). More particularly, the system is based on an optical device that is provided at a known position in space and a second device that is mounted at a known, fixed location on the line (BROWN, 2001).

2.3 BRAZILIAN REGULATORY ASPECTS FOR TRANSMISSION LINES REMUNERATION

Some Brazilian normative resolutions provide guidelines for the remuneration of transmission lines. The REN N° 191 and REN N° 729, from *Agência Nacional de*

Figure 2.13 – Sagometer.

(a) Second-generation camera (b) Target installed on the line

Source: adapted from EPRI (2001).

Energia Elétrica (ANEEL), address procedures to determine the operative capacity of transmission installations and establish guidelines related to the quality of transmission system public service (associated with availability and operative capacity of the transmission installations), respectively (ANEEL, 2005b, 2016).

In Brazil, the transmission lines base payment (BP), which comes from granting process, is generally based on the long-term operative capacity. This value is declared by transmission companies in the *Contrato de Prestação de Serviços de Transmissão* (CPST). In this contract, details about the transmission installation are exposed.

The long-term operative capacity of a transmission line is specified at the design phase for normal conditions of operation. The static capacity is determined considering usually the worst boundary conditions and the value is obtained by using the standard produced by CIGRE WG22-12. On the other hand, the short-term operative capacity of a transmission line is the value allowable during emergencies and it is calculated based on an overload factor that is established according to the conductor design temperature, as presented in Table 2.1.

Table 2.1 – Design temperature and overload factor.

℃	50	55	60	64	65	70	75	80	90
Factor	1.42	1.33	1.26	1.24	1.23	1.19	1.17	1.15	1.12

Source: adapted from ANEEL (2005b).

Regarding the service quality and reliability, the BP may be discounted whether some aspects related to the service are not being attended to. In this sense, three variable shares are utilized to guide the service evaluation by the ANEEL:

- *Parcela Variável por Atraso na Entrada em Operação* (PVA): it establishes payment discounts based on the delay time observed to start the operation of a certain transmission line taking into account the day established for its operation beginning.

- *Parcela Variável por Indisponibilidade* (PVI): unavailability of transmission lines due to schedule or non-schedule out of operation (maintenance).
- *Parcela Variável por Restrição Operativa* (PVRO): it is related to the operative restrictions of a transmission installation may present.

To illustrate the number of parameters involved on the financial variable share related to operative restrictions (PVRO), it can be defined mathematically as:

$$PVRO = \frac{BP}{24 \times 60 \times D} \left(\sum_{i=1}^{NRL} (ROL_i DROL_i) + \sum_{s=1}^{NRS} (ROC_s DROC_s) \right) \tag{2.8}$$

where D is the number of days in occurrence month, $24 \times 60 \times D$ is the number of minutes in occurrence month, BP is the base payment of transmission function related to initial month of event occurrence, ROL is the proportional reduction of long duration operative capacity, ROC is the proportional reduction of short duration operative capacity, $DROL$ is the duration, in minutes, of an operative restriction of long duration that has occurred during the month for the transmission function submitted to restriction, $DROC$ is the duration, in minutes, of an operative restriction of short duration that has occurred during the month for the transmission function submitted to restriction, NRL is the number of operative restrictions of long duration in a month and NRC is the number of operative restrictions of short duration in a month.

Assuming as a reference the nominal value agreed (independently of the operational need of the system), the reduction in operative capacity, either long or short duration, is occasioned, usually, due to three limiting factors: surpassing of equipment nominal capacity, interference on transmission line right of way causing reduction on the clearance-to-ground and deficiency on the normal state of operation of equipment, such as power transformers. These situations can cause discounts on the base payment.

2.4 GENERATION SYSTEMS RELIABILITY ASSESSMENT

The sufficient generation capacity amount determination to supplying the load continuously is an issue approached by Hierarchical Level (HL) I. The task is to plan a generating system to meet the system load requirement as economically as possible with an acceptable level of reliability. Figure 2.14 depicts the usual system representation applied to solve HL-I problems, where it is assumed that the total generation and system loads are connected to a single bus (BILLINTON; LI, 1994; CARVALHO, 2013).

The long-term adequacy generation system studies can be viewed according to two different perspectives: static and operating reserve. However, at the end of the 20th century, the focus of planning studies has been on static reserve assessment, which evaluates if the installed capacity satisfies the system load by means of estimating risk

Figure 2.14 – System model for HL-I adequacy assessment.

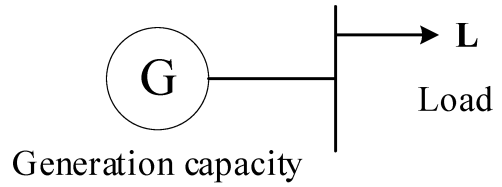

Source: adapted from Billinton and Li (1994).

of failure (BILLINTON; LI, 1994). The events of insufficient static reserve (R_{static}) occur when the generating capacity is less than the load, according to (2.9):

$$R_{static} = G - L < 0 \tag{2.9}$$

where G represents the system available capacity and L the total system load. Probabilistic static reserve models may include planned (preventive maintenance) and/or forced (unscheduled) outages of the generating units, capacity fluctuations, and short- and long-term load uncertainties (LEITE DA SILVA; SALES, et al., 2010; CARVALHO, 2013).

With the increased amount of renewable energy sources in power systems, deal with the time-dependent generating capacity in the operating reserve perspective is mandatory (LEITE DA SILVA; SALES, et al., 2010). The operating reserve studies are concerned with the long-term analysis of the flexibility of the generating system to cope with the short-term variations which can occur during the system operation (CARVALHO, 2013). Hence, there is a risk associated with the system be not capable to respond to specific operating situations, as follow up reserve requirements (e.g. loss of a generating unit, wind capacity fluctuations, or gross errors in load forecast). Operating reserve, more specifically the spinning one (G_s), is the synchronized generation capacity ready to respond to load uncertainties in short-time intervals, requiring rapid and automatic responses. The reserve criterion can be (LEITE DA SILVA; SALES, et al., 2010):

1. a percentage of the hourly load;
2. a fixed amount: considering uncertainties related to variable generation, forecast errors, and/or pre-defined security levels;
3. the largest synchronized unit;
4. a combination of 1 and 3.

The non-spinning (tertiary) reserve is called to replace the spinning reserve for posterior availability or help in cases of huge perturbations (loss of load or unexpected

load changes) (CARVALHO, 2013). In broad terms, the insufficient operating reserve capacity ($R_{operating}$) events can be identified according to (2.10) (MATOS et al., 2009):

$$R_{operating} = G_s + G_{ns} - [L + (\Delta L + \Delta P_{vRES} + \Delta G)] \leq 0 \tag{2.10}$$

where G_s is the capacity of the synchronized units scheduled to meet the forecast load (L), the primary reserve (R_P) and the secondary reserve (R_S). G_{ns} is the fast tertiary reserve not synchronized, which is composed of those generators that can assume load within 1 h. ΔL and ΔP_{vRES} account for short-term deviations on load and variable renewable sources forecasts, respectively, whereas ΔG represents generating units' shortage due to forced outages during the operating period (MATOS et al., 2009). A unit commitment of the available generating units must be performed to calculate the $R_{operating}$ (CARVALHO, 2013).

Figure 2.15 shows the operating reserve approach and describes the risk of changes in the load, wind and solar power capacity, and generating outages not being duly covered by the amount of spinning and tertiary reserves (MATOS et al., 2009).

Figure 2.15 – Operating reserve assessment.

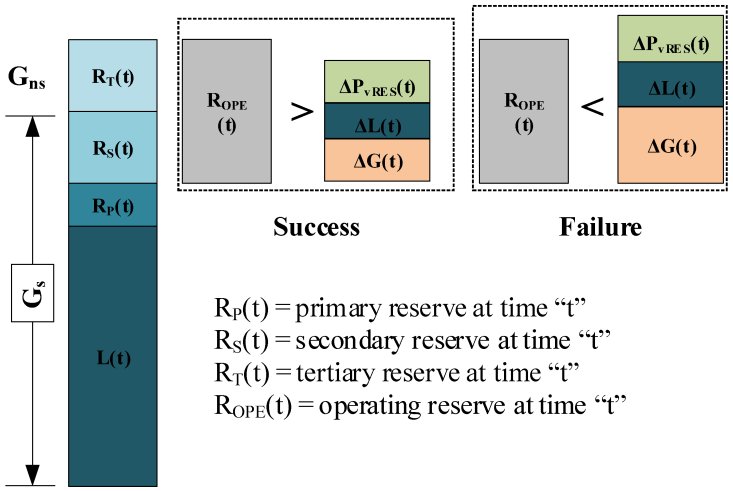

Source: adapted from Matos et al. (2009).

2.4.1 Generating units operational flexibility

The flexibility assessment of the generating units is concerned with evaluating which generating units have the technological features to provide reserve services. When the unit commitment is carried out to meet the load, generating units' stochastic failures may occur and/or uncertainties of generation and load forecast. The flexibility, in its turn, comes mainly from controllable or dispatchable units that allow the control of their operation by TSO. There are some properties and constraints that impact flexible units response, such as (WOOD; WOLLENBERG; SHEBLÉ, 2014; MIRANDA, 2020):

- Ramp rates: represent the generating unit capacity in response to increasing or reduction on its generation in a determined period, in MW/min.
- Minimum operation power: operational constraint related to minimum power value that the unit can operate synchronized to the grid, in MW.
- Minimum technical power: some units present a minimum generation constraint higher than its minimum operation power, imposed by the operator agent to assure system security.
- Start-up time: maximum time that a generating unit takes to operate, considering the state condition of cold, warm or hot start, in hours.
- Minimum Down Time (MinDT): once the unit is decommitted, there is a minimum time before it can be recommitted.
- Minimum Up Time (MinUT): once the unit is running, it should not be turned off immediately.
- Must Run (MR): some units are given a must-run status during certain times of the year for the reason of voltage support on the transmission network.

The conventional generation technologies can be organized into flexibility levels (GONZALEZ-SALAZAR; KIRSTEN; PRCHLIK, 2018):

- Inflexible generation: designed to operate in load base, while start-up and ramping operations are rare and time-consuming. The technologies include inflexible nuclear, coal power plants, and certain steam turbines.
- Flexible generation: designed to operate as mid-merit plants that can adjust their generation level to cope with load variations and short start-up time. The technologies comprise flexible gas turbine combined cycle, biomass, biogas, and flexible coal.
- Highly flexible generation: this type of generation presents a high capacity to cope with load variations. Start-up time, minimum downtime, and minimum uptime very low. Power plants such as hydro, mini-hydro, and a sub-set of simple cycle gas turbines.

The waste of renewable sources means an inflexible moment of the system where shutting down a clean and low-cost energy source is necessary. Solar and wind generating units are not controllable (vRES), presenting particular variability, over shorter time scales, and raising specific operational challenges when large amounts of those technologies are integrated into the power system. Actually, high shares of

vRES are likely to require more investment in flexibility measures to maintain system balance at all times (IRENA, 2017). In this sense, the reserve flexibility assessment can be divided into two situations (MIRANDA, 2020):

- Up Operating Reserve (UOR): operation situations with sudden load increase, loss of generation not scheduled, production reduction due to primary resources availability, transmission system restrictions, or even importation reduction from neighboring areas. In general, it involves situations in which the generation is inferior to the system load.
- Down Operating Reserve (DOR): operation situations with sudden load reduction, quick renewable generation due to availability of primary resources (wind, solar irradiance), or transmission system restrictions that take the system to a unbalance with generation beyond of load preventing the flow of surplus generation. In general, it involves situations in which the generation is higher than the system load.

Figure 2.16 presents situations involving the need of load curtailment (lack of UOR) and vRES shedding (lack of DOR).

Figure 2.16 – Flexibility requirements in a system with high penetration of vRES.

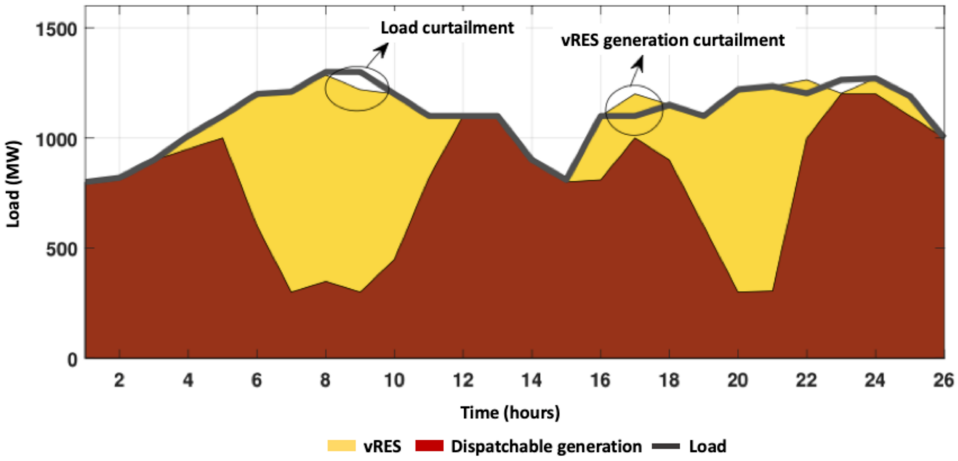

Source: adapted from Miranda (2020).

The method proposed to evaluate the UOR and DOR requirements encompasses three general distinct stages (MIRANDA, 2020):

Stage 1: this stage assess if the generators scheduled to meet the load, during the phase of operation planning, have the technical and technological characteristics to meet the operational situations, such as the variability of energy resources and load, without considering any remedial action. Whether this is a state of failure, there is a lack of generation technological

resources to meet the load (UOR), or the generators are not sufficiently flexible to avoid renewable energy wasting (DOR).

Stage 2: the remedial actions are considered trying to eliminate the failure identified in the previous stage. Operational actions may be used during the simulation process. Actions are taken to avoid the waste of renewable generation (DOR) or load shedding (UOR).

Stage 3: the need of load shedding (UOR) or generation shedding (DOR), as an extreme remedial action, is assessed.

The generation flexibility evaluation methodology is illustrated in Figure 2.17, where ΔUNC is the variation of $\Delta L + \Delta G + \Delta vRES$, $R_{flex}^{up,down}$ represents the ramp down or up capacity, considering a specific period, i.e., the capacity of increase or reduce the generation in a determined instant, $RAN^{up,down}$ represents the need for remedial actions when the first stage does not attend the requirement.

Figure 2.17 – Operating reserve assessment considering flexibility aspects.

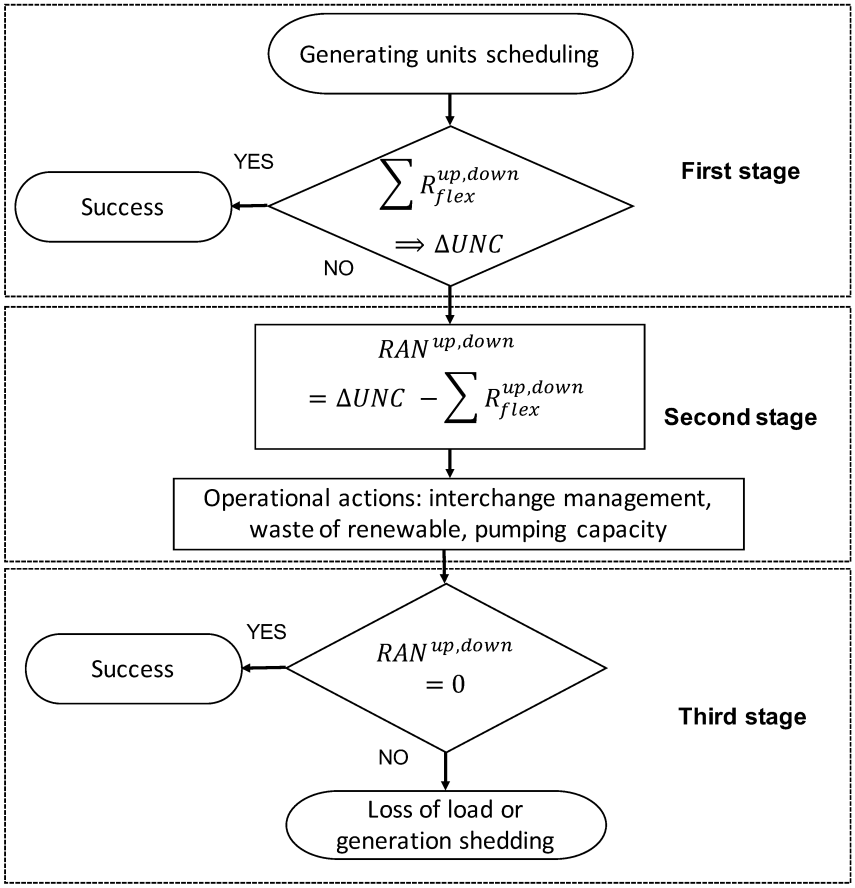

Source: adapted from Miranda (2020).

In Miranda (2020), some performance indices to evaluate the risk of lack of flexibility both for UOR than DOR are proposed. The indices are related to the frequency,

duration, and severity of events occasioned by the excess or deficit of generation in the power system. DOR indices, specifically, can be used to measure the ability of the system in reducing its conventional generation to meet demand, avoiding the waste of renewable intermittent sources.

2.5 COMPOSITE SYSTEMS RELIABILITY ASSESSMENT

The adequacy assessment of composite generation and transmission systems, or simply composite system, belongs to HL-II type of studies (BILLINTON; ALLAN, 1996; CARVALHO, 2013). This generation and transmission adequacy analysis needs to address with the bulk electric system's ability in delivering energy to major points of consumption.

The system analysis is significantly more complicated at HL-II, besides generating units detailed models and the system load, the transmission circuits stochastic behavior and constraints such as voltage limitations, maximum loading limits of the transmission circuits, and real and reactive power, are also considered (CARVALHO, 2013). In the literature, the maximum loading limits are usually fixed, based on static ratings. Figure 2.18 illustrates a basic network configuration that can be used on composite system evaluation under the adequacy approach.

Figure 2.18 – Example of a simple network configuration for HL-II adequacy assessment.

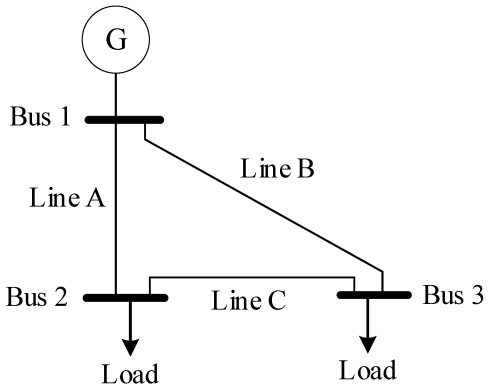

Source: adapted from Billinton and Allan (1996).

Therefore, in addition to the generating system adequacy perspective, HL-II studies have a second element involved in the planning process that is the development of a suitable transmission network to convey the energy generated to the points of consumption. The adequacy analysis consists of verifying if the operative constraints are being attended or if it is necessary some corrective measures to avoid load shedding. Usually, at this stage, Power Flow (PF) solution techniques (non-linear or linear) are required, whether not enough to attend the operative limits, non-linear or linear Optimal Power Flow (OPF) problem is solved (PEREIRA; BALU, 1992; CARVALHO, 2013).

In a long-term planning analysis, these studies can capture more accurately the effect of geographic dispersion of the loads and primary energy resources. Besides, composite systems assessments intend to identify weak points in the system through the individual load point adequacy indices (CARVALHO, 2013), where different load curtailment priorities for the load can be used (PEREIRA; BALU, 1992).

The adequacy results can be evaluated also by separating the system into subsections, such as generation and transmission failures (PEREIRA; BALU, 1992). For instance, a failure involving the generation subsystem is characterized by the inexistence of sufficient generating capacity to supply the system load whereas a transmission subsystem failure happens when there is load curtailment although the generating capacity is sufficient to supply the system load (CARVALHO, 2013).

2.6 MULTI-AREA SYSTEMS RELIABILITY ASSESSMENT

Multi-area configuration encompasses the operation of different systems interconnected through tie transmission lines. The adequacy of a power system can be improved by interconnecting the system to other electrical areas. When an area has insufficient generation capacity to meet its load, assistance can be received from neighboring areas. The amount of assistance depends on the following factors (BILLINTON; LI, 1994):

- The load level of the supported area.
- The available generating capacities of the supporting areas.
- The tie line constraints.
- The import/export agreement between the areas.

The supporting area is that one, which has surplus generation capacity in relation to its demand. On the other side, the supported area is the area, which has a generation deficit. The static reserve capacity of each area (R_{static_i}) can be defined as (BILLINTON; LI, 1994):

$$R_{static_i} = G_i - L_i + \sum_{j \in \Omega_i} I_j \tag{2.11}$$

where I_j is the interchange power capacity (importation or exportation), related with area j, which goes through the interconnections. Ω_i is the set of all areas interconnected to area i. Considering a power system pool composed of N_A interconnected areas, the total reserve capacity of the system (R_{system}) is:

$$R_{system} = \sum_{i=1}^{N_A} R_{static_i} \tag{2.12}$$

Similarly to the single area studies, the operating reserve ($R_{operating_i}$) for a specific electrical area can be defined as (VIEIRA, 2020):

$$R_{operating_i} = R_{S_i} + R_{T_i} + \sum_{j \in \Omega_i} I_j \tag{2.13}$$

where R_{S_i} and R_{T_i} are the secondary and tertiary reserve requirements for area i. In planning studies, considering the amounts of the interchange (I_{ij}) established by multi-area strategies, it is necessary to calculate the power flow values at tie and transmission lines, verifying the eventual violation of power limits. These new conditions demand a novel restriction in OPF modeling, considering the exportation and importation limits of each participating area of the interconnected system. The details of the algorithm utilized to evaluate the system state for multi-area systems assessments, and proposed indices to quantify the events according to the procedures established by strategy operation, are presented in Vieira (2020).

Most of the works published in the literature has dealt with the adequacy assessment of multi-area systems representing each area as that total system generation and total system load are connected to the same bus (HL-I) as in Billinton and Li (1994) and Haringa, Jordan, and Garver (1991) or considering the representation of the tie lines (SINGH; LAGO-GONZALEZ, 1989; TÓMASSON; SÖDER, 2016). On the other hand, in Nagarajan (2009), it is carried out a study considering a multi-area test system with a complete representation of the transmission network and interchanges.

Indices, for each electrical power system area, are calculated to estimate the reliability of these typologies. To accomplish that, a supporting strategy must be specified. Distinct policies result in different amounts of interchange and consequently distinct reliability indices. The following two basic emergency action philosophies can be used in a loss of load situation (BILLINTON; LI, 1994):

- The loss of load sharing philosophy: each area shares the unserved demand according to a supporting strategy, recognizing tie-line constraints.
- The no-load-loss sharing philosophy: each area attempts to meet its demand. If there is excess capacity, it is supplied to supported areas by an agreed supporting strategy.

Distinct supporting strategies based on the two philosophies of emergency actions aforementioned are proposed in Billinton and Li (1994). However, on the framework of this thesis, three representations are used to study the DLR as planning alternative, which involve single area and multi-area representations. The composite system analysis is considered as Representation 01 (Figure 2.18) and multi-area assessments are conducted by two other representations (VIEIRA, 2020):

a) Representation 02 - multi-area system with interconnections: tie lines are represented considering operating procedures and/or market policies between areas, as well as capacity restrictions (Figure 2.19);

Figure 2.19 – Multi-area single bus with interconnections.

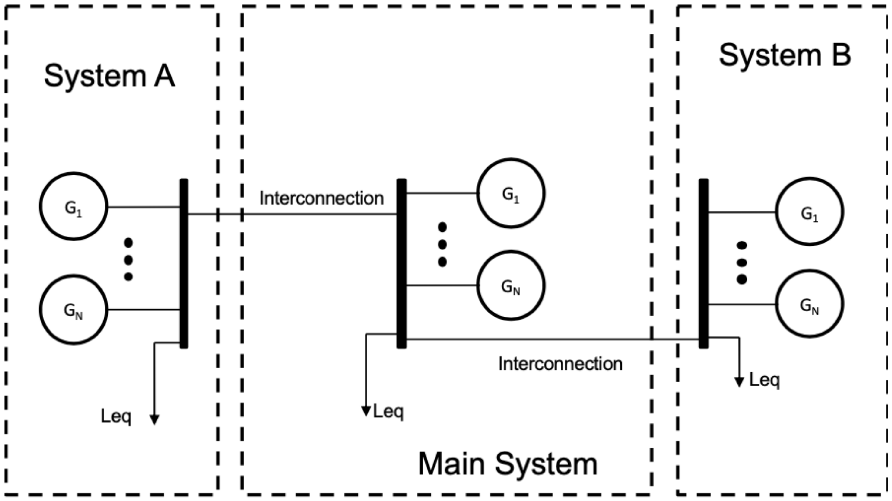

Source: adapted from Vieira et al. (2020).

b) Representation 03 - multi-area system with transmission network of the main system: it considers the representation of the main system connected to distinct electric areas, as depicted in Figure 2.20.

Figure 2.20 – Multi-area with transmission network.

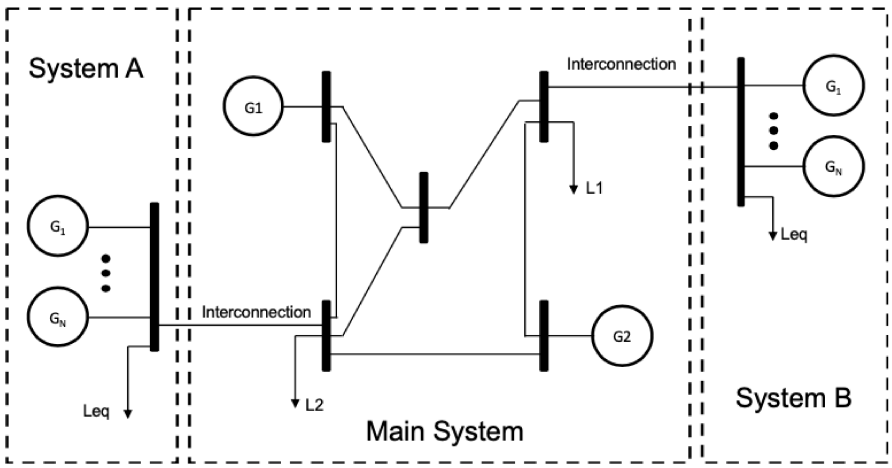

Source: adapted from Vieira et al. (2020).

Agreements (market policies) among the operating agents control the power amounts allowed in the interchanges between areas. The correct representation of these policies allows a simulation more adherent to the expected behavior of the system.

Three interchange policies are considered to assess the performance of interconnected operation (VIEIRA et al., 2020):

- Assistance strategy: each system performs the unit commitment on an individual basis, aiming at fulfilling the generation amounts necessary to meet the expected load and reserve needs of its area. Each system tries to meet its load with its generation and if necessary tries to cover the deficit through import action whether there is available capacity to export in neighboring areas. The exporting capacity of a given area corresponds to the amount of committed generation that is not utilized to supply its load. Eventually, if more than one system needs support, a priority list is used to decide which area will have support priority.
- Market strategy: permits commercial trades between areas, allowing that generating units with lower cost to be allocated in neighboring areas. It means that the process of allocating generating units is carried out together, therefore the generating units of any area can be scheduled to meet the load and reserve requirements of other areas. If there is the necessity of load curtailment due to generation deficit, the priority list of supported areas is used.
- Hybrid strategy: it presents characteristics from the two previous policies. To meet the system load forecast needs, the scheduling of generating units is performed looking for units in any interconnected areas, prioritizing those with lower operational cost. On the other hand, the scheduling of units to cover reserve needs is carried out individually, where each area should schedule generating units from its area.

2.7 RELIABILITY INDICES

There is a wide range of reliability indices that can be used to measure both the past reliability performance and to predict the future power systems performance in terms of reliability, i.e., performance indices are used to quantify the risk of loss of load (BILLINTON; SATISH, 1994). Reliability indices can appear with different names depending on the HL being analyzed. Traditionally, they can be categorized into three groups: probability indices, frequency and duration indices, and energy indices (CARVALHO, 2013). The probability indices are (BILLINTON; ALLAN, 1996):

- Loss of Load Probability – LOLP, which gives the probability of load curtailment.
- Loss of Load Expectation – LOLE (hour/year, day/year, or week/year), indicates the average number of hours, days, or weeks in a given evaluation period that the system cannot meet the load.

Examples of frequency and duration (F&D) indices are (BILLINTON; ALLAN, 1996):

- Loss of Load Frequency – LOLF (occurrence/year), which represents how many times, on average, the loss of load occurs during a determined period.
- Loss of Load Duration – LOLD (hour/occurrence, day/occurrence or week/occurrence), indicates the average duration of a load curtailment event.

Examples of energy-related indices are (BILLINTON; ALLAN, 1996):

- Expected Power Not Supplied – EPNS (MW), which gives the average amount of load curtailment.
- Expected Energy Not Supplied – EENS (MWh/year), which indicates the average energy curtailed during the evaluation period (usually a year).

Aiming to obtain a complete picture of bulk and multi-area power systems adequacy evaluation, the reliability indices can be also divided into two groups or perspectives of assessment which are complementary: system indices and load-point indices (BILLINTON; SATISH, 1994). Individual load-points can be used to identify weak points in the system while overall system indices provide a global vision (quantitative) of the composite system adequacy and may be used by planners to compare different power systems design alternatives (CARVALHO, 2013).

Despite the valuable information the aforementioned indices convey (point and system reliability indices), they can not account for load curtailment costs. According to Carvalho (2013), the overall economic impact of an interruption depends on the type of consumer disconnected: consumer class (residential, commercial, and industrial), the customer's dependence on electricity, the nature of the interruption, the economic value of the activity being disrupted, and on the several characteristics of the interruptions, such as the amount of unserved energy (curtailment depth) and respective duration, frequency, time of occurrence, geographical coverage or even if the consumer was warned (LEITE DA SILVA; PEREZ A., et al., 1997; MELLO; PEREIRA; SILVA, et al., 1997). A variety of methods has been utilized to evaluate these unit individual interruption costs (currency/kWh) through various indirect analytical evaluations, actual blackouts, and customer surveys where the last method has been considered the most accurate way to determine the monetary losses that consumers have due to interruption on their supply (MASSAUD; SCHILLING; HERNANDEZ, 1994; MELLO; PEREIRA; SILVA, et al., 1997).

The outcome of these studies is the customer damage function, which represents the average cost that each customer class incurs after an interruption as a function of time (CARVALHO, 2013). Since these damage functions are available to each consumer class, producing sector customer damage functions, they can be aggregated at

any particular load point in the system to produce a composite customer damage function at that load point. Then, the reliability worth can be accurately measured through the following index (LEITE DA SILVA; PEREZ A., et al., 1997; MELLO; PEREIRA; SILVA, et al., 1997):

- Loss of Load Cost – LOLC (currency/year), which represents the average cost of load curtailment during the evaluation period (generally a year).

Reliability studies require the use of test functions to estimate the performance indices, these functions convert the definition of the indicators into mathematical formulae. Test functions are utilized to verify if the system states are of success or failures. Therefore, reliability indices are determined by the test functions' expected value that have an underlying probability distribution associated (CARVALHO, 2013; PEREIRA; BALU, 1992).

2.8 RELIABILITY ASSESSMENT METHODS

The reliability indices of a power system adequacy analysis can be assessed using two basic categories of probabilistic methods: direct analytical techniques and stochastic simulation (BILLINTON; LI, 1994; BILLINTON; ALLAN, 1996). The difference between these approaches lies in the way in which the reliability indices are evaluated. Analytical methods rely on mathematical solutions to calculate the exact value of the reliability indices. Monte Carlo Simulation (MCS) methods, on the contrary, estimate the indices bounded by an interval of confidence by simulating the actual process and random behavior of the system (CARVALHO, 2013). The primary assumption in most adequacy assessment methods is that the component failures in the system are independent events. Even though, common-mode failure events, which are defined as an event having a single external cause with multiple failure effects where the effects are not a consequence of each other (BILLINTON; ALLAN, 1996), can be considered depending on the level of detail required.

2.8.1 Simulation-based methods

The simulation methods are based on Monte Carlo (MC) techniques which involve simple algorithms for computing numerical quantities (expectations, probabilities) that are formulated in terms of basic random objects (series of experiments, stochastic processes) (PEREIRA; BALU, 1992; CARVALHO, 2013). The advantage of MCS over analytical methods is that the required number of samples for a given accuracy is independent of the size of the system but rather on its reliability and therefore it is suitable for real power system evaluation. MC methods are also more flexible than

analytical methods and are favored when complex features such as reservoir operating rules in hydroelectric systems, complex correlated load models, chronological simulation, maintenance schedules, wind power variation, etc. need to be represented (PEREIRA; BALU, 1992; CARVALHO, 2013). Lastly, the Monte Carlo methods estimate the probability and other indices by counting the number of times an event occurs.

MCS techniques can be classified according to how system states are sampled. If a state-space representation is used, then the MCS method is called non-sequential. Conversely, when system states are sampled taking into account the chronology of events, the method is called sequential (CARVALHO, 2013). Other kinds of MCS methods, that combine characteristics of a state-space and chronological representations, have been proposed in the last decade of the 20th century, such as pseudo-sequential (MELLO; PEREIRA; LEITE DA SILVA, 1994) and pseudo-chronological (LEITE DA SILVA; MANSO, et al., 2000).

The convergence of the MCS methods is monitored by the coefficient of variation β of the estimates of the reliability indices (BILLINTON; ALLAN, 1996; PEREIRA; BALU, 1992). Considering H (H is normally a scalar function) as a test function representing a given performance function, the coefficient of variation or relative error is calculated according to (2.14):

$$\beta = \frac{\sqrt{V[\tilde{E}[H(x)]]}}{E[H(x)]} \tag{2.14}$$

where $E[H(x)]$ is the estimate of a given reliability index, $\tilde{E}[H(x)]$ is an unbiased estimator of the unknown quantity $E[H(x)]$ and $V[\tilde{E}[H(x)]]$ is the variance of the estimator of the reliability index. The sample variance can be estimated using the unbiased estimator:

$$V[\tilde{E}[H(x)]] = \frac{1}{N-1}\sum_{y=1}^{N}(H[x_i] - \tilde{E}[H(x)])^2 \tag{2.15}$$

where N is the number of samples and x_i is one system state over the N sampled. The suitable test function for each reliability index depends on the MCS method. By the strong law of large numbers and the Central Limit Theorem (CLT) (BILLINTON; LI, 1994), the distribution of any sequence of independent identically distributed (iid) random variables, each one with mean μ and variance σ^2, tends to the Normal distribution with zero mean and variance 1 as $N \to \infty$, being σ the standard deviation. The approximate $(1-\alpha)$ confidence interval for $E[H(X)]$ is given by:

$$\left(\tilde{E}[H(x)] - z_{1-\alpha/2}\frac{\sigma}{\sqrt{N}}, \tilde{E}[H(x)] + z_{1-\alpha/2}\frac{\sigma}{\sqrt{N}}\right) \tag{2.16}$$

where $z_{1-\alpha/2}$ is the quantile of the standard normal distribution, $\mathcal{N}$ (0,1). For instance, the 95% $(\alpha = 0.05, z_{0.975} = 1.96)$ confidence interval of $E[H(X)]$ is given by (2.17):

$$\left(\tilde{E}[H(x)] - 1.96\frac{\sigma}{\sqrt{N}}, \tilde{E}[H(x)] + 1.96\frac{\sigma}{\sqrt{N}}\right) \tag{2.17}$$

The necessary criteria and definitions to implement the Sequential Monte Carlo Simulation (SMCS) method are detailed in Appendix B.

2.9 POWER SYSTEM COMPONENTS MODELING

The methods used to evaluate power system adequacy include the application of models intended to represent system real operation, such as: (a) availability of the generating units; (b) hydro capacity fluctuation; and (c) the chronology of the load (representing power-consuming habit). Essentially, the capacity of system components depends on two distinct aspects: the failure/repair cycle stochastic model and the time-dependent capacity model (PEREIRA; BALU, 1992; CARVALHO, 2013).

The failure/repair cycle stochastic model is related to the component stochastic behavior of forced outages (physical failures). It defines the availability of the component, i.e., the transitions between the up and down states. The Markov model approach can be applied to represent the random behavior of systems that vary continuously or discretely with relation to space and time. Markov representation also considers that the system is stationary, i.e., the component probability to transit from one state to another is the same during the entire time (BILLINTON; ALLAN, 1996).

The failure/repair cycle of equipment can be dictated by Markov models (BILLINTON; LI, 1994; BILLINTON; ALLAN, 1992; DA ROSA et al., 2016). Bearing in mind the Figure 2.21, a component, whose stochastic behavior is represented by the two-state Markov model, has its maximum capacity available when in the up state. In the down state, the capacity is zero. Two state transition rates rule the state's transition (CARVALHO, 2013):

- λ is the failure rate (occurrence/year or occurrence/hour).
- μ is the repair rate (occurrence/year or occurrence/hour).

Figure 2.21 – Two-state Markov model.

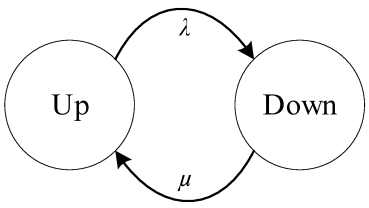

Source: adapted from Billinton and Allan (1996).

It is considered that the state transition rates are constant, also, it is common to determine these transition rates using the parameters Mean Time To Failure ($MTTF$)

and Mean Time To Repair ($MTTR$). Hence, failure and repair rates can be obtained by (2.18) and (2.19), respectively.

$$\lambda = \frac{1}{MTTF} \tag{2.18}$$

$$\mu = \frac{1}{MTTR} \tag{2.19}$$

The two-state Markov model is a simple but reasonably robust representation. The component availability (A) and unavailability (U) or Forced Outage Rate (FOR) are given by (2.20) and (2.21), respectively:

$$A = \frac{\mu}{\lambda + \mu} \tag{2.20}$$

$$U = \frac{\lambda}{\lambda + \mu} \tag{2.21}$$

Considering a chronological Monte Carlo simulation and assuming that the states duration is exponentially distributed, the component residence time in the up (operating) and down (unavailable) states is given by the inverse transform method (BILLINTON; LI, 1994), according to (2.22) and (2.23), respectively:

$$T_{up_i} = -\frac{1}{\lambda_i} ln(U_i) \tag{2.22}$$

$$T_{down_i} = -\frac{1}{\mu_i} ln(U_i) \tag{2.23}$$

where T_{up_i} is the residence time in the up state for component i, T_{down_i} is the residence time in the down state for component i, U_i is the random uniformly distributed number sampled from the interval $[0, 1]$, and μ_i and λ_i represent the repair and failure rates for component i, respectively.

The multi-state Markov model, in its turn, can be used to represent the wind farms and solar plants failure/repair cycle as an aggregation of N components iid, as shown in Figure 2.22 (CARVALHO, 2013; LEITE DA SILVA; MANSO; SALES, et al., 2007; LEITE DA SILVA; MANSO; FLÁVIO, et al., 2013).

Figure 2.22 – Multi-state Markov model.

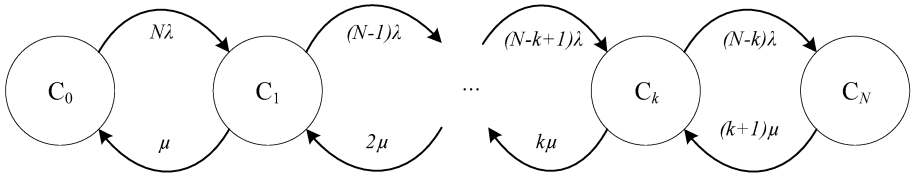

Source: adapted from Leite da Silva, Sales, et al. (2010).

In this case, the maximum capacity of the state C_k, which is a state that contains $N-k$ components in the up state, is (2.24) (CARVALHO, 2013):

$$C_{C_k} = (N-k)C \tag{2.24}$$

where N is the number of iid components, $k = 0, 1, ..., N$ and C is the capacity of one component. If the duration of the states is exponentially distributed, the residence time in the states C_0 and C_N is (CARVALHO, 2013):

$$T^{C_0} = -\frac{1}{N\lambda} ln(U_i) \tag{2.25}$$

$$T^{C_N} = -\frac{1}{(k+1)\mu} ln(U_i) \tag{2.26}$$

where T^{C_0} is the residence time in the state C_0, T^{C_N} is the residence time in C_N, and λ and μ are rates related to one component of the aggregation. For the remaining states, the residence time is calculated using (2.27).

$$T^{C_k} = min\left\{-\frac{1}{(N-k)\lambda} ln(U_i), -\frac{1}{k\mu} ln(U_i)\right\} \tag{2.27}$$

Finally, the modeling of hydropower plants, wind and solar power plants time dependence capacity is of total importance since their capacity exhibits an hourly, monthly, or even yearly variation (LEITE DA SILVA; MELO; CUNHA, 1991; PEREIRA; BALU, 1992). This time-dependent characteristic is captured by an hourly or monthly series with probabilities associated (MELLO; PEREIRA; LEITE DA SILVA, 1994). Generally, these series are obtained for several years of observations.

2.9.1 Transmission lines and transformers

The up/down cycle, for transmission lines and transformers, is represented by the two-state Markov model, with transitions that follow an exponential probability distribution. Traditionally, no time dependence on the capacity of these components is considered (CARVALHO, 2013). However, the power capacity of those types of equipment can follow models that consider the dynamic thermal behavior (time-dependency capacity) based on actual weather conditions. Equipment thermal models may determine the power capacity on an hourly, monthly or seasonal basis (BOLACELL; DA ROSA, 2020).

2.9.2 Wind generating units

Traditionally, the wind generating units within wind farms are equal, which allows to model using a multi-state Markov model. Similar to the capacity time-dependent

model of hydro units, the maximum capacity of the states is multiplied by the corresponding value taken from the hourly wind series. Using the SMCS there is no necessity to build models for spatial and temporal correlations for wind power units located in different regions since these correlations are implicitly considered at historical series.

The wind power forecast uncertainties are modeled using a persistence model (VIEIRA, 2020). It considers that the wind power at a certain time instant i is equal to the wind power at $i-1$. Therefore, the forecast error in wind generation can be calculated by (2.28).

$$\Delta W_i = W_i - W_{i-1} \tag{2.28}$$

where W_i and W_{i-1} are the realized values at time instant i and $i-1$, respectively, obtained from the wind series and ΔW_i represents the wind forecast error. The error will generally be different from zero because of the wind generation constant variation.

2.9.3 Solar generating units

Similarly to wind generating units, the multi-state Markov model is utilized to represent the failure/repair cycle and the time-dependent capacity is modeled using irradiance hourly series defined for each geographical region of the system. The total uncertainty for the solar power forecast is computed using (2.29) (VIEIRA, 2020).

$$\Delta S_i = S_i - S_{i-1} \tag{2.29}$$

where S_i and S_{i-1} are the realized values at time instant i and $i-1$, respectively, obtained from the solar irradiance series and ΔS_i represents the solar forecast error. Similar to wind energy, the error will generally be different from zero because of the constant solar irradiance variation.

2.9.4 Conventional generating units

Conventional generating units are typically thermal power plants based on the two-state Markov model, as a consequence, all thermal power technologies, such as nuclear, coal, oil, gas, among others, can be represented. The residence time to each state is assumed to be exponentially distributed. When in the up state, a conventional generating unit can produce its maximum capacity. Conversely, the capacity is zero when in the down state. Moreover, thermal power plants can be modeled with a multi-state (derated) Markov model, in which instead of two states, the generating model is based on three-state representation: full output (up), that has the maximum capacity available, derated state, in which the generating unit is operating with a reduced capacity, and the failed state (CARVALHO, 2013).

2.9.5 Hydro generating units

The failure/repair cycles for all hydropower plants are represented based on a two-state Markov model, presented in Figure 2.21. State transitions follow an exponential probability distribution. In hydropower plants, the available power is assumed to depend on the up/down cycle and water storage of each reservoir. Nevertheless, the levels of water storage of each reservoir vary due to several aspects, such as water coordination policies, yearly or monthly hydrological conditions, daily hydro-thermal coordination, inflows, and others. Then, as a simple but robust approach, it is common to use several hydrological series, which are based on the historical observations and have probabilities associated, that capture a proportional relationship between the total water stored in the reservoir and the power produced by the corresponding hydro generating unit in each month of the year (MELLO; PEREIRA; LEITE DA SILVA, 1994; LEITE DA SILVA; MELO; CUNHA, 1991).

The active series is sampled from historical yearly series volumes per power plant and per month. The use of simplified models to represent hydro generating units can be justified due to the high complexity involved in monitoring the dispatch conditions in long-term planning horizons. Therefore, each hydro unit's capacity available in each month is calculated by multiplying the maximum capacity, which is obtained from the up/down stochastic model, by the corresponding monthly value of the hydrological series (VIEIRA, 2020).

In addition, the hydro generating units can be modeled also using an energetic-based approach (VIEIRA, 2020). This model consists of assessing the water availability in the reservoir. More specifically, the model follows a series of available volumes (in hm^3) which can be turbined during a week. This model is based on the net load value for each hour of the week:

$$NL_i = L_i - \sum_{j=1}^{N_r} C_{j,i} \tag{2.30}$$

where NL_i is the net load for an hour i that represents the system load level not supplied by non conventional sources, L_i is the load forecast value, N_r is the number of non conventional sources and $C_{j,i}$ is the generation capacity of each non conventional source available (e.g., wind, solar, biomass, co-generation).

The model also includes reversible hydro plants representation (VIEIRA, 2020). During the week, those generators can be utilized to pump water and this reverted energy is turbined in convenient hours. The extra generation capacity due to pumping is already included in the production series described previously. However, when those generators operate in a reversible way they insert additional load into the system. It is utilized a production coefficient and the pumping cycle efficiency of each power plant to convert energy volume into electrical energy ($hm^3 \rightarrow MWh$).

2.9.6 Mini-hydro generating units

Mini-hydro units are represented by a two-state Markov model and the fluctuations of capacity follow historical series, which contain percentual values that correlate the nominal power of the unit and the water availability. The water volume depends on inflow regimes and operator decisions, it is used on a weekly basis in historical data. Due to the lack of specific data about the hydrological basin where they are located, only one equivalent reservoir (average series per year) is utilized to model the capacity variations with time (VIEIRA, 2020).

2.9.7 Alternative generating units

Some special regime units are not included in the previous models. Those units are based on alternative sources, namely: biomass, co-generation, etc. In this case, it is utilized the two-state Markov model to represent the failure/repair cycle. Moreover, an hourly utilization factor is specified, modulating the actual power value of generation utilized by the system. This factor varies during the year following the tariff attractiveness and/or the industrial production cycle (VIEIRA, 2020).

2.9.8 Load

The load can be modeled using a fixed level of demand, samples from probability distributions, or a chronological representation that contains a load level for each hour of the year (8760 values). The chronological MCS will sequentially follow these load steps during the simulation process. Also, each load bus has its hourly load profile in a percentage of its peak load (CARVALHO, 2013).

Furthermore, short- and long-term load forecast uncertainties can also be included in power system performance simulation (VIEIRA et al., 2020). The short-term uncertainty consists of adding an aleatory number sampled by $\mathcal{N}(0, \sigma_{ST})$ to the nominal hourly value, where σ_{ST} is the short-term standard deviation that controls the uncertainty amplitude. The long-term uncertainty is modeled by adding an aleatory number sampled by $\mathcal{N}(0, \sigma_{LT})$, where σ_{LT} is the long-term standard deviation. Both standard deviations are specified at the beginning of the simulation.

Therefore, the real load level (L_{real_i}) is computed using (2.31).

$$L_{real_i} = \left[L_{plan_i} + L_{nom}\delta l_{LT_y}\right]\left(1 + \delta l_{ST_y}\right) \tag{2.31}$$

where L_{plan_i} is the planned load level for hour i, obtained from load curve profile. L_{nom} is the nominal system load value. δl_{LT_y} represents the percentual value of long-term uncertainty for the year y, since $\delta l_{LT_y} \sim \mathcal{N}(0, \sigma_{LT})$ and δl_{ST_y} represents the percentual value of short-term uncertainty for the year y, since $\delta l_{ST_y} \sim \mathcal{N}(0, \sigma_{ST})$.

It is assumed that only the share of short-term uncertainty is considered as forecast error on the moment of generating scheduling. Hence, the load uncertainty (ΔL_i), that affects the operating reserve at hour i, is calculated by (2.32):

$$\Delta L_i = L_{real_i} - \left[L_{plan_i} + L_{nom}\delta l_{LT_y}\right] \tag{2.32}$$

2.10 METHODOLOGIES FOR COMPOSITE SYSTEM EVALUATION

The SMCS method algorithm, for the composite system adequacy assessment, can be dictated by the following general steps (CARVALHO, 2013; BILLINTON; ALLAN, 1996; BILLINTON; LI, 1994):

Step a) Define the tolerance for the relative error/uncertainty (β), the maximum number of years to be simulated, N_{MAX}, set the simulation time, h, to 0, set the number of years simulated, N_{YEAR}, to 1, and sample the initial operating state of each component.

Step b) Update the simulation time: $h \leftarrow h + 1$.

Step c) Select a system state, i.e., identify the next state transition, the shortest state duration of the respective component. Select the availability of the components according to their stochastic failure/repair cycle and the capacity time-dependent model, select the load level, etc.

Step d) Evaluate the system state selected: compose the state and check if the load level can be supplied with the available generating and/or transmission capacity without violating operating limits; if not, apply remedial actions, such as generation redispatch and/or load curtailment.

Step e) Update the test functions outcome and corresponding indices;

Step f) If the number of hours (h) reaches 8760, store the reliability indices, update their relative error and advance to Step g); otherwise, go back to Step b).

Step g) If N_{YEAR} is equal to N_{MAX} or if the relative uncertainties of the reliability indices are less than the specified tolerance, stop the simulation; otherwise, $N_{YEAR} \leftarrow N_{YEAR} + 1$, $h = 0$, and go back to Step b).

In composite system adequacy, the analysis is related to the existence of sufficient facilities to satisfy the customer load or system operational constraints (PEREIRA; BALU, 1992), thus being associated with static conditions. Therefore, the first procedure consists of determining the connectivity between buses (grid configurator) since transmission circuits are prone to fail. Subsequently, a dispatch procedure is made to

distribute the load to the available generating units. After that, the state of the transmission system is assessed by running a PF (GRAINGER; STEVENSON JR., 1994). If there are circuits with operating limits violated, then an OPF is executed to apply remedial actions and determine the minimum load curtailment or minimum loss of load cost (GRAINGER; STEVENSON JR., 1994; CARVALHO, 2013).

The following subsections present the methodologies associated with the transmission network configuration, generating units dispatch, and PF and OPF analyses.

2.10.1 Transmission network configuration

The transmission network configuration procedure is based on a list search method or graph's theory. This method assumes that the network is described by a node/branch representation, i.e., a node is a bus and a branch is a transmission circuit or transformer. All nodes are numbered, and each branch connects two different nodes. The main objective is to identify possible electric islands and the node/branch they enclose. The algorithm is as follow (CARVALHO, 2013; COSTA; SALGADO, 2002):

Step a) Initialize a vector $\mathbf{v}$, which is named vector of auxiliary indicators, by assigning each entry i an indicator, according to $v_i = i$.

Step b) Create a temporary vector, $\mathbf{v_T} = \mathbf{v}$ and browse the list of branches until all branches are checked. If the branch connecting node i to j is in the up state, then v_i and v_j are updated according to (2.33):

$$v_i = v_j = min\{v_i, v_j\} \tag{2.33}$$

If the branch connecting node i to j is in the down state, then go to the next branch.

Step c) If $\mathbf{v} \neq \mathbf{v_T}$, then go to Step b); otherwise, continue to Step d).

Step d) Assign each node an electric island: the nodes belonging to the same electric island have the same indicator; the number of different electric islands is equal to the number of different indicators in $\mathbf{v}$.

2.10.2 Generating units dispatch

The essential constraint on this procedure consists of allocating hourly load to the available generating units taking into account their restrictions, i.e., the sum of the output powers must equal the load demand. It can follow a merit order, a proportional strategy, or deal with the minimum cost of power production (economic issues) (GRAINGER; STEVENSON JR., 1994). For instance, the merit order strategy is according to the following steps (CARVALHO, 2013):

Step a) Find the next available generating unit with the highest merit that has not been dispatched yet.

Step b) Dispatch the generating unit with its full capacity or with the remaining load, whichever is lower.

Step c) If all load has been allocated end the process; otherwise go to Step a).

2.10.3 DC power flow model

The PF analysis aims to determine the complex voltage at buses and power flow distribution at lines, hence composing a steady-state representation of power grid operation (MONTICELLI, 1983). The Direct Current (DC) or linearized PF task consists of checking if transmission lines or transformers are operating outside their loading limits. This representation can not analyze the impact of reactive power and bus voltages on the adequacy of the system (CARVALHO, 2013).

Considering the problem dimension, long-term analysis perspective (planning studies), and computational effort involved, the choice of DC PF is very attractive, due to its simplicity and fast convergence. It represents Kirchoff's first and second laws for the active power flow in the system and it is based on the coupling of active power and voltage angle (CARVALHO, 2013). Also, it has a reasonable compromise between accuracy and computational cost. The problem linearization considers the following aspects (VIEIRA, 2020):

- The angular difference, in radians, between buses i and k is always very small, as:
  - $cos\theta_{ik} \approx 1$
  - $sin\theta_{ik} \approx \theta_i - \theta_k$
- The voltage magnitude in all buses is fixed in $1\,pu$ and there is no reactive power flow.
- The resistance of the lines is very small in relation to the reactance ($R \ll X$), and then it can be neglected.

The DC PF comprises solving the following system of linear equations (CARVALHO, 2013; PEREIRA; BALU, 1992):

$$\mathbf{P}_G - \mathbf{P}_L = \mathbf{B}'\boldsymbol{\theta} \tag{2.34}$$

where $\mathbf{P}_G$ and $\mathbf{P}_L$ are, respectively, the vectors of active power produced and consumed at buses. $\mathbf{B}$' is the susceptance matrix of the DC representation and $\boldsymbol{\theta}$ is the vector

of bus voltage angles. Given $\mathbf{P}_G$ and $\mathbf{P}_L$, the linear system is solved by fast sparse techniques to obtain $\boldsymbol{\theta}$. The entries of the susceptance matrix are calculated as follow:

$$B'_{ik} = -\frac{1}{x_{ik}}, \forall\, i \neq k \tag{2.35}$$

$$B'_{ik} = -\sum_{i=1,\, i\neq k}^{NB} \frac{1}{x_{ik}}, \forall\, i = k \tag{2.36}$$

where NB is the number of buses and x_{ik} the reactance of the branch connecting bus i to k. The system of linear equations represented by (2.34) is undetermined. By zeroing the bus voltage angle of one bus, it is possible to solve the system by eliminating one equation (2.37):

$$\hat{\mathbf{P}}_G - \hat{\mathbf{P}}_L = \hat{\mathbf{B}}'\hat{\boldsymbol{\theta}} \tag{2.37}$$

Therefore, the real power flow through the branch connecting bus i to k is determined using (2.38).

$$P_{ik} = \frac{\theta_i - \theta_k}{x_{ik}} \tag{2.38}$$

2.10.4 DC optimal power flow model

Whether at the end of the PF task transmission lines and transformers are operating outside their loading limits, an OPF is run (PEREIRA; BALU, 1992). This analysis tool enforces the operating limits of the system by generation and reactive power rescheduling, tap changes, circuit switching, and, in the most severe cases, controlled load curtailment. The objective is to minimize the total load curtailed if there is a need for such corrective measures. In mathematical form, the DC OPF is (CARVALHO, 2013):

$$min. \quad z = \sum_i M_i P_{GFi} \tag{2.39}$$

$$s.t. \quad \mathbf{0} \leq \mathbf{P}_{GF} \leq \mathbf{P}_L \tag{2.40}$$

$$\underline{\mathbf{P}}_{\mathbf{G}} \leq \mathbf{P}_G \leq \overline{\mathbf{P}}_{\mathbf{G}} \tag{2.41}$$

$$\underline{\mathbf{P}}_{\mathbf{ik}} \leq \boldsymbol{\Gamma}\hat{\mathbf{Z}}\hat{\boldsymbol{\theta}} \leq \overline{\mathbf{P}}_{\mathbf{ik}} \tag{2.42}$$

$$\mathbf{P}_{\mathbf{G}} + \mathbf{P}_{GF} - \mathbf{P}_L + \hat{\mathbf{B}}'\hat{\boldsymbol{\theta}} = \mathbf{0} \tag{2.43}$$

where M_i is a constant that reflects the load curtailment priority of the load at bus i, $\mathbf{P}_{GF}$ is the vector of real power produced by the fictitious generating units that model the load curtailment, $\mathbf{P}_G$ is the vector of the real power produced by the generating units, $\mathbf{P}_L$ is the vector of real power loads (consumption), $\boldsymbol{\Gamma}$ is a diagonal matrix whose entries are

the inverse of the branches reactance (i.e., susceptance), $\mathbf{Z}$ is the branch-bus incidence matrix, $\boldsymbol{\theta}$ is the vector of bus voltage angles and $\mathbf{B}$' is the susceptance matrix of the DC PF.

A variety of methods are available to solve the problem presented in (2.39)-(2.43), such as: (a) Simplex method; and (b) Interior-Point method.

2.11 CONCLUSION OVER STATE OF THE ART: PAST, PRESENT AND FUTURE TRENDS

Evaluating the discussion over this chapter, it is possible to notice that there is an ongoing energy transition happening in the electric sector which is posing new energetic and electric challenges. In this sense, new methodologies of analysis need to be considered in order to cope with new characteristics arising in nowadays hybrid power systems, which are composed of synchronous and asynchronous shares.

With the increasing penetration of vRES, new models need to be created in order to plan reliable and secure hybrid power systems. Taking those concerns into account, a task force in the area of power system stability has revisited and revised the traditional definition of stability since a considerable share of the system load would be supplied by intermittent generating units that do not provide inertial response, indicating two new stability categories (HATZIARGYRIOU et al., 2021).

Therefore, the impact of the combination of AC and DC transmission lines, and of synchronous and converter interfaced generation, in actual power systems, need to be deep assessed in order to maintain a secure operation and plan reliable and flexible power systems.

Part I

Technological Approaches

3 OPTICAL MONITORING SYSTEM PROTOTYPE DEMONSTRATION IN AN OPERATING ENVIRONMENT

The objective of this chapter is to present the technological contributions of this thesis. Those approaches are connected with TECCON II research project development, in which the author has participated and contributed in distinct fields of study. To make clear the technological advances, a maturity scale is utilized to identify the main research project results and author contributions. To clarify the understanding and point out the contributions in an appropriate manner, during the text of this chapter, frames are positioned specifying the main activities or contributions on the results for the technology reaches a specific level of maturity. The frame presents in which TRL the results achieved until that moment are positioned and which tasks the author has performed to migrate the TRL. The TRL can be interpreted as an approach of qualitative assessment that can be used in scientific works to make clear technological results.

The TRL is an approach utilized to assess the maturity level of a specific technology. Each new technology in development is evaluated through parameters established for each technology level and then it is assigned a TRL rating based on its progress. This methodology has been first used by National Aeronautics and Space Administration (NASA) during the 1970 decade (NASA, 2019). Figure 3.1 presents the parameters associated with each TRL.

There are nine technology readiness levels. TRL 1 is the lowest level representing the basic principles observed and reported of a specific technology and TRL 9 is the highest and represents the end of the innovation chain where the actual system is ready to be utilized in large scale. The specialists in the innovation of the multidisciplinary team of the TECCON II research project have studied the project potentialities and positioned the project technology at TRL 5 at the beginning of the project and indicated that at the end of the project the results could reach the TRL 7 (INESC P&D BRASIL, 2020). In this sense, the contributions of the author in the activities to improve the TRL from 5 to 7 are presented and highlighted in sections 3.2 and 3.3, representing explicitly the technological contributions of this thesis.

The optical monitoring system technology is part of the outcomes developed in TECCON I and TECCON II research projects. The main products and the scope of the projects are discussed briefly in Appendices C and D. Following, section 3.1 describes main results related to TECCON MS in a laboratory environment, section 3.2 highlights advances in a relevant environment (high voltage laboratory), section 3.3 shows system in an operating environment (high voltage transmission line), and section 3.4 outlines collected data using TECCON MS infrastructure.

Figure 3.1 – NASA Techonology Readiness Levels.

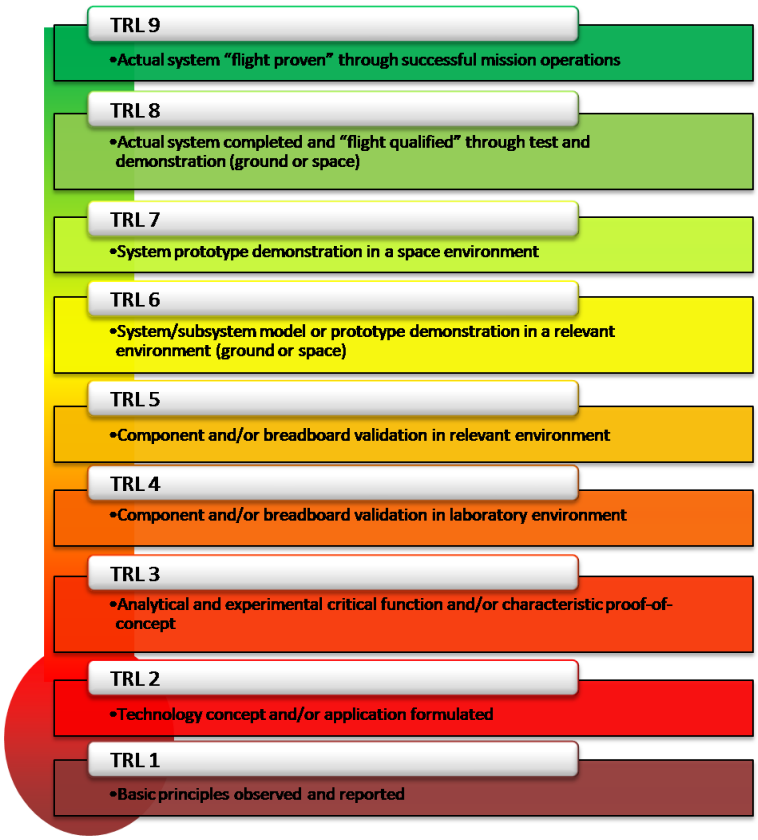

Source: adapted from NASA (2019).

3.1 TECCON MONITORING SYSTEM IN A LABORATORY ENVIRONMENT

From the multidisciplinary perspective of the TECCON II project, the author of this doctoral thesis is positioned in the project integration team, which has been responsible for integrating the different results achieved in each project unit. The integration team has sought to reexamine all the initial specifications of the units developed in order to promote the installation in an operational environment. Thus, the author could revisit all the specifications originated by the project's research team and propose solutions to enable a joint operation of TECCON MS units in an operational environment.

This section presents the main activities developed by the author of this doctoral thesis and the multidisciplinary team of the TECCON II research project in the laboratory environment. Those tests are based on initial project specifications, which have been considered in the first studies for every unit of the TECCON MS. The five units have been tested separately and using two or three units in a laboratory environment. The main tasks performed for each unit are described as follows:

- Unit 1: electrical and mechanical tests with the insulator. The author has not participated in such activities, only accompanied the results;
- Unit 2: the optical sensors have been calibrated and the weather station tested

properly considering project initial specifications. However, during the tests, the author has proposed a new setup, discussed in section 3.3, aiming at the field application;

- Unit 3: the Opto-Electronic Signals Processing Unit (OESPU) has been tested receiving and interpreting the information provided by the optical sensors and the weather station considering the research project initial specifications provided by the specialists of this unit;
- Unit 4: the energy supplying unit has been installed in a laboratory to verify the energy-consuming of the TECCON MS, considering the dimensioning proposed in the research project initial specifications provided by the specialists of this unit. The author has proposed an update of supplying energy capacity aiming at field application (see section 3.3);
- Unit 5: the real-time CM and media converters have been tested in a laboratory environment considering the research project initial specifications provided by the specialists of this unit. Some improvements in this unit have been proposed by the author, as identified in section 3.3.

In broad terms, tests with the TECCON MS have been performed to know the behavior of each unit of the monitoring system unit in the laboratory environment. To establish a milestone in the maturity scale methodology proposed, Table 3.1 presents the TRL for each unit that composes the TECCON MS considering the stage of developments achieved in laboratory tests, i.e., after finishing tests in a laboratory environment each unit presented a specific technological maturity level.

Table 3.1 – TRL of each unit that composes the TECCON MS on this stage of development.

TRL	Level 5
Task 1	Unit 1: the polymeric insulator with an optical fiber has been submitted to relevant environment operation.
TRL	Level 4
Task 2	Unit 2: optical sensors have been calibrated and tested in laboratory environment.
Task 3	Unit 3: OESPU has been tested with sensors unit in laboratory environment.
Task 4	Unit 4: photovoltaic energy supplying has been tested with OESPU as load in laboratory environment.
Task 5	Unit 5: real-time condition monitoring and optical communication channel have been tested in laboratory environment.

Source: own.

Unit 1 has presented the highest TRL due to the characteristics of the tests developed in the relevant environment. Other units have presented TRL 4 that indicates the validation of the components in the laboratory environment.

The following subsections emphasize some of the developments performed in a laboratory environment, which the author has participated in and/or accompanied with the team of the research project. Tests with unit 2 are presented in subsections 3.1.1, 3.1.2, 3.1.3, and 3.1.4, involving task 2. Subsection 3.1.5 addresses the tests related to task 3. Task 4 is described in subsection 3.1.6. Regarding task 5, the TECCON application programming interface has been tested in the laboratory environment in order to identify necessary aesthetic enhancements. Improvements to include in the web application all types of measures obtained by TECCON MS, in an organized way, are discussed in section 3.3.

3.1.1 Tests with optical electric current sensor

The optical bulk sensor has a center wavelength of 1550 nm, operating temperature from -5 to 70 ℃ and the optical power needs to be $\leq$ 500 mW. An optical source with amplified spontaneous emission is used for sensor calibration, the source has a wide spectrum and is depolarized.

Hence, the scheme has, basically, a wide spectrum optical source, a linear polarizer, a Faraday rotator Rare-earth Iron Garnet (RIG) single crystal, a Polarizing Beam Splitter (PBS) and two photodetectors (S_1 and S_2). The system is interrogated using a National Instruments Data Acquisition (NI DAQ™) device connected to a computer with the LabVIEW software, which is acquiring the sensor data in real-time. The experimental scheme is presented in Figure 3.2.

Some couplers or attenuators may be necessary to reduce the optical power, depending on the type of the Photodetector (PD) and the optical source power. The optical sensor is interrogated using a quadrature polarimetric configuration. This light is polarized with 45° of relative phase with each one of the PBS axes. The signals (S_1 and S_2) are in phase opposition with maximum sensitivity to the polarization plane variations (rotations) induced by the magnetic field, which is proportional to the electric current of the conductor (Faraday effect).

The signal S, computed using (3.1), represents the result of the quadrature polarimetric configuration, which uses the signals of two PDs that combined offer a response immune to interference.

$$S = \frac{S_1 - S_2}{S_1 + S_2} \tag{3.1}$$

where S_1 and S_2 are normalized before the processing:

Figure 3.2 – Setup for optical current sensor calibration.

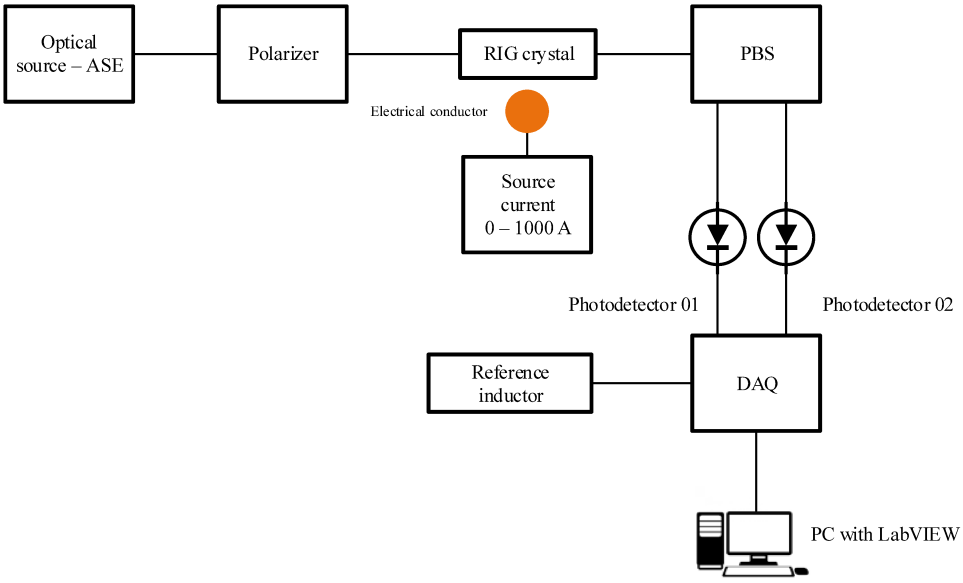

Source: own.

$$S_1 = \frac{S_{1ac}}{S_{1dc}} \qquad S_2 = \frac{S_{2ac}}{S_{2dc}} \tag{3.2}$$

To analyze the response of the bulk sensor, losses are introduced in the fibers after the PBS, i.e., in the fibers that connect the PBS outputs to the PDs. Figure 3.3 illustrates the decay in voltage DC level of PDs while losses are applied to the optical system.

Figure 3.3 – DC values for S_1 and S_2 with punctual losses.

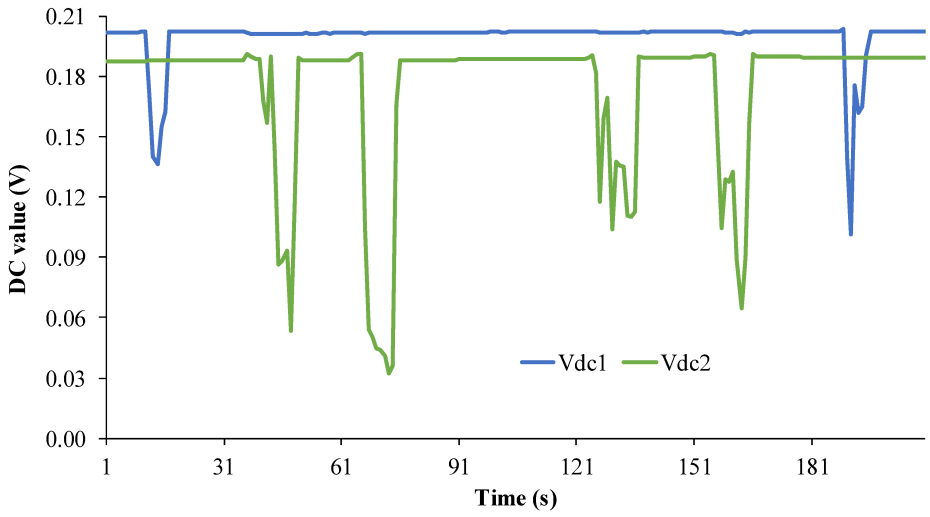

Source: own.

The electric current sensor has received distinct steps of electric current at every

30 seconds roughly. Figure 3.4 demonstrates the voltage signals of PDs output and signal S processed for each step.

Figure 3.4 – Photodetectors normalized signals and signal S processed.

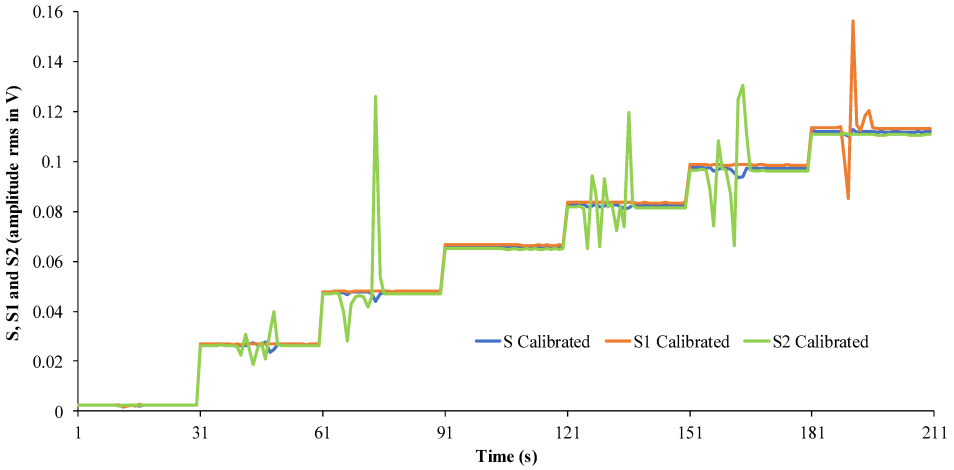

Source: own.

Figure 3.5 presents the sensor response when losses are introduced in the optical system. As can be noted, the sensor is not losses sensitive. Distinct losses have been applied in S_1 and S_2 signals and the linear relation between PDs signals and electric current remains.

Figure 3.5 – Sensor response: calibration curve SxI with losses after the PBS.

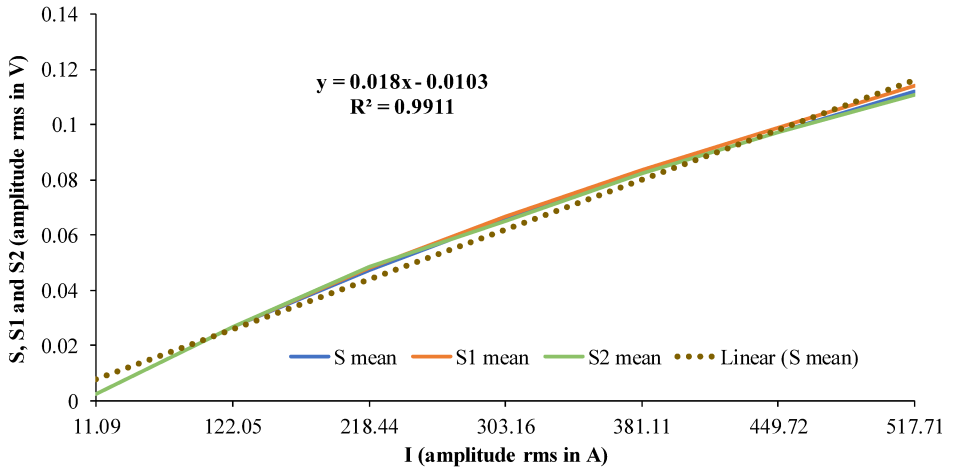

Source: own.

3.1.2 Tests with optical mechanical tension sensor

To monitor sags and clearances on critical spans, TECCON MS obtains conductor traction in real-time through an indirect measurement. Therefore, intending to measure the mechanical characteristic of an anchorage hardware piece of the transmission

line, where the strain sensor is welded, a mechanical tension test with a deformation rate of 0.05 mm/min has been developed with a sheet-type specimen (ASTM INTERNATIONAL, 2015). Figure 3.6 illustrates the characteristic elastic region curve for that material and it has been identified Young's modulus (E) of roughly 215.00 GPa, which defines the relationship between stress and strain in the linear elasticity regime.

Figure 3.6 – Elastic region curve of anchorage piece specimen submitted to tension test.

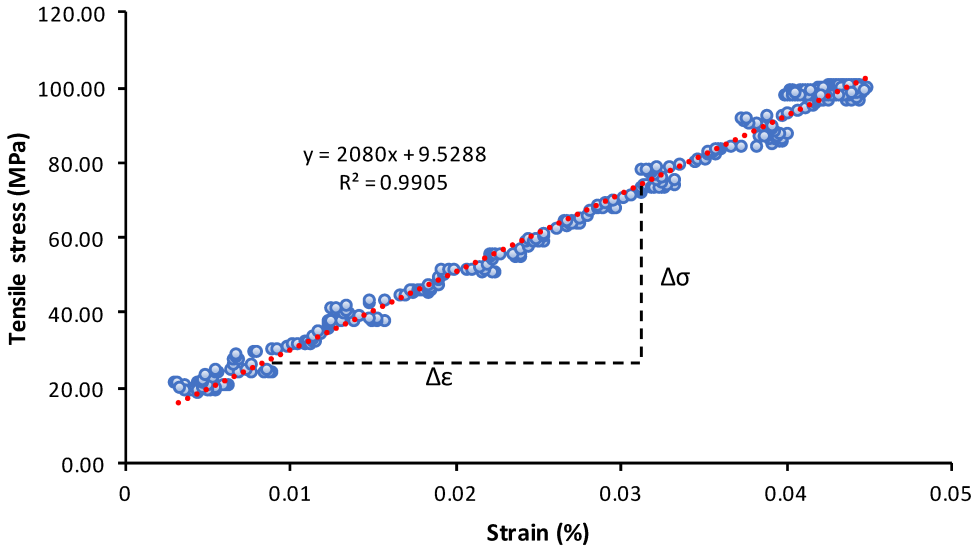

Source: own.

The elastic region of the material is where the strain sensor operates. Figure 3.7 displays a FBG strain sensor positioned on the anchorage hardware piece. Accordingly, real-time monitoring of the conductor strain and temperature aims to avoid excessive sag of the conductor leading to violation of minimum clearance to the ground and other conductors, besides avoiding annealing aluminum strands due to conductor overheating. In these situations, alerts should be emitted to the operator at the AMC.

3.1.3 Tests with optical temperature sensor

A controlled temperature ambient has been used for the FBG temperature sensor calibration. The process is to follow the Bragg wavelength variation with the temperature increase. Figure 3.8 illustrates the calibration curve for the TECCON MS specific temperature sensor.

The Bragg wavelength variation with the temperature is analyzed and a 10 pm/°C sensitivity is identified, which is a value expected for this sort of sensor. With the FBG sensor for temperature measurements is possible to emit alerts when the conductor reaches its maximum allowable temperature, avoiding problems for the operator with

Figure 3.7 – FBG mechanical tensile sensor positioned on the central rod of the anchorage piece.

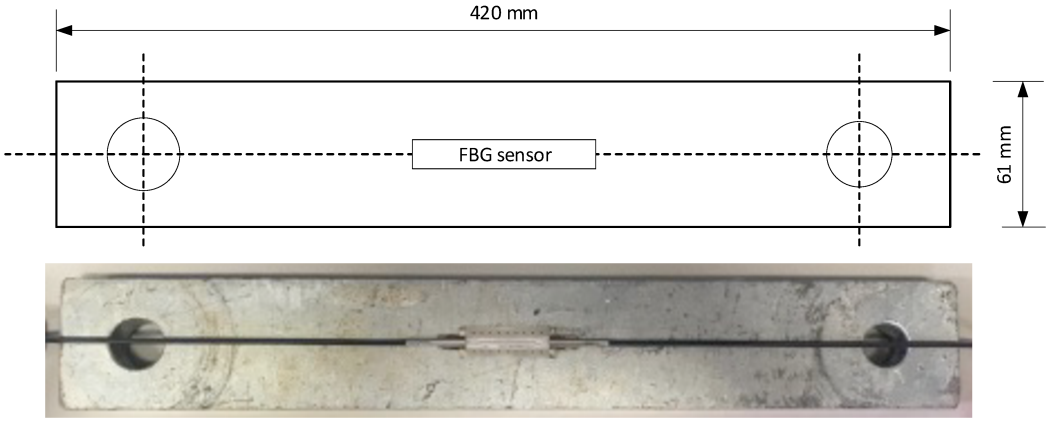

Source: own.

Figure 3.8 – FBG temperature sensor calibration curve.

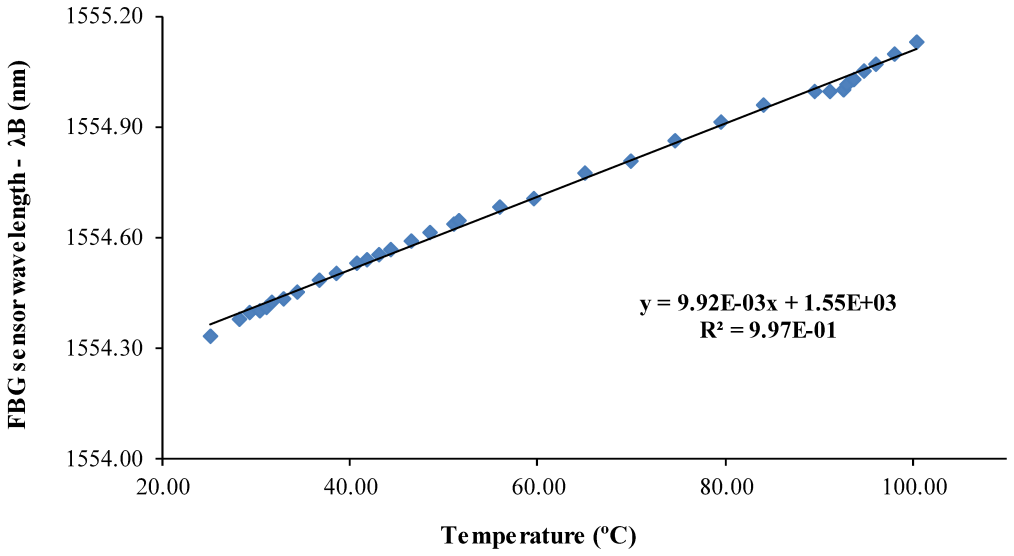

Source: own.

the conductor integrity. Also, the temperature FBG sensor provides the necessary information for the optical DLR implementation.

The temperature sensor has been calibrated using a specific stove at *Laboratório de Fibras Especiais* (LaFE), *Universidade Estadual de Campinas* (Unicamp), Campinas, São Paulo, as shown in Figure 3.9. The temperature FBG sensor has received successive increments of temperature from 25 to 100.4 ℃ in order to obtain the calibration curve presented in Figure 3.8.

Figure 3.9 – FBG temperature sensor calibration process.

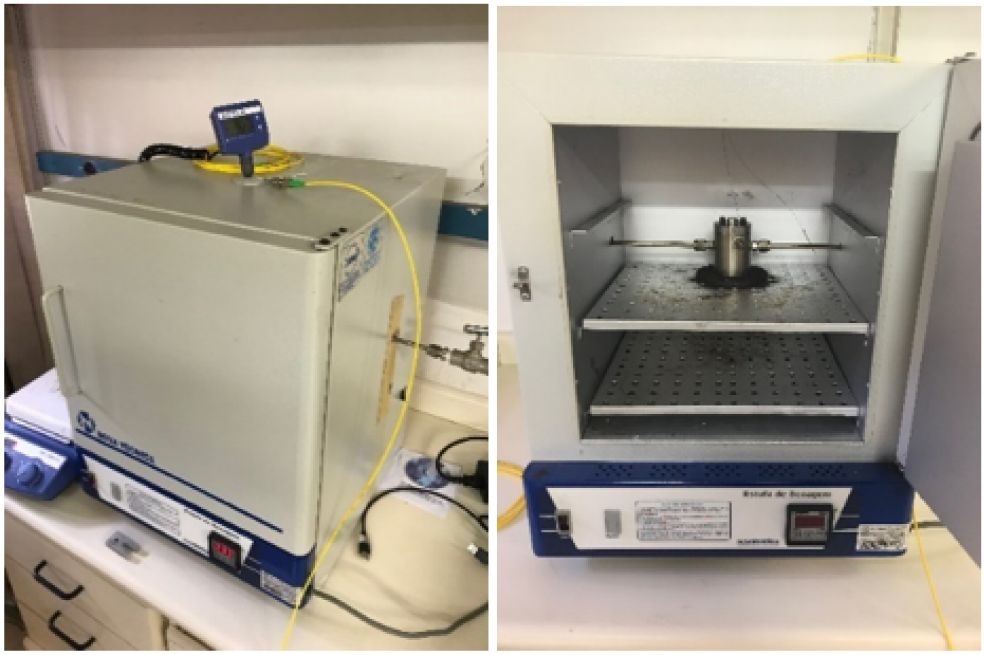

(a) Stove closed and the termocouple PT100 used for the calibration.

(b) Stove with the FBG temperature sensor positioned inside.

Source: own.

3.1.4 Tests with weather station

The initial experiments with the weather station have been carried out at *Universidade Federal de Santa Catarina* (UFSC), in a laboratory environment. Figure 3.10 exposes the graphical interface that allows interaction between the user and the weather station sensors, providing visual indicators of the meteorological variables.

The software is the MetView, from GILL Instruments. The weather station has been connected to the computer using an interface RS232. The values indicated in the digital icons have been collected in the laboratory intern ambient.

3.1.5 Tests with opto-electronic signals processing unit

After the successful connection of the weather station with the MetView software, the next step was connecting the meteorological station to the OESPU. The results from the experimental setup have denoted that the software implemented is ready to identify the data that the weather station is sending.

Figure 3.11 shows seven strings that have been identified in a preliminary test. It is noticed that the weather station output rate has been defined as 1 Hz, hence, one string is sent by second, being equally spaced in Figure 3.11.

Each string is related with a package reference number. Taking into account the example presented, the format of one of the strings identified in Figure 3.11 is

Figure 3.10 – Graphical interface from MetView.

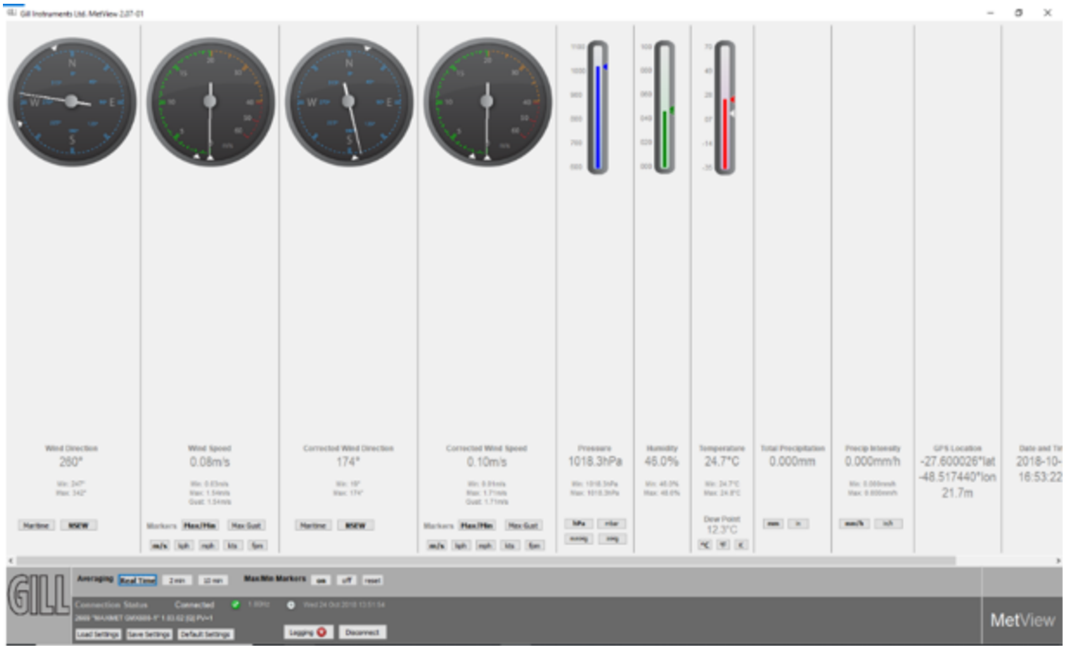

Source: own.

Figure 3.11 – Strings from the weather station being processed by the OESPU.

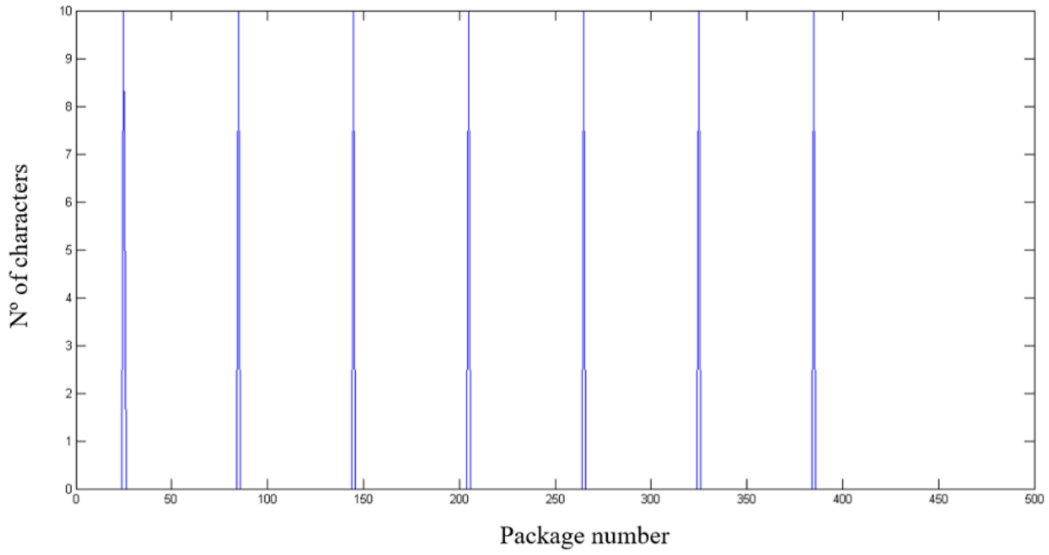

Source: own.

presented as follows:

- Q,097,000.04,071,000.04,1008.3,063,+025.0,+017.6,00000.0,000.0, -27.600114:-048.517416:+0014.80,2018-10-26T18:21:23.9,+12.1,0002.

where the meaning of each field of the string is specified in Table 3.2.

Assessing the string printed by the software and Table 12, it is concluded that the Global Positioning System (GPS) location is available. The status 0004 indicates

Table 3.2 – Description of the string data sent by the weather station.

Data	**Function**	**Unit**
Q	GPS node	-
097	Wind relative direction	°
000.04	Wind relative speed	m/s
071	Wind corrected direction	°
000.04	Wind corrected speed	m/s
1008.3	Atmospheric pressure	hPa
063	Relative humidity	%RH
+025.0	Ambient temperature	℃
+017.6	Dewpoint	℃
00000.0	Precipitation	mm/day
000.0	Precipitation intensity	mm
-27.600114:-048.517416:+0014.80	Latitude, longitude and altitude	0.06050
2018-10-26T18:21:23.9	Date and hour	y/m/d-h:m:s
+12.1	Voltage supply	V
0004	Status	-

Source: own.

that the GPS has been responsible to correct the wind direction. It happens when the weather station marker is not perfectly aligned with the geographical north.

The confirmation of the location coordinates provided by the weather station is carried out to ensure the GPS precision. The location founded in Google Maps is exactly where have been developed the measurements: *Laboratório de Planejamento de Sistemas de Energia Elétrica* (LabPlan), UFSC, Florianópolis, Brazil.

The second test performed with the Printed Circuit Board (PCB) has aimed to check the technique of the electric current retrieving process presented in this thesis. Figure 3.12 shows the amplitude of the voltage signal processed by one PD.

The result affirms the OESPU adequate operation of the optical sensor. Tests have been performed at Unicamp and UFSC with the Hi-Bi TECCON and µTECCON sensors and the results show the effectiveness of the proposed approaches even with small values for the electric current, for instance, 50 A.

3.1.6 Tests with solar energy supply

In the scope of laboratory environment tests, two energy supply setups have been installed: one at UFSC, Florianópolis, SC, Brazil, and one at *Universidade Federal do Maranhão* (UFMA), São Luís, MA, Brazil. In both systems, a datalogger with Internet of Things (IoT) has been used to monitor the system in real-time and get data from battery voltage, photovoltaic power generation, load power, generation current, and load current. The information in the following graphs has been extracted from experimental monitoring systems using Arduinos.

Figure 3.12 – Photodetector signal on electrical current retrieving process with the μTECCON.

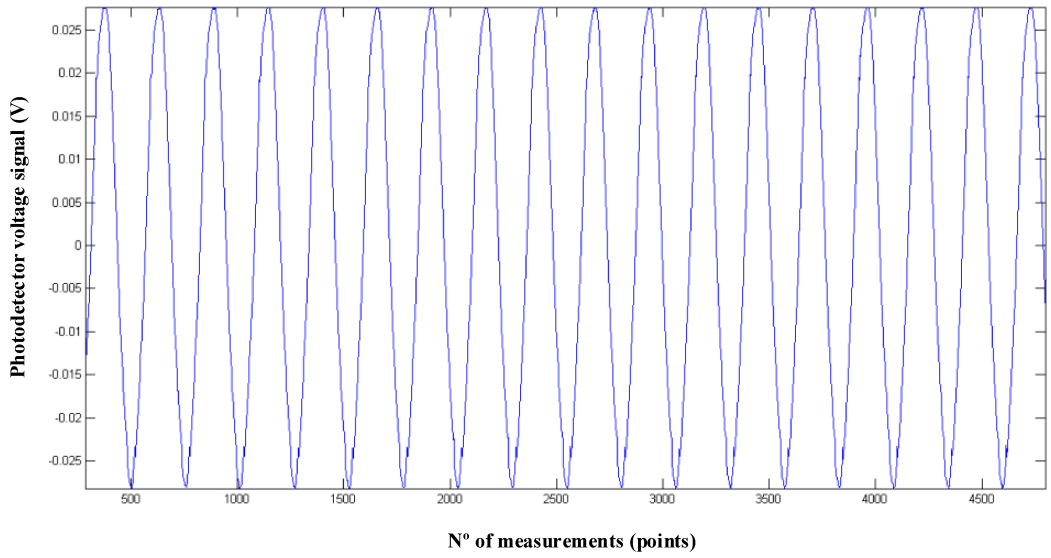

Source: own.

Figure 3.13 shows an observation about the electric current generated at photovoltaic panels from November 21 until November 22, 2018.

Figure 3.13 – Current generated by the photovoltaic panels in UFMA and UFSC.

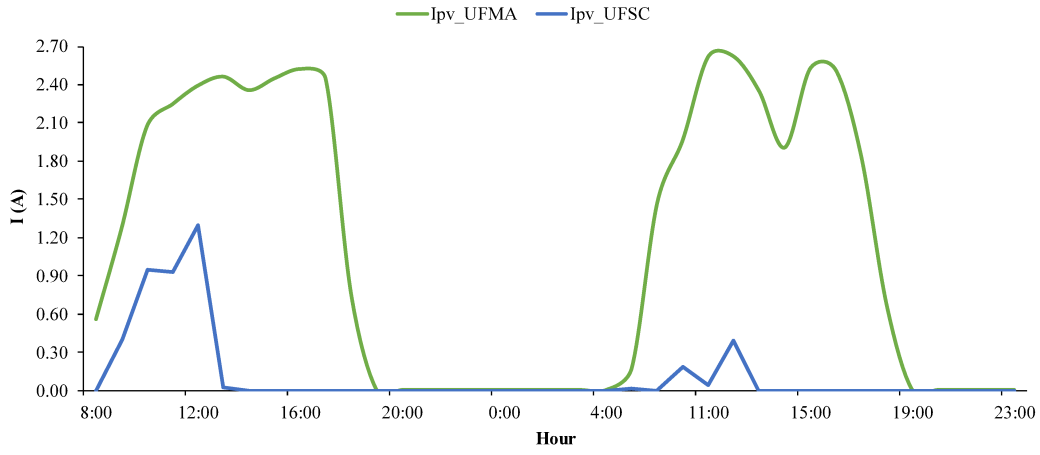

Source: own.

As can be noted, the current generated in UFSC is significantly lower than the capacity of the solar system in UFMA. For instance, at 12:00 pm of November 21, the electric current generated in UFMA is more than two times higher than the generation in UFSC, as expected due to the region's microclimate. In fact, there is a well-defined pattern in a photovoltaic generation: the current begins with a very low value during the first hours of the morning, due to the lower values of irradiance, reaching the generation peak at noon. The decrease in generation starts at the end of the afternoon.

Another very important aspect to be analyzed is that the load controller installed in both systems is limiting the generation current as the maximum power current (I_{mp}) is never reached (6.16 A). A reason for that is to not stress the battery in the charging process. Secondly, Figure 3.14 depicts the load current for the load in UFSC and UFMA.

Figure 3.14 – Load current in the UFMA and UFSC systems.

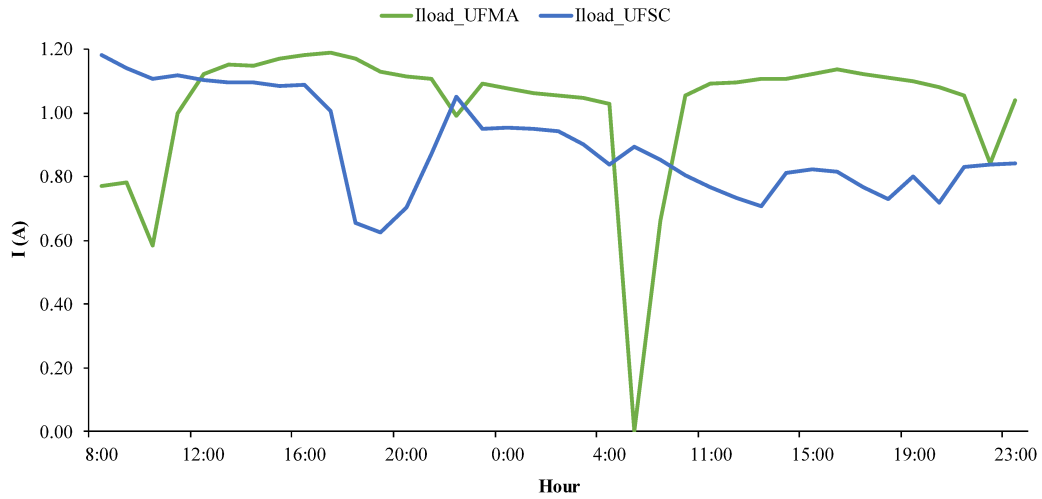

Source: own.

For the tests, the load in UFMA is resistive and in UFSC it is a LED light of 8 W. Analyzing Figure 3.14, it is observed that since the load is not connected directly to a converter with constant output voltage, the current varies with the voltage of the battery bank, which in turn varies according to the state of charge of the battery bank. Moreover, the behavior of the battery voltage during those two days of assessment is demonstrated in Figure 3.15.

Figure 3.15 – Battery voltage for the system in UFSC and UFMA.

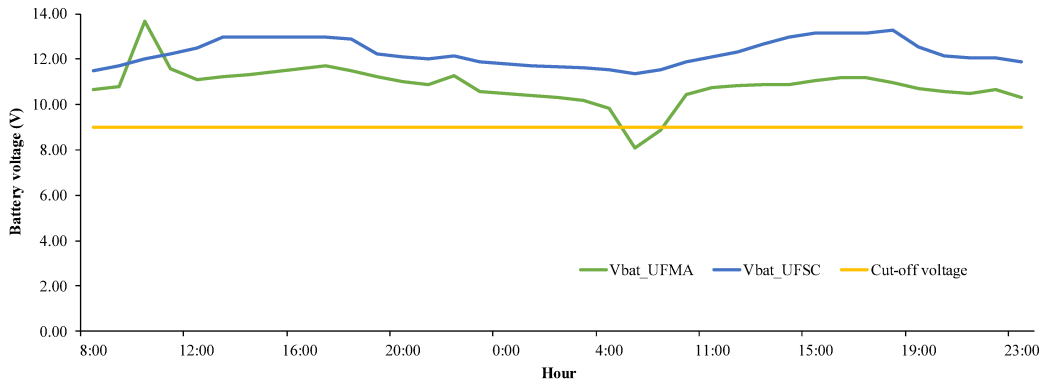

Source: own.

The tests performed have validated the correct functioning of the solar system proposed to supply energy to TECCON MS load For operating environment application, an alternative photovoltaic system must be implemented to avoid any risk of energy

deficit for the TECCON MS, as the one happened during the beginning of the morning in UFMA (Figure 3.15) when the battery voltage has been less than the energy cut-off voltage.

3.2 TECCON MONITORING SYSTEM IN A RELEVANT ENVIRONMENT

To clarify the main contributions of the author of this doctoral thesis within the scope of the TECCON II project, it is important to highlight two distinct phases of the project's development. The first phase (addressed in section 3.1), developed over 36 months, had the participation of a multidisciplinary team (21 researchers) and the development of 5 individual units that together made up the TECCON MS. The second phase, developed over 24 months, counted on the participation of an integration team (5 researchers), where some developments stand out that characterize the unique contributions of the author of this doctoral thesis. This section and section 3.3 present these developments.

After the tests in the laboratory environment and before the final implementation of the TECCON MS on the transmission line, there is a stage in which some tests with all components (units) need to be carried out in a High Voltage Laboratory (HVL), such as partial discharges and impulse voltage tests. These tests guarantee the TRL 6 for TECCON MS technology, i.e., the prototype demonstration on a relevant environment. The goal is to ensure the normal (adequate) operation of the system in a high voltage relevant ambient and verify the accuracy of the optical measurement and its accessories (A/D conversion, signals filtering process, etc.) and eventual saturation occurrences. To measure electric current impulses (partial discharges spikes), the following methodology has been proposed:

i. The insulator prototype, together with the optical sensors and the OESPU (a subsystem of TECCON MS), is suspended in the HVL in an adequate height for current impulses application (duration of roughly 500 μs) with distinct crest values.

ii. The optical and electronic modules should be activated to operate, recording the existing signals.

iii. The OESPU needs to be positioned at a safe distance from the electric conductor.

iv. Should be applied the electric current impulse, which must be registered by the TECCON MS.

To make feasible the tests and the migration in the technological maturity scale level, the author has contributed in identifying a methodology to measure the electric current of partial discharges (transitory event) and in the positioning and encapsulating

of all parts of the TECCON MS, bearing in mind the final configuration of the monitoring system in the tower of the real transmission line.

The TECCON MS has been mounted in a HVL, located at Unicamp, Campinas, Brazil, to reproduce the test proposed. Figure 3.16 presents the mounted scheme in the HVL. The results of the partial discharges test are exposed in Table 3.3, which presents the magnitudes of impulse current applied in the test and the sensor signal amplitude results. The aim is to simulate partial discharges that can occur in an operating environment and analyze if the electric current optical sensor is capable to measure/interpret such transitory conditions.

Figure 3.16 – Scheme mounted in HVL.

Source: own.

The first column of Table 3.3 depicts the voltage used to charge the capacitor bank devoted to producing the electric current impulse. The second column exposes the electric current impulse value generated due to the capacitor bank discharge and the third column outlines the amplitude of the signal (in Volts) of the electric current sensor. Figure 3.17 presents the curve that relates the sensor signal amplitude, in V, and the crest value of the electric current impulse, in kA.

It is noticed that the sensor is capable to identify/measure partial discharges (high current impulse measurements) and it saturates for impulse currents higher than

Table 3.3 – Partial discharges test.

Voltage applied to charge capacitor bank (kV)	Crest of current impulse (kA)	Sensor signal amplitude - S1 (V)
5.5	6.2	0.02054
7.5	8.7	0.02784
9.5	10.9	0.03876
10.2	12.2	0.04207
12.0	13.9	0.04776
14.0	16.3	0.06277
16.0	18.6	0.06355
18.0	21.0	0.06050

Source: own.

Figure 3.17 – Relation between sensor signal amplitude and crest of current impulse.

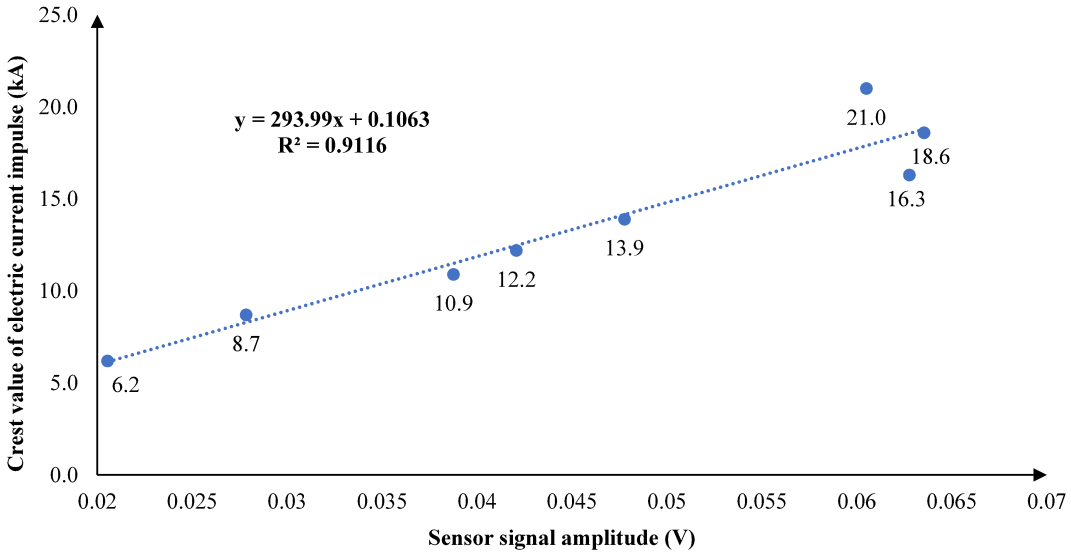

Source: own.

18.6 kA. The waveform of sensor response is illustrated in Figure 3.18 for an application of an impulse electric current equal to 6.2 kA.

The results related to the tests developed in the HVL with the TECCON MS technology elevate the system's TRL to rating 6, according to the definitions described in Figure 3.1. Table 3.4 presents the TRL after the tests (prototype demonstration) in the relevant environment, the author's main contributions, and future applications of the outcomes associated with this section.

3.3 TECCON MONITORING SYSTEM IN AN OPERATING ENVIRONMENT

Some particular improvements related to the initial project specifications for units 2, 4, and 5 have been implemented to make possible the field installation of the TECCON MS. These enhancements have been identified by the author through the tests performed in two environments: laboratory and relevant (HVL).

In few words, robust encapsulations and optical circuit modifications have been

Figure 3.18 – Electric current signal for high current impulse test.

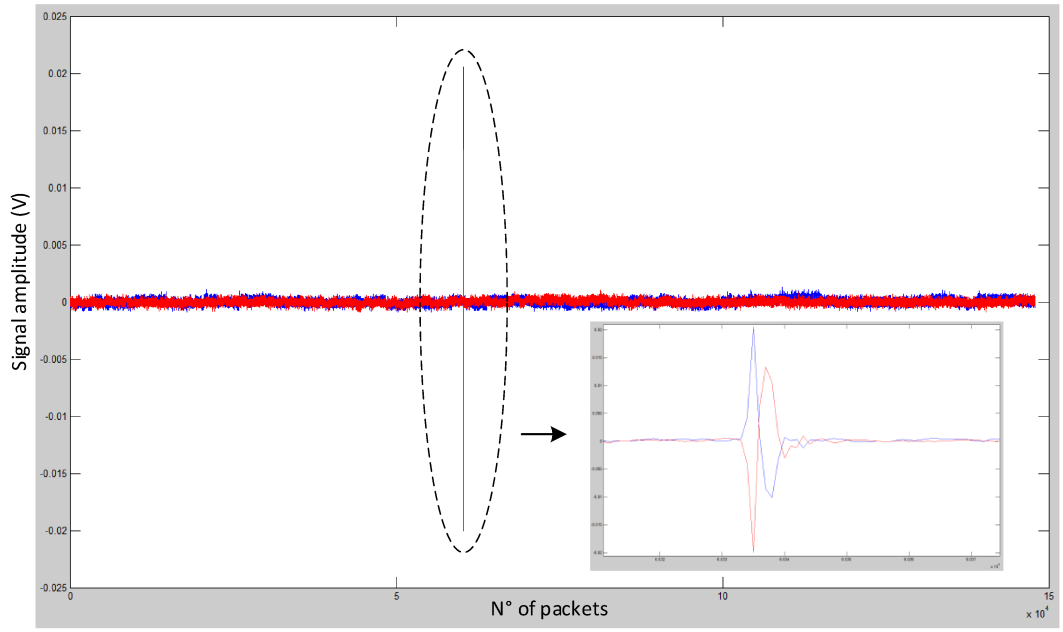

Source: own.

Table 3.4 – Contributions related to TECCON MS in a relevant environment.

TRL	Level 6
Contribution 1	Positioning and encapsulating of all components of the TECCON MS for proper operation in relevant ambient
Contribution 2	Methodology to measure electric current impulses (partial discharges)
Future applications	Methodology for recognition and identification of transitory events signatures

Source: own.

performed devising to demonstrate the system prototype in a high voltage operating environment (TRL 7), i.e., a real transmission line. A summary of the decisions/tasks required to take the technological solution to the operating environment is presented in Table 3.5. It outlines the main contributions of the author to improve the TRL of TECCON MS technology from rating 6 to 7 and suggests future applications.

Following the implementation of those contributions presented in Table 3.5, the field installation has been possible. The explanation of every contribution is organized as follows. Subsection 3.3.1 describes the optical circuit update, highlighting contribution 1. Subsection 3.3.2 outlines the main aspects connected with contribution 2, presenting the calibration curve for the FBG strain sensor. Subsection 3.3.3 presents the Dense Wavelength-Division Multiplexing (DWDM) utilized and the calibration curve for the temperature FBG sensor (contribution 3). Contribution 4 is posed in subsection 3.3.4, indicating the calibration curves for the electric current sensor. Contribution 5, which is related to web application updates, is described in subsection 3.3.5. Contributions 6

Table 3.5 – Contributions to make feasible the field installation of the TECCON MS.

TRL	Level 7
Contribution 1	Optical circuit update: specification of DWDM filters, addition of couplers and pre-amplifiers
Contribution 2	Calibration of the FBG strain sensor for operating environment installation
Contribution 3	Calibration of the FBG temperature sensor for operating environment installation
Contribution 4	Calibration of the electric current for operating environment installation
Contribution 5	Modifications in web application and software update to proper real-time monitoring, encompassing all variables monitored
Contribution 6	Positioning and encapsulating of all units for TECCON MS installation and proper functioning in operating environment
Contribution 7	New dimensioning of solar energy supplying system
Future applications	Identification of transitory events in operating environment

Source: own.

and 7 are detailed in subsection 3.3.6.

3.3.1 Optical circuit update

In order to take the system to the operating environment modifications in the optical scheme firstly proposed have been mandatory. The part of the electric current sensor has been needed an update to correct operation: a DWDM CH 32 has been added to the optical circuit for the correct operation of the bulk sensor. As a broadband optical source has been utilized, the DWDM is utilized to restrict the photons group, providing the proper operation of the bulk sensor. Figure 3.19 presents the upgrade in optical circuit.

It is identified that the pre-amplifiers are utilized to enhance (amplify) the optical signals reflected by the FBGs in order to be able to measure them using the PDs attached to the PCB (OESPU module). The optical signals need to be amplified to compensate attenuation provided by the DWDMs and the Coarse Wavelength-Division Multiplexing (CWDM).

Besides, the PD originally specified by the project team has been replaced by another one with a higher gain to convert the optical signals of the FBG sensors (temperature and strain) in electric signals. Although, the first one specified has worked adequately to measure electric current using the bulk sensor.

Table 3.6 makes a comparison between the two types of PDs. The calibration tests analyze the PDs response (mV) related with the optical power variation at PD input.

Figure 3.19 – Optical circuit for operating environment.

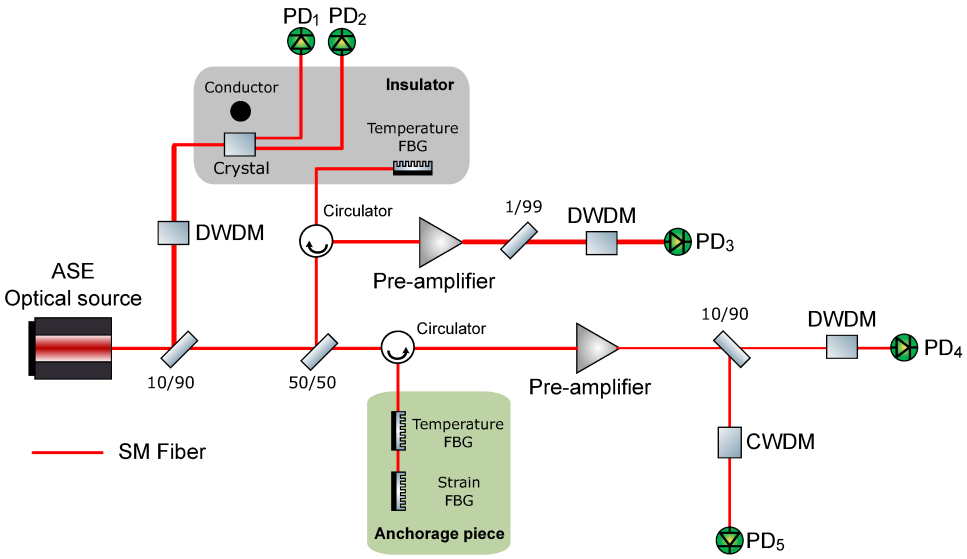

Source: own.

Table 3.6 – Photodetectors response.

dBm	Voltage (mV)	
	PD 1	PD 2
-1.90	-4.6912	-
-2.77	-3.7933	-
-3.63	-3.1145	0.1741
-4.35	-2.6682	0.1743
-5.22	-2.1981	0.1744
-6.60	-1.6000	0.1751
-7.50	-1.3018	0.1752
-8.50	-1.0374	0.1753
-9.35	-0.8561	0.1756
-10.60	-0.6456	0.1755
-11.50	-0.5233	0.1752
-12.90	-0.3794	0.1750

Source: own.

The outcomes show that the replacement is mandatory for the correct operation of the measurement system. The PD 2 is not adequate for the application of FBGs with DWDM filters since the objective is to capture the variation of optical power in terms of the electric voltage signal (mV) as the Bragg wavelength changes according to the physical property (temperature or strain) being measured. Due to the low gain of the PD 2, the optical power variation is practically undetected by the PDs and the OESPU module.

Future applications will improve the gain provided by the OESPU in order to interpret low amplitude signals from PDs with low gain.

3.3.2 FBG strain sensor operation using the PCB

To calibrate the measure using the optical strain sensor and the PCB, a sheet-type sample of the anchorage piece has been submitted to a standard tension test. The elastic region of the material of the extender has been characterized to estimate the maximum deformation that might be imposed on the extender of the transmission line.

The FBG sensor utilized in TECCON MS has its Bragg wavelength (λ_B) centered in 1540.43 nm and a sensitivity of 854 $(\mu m/m)/nm$.

A DWDM can be used as an optical power reference value for the system. The objective of the utilization of a DWDM is to support the calibration and measurement of the system when it is placed on the transmission line (operating environment).

The processing of this optical signal is performed through using a CWDM, which actuates as a passive filter. The aim is to position the Bragg wavelength in the lateral band of the CWDM, as shown in Figure 3.20. Hence, the variation in the mechanical tensile will reflect in distinct optical power values and as consequence voltage signals, converted by the PD attached to the PCB.

Figure 3.20 – CWDM for the modulation of optical power in the lateral band.

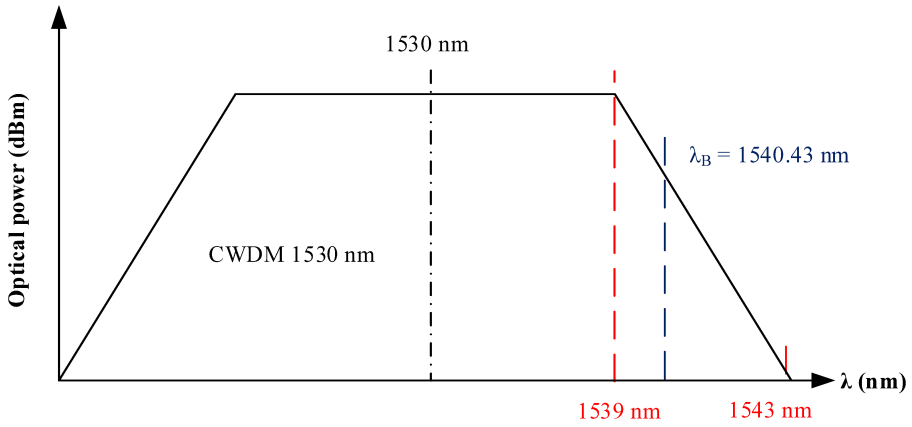

Source: own.

Table 3.7 presents the results in terms of voltage signal and optical power obtained during the mechanical (tension) test, considering the optical circuit presented in Figure 3.19 and the signal filtered by the descendent lateral band of the CWDM Channel (CH) 1530 nm.

The FBG strain sensor calibration curve, that relates stress x PD voltage (MPa x V), utilized on the web application (Asset Management Center (AMC)), is illustrated in Figure 3.21. Using this curve is possible to convert the information provided by the PCB into useful information for the operation and planning teams of the TSO.

Figure 3.22 presents the behavior of the Bragg wavelength in terms of stress variation.

Table 3.7 – Data for calibration of the FBG strain sensor.

Stress (MPa)	Optical power (dBm)	Voltage at PCB (V)
10.0	-3.46	-3.56
20.0	-3.51	-3.52
30.0	-3.56	-3.48
40.0	-3.62	-3.43
50.0	-3.70	-3.36
60.0	-3.79	-3.29
70.0	-3.89	-3.22

Source: own.

Figure 3.21 – Calibration curve for the FBG strain using the PCB.

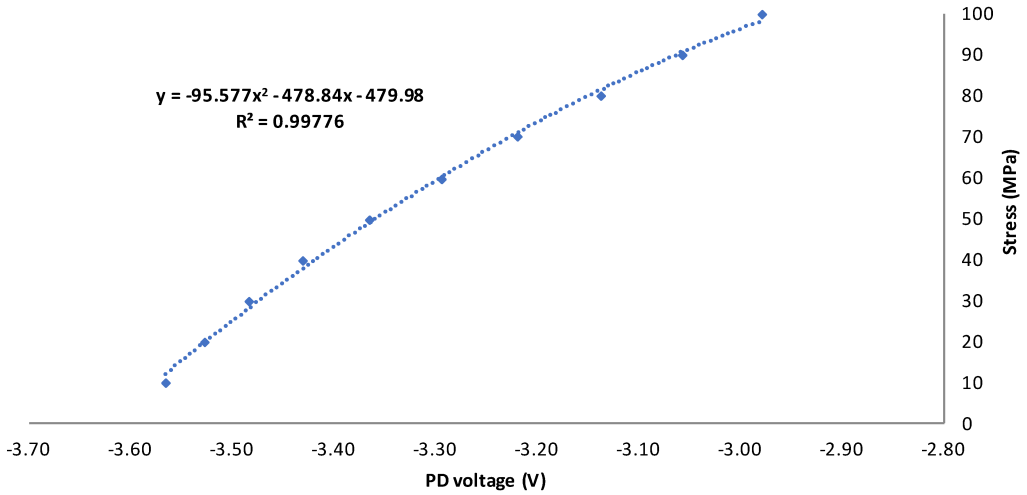

Source: own.

3.3.3 FBG temperature sensor operation using the PCB

The FBG temperature sensor used has a λ_B equal to 1554.3 nm. Considering the same idea exposed for the optical signal processing for the FBG strain sensor, a CWDM, with a central wavelength of 1550 nm, can be utilized as a reference for optical power in the interrogation process.

For purpose of illustration, considering that FBG temperature sensor has a sensitivity of 10 pm/℃ and assuming an initial conductor temperature of 25 ℃ and a maximum allowable temperature for the conductor equal to 100 ℃, there is a temperature variation range of 75 ℃. Therefore, in terms of Bragg wavelength, a displacement of $\Delta\lambda_B$ = 0.75 nm can be estimated.

The DWDM CH 27 is an alternative to measure this variation of temperature. Using this DWDM channel, the incremental variation of the Bragg wavelength will be captured in the PD output by the OESPU. Figure 3.23 illustrates the functioning of the optical interrogation in the lateral band of the filter.

Table 3.8 presents the results obtained during the test performed at TBE Lages

Figure 3.22 – Stress and Bragg wavelength relation for FBG strain sensor.

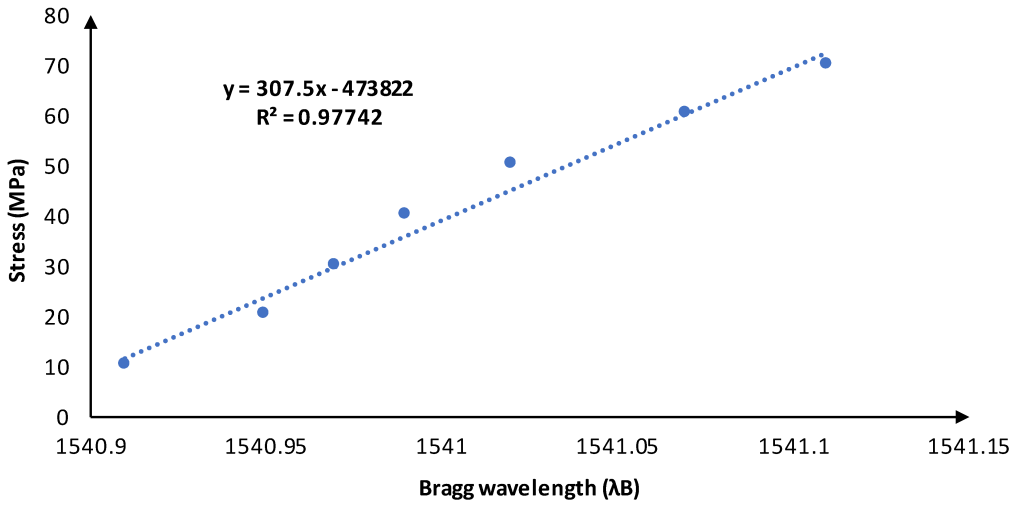

Source: own.

Figure 3.23 – Temperature FBG sensor in the lateral band of a DWDM CH 27.

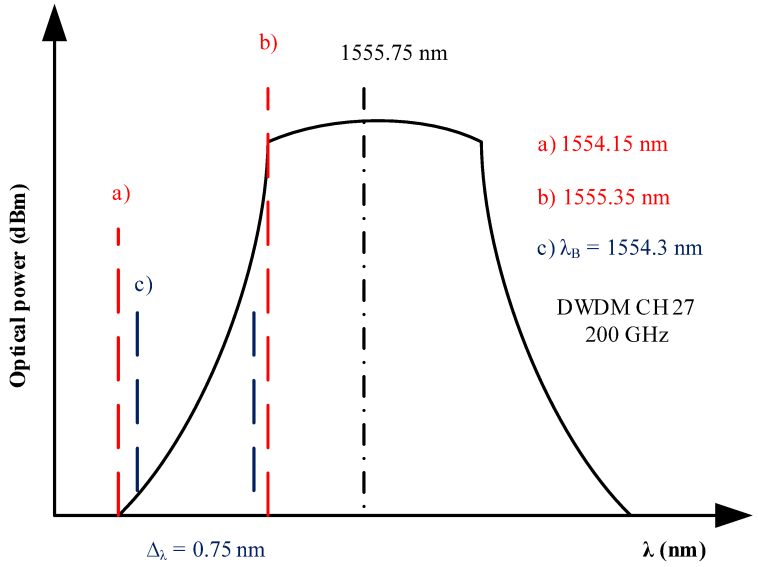

Source: own.

substation, using a calibrated oven as reference. The variation of the optical power and voltage at OESPU according to temperature changing can be noted.

The behavior of the FBG temperature sensor is segmented into two curves (℃ x V) to support the interpretation of the information on the web application (AMC) as illustrated in Figure 3.24.

3.3.4 Bulk optical electric current sensor operation using the PCB

The bulk electric current sensor has been selected to operate in the operating environment initially. The necessary modifications on the optical circuit for the proper

Table 3.8 – Data for calibration of the FBG temperature sensor.

Temperature (°C)	Optical power (dBm)	Voltage at PCB (V)
16.6	-10.40	-0.6609
20	-10.40	-0.6735
25	-10.20	-0.6895
30	-10.10	-0.7016
35	-10.00	-0.7167
40	-9.87	-0.7368
45	-9.71	-0.7680
50	-9.48	-0.8259
55	-9.36	-0.8776
60	-9.01	-0.9351
65	-8.52	-1.0490
70	-7.40	-1.2505
75	-5.98	-1.6884
80	-5.08	-2.4027
85	-3.15	-3.6016

Source: own.

Figure 3.24 – Temperature x PD voltage calibration curve.

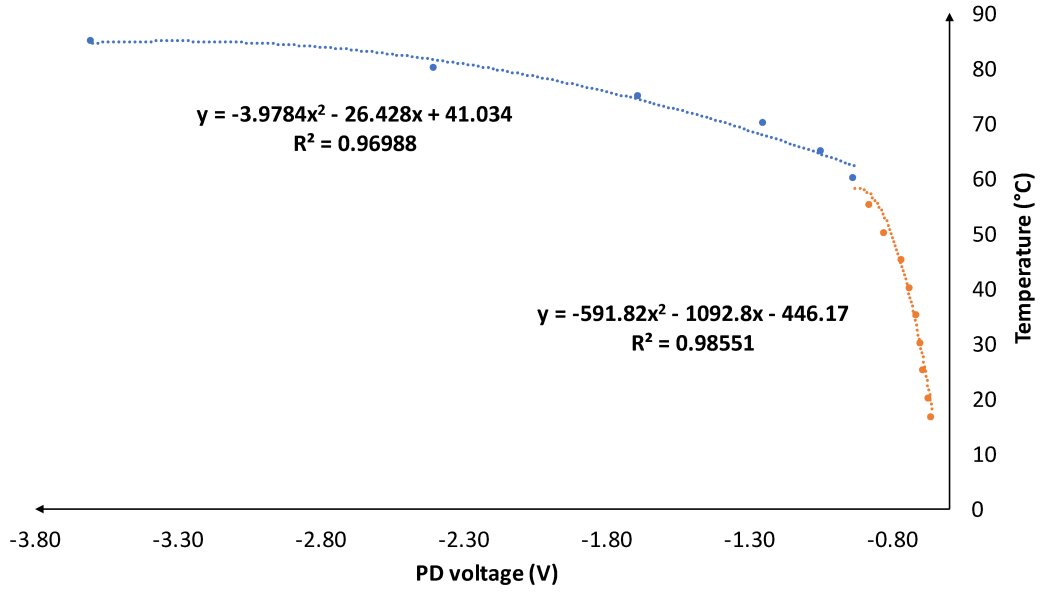

Source: own.

operation of the electric current sensor have been highlighted in section 3.3.1.

The calibration of the crystal sensor using the PCB has been divided into two curves: one for electric currents higher than 100 A and one for values less than this threshold. This is justified due to the sensor sensitivity. The curves relate the Fast Fourier Transform (FFT) amplitude mean value of the 60 Hz signal to the electric current that is passing through the line. Figure 3.25 presents the response of the sensor using the OESPU for electric currents lower or equal than 100 A.

Figure 3.26 presents the response of the sensor using the OESPU for electric currents higher than 100 A.

Figure 3.25 – Calibration curve for electric currents lower or equal than 100 A.

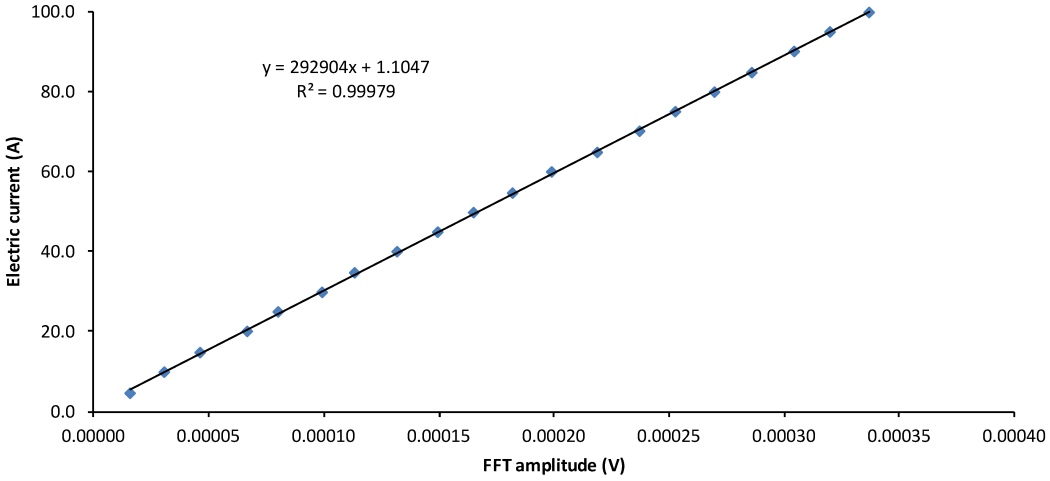

Source: own.

Figure 3.26 – Calibration curve for electric currents higher than 100 A.

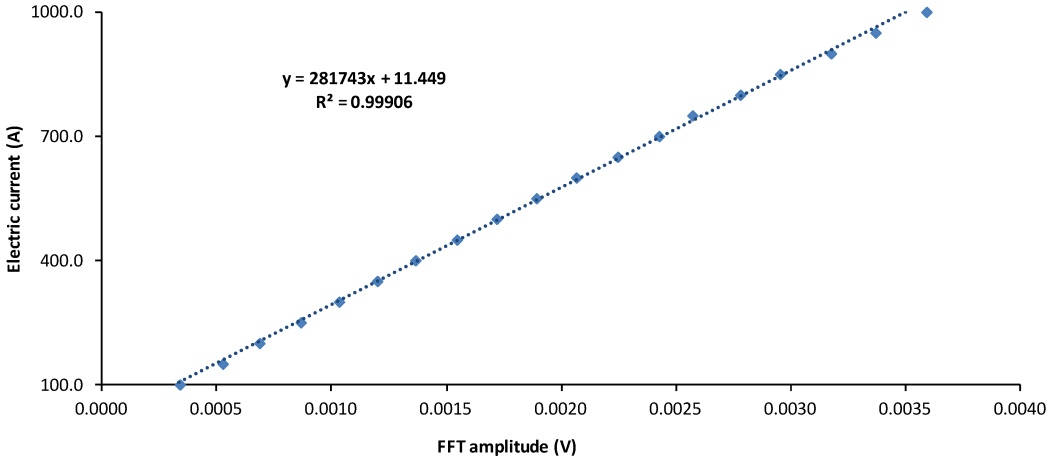

Source: own.

A very linear response is noted for this kind of sensor, those curves are implemented on the web application on AMC to support the TSO decision-making processes.

3.3.5 TECCON Application Programming Interface

The TECCON Application Programming Interface (API) is composed of five major components, as follows.

- receptor: it gets measurement data through ethernet port;
- estimator: it validates gathered data;
- connector: it manages communication with the project database;
- controller: it manages the API server;

- sockets: it streams data gathered by the receptor to listeners.

Modifications have been required in the software to receive the weather station data and to process signals from the electric current sensor and FBG sensors. The calibration curves of the optical sensors have been added to the software code.

The original configuration of the web application has been updated aiming to include all measurements properly. Figure 3.27 presents the TECCON II web application.

Figure 3.27 – Interface of TECCON website.

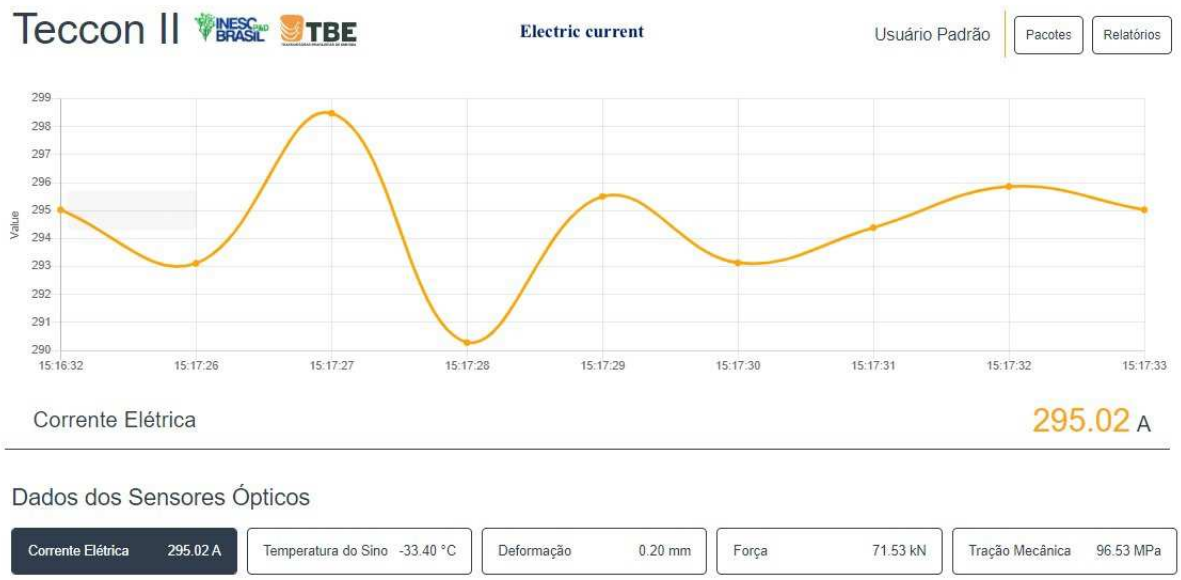

Source: own.

In this illustration, the electric current measurement has been selected to show values on the graph. It is a real value of the Lages x Abdon Batista transmission line, on July 19, 2020, at 3 p.m. Every variable being measured at TECCON MS can be plotted on the main graph of the web application. The web application is available through the link http://teccon2.inescbrasil.org.br.

Another functionality of the web application is the map of the sensors. It presents the geographical location of TECCON MS around the globe. Figure 3.28 presents the actual map of the sensors. Until the present moment, only one TECCON MS has been installed, as highlighted on Figure 3.28.

3.3.6 Installation of the TECCON MS on the tower and solar energy supplying update

The TECCON MS has been installed on tower number 23/1 of the transmission line that connects the substations of Abdon Batista and Lages (SC), 230 kV, from TBE. System infrastructure installation layout is displayed in Figure 3.29 (3D software

Figure 3.28 – Map of the sensors.

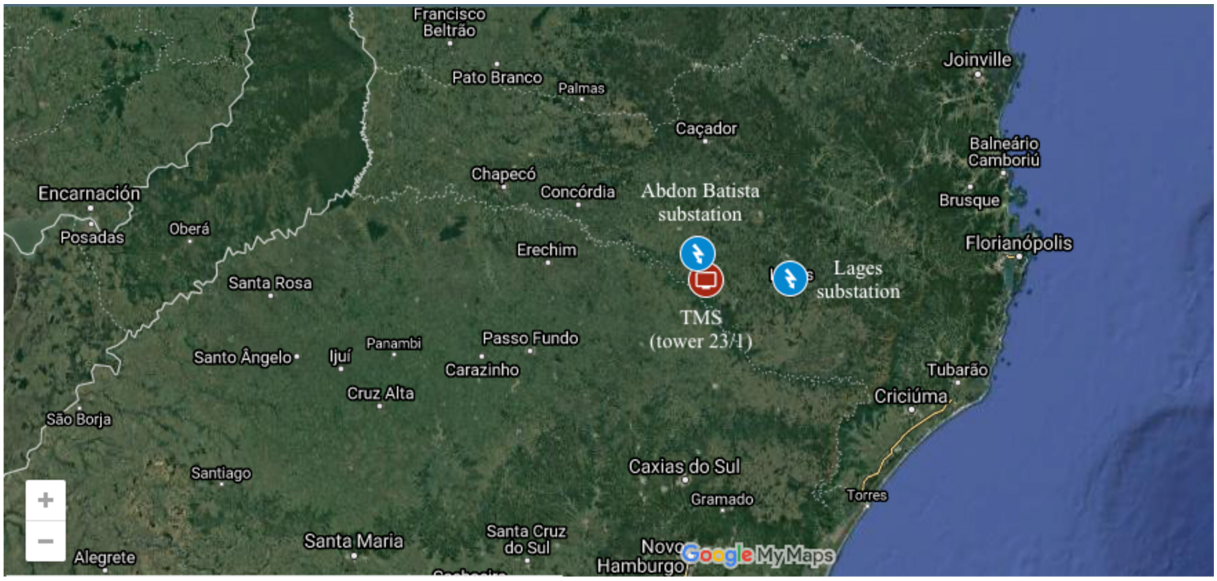

Source: own.

perspective) and Figure 3.30 depicts TECCON MS onto tower, highlighting the position and details of some equipment.

The illustrations display the layout of the components at the transmission line tower. The transmission line has two electrical circuits. The housing for the OESPU and the enclosure of the solar energy system components (battery, load controller) are placed near the meteorological station.

The energy supplying system had to be updated due to the load of the new PDs and optical pre-amplifiers. Two solar panels of 330 Wp each and an ion-lithium battery with a capacity of 200 Ah are utilized to supply the load on the tower.

Due to the shadowing firstly observed when the panels have been positioned on the tower for initial tests, the panels are located on two different positions on the tower as exposed in Figure 3.29. Notice that one photovoltaic panel is placed on the top of the tower under the Optical Ground Wire (OPGW)s and another one is positioned on the highest cross arm. This arrangement has been implemented to avoid electrical discharge effects, prevent vandalism and reduce the shadowing on the panels.

One instrumented polymeric insulator is placed in one phase of the line embedding the sensors devoted to measuring electrical current and temperature. The optical and electrical losses related to solution arrangement on the tower are reduced, mainly the first one, due to the distances involved in the placement of the components. Figure 3.31 highlights the instrumented polymeric insulator installed on electrical circuit 2 (C2) of Lages x Abdon Batista 230 kV transmission line.

As addressed before, the electromagnetic compatibility of the enclosures and the electromagnetic interference on the photovoltaic panels have been tested and the proper operation of the system was verified. As consequence, the TECCON MS

operates properly on the operating environment, achieving the TRL 7.

3.4 COLLECTED DATA USING TECCON MS INFRASTRUCTURE

The TECCON MS has been collecting electric, physical and mechanical variables related to the transmission line, since the year 2020. The objective of this section is to present practical results of the TECCON MS real operation. The behavior and characteristics of those variables that are being measured on the Lages x Abdon Batista transmission line are discussed. The monitoring system provides information about the following variables:

- Physical variables: wind relative speed, wind corrected speed, wind relative direction, wind corrected direction, atmospheric pressure, ambient temperature, line conductor temperature, relative humidity, dewpoint, precipitation, total precipitation intensity;
- Geographical and general information: latitude, longitude and altitude, date and hour, voltage supply and status;
- Electric variable: electric current on circuit 2 of the line;
- Mechanical variables: tensile stress, mechanical force, and deformation of line conductor.

Table 3.9 presents the set of measurements acquired using TECCON MS for December 10, 2020, at 06:00 pm.

Table 3.9 – Collected data from a specific time instant.

Optical sensors data				
Electric current (A)	Conductor temperature (℃)	Deformation (mm)	Mechanical force (kN)	Tensile stress (MPa)
247	27.0	0.11	37.57	50.70
Weather station data				
Wind rel. speed (m/s)	Wind cor. speed (m/s)	Wind rel. direction (°)	Wind cor. direction (°)	Ambient temperature (℃)
0.91	0.91	31	5	27.9
Atm. pressure (hPa)	Rel. humidity (%)	Dewpoint (℃)	Precipitation (mm/day)	Total precipitation (mm)
901.4	38.0	12.5	-	-
Voltage supply (V)	Status			
12.2	4			

Source: own.

The status, attributed as 4 on the example of Table 3.9, indicates that the GPS has been responsible to correct the wind direction. It happens when the weather station is not perfectly aligned with the geographical north. The voltage supply is at 12.2 Vdc in this case. The weather station operates properly from 5 to 30 Vdc and its nominal voltage is 12 Vdc. TECCON MS geographical position is at 27°S and 51°W and it is placed at an altitude of 996.10 m. Another analysis can be performed looking at the behavior of the electric current during the Sunday of December 13, 2020. The graph on Figure 3.32 presents the data gathered using the electric current optical sensor.

The results show that this sensor can be utilized as a real-time monitoring system since it has a high resolution rate. The waveform sampling can be also obtained from this measurement. The electric current optical sensor provides results that can be observed in terms of harmonics and waveform. The amplitude curve, exposed in Figure 3.32, has been validated with Supervisory Control and Data Acquisition (SCADA) system of the transmission utility.

This group of information allows the operator to yield insights about the loading of the line, horizontal and perpendicular strengths may be calculated. Also, the catenary of the line can be estimated taking into account the data obtained. The monitoring system is positioned on a multi-span tension section, comprising a total of 23 unequal spans.

Many studies can be made based on the data collected. The existing correlations between the physical variables on a transmission line can be evaluated when a TECCON MS is installed on an anchorage tower. It may yield insights about the improvement of conductor tensile stress due to high wind speeds, for instance. The sag can be estimated using the span length, tensile stress, and known mass per unit length of the conductor.

Traditional power systems have been built and operated using SCADA systems, which report measured grid conditions every 4 to 6 seconds. More recently, transmission utilities have been installing phasor measurement units (PMUs) that continuously report from 30 to 60 samples/sec., using the UTC-synchronized data for event analysis, model development, and operations support. The development of new measurement technologies, such as optical sensor devices and TECCON MS, needs to be carried out to make feasible higher-resolution, time-synchronized POW data. A POW measurement device reports the sampled waveform directly, typically at rates of 256 samples/sec. or higher (NASPI, 2020). The TECCON MS provides information with a sample rate of 15,360 samples/s (15.36 kHz), complying with the requirements for POW applications.

3.4.1 Real-time measurements

TECCON MS provides measurements at each second using OPGW, transmitting data from transmission line intermediate tower to AMC (roughly 72 km). This subsection aims to present additional outcomes yielding insights about the real-time condition

monitoring of the Lages x Abdon Batista transmission line. Some specific days are selected for evaluation. Illustrations are positioned on Appendix E and nominal reference limits are emphasized in such curves. Firstly, three variables monitored (conductor temperature, mechanical traction, and electrical current) are assessed independently:

- Figure E.1 presents the conductor temperature variation during Feb. 2, 2021: it is noted an average temperature of 51.3℃, which is lower than design temperature and than conductor maximum allowable temperature. It is an example of a typical day which the line could be more exploited using DLR;
- Figure E.2 presents mechanical traction (kgf) variation on conductor anchorage point (Feb. 2, 2021): the graph shows that mechanical traction is around design value, however, it is constantly varying accordingly to boundary conditions, mainly, wind speed and direction. Conductor tangent mechanical traction can be utilized to monitor sags;
- Figure E.3 presents the electrical current variation during the 24 h at Feb. 2, 2021: it exhibits that the conductor is, on average, operating under transmission line and conductor static limits, indicating possible situations in which line could be more exploited.

The inter-dependency between climatic elements and transmission line mechanical and electric parameters is evaluated using another set of graphs (Appendix E):

- Figure E.4 presents the relation between ambient temperature (℃) and mechanical stress (MPa) on anchorage point on Feb. 5, 2021: the graph shows that mechanical stress is increased during the period which the ambient temperature is also on a high range (from 09:00 am to 06:00 pm);
- Figure E.5 presents mechanical stress (MPa) and wind speed (m/s) variation (Feb. 5, 2021): the graph shows the behavior of mechanical stress against wind speed, complementing the insights provided by analyzing Figure E.4. The wind speed, as expected, varies instantaneously, justifying the need for dynamic rating techniques to optimize line exploitation. Also, the variation of mechanical stress impacts directly on the line clearance-to-ground and sag;
- Figure E.6 presents the relation between electrical current and ambient temperature (Feb. 2, 2021): it shows that the line is more loaded during the afternoon, having its lowest value at roughly 03:00 am. The ambient temperature becomes to increases at 09:00 am and reaches its peak at 03:00 pm. The graph displays a traditional summer weekday.

Figure 3.29 – The placement of TECCON MS components on tower 23/1.

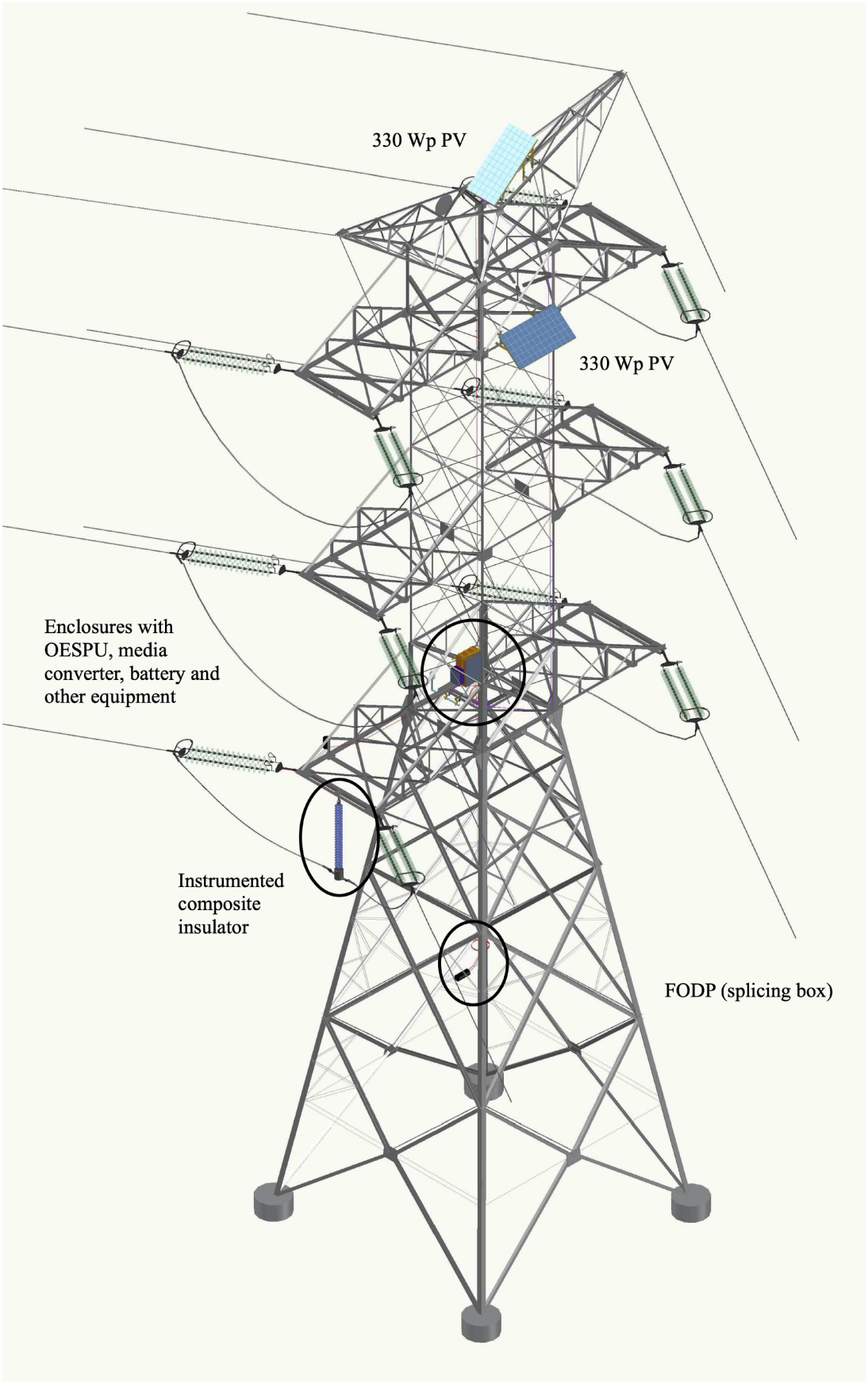

Source: own.

Figure 3.30 – TECCON MS infrastructure on tower 23/1.

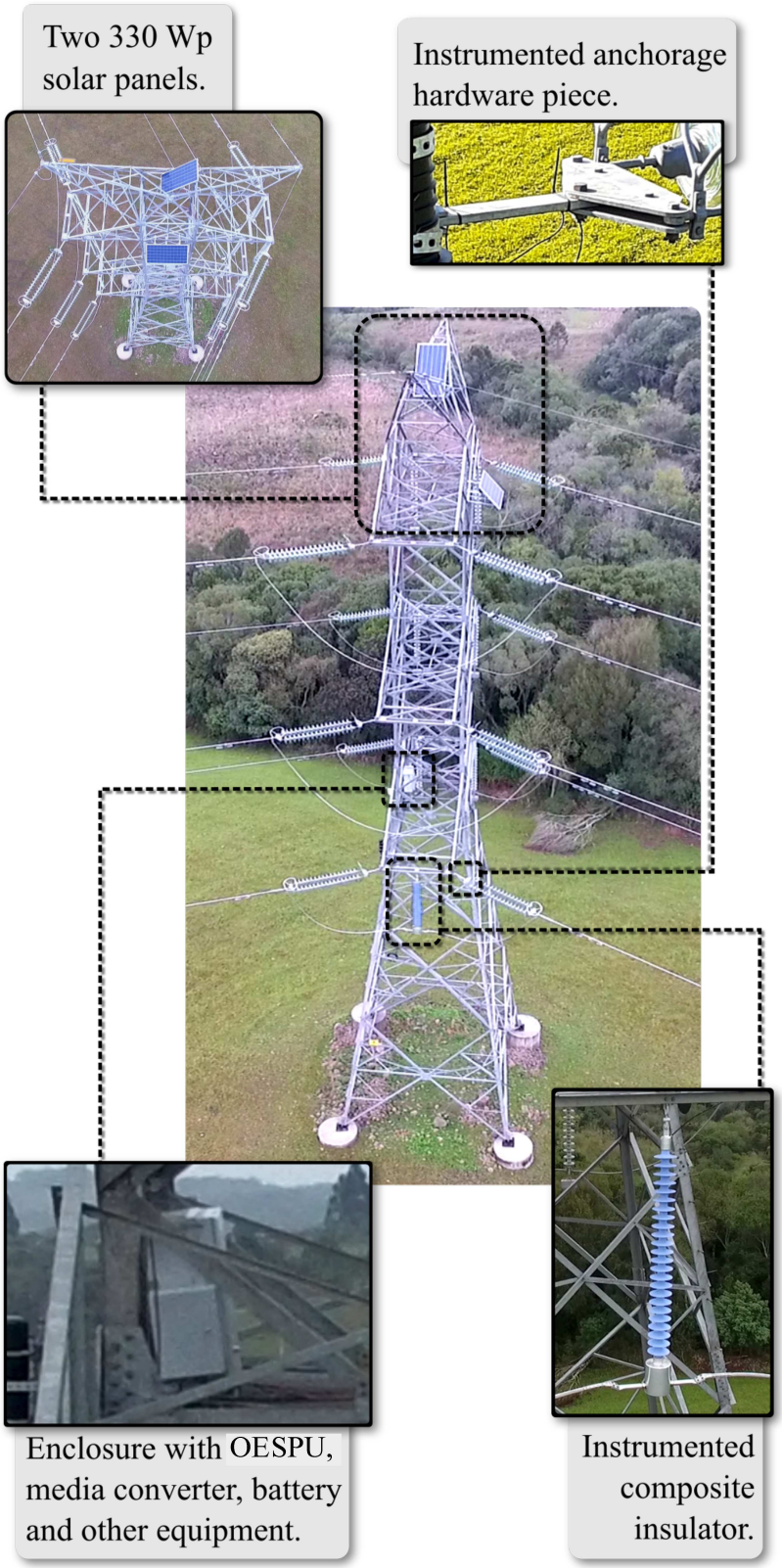

Source: own.

Figure 3.31 – Instrumented polymeric insulator positioned on C2 of Lages x Abdon Batista transmission line.

Source: own.

Figure 3.32 – Electric current measurement at December 13, 2020.

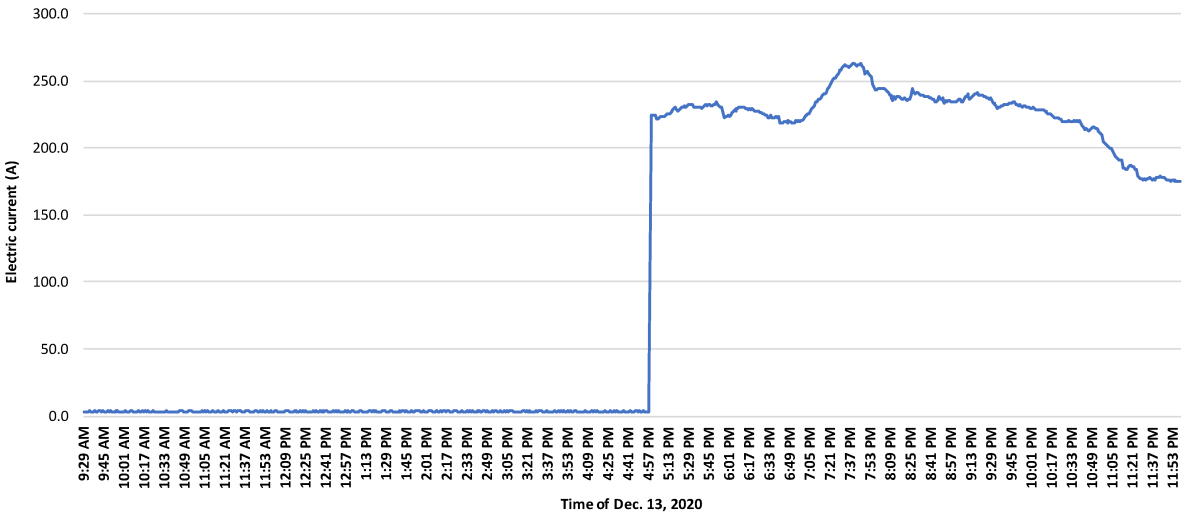

Source: own.

Part II

Scientific Approaches

4 METHODOLOGY FOR POWER SYSTEM ASSESSMENT CONSIDERING OPERATIONAL FLEXIBILITY

The proliferation of systems that estimate in real-time the ampacity of specific transmission lines requires novel representations to be aggregated to power system evaluations. The TECCON MS, for instance, is a novel technological infrastructure added to the power system. The installation of this device yields a variety of dimensions of applications, such as the DLR. This method, in its turn, can be utilized as a source of real-time ampacity, serving as a solution that provides transmission line flexibility. Devising to accommodate such methods in power system performance evaluations, a DLR representation is proposed. This modeling connects technological contributions with scientific ones.

In this sense, this chapter presents the proposed method to calculate the real-time ampacity of transmission lines based on DLR and the probabilistic DLR-based technology method for evaluating power systems reliability.

4.1 DLR TECHNOLOGY IMPLEMENTATION

It is possible to variate the transmission line power capacity according to the weather conditions and physical characteristics of the conductor using the equation (A.3). The real-time conductor temperature can be evaluated using numerical methods that consist of solving the equation (A.3) for determined time intervals. The proposed methodology considers that both weather conditions and electric current remain constant for one hour and that at the end of 1200 s (20 min) the conductor must reach its maximum temperature. From the input variables (weather series, type of conductor, meteorological region), the rating of the transmission line is computed for a future time of interest, for instance, 20 min (BOLACELL; DA ROSA, 2020; FERNANDES; DA ROSA; ISSICABA, 2020).

The procedure utilized for DLR calculation is illustrated in Figure 4.1. Initially, the conductor temperature (T_c) is compared with its maximum allowable temperature (T_c^{max}). If $T_c > T_c^{max}$, a negative electric current step is applied, otherwise, positive. After that, the time counter (t) and numerical computation of equation (A.3) are initiated for a time increment (e.g., k = 1 second). At the analysis end time (20 min), if T_c is roughly equal to T_c^{max}, an error margin of 5% is assumed, the dynamic rating for the transmission line has been found and the process is ended. Otherwise, T_c returns to its original value and the procedure is reinitiated utilizing distinct electric current step values.

The DLR implementation provides the modulus of maximum electric current (I_{max}), in Ampere (A), which the conductor supports under specific weather conditions. The modulus of the three-phase maximum apparent power (S_{max}), in VA, for a specific

Figure 4.1 – DLR implementation flowchart.

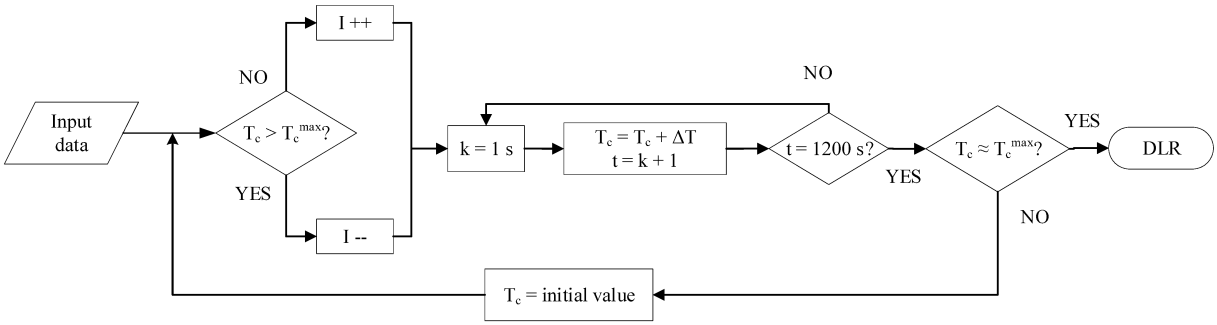

Source: own.

hour of the simulation is computed using (4.1).

$$S_{max} = \sqrt{3} V_{nom} I_{max} \tag{4.1}$$

where V_{nom} is the modulus of the nominal voltage (V). Using (4.1) and annual hourly series for weather conditions, it is possible to generate an hourly transmission power capacity series based on DLR devised to be utilized in power system performance assessments. The model requires the specific weather data, type of conductor, and voltage level for each transmission line of the power system, which the methodology of varying the power capacity will be applied.

Figure 4.2 illustrates the framework of analysis proposed to reproduce the variation of the transmission power capacity employing the dynamic rating methodology presented in detail by Figure 4.1. Therefore, the modeling of the transmission line has a time-dependent capacity that depends on the climate conditions and the maximum conductor temperature and a failure/repair cycle that represents the physical availability of the component.

Figure 4.2 – Framework of analysis considering the time-dependant capacity of transmission lines.

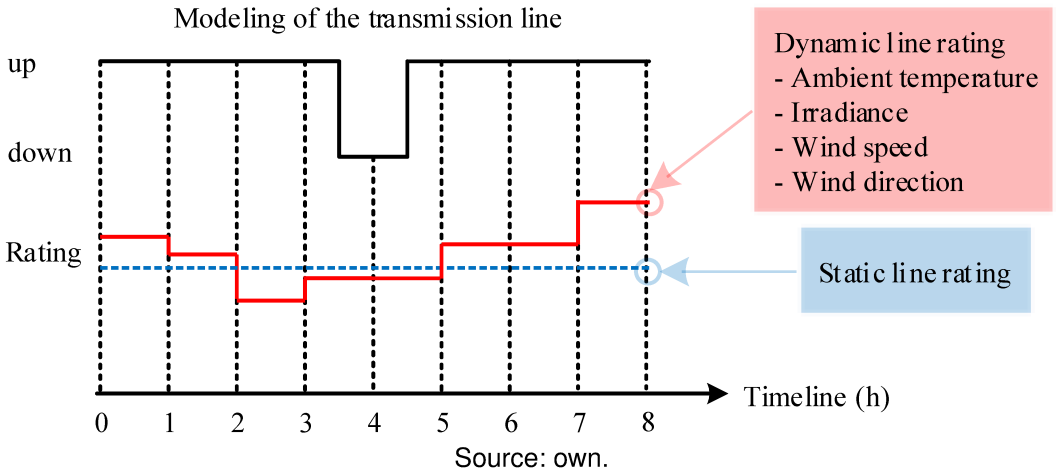

Source: own.

On traditional reliability evaluations, the transmission line has a fixed static rating during the SMCS, as depicted in blue color in Figure 4.2. However, to change this paradigm, evaluations considering the DLR are proposed based on hourly series of ambient temperature, irradiance, wind speed, and direction. The time-dependent capacity adds a new element to provide more realistic modeling of transmission systems regarding the challenges faced with the technological transformation of the 21st century.

To highlight the DLR implementation, the transmission utilization factor (TUF), given in pu or %, is evaluated in some case studies. It can be defined as the ratio of power transmitted (PT_{PF}), given by power flow computation (VA), by dynamic transmission capacity (S_{max}).

$$TUF = \frac{PT_{PF}}{S_{max}} \tag{4.2}$$

4.2 PROBABILISTIC DLR METHOD

On traditional reliability evaluations, the transmission line has a fixed static rating during the, for instance, SMCS studies, as highlighted in Figure 4.2. However, to change this paradigm, reliability performance evaluations considering the DLR technology as a planning alternative are proposed following the general steps of the Algorithm 1, which is utilized to study composite and multi-area systems.

It is important to highlight that $\overline{\mathbf{P}}_{\mathbf{ik}}$ (maximum transmission line capacity) is updated at each hour based on DLR implementation. Furthermore, the evaluation of the system state, indicated in the step number 38 of the Algorithm 1, presents the highest computational effort on a SMCS. The flowchart illustrated in Figure 4.3 presents the general steps to assess the system state for composite systems (R01), including the modeling of the transmission network and generation operational flexibility aspects.

As shown in Figure 4.3, at each new SMCS state initially is made a generation dispatch to distribute the load to the available generating units taking into account only the production cost of the generators. Supposing that the amount of available generation is not sufficient to meet the load, it is counted as a loss of load event:

$$P_c(t) = L(t) - G(t) \tag{4.3}$$

where $G(t)$ is generation capacity at time t, $L(t)$ is the system load at time t and $P_c(t)$ is the load curtailment at time t. Subsequently, $P_c(t)$ is distributed in all load buses, prioritizing those with lower cost and minimizing the total loss of load cost, until the relation presented in (4.4) be satisfied.

$$L(t) - \sum_{i=1}^{N_b} P_{c_i}(t) = G(t) \tag{4.4}$$

where $P_{c_i}(t)$ is the load curtailment at bus i at time instant t and N_b is the system number of buses. After that, the state of the transmission system is assessed by running a DC PF (GRAINGER; STEVENSON JR., 1994; WOOD; WOLLENBERG; SHEBLÉ, 2014). If there are circuits with operating limits violated, then an OPF is executed to apply remedial actions. As a result, the OPF may indicate two scenarios: the first is a new feasible point of operation, achieved with a generation redispatch, meeting the load. The second, however, indicates that is not possible to find a feasible state with the actual system configuration, being necessary a load curtailment, to be incremented at $P_c(t)$ value.

To assess the performance of the system considering generating units' operational flexibility parameters, some performance indices are computed via SMCS. Four indices are proposed to quantify events related with the DOR requirements, similar to indices presented in section 2.4.1:

- Generation Shedding Expectation (GSE), indicates the average number of yours in a given period that the system is not able to reduce its conventional generation (lack of flexibility) to meet the load, in hour/year.
- Generation Shedding Frequency (GSF), indicates the frequency of conventional generation shedding necessary to avoid the excess of generation, in other words, it counts the number of events that lack of flexibility has been experienced, in occurrence/year.
- Waste of Intermittent Generation Expectation (WIGE), represents the expectation of waste of intermittent, not controllable, generation actions demanded trying to fulfill DOR requirement ($G = L$), in hour/year.
- Waste of Intermittent Generation Frequency (WIGF), represents the frequency of events with a waste of intermittent generation, indicating system conditions that variable renewable generation needs to be wasted trying to meet the load ($G = L$), in occurrence/year.

The indices can support power system flexibility assessments, estimating the expectation of a lack of downward reserve capacity. To accomplish with multi-area systems analyses, some simulation criteria are adapted based on the methodology proposed in Vieira (2020), following the general idea presented in Figure 4.3.

Algorithm 1 Probabilistic DLR method

Initiate DLR estimation, for each hour h, using historic weather data.
while $h < 8760$ hours **do**
  if $T_c > T_c^{max}$ **then**
    Increment line electric current;
  else
    Decrease line electric current;
  end if
  Compute ΔT_c via dynamic T_c equation (A.3); k = 1 min;
  $T_c = T_c + \Delta T_c$; $t = k + 1$;
  if $t = 20$ min **then**
    if $T_c \approx T_c^{max}$ **then**
      Maximum electric current (I_{max}) for hour h;
      $h = h + 1$, and go back to step 2;
    else
      $T_c =$ initial T_c, and go back to step 3 (set new I);
    end if
  else
    Go back to step 8;
  end if
end while
Compute hourly power capacity series for each transmission line: $S_{max} = \sqrt{3} V_{nom} I_{max}$;
Start SMCS;
Sample the state and state residence time (t_i) of each component, and the hourly power capacity series;
$t_{clock} = \min(t_1, \ldots, t_n)$, where n is the nº of components;
while $\beta < \beta_{max}$ or $y < N_{max}$ **do**
  while t_{clock} does not cross a year **do**
    Perform next state transition;
    if component i transits to down state **then**
      Sample repair time using: $T_i = -\frac{1}{\mu_i} \ln U$;
    else
      Sample the operating state duration: $T_i = -\frac{1}{\lambda_i} \ln U$;
    end if
    $t_i = t_i + T_i$;
    $t_{clock} = \min(t_1, \ldots, t_n)$;
    if t_{clock} is a new simulation hour **then**
      Update lines capacity for the specific hour (S_{max});
    end if
    Evaluate the system state;
    Update all test functions;
  end while
  Estimate indices and compute β; $y = y + 1$;
  Sample hourly power capacity series;
end while

Figure 4.3 – General steps of system state assessment.

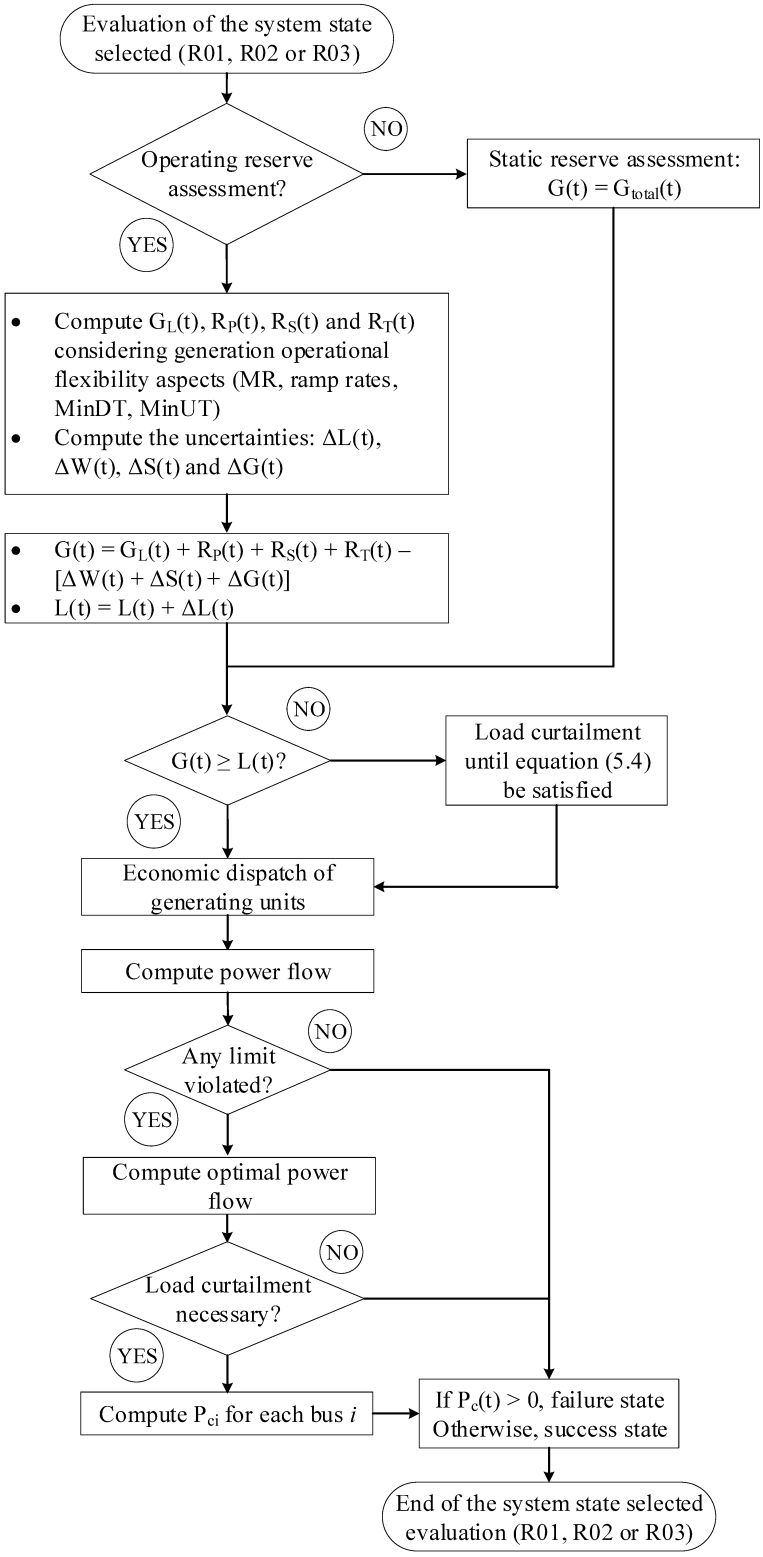

Source: adapted from Vieira (2020).

5 RESULTS

In the first part of this chapter, the proposed method to estimate the steady-state and dynamic rating of transmission lines is validated through the utilization of real transmission lines from the South Brazilian Interconnected System and benchmark cases. The DLR implementation is validated using benchmark results in order to apply the method as an option to provide transmission line flexibility.

Secondly, IEEE test systems and the Iberian Peninsula (Portugal and Spain) real power system are utilized to illustrate the methodology proposed to assess reliability perspective considering flexibility aspects of the generating units and transmission lines. The impact of the introduction of these models into simulations that are envisioned to evaluate the performance of power systems is discussed. The reliability results encompass the distinct representations to assess the power system from a long-term perspective considering single and multi-area systems.

The software utilized in the analysis has been coded in C++/CLI. Simulations have been carried out in an INTEL® CORE™ i5 CPU 3.20 GHz.

5.1 IMPACT OF DLR ON TRANSMISSION POWER CAPACITY

The DLR methodology is intended to support the evaluation of the profits that may arise when the transmission system flexibility is considered on power system reliability assessments. Advantages in considering variable transmission line limits are assessed and the impact of voltage level and weather conditions in the ampacity is also presented. Furthermore, it is considered that the monitoring system used for DLR purpose is not susceptible to failures, hence, it is 100% reliable.

A critical span (weakest span) is considered as representing the whole transmission line and the sag is not a limiting factor. The conductor is mechanically properly designed to support the maximum allowed conductor temperature in all simulations involving DLR. The conductor maximum allowable temperature is considered to be equal to 80, 90, or 100 ℃, depending on the study case (ENTSO-E, 2015).

In order to validate and verify the accuracy of the conductor thermal model implementation for the steady-state and dynamic cases, the steady-state thermal rating and the temperature tracking calculation have been performed considering the data available in CIGRE (2014). Table 5.1 presents the data used to assess the fidelity of the steady-state thermal rating model.

The results for the steady-state ampacity calculation using the equations presented in section A are exposed in Table 5.2. The outcome is compared with the steady-state thermal rating presented in CIGRE (2014) and relative errors are exhibited.

It can be noticed that the conductor thermal model implemented is adequate to

Table 5.1 – Conductor characteristics and ambient conditions.

Conductor characteristics	**Drake 26/7 ACSR**
Conductor outside diameter (mm)	28.143
Core diameter (mm)	10.4
Outer strand diameter (mm)	4.44
Emissivity, ϵ	0.8
Solar absorptivity, α	0.8
Conductor ac resistance at 25°C (Ω/km)	0.0727
Conductor ac resistance at 75°C (Ω/km)	0.0872
Ambient conditions	
Ambient air temperature (°C)	40
Wind speed (m/s)	0.61
Wind angle of attack (direction) (deg)	60.0
Inclination β to the horizontal (deg)	0
Height above sea level y (m)	0
Solar conditions	
Azimuth of line (deg)	90 (east-west direction)
Latitude (deg)	30
Clearness of atmosphere	clear ($N_s = 1$)
Date	11 a.m. 10th June
Reflectance of the ground (albedo)	forest ($F = 0.1$)

Source: own.

Table 5.2 – Results for the steady-state thermal rating and thermal balance.

Description	**Value**	**(CIGRE, 2014)**	**Unit**	**Relative error (%)**
Electric current (I)	976.79	976	A	0.0809
AC resistance at 100°C	9.3905×10^{-5}	9.3905×10^{-5}	Ω	-
Heat gain by Joule effect (P_j)	89.60	-	W/m	-
Solar heat gain (P_s)	27.25	27.2	W/m	0.1838
Heat loss by radiation (P_r)	39.13	39.1	W/m	0.0767
Heat loss by convection (P_c)	77.72	77.6	W/m	0.1546

Source: own.

calculate the ampacity (static rating). The next set of results addresses the algorithm's capability to implement the dynamic conductor thermal behavior. The first 10 minutes time interval between midnight (00:00 h) and 10 min after midnight (00:10 h) is considered. In this particular case, the weather conditions and the line current are averaged over each 10 min and assumed constant during this time interval (CIGRE, 2014). Table 5.3 describes the initial conditions utilized to assess the fidelity of the dynamic rating model.

Table 5.4 exposes the results for conductor final temperature (T_{final}) in each time step, for the first five minutes of a study case considering the Drake 26/7 Aluminum Conductor Steel Reinforced (ACSR) conductor, line located at sea level and that all the parameters are monitored every 10 minutes. Thus, the effective values considered for the 10 minutes interval are the average values in this interval, obtained from real-time monitoring systems.

It is concluded that the transient conductor temperature can be evaluated through

Table 5.3 – Initial conditions: measured values (10 min. average).

Interval (hh:mm)	00:00 - 00:10
Ambient temperature (°C)	23.7
Wind speed (m/s)	1.7
Wind direction, δ (deg)	62.0
Solar radiation (W/m^2)	0.0
Current (A)	819.0
Initial conductor temperature (°C)	42.01

Source: own.

Table 5.4 – Temperature tracking calculation - DLR.

Steps	$\mathbf{T_{final}}$ **(CIGRE, 2014)**	$\mathbf{T_{final}}$	**Relative error (%)**
1 (00:00 - 00:01)	42.175	42.175	0.0000
2 (00:01 - 00:02)	42.321	42.319	0.0047
3 (00:02 - 00:03)	42.449	42.447	0.0047
4 (00:03 - 00:04)	42.562	42.559	0.0070
5 (00:04 - 00:05)	42.662	42.658	0.0094

Source: own.

the proposed methodology. In reliability simulations, from section 5.3, the weather data are provided by annual hourly series (data from one-hour intervals) in order to include the dynamic conductor temperature tracking into SMCS. The main idea associated with this point is to use as much as possible the capacity of the conductors without violating safety criteria.

5.1.1 Thermal rating of Abdon Batista - Lages transmission line

As addressed in chapter 3, the TECCON MS has been installed on the South Subsystem of the Brazilian Interconnected System. The TECCON MS is located on a transmission line that has originated from the sectioning of Barra Grande - Lages transmission line. Originally, the basic project has been based on the specifications to attend the ANEEL public notice nº 001/2005 that demanded a 230 kV transmission line, connecting Barra Grande - Lages - Rio do Sul, double circuit, with 195 km of extension. A illustrative map is presented in Figure 5.1.

The transmission lines originated from the sectioning are highlighted through red dashed lines on Figure 5.1. The instrumented polymeric insulator with optical sensors has been installed on the 230 kV Abdon Batista - Lages transmission line.

This subsection aims to assess the steady-state and dynamic rating conditions associated with Abdon Batista - Lages transmission line. The sensors information is being sent to the data center (AMC), located in TBE substation. These data support the DLR application.

Table 5.5 exposes the general data related to thermal behavior and electric parameters of the conductor selected to be utilized by the utility to build the transmission

Figure 5.1 – Electro-geographic map presenting the main transmission lines on Santa Catarina region.

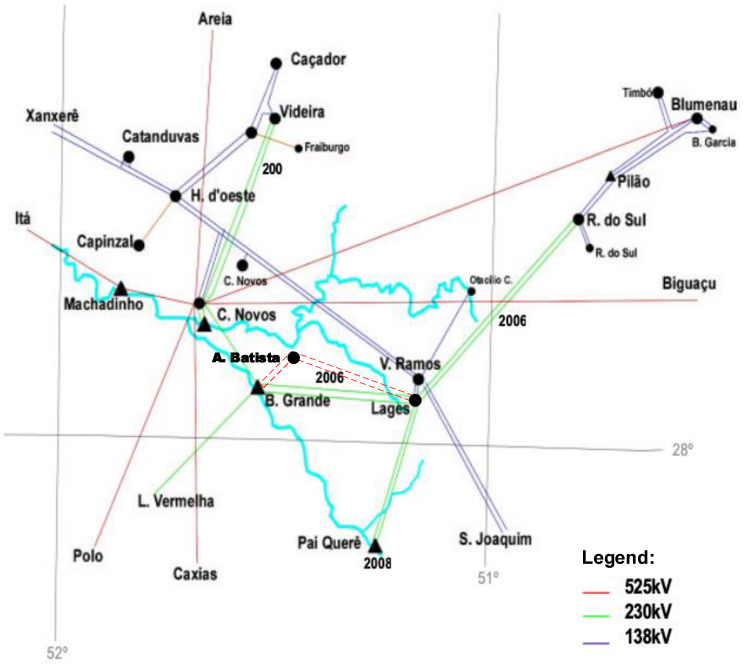

Source: adapted from ANEEL (2005a).

line. Regarding the information utilized by the executor of the line design (STC, 2006), the calculation of the steady-state thermal rating has been performed to guarantee that each circuit of the transmission line could support an electric current of 879 A without violating any performance criterion, following the criteria imposed by ANEEL public notice (ANEEL, 2005a; STC, 2006).

The emissivity and absorptivity values have been established in order to represent an aged conductor, providing conservative results. Table 5.6 presents the results that have been provided in the line basic design (STC, 2006).

Some parameters, namely the wind direction angle, the date considered, and albedo (F), which are of the utmost relevance for correct calculation of the steady-state ampacity are not specified in the transmission line basic design (STC, 2006). These values impact directly on the thermal behavior of the conductor, see equation (A.1).

In order to validate the results presented in Table 5.6, four different scenarios are posed intending to understand and study the specifications used to determine the thermal rating of the transmission line. The scenarios have been created devising to assess the impact of those parameters not specified at line basic design on conductor thermal balance calculation. These variables have straightforward impact on equations (A.7), (A.10), for instance, which will influence on final values of solar heat gain, equation (A.6), and convective heat cooling, equation (A.15). The scenarios are:

- Scenario 1: F = 0.1 (forests), date is June 1st, and wind direction is 90°;

Table 5.5 – Transmission line of the TECCON MS: conductor characteristics and ambient conditions.

Conductor characteristics	**Bluejay 45/7 ACSR**
Conductor outside diameter (mm)	31.98
Core diameter (mm)	7.98
Outer strand diameter (mm)	4.00
Emissivity, ϵ	0.70
Solar absorptivity, α	0.90
Conductor ac resistance at 25°C (Ω/km)	0.0538
Conductor ac resistance at 75°C (Ω/km)	0.0656
Ambient conditions	
Ambient air temperature (°C)	28.00
Wind speed (m/s)	1.00
Wind angle of attack (direction) (deg)	-
Inclination β to the horizontal (deg)	0.00
Height above sea level y (m)	700.00
Solar conditions	
Azimuth of line (deg)	90.00 (east-west direction)
Latitude (deg)	-28.00
Local hour	12 p.m.
Date	-
Clearness of atmosphere	clear ($N_s = 1$)
Reflectance of the ground (albedo)	-

Source: adapted from STC (2006).

Table 5.6 – Relation between conductor temperature, electric current and transmission power capacity.

Maximum conductor temperature (°C)	**Electric current (A)**	**Power (MVA)**
61	858	684
62	880	701
63	900	717
64	920	733
65	940	749
66	959	764
67	978	779

Source: adapted from STC (2006).

- Scenario 2: F = 0.1 (forests), date is January 1st, and wind direction is 90°;
- Scenario 3: F = 0.2 (soil, grass and crops), date is January 1st, and wind direction is 90°;
- Scenario 4: F = 0.2 (soil, grass and crops), date is January 1st, and wind direction is 60°;

Figure 5.2 presents the ampacity of the Bluejay conductor for the four scenarios previously described, considering the base data for the region of the line provided in Table 5.5. The maximum conductor temperature has been fixed at 65 °C.

Figure 5.2 – Steady state thermal rating for Abdon Batista - Lages transmission line.

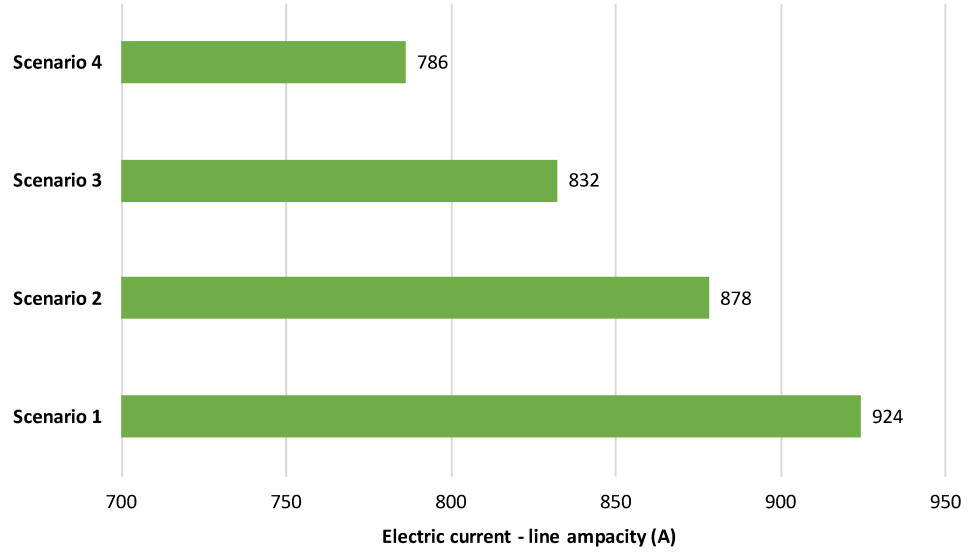

Source: own.

Some important conclusions can be made by analyzing Figure 5.2. Looking at scenarios 2 and 3, the impact of albedo (F) is emphasized, it represents the reflectance of the ground of the line corridor. This parameter produces a higher solar heat gain on the conductor as it is higher, reducing the ampacity. Scenario 2 has a higher static rating (878 A) than scenario 3 (832 A) since scenario 2 has a F = 0.1 being lower than the value established for scenario 3 (F = 0.2).

Another important aspect to be observed is the impact of the wind direction angle on the line ampacity. Scenarios 3 and 4 have been proposed to emphasize explicitly this situation. In scenario 3, the perpendicular wind speed provides better cooling conditions, leading the line to a higher ampacity (832 A) than scenario 4, which has a wind angle of attack of 60° (786 A).

Scenario 1 has the most favorable conditions for line ampacity, i.e., the effective cooling is suitable (P_c) and the solar heat gain (P_s) is the lowest between all scenarios since the albedo is defined as for forest terrains (F = 0.1) and the calculus is positioned at June, impacting positively on the declination of the sun (reducing the direct beam radiation).

Moreover, to complement the analysis in steady state, a study about the level of utilization of the transmission line is undertaken based on a DLR analysis. The risk of transmission line overloading is assessed. Devising to represent in which extent an electric current exceeds the line rating, a relative loading margin (M_{rel}) can be defined as (HAJEFOROSH; BOLLEN, 2020):

$$M_{rel} = 1 - \frac{I_{h_l}}{I_{h_r}} \tag{5.1}$$

where I_{h_l} is the current through the line for a given hour and I_{h_r} is the static or dynamic rating for that hour. In this case, the electric current value is provided through the bulk optical sensor of TECCON MS.

Figure 5.3 presents the frequency distribution of relative loading margin of the transmission line using the data gathered by optical sensors installed on the transmission line, where I_{h_r} is the static rating of 879 A (criteria imposed by the public notice of the line construction). There is a probability of 19% of having a load margin available of 75%. The data have been acquired from July to August 2020, comprising roughly 39 days of data acquisition.

Figure 5.3 – Frequency distribution of the relative margin with static line rating.

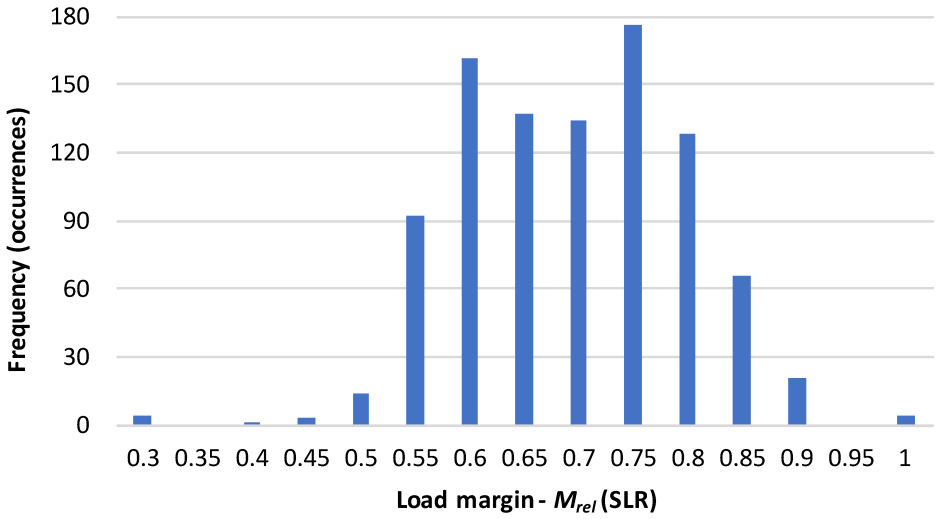

Source: own.

The next evaluation, illustrated in Figure 5.4, presents the frequency distribution of relative loading margin of the transmission line using the dynamic rating and considering the weather data for the region where the system is positioned for a year (JRC-PVGIS, 2020).

As there are no sensors data for an entire year, an average value for the electric current passing through the transmission line is assumed as equal to 300 A. This value has been determined taking into account the measurements undertaken during the 39 days mentioned, which is the period that the sensors have worked properly.

The usage of DLR aids in the integration of vRES to the grid and makes it easier to mitigate overhead line congestion due to high demand. Most of the time (probability of 47%), by evaluating Figure 5.4, there is a loading margin of 85% that can be utilized to transmit power without jeopardizing the reliability of the system, respecting the conductor maximum allowable temperature. Assessing the illustration of Figure 5.4, it is noted that, in general, the Abdon Batista - Lages transmission line is being underutilized.

Figure 5.4 – Frequency distribution of the relative margin with dynamic line rating.

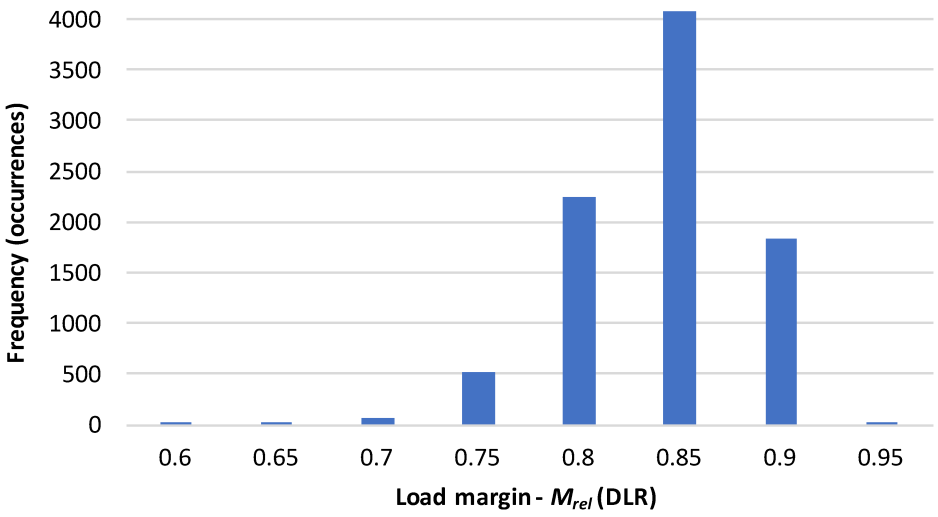

Source: own.

The potential of DLR can be analyzed from plenty of perspectives. The studies presented may help yield insights from two other viewpoints: real-time monitoring may decrease the number of unnecessary load curtailments, identifying real operational capacity reductions, and also activating or ordering out of operation states when there is a real risk of violating safety conditions of the line. As exposed in section 2.3, these actions may reduce the discounts imposed by regulatory aspects when the line capacity is reduced. The PVRO factor can be improved or modified taking into account the outcomes provided by the nature of DLR application on planning and operation outlook. The TECCON MS is envisioned to act as an equilibrium point for discussions between the TSO and the utility responsible to maintain the line operation conditions adequate.

5.1.2 Dynamic line rating for IEEE test systems

In the evaluation intended in this section, the IEEE-RTS 79 is presented in a general perspective, identifying the characteristics of the transmission lines. This test system has two nominal voltage levels: 138 kV and 230 kV. The first voltage level has transmission lines with a static rating of 175 MVA and the 230 kV subsystem has lines with static limits of 500 MVA. On section 5.2.1, for simulation effects, it is introduced the test systems in more details.

To verify the impact of DLR in reliability studies performed using the IEEE Reliability Test Systems (RTS), distinct types of conductors and meteorological regions have been assumed for simulations. Weather data from Porto (Portugal), Florianópolis (Brazil) and Saskatoon (Canada) have been used in the simulations. The data have been acquired from Huld, Müller, and Gambardella (2012), JRC-PVGIS (2020) and

Jager and Andreas (1996). In this case, the maximum allowable conductor temperature is 80 °C for all regions. Table F.1, in Appendix F, exposes the configurations (meteorological region and type of conductor) utilized for each transmission line to represent the variation of available power capacity for each hour.

Figure 5.5 demonstrates the hourly capacity variation of a transmission line, at 230 kV level, submitted to the dynamic rating application over Florianópolis weather conditions. The DLR average power capacity (566.97 MVA) for this type of transmission line, built with Bluejay conductor, is 13.39% higher than the static limit. The analysis indicates that, on average, the transmission line can be more exploited since the conductor thermal limit of 80 °C is being respected.

Figure 5.5 – Hourly average transmission capacity variation, 230 kV line - Florianópolis.

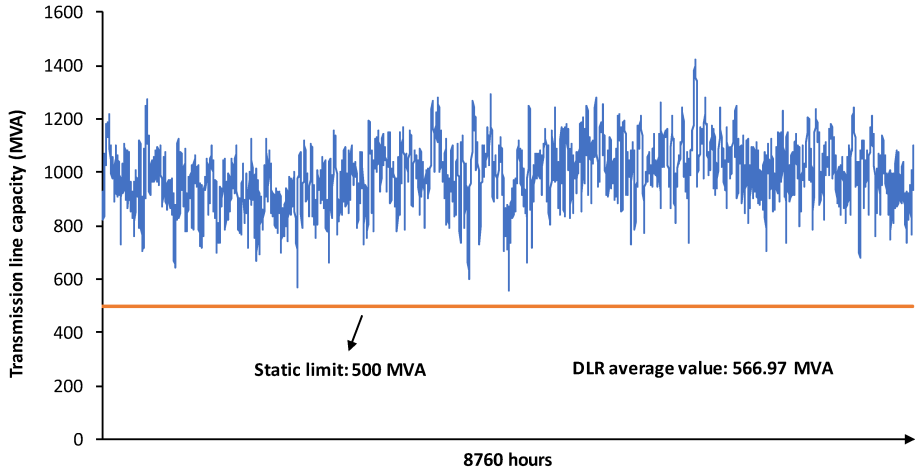

Source: own.

Figure 5.6 and Figure 5.7 demonstrate the hourly capacity variation of a transmission line at 138 kV level submitted to Porto and Saskatoon weather conditions, respectively, supposing that both have been built using Drake conductor. The illustrations show that the average power capacity for a 138 kV line in Porto is 421.90 MVA, representing an increase of 141% related to line static rating (175 MVA). Whereas in Saskatoon, Figure 5.7 shows even a better condition, the DLR average value is 513.53 MVA, indicating an enhance of 193% comparing with 175 MVA static limit.

Transmission lines at Saskatoon weather conditions have, on average, 21.72% more transmission power capacity than in the Porto region. Thus, the results indicate that a transmission line, with the same conductor and design characteristics, can have distinct power capacity limits depending on the region it is constructed since the conductor thermal limit is considered as power capacity restriction.

It is concluded that, on average, during the entire year, the transmission lines may be conveying a higher power capacity than the static limits (175 MVA and 500 MVA) if the dynamic rating is exploited.

The utilization of historical series to support the estimation of the ampacity of the

Figure 5.6 – Hourly average transmission capacity variation, 138 kV line - Porto.

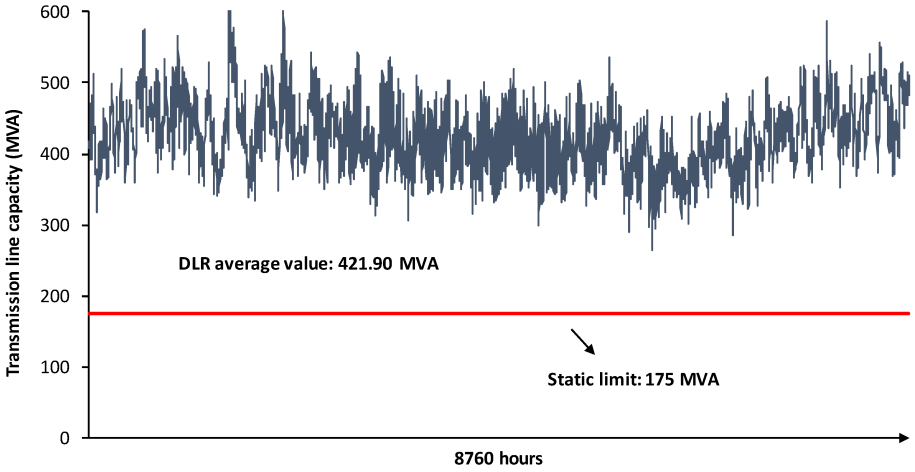

Source: own.

Figure 5.7 – Hourly average transmission capacity variation, 138 kV line - Saskatoon.

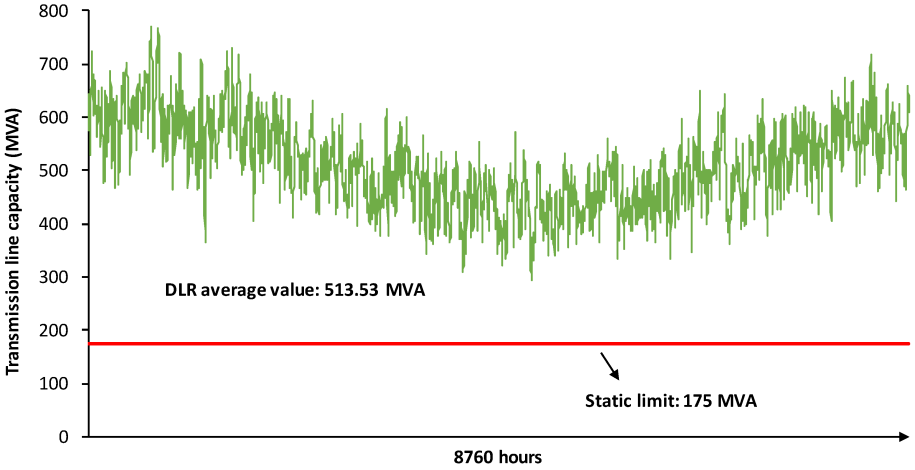

Source: own.

transmission lines in the planning phase has a significant impact on the line capacity limit. The results presented in this section illustrate that in general, the transmission line has an underestimated static limit, which is much below the average value calculated considering the dynamic conductor limit. Clearly, during few hours of the year, the dynamic ampacity may be lower than the static limit, which corroborates the relevance of the dynamic rating consideration.

On the operation of transmission lines, TSO can use this information to redispatch or add load in a specific transmission line, taking into account that its thermal limit is not being violated and as consequence, the line will not have problems related with sags and clearance-to-ground.

This section has addressed the impact of DLR on transmission lines' power capacity. The next section is focused on discussing the details and characteristics of the IEEE test systems and the Iberian Peninsula's real power system. These systems have

been utilized to illustrate the methodology proposed considering operational flexibility aspects for generation and the transmission network in reliability assessments.

5.2 DESCRIPTION OF POWER SYSTEMS SIMULATED

The IEEE test systems are utilized to validate the SMCS method and test the proposed methodology with their variants. The small-sized IEEE-RTS 79 and the medium-sized IEEE-RTS 96 are considered with variants that include the time-dependency of hydrological and wind resources. Also, the most recent update of the IEEE's Reliability Test System (RTS), named IEEE-RTS GMLC 2019, is utilized to illustrate the methodology presented in chapter 4.

Moreover, the Iberian Peninsula's real power system is simulated taking into account three distinct multi-area operation strategies. Another objective of these simulations is to analyze the impact of dynamic rating on the reliability of real power systems. The following two subsections describe in detail the IEEE test systems and the Iberian Peninsula power system, respectively.

5.2.1 IEEE test systems

The IEEE-RTS 79 is utilized to test and compare results (GRIGG et al., 1999). This test system has been developed to test different adequacy assessment methods. The original configuration of this test system is composed of 24 buses, 32 generating units, 33 transmission lines, and 5 transformers. The system load model consists of 8760 hourly peaks with an annual peak load of 2850 MW. The hourly system load is distributed among the respective load buses according to fixed percentages. The total installed capacity is 3405 MW. The IEEE-RTS 79 single-line diagram is shown in Figure 5.8 (IEEE, 1979).

In order to account for the variability of hydropower and wind power, two modifications of the IEEE-RTS 79 are proposed. The first configuration is called IEEE-RTS 79 H and it is considered that the 300 MW of hydro capacity varies monthly according to five historical series. These series are obtained from Leite da Silva, Sales, et al. (2010) (corresponding to those of Area 1). The second configuration, named IEEE-RTS 79 HW, consists of adding 400 MW of wind power to the IEEE-RTS 79 H configuration. The power amount is divided into three wind farms (CARVALHO, L. M. et al., 2012).

To evaluate multi-area systems operation, the IEEE-RTS 96 is utilized. It consists of three interconnected areas. Each area is an IEEE-RTS 79 system, as depicted in Figure 5.9. The original configuration of IEEE-RTS 96 has 96 generating units with a total installed capacity of 10215 MW. Its transmission system includes 104 transmission lines and 16 transformers (GRIGG et al., 1999).

The annual peak load of this system is 8550 MW. The load model is represented

Figure 5.8 – IEEE Reliability Test System.

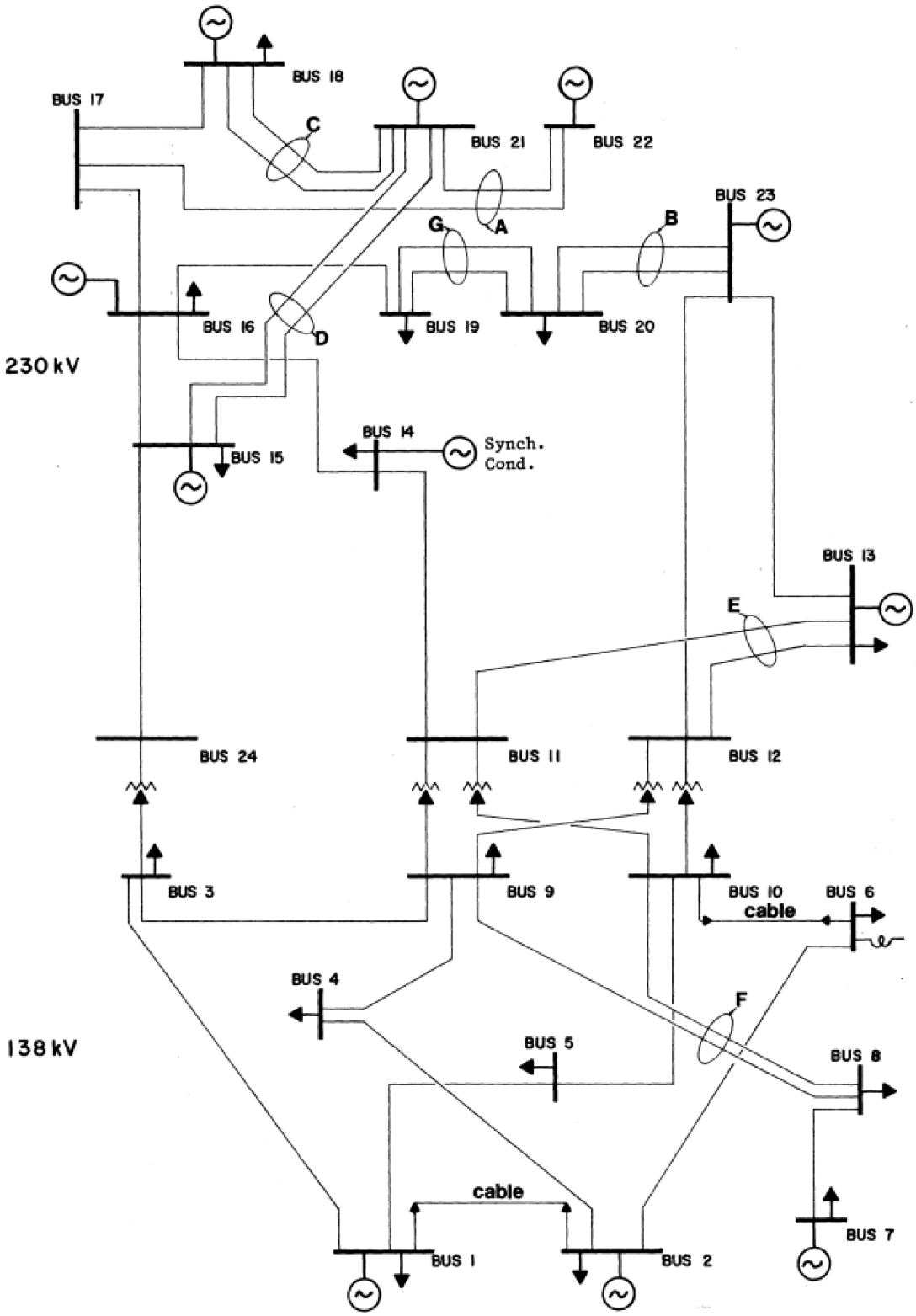

Source: adapted from IEEE (1979).

by 8760 hourly peaks. Like the case of IEEE-RTS 79, the load of the system is distributed by the load buses according to fixed percentages. Three transmission lines make the interconnection between Area A and Area B: AB-1 connects bus 107 with

Figure 5.9 – Illustration of the interconnection between the three areas of the IEEE-RTS 96.

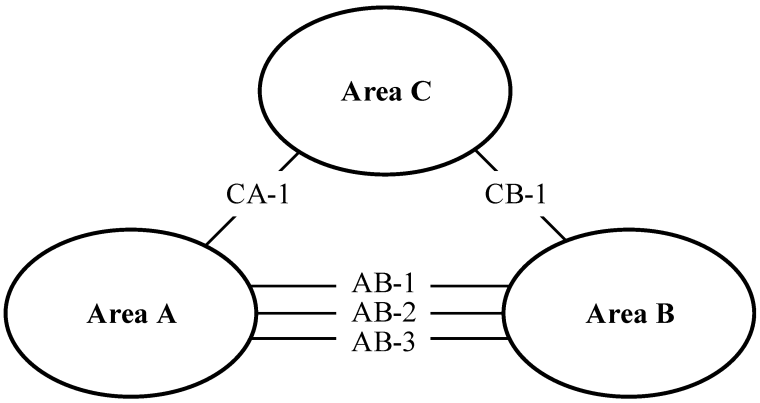

Source: adapted from Carvalho (2013).

bus 203; AB-2 connects bus 113 with bus 215; AB-3 connects bus 123 with bus 127. Area C is connected to Area B through line CB-1, which links bus 318 with bus 223. The transmission line CA-1 interconnects buses 325 and 121. The two-terminal DC transmission lines between bus 113 and bus 316 have not been considered. Table A.1, in Annex A, summarizes the interconnections between the areas of the IEEE-RTS 96.

Similar to the IEEE-RTS 79 case, IEEE-RTS 96 is modified to consider the variability of renewable resources. First, the hydro variability is considered and it is called IEEE-RTS 96 H (LEITE DA SILVA; SALES, et al., 2010). The second modification consists of replacing the coal unit of 350 MW with 1526 MW of wind power, increasing the total generation capacity to 11391 MW. This configuration is called IEEE-RTS 96 HW. However, in this case, the three areas are not identical due to the removal of the coal thermal unit and the wind farms addition. The three areas are composed by the groups of generation presented in Table A.2 (Annex A).

Therefore, Area A has a total generation capacity installed of 3939 MW, the generation capacity of Area B is equal to 3863 MW and Area C has the smallest generation capacity, 3589 MW.

To yield insights using the present state of the art, the IEEE-RTS GMLC 2019 is also utilized to test the algorithm proposed. It is an update of IEEE-RTS 96, proposed in Barrows et al. (2020), intended to introduce aspects adherent to modern power systems. The total generation capacity of region 1 is equal to 3628 MW. Changes in the generation system have been carried out, some generating units have been removed and some power plants using new technologies have been added. An additional generation has been added to some buses for each area. Table A.3, in Annex A, describes the amount of generation power capacity added to each bus (RTS-GMLC, 2018).

In addition, transmission lines 111-113, 211-213, and 311-313 have been removed to add transmission congestion on economic dispatch. The load of some buses, presented in Table A.4 (Annex A), have been changed for each region (area). The

capacity of the lines 114-116, 214-216, and 314-316 have been reduced to 350 MW. A new hourly regional load profile is utilized on system simulations (RTS-GMLC, 2018). The same levels of load uncertainty presented previously for other test feeders are utilized.

5.2.2 Iberian Peninsula power system

To perform simulations for real power systems, the Iberian Peninsula's equivalent interconnected power system is utilized. It is composed of the Portugal and Spain power systems. The data have been provided by the Portugal system operator, Redes Energéticas Nacionais (REN), taking into account the system of the year 2016. The Portugal electric power system has an annual peak load of 8.2 GW and a generation system with a nominal capacity of 19.62 GW, detailed by technology in Table B.1 (Annex B). The Portugal transmission system is composed of 512 buses, 466 transmission lines, and 300 transformers. Additional information, for instance, the type of conductors and static ratings for each season, have been obtained from REN (2018).

The Spanish electric power system has an annual peak load of 40.2 GW and an installed power capacity of 99.74 GW. The generation system is presented in Table B.2 (Annex B). The interconnections between Portugal power system and Spanish power system are presented in Table B.3 (Annex B). The hydro generating units of Portugal follow the hydro model of turbined volume to represent the fluctuations of capacity.

5.3 COMPOSITE SYSTEM RELIABILITY ASSESSMENT

This section aims to validate the SMCS method using the static reserve concept, present results about the impact of operating reserve requirements, and assess the performance of the system when operational flexibility aspects are considered on composite power system evaluations. Representation 01 is considered for all simulations of this section.

Models to represent the transmission network capacity variation and operational parameters of generating units are added to the SMCS. The analysis of these situations is addressed in the next subsections.

5.3.1 Validation of the SMCS algorithm

The validation of the SMCS method is performed using the IEEE-RTS 79 and the IEEE-RTS 79 HW configurations considering static reserve requirements. Table 5.7 contains the estimates of the LOLE, EENS, LOLF, and LOLD indices for the composite system of the IEEE-RTS 79 provided by the SMCS and the respective coefficients of variation (β) and intervals of confidence.

Table 5.7 – Composite system adequacy indices for the IEEE-RTS 79.

Indice	**SMCS**	**99% interval of confidence**	β **(%)**	**(LEITE DA SILVA; RESENDE, et al., 2008)**	**(CARVALHO, L. M. et al., 2012)**
LOLE (h/yr)	10.98	[9.97, 11.99]	3.56	10.483	10.733
EENS (MWh/yr)	1,384.0	[1,205.75, 1,562.24]	5.00	-	1,370.43
LOLF (occ/yr)	2.262	[2.10, 2.42]	2.81	2.265	2.293
LOLD (h/occ)	4.854	[4.30, 5.41]	4.44	4.728	4.681

Source: own.

The short- and long-term uncertainties, related to the load, are not considered for the analyzes using the static reserve concept. The estimates of the reliability indices are compared with the ones published in Leite da Silva, Resende, et al. (2008) and L. M. Carvalho et al. (2012). The confidence intervals have been calculated considering a 99% probability level.

The comparison of the intervals of confidence obtained with the SMCS method with the estimates of the indices reported in Leite da Silva, Resende, et al. (2008) and L. M. Carvalho et al. (2012) shows with 99% of confidence that the LOLE, EENS, LOLF, and LOLD intervals include the estimates obtained in these references (Table 5.7). The outcomes prove that the SMCS is suitable to assess the adequacy of power systems.

The estimates of the loss of load indices for the IEEE-RTS 79 HW (with 400 MW of wind capacity) are presented in Table 5.8 and they are compared with the ones published in L. M. Carvalho et al. (2012).

Table 5.8 – Composite system adequacy indices for the IEEE-RTS 79 HW.

Indice	**SMCS**	**99% interval of confidence**	β **(%)**	**(CARVALHO, L. M. et al., 2012)**
LOLE (h/yr)	11.60	[10.56, 12.63]	3.47	11.68
EENS (MWh/yr)	1,517.64	[1,322.22, 1,713.06]	5.00	1,531.96
LOLF (occ/yr)	2.39	[2.22, 2.55]	2.74	2.42
LOLD (h/occ)	4.86	[4.32, 5.40]	4.34	-

Source: own.

Assessing the intervals of confidence established using the SMCS, it is observed that the estimates of the adequacy indices published in L. M. Carvalho et al. (2012) are inside the intervals for all adequacy indices. Therefore, the results show that the proposed algorithm can model the time-dependency capacity of hydro and wind power plants.

Note that the performance of IEEE-RTS 79 HW in terms of adequacy indices is worse than the performance estimated for IEEE-RTS 79, even though an additional 400 MW of wind power plants has been added. As the main reason, the fluctuations related to the hydro and wind power capacity cause reductions in the generation capacity of

these power plants, diminishing the total system generation capacity.

5.3.2 Impact of operating reserve requirements

The approach presented herein is devised to highlight the influence of considering operating reserve requirements on reliability studies, reflecting a more realistic representation of the system's operation point of view. The pre-defined levels of the spinning reserve are established based on requirements indicated in ONS (2018), which reflects the concerns of the TSO about the Brazilian Interconnected System. The primary reserve is stated as 1% of the total load of the control area and the secondary reserve is 4% of the total load (2850 MW) of the area plus 6% of the wind power generation capacity. Taking it into account, the operating reserve requirements are settled as:

- Primary reserve = 28.5 MW;
- Secondary reserve:
  - RTS 79 and RTS 79 H = 114 MW;
  - RTS 79 HW = 138 MW.

Some relevant criteria of these simulations group are: short- and long-term load uncertainties are considered equal to 2% and 1%, respectively, and maintenance schedules of generators and transmission lines are not included in the simulation. The cycle up and down of generating units and transmission lines is considered. Table 5.9 shows the estimates of the reliability indices for three IEEE-RTS 79 configurations. All of the estimates of the reliability indices have achieved a relative error less than or equal to 5%.

Table 5.9 – Composite system (R01) reliability evaluation considering operating reserve requirements.

Indice	IEEE-RTS 79	IEEE-RTS 79 H	IEEE-RTS 79 HW
LOLE (h/yr)	28.93	41.02	26.47
EENS (MWh/yr)	2,942.73	4,916.17	2,655.40
LOLF (occ/yr)	23.75	27.24	21.68
LOLD (h/occ)	1.22	1.50	1.22

Source: own.

The uncertainty associated with wind power capacity is modeled using a persistence model. In an evaluation of the results presented in Table 5.9, the consideration of hydro capacity fluctuation, inherent to hydropower generating units, jeopardizes the system reliability. Namely, LOLE increases from 28.93 occ/yr to 41.02 occ/yr. On the other hand, the addition of 400 MW of wind power nominal capacity improves the reliability of the system, EENS is reduced by 37%, even though power fluctuations related

to wind capacity are also assumed. Similar behavior has been noted for static reserve simulations.

In an evaluation of the static and operating reserve perspectives, comparing the results presented in Table 5.7, Table 5.8 and Table 5.9, the operating reserve requirements bring with them to the simulation more realistic criteria, i.e., the total generation capacity is not available (scheduled) to meet the load due to operational costs. Since some generating units are not scheduled to meet the load, the short-term capacity variation related with the vRES, load uncertainties, and the generation stochastic behavior are factors that contribute to the system experiencing more failure states. The process of eliminating the hypothesis that all generating units of the system are available to meet load at any time required produces an analysis closer to reality, involving real challenges faced during the actual system operation.

5.3.3 IEEE-RTS 79 HW with generating units flexibility parameters representation

The results discussed in this section try to highlight the impact of generating units' operational constraints on the performance of composite power systems. Representation 01 (see section 2.6) is utilized in the simulations of this section. The proposed approach encompasses the operating reserve requirements considering additional aspects related to the generation flexibility. This methodology has been extended from Miranda (2020). The primary and up operating reserve amounts are the same as the ones utilized in IEEE-RTS 79 HW previous simulations and the down operating reserve is equal to 2.5% of the system nominal load plus 6% of the wind capacity (ONS, 2018), i.e., 95.25 MW.

The load uncertainties of the short and long-term are also considered. The operational parameters of dispatchable units, such as, ramp rates (MW/min), minimum operation power and MinDT, are presented in Table 5.10 (MIRANDA, 2020).

Table 5.10 – Generating units flexibility parameters for IEEE-RTS 79 HW assessments.

Unit size (MW)	Technology	Minimum down time (h)	Ramp rate (MW/min)	Min. power (MW)
12	Oil/Steam	2	1	3.6
20	Oil/CT	1	1	6.0
50	Hydro	-	7.5	2.5
76	Coal/Steam	4	2	22.8
100	Oil/Steam	8	7	30.0
155	Coal/Steam	8	3	46.5
197	Oil/Steam	10	3	59.1
350	Coal/Steam	48	4	105.0
400	Nuclear	1	20	200.0

Source: adapted from Miranda (2020).

To provide flexibility, as remedial action to generation meet the load, three hydro

units of 50 MW are assumed as having pumping capacity, so, they can operate as generation or load, according to the system requirements (UOR or DOR). The ramp rate data and MinDT are based on values presented in Christie and Dabbagchi (1993), where the up and down ramp rates are assumed the same. The minimum operation power is detailed for the main technologies in Schröder et al. (2013). The simulations have considered only generating units hot starts and dispatch is made through generation stacking considering economic criteria.

Another important parameter to be settled on evaluations considering the generation flexibility is the MR capacity. Specific generating units are selected to supply a minimum margin of stability (security operation) for the system. The MR total power generation is specified as 600 MW for the IEEE-RTS 79 HW. The MR capacity per bus is assigned as follows:

- 60 MW of a 76 MW unit connected to bus 102;
- 90 MW of a 100 MW unit connected to bus 107;
- 100 MW of a 155 MW unit connected to bus 115;
- 100 MW of each 155 MW unit connected to bus 123;
- 150 MW of a 197 MW unit connected to bus 113.

On the proposed approach, the capacity reduction of the flexible generation technologies is assigned as the main operational action. Eventually, this action may be not possible due to technical requirements and system uncertainties, causing intermittent technologies to get out of operation and/or hydropower plants to operate with pumping capacity.

Four indices are utilized to quantify events over DOR perspective, indicating events that are related to lack of flexibility to meet the load. The outcomes are presented in Table 5.11 for HL-I and HL-II (Representation 01). The composite system simulation considers generating units' and transmission lines' stochastic behaviors.

Table 5.11 – IEEE-RTS 79 HW downward reserve analysis considering generation flexibility.

Indice	**HL-I**	**HL-II**
GSE (h/yr)	4.73	1.97
GSF (occ/yr)	46.78	12.61
WIGE (h/yr)	56.95	30.51
WIGF (occ/yr)	154.74	62.48

Source: own.

The results presented in Table 5.11 characterize states with lack of flexibility. These states are characterized by conventional generation shedding where the waste

of renewable generation and/or pumping increasing (remedial actions) have not been enough to avoid conventional generation shedding necessary to power balance ($G = L$).

The impact evaluation of the spatial distribution of the generating units, which can be reproduced in composite system assessment, yields relevant insights about the performance of the power system when the flexibility aspects (parameters) of generating units are considered. In some situations (system state analysis), the violation of transmission circuit limits may occur and some remedial actions are necessary to avoid load shedding ($G < L$) or waste of renewable and/or conventional generation shedding ($G > L$), such as generation redispatch on OPF. The new operation point indicated by OPF may be sometimes not feasible due to operational constraints that restrict the increase/decrease of generation capacity from a specific generating unit, characterizing a system state with a lack of flexibility.

Moreover, there are other interesting insights to analyze when ramp rates and other flexibility parameters are assumed as conventional generating unit restrictions to meet load and respond quickly to renewable sources variations. In most real operation situations, the synchronous generating units control actuates to rapidly meet the load variations or cover renewable sources capacity variations, as consequence, no failure state is identified since it is almost instantaneous. The control associated with those units is not modeled on the representation of flexibility and then many of these failure states could not be avoided, however, if control aspects are represented adequately responding to small frequency variations.

On the other hand, the assessment of DOR requirements presents an interesting point of view for expansion and operation planning. The estimates for downward operating reserve indicate the expectation of experiencing waste of an intermittent and renewable generation. Therefore, this analysis aims to identify system states in which the excess of generation causes waste of renewable and intermittent generation technologies, generally, with low cost.

To improve the discussion over the influence of generating units' operational parameters representation into reliability evaluations, seven additional simulation cases have been proposed aiming to assess the impact of technological aspects connected with each generating unit. The proposal is to vary internal generating unit parameters, such as ramp rates and minimum operating power. Also, system inertial response is modified via MR power capacity criterion. The study cases are:

- Case A: ramp rates of generating units presented on Table 5.12, except the 76 MW unit, have been increased, and MR power capacity is maintained (600 MW);
- Case B: ramp rates are the same of Case A and individual MR power capacity has been spatially rearranged among generating units, as presented on Table

5.12. However, 600 MW has maintained as system MR power capacity;

- Case C: ramp rates are the same as Case A, however, MR power capacity of each generating unit settled on Case B is reduced by 50%. System MR power capacity is 300 MW;
- Case D: similar conditions of Case C with only an exception, system MR power capacity is unconsidered (0 MW);
- Case E: ramp rates of Case D are maintained for generating units of Table 5.12. Regarding 76 MW, 20 MW, and 12 MW units, the ramp rates are updated to 10 MW/min, 10 MW/min, and 6 MW/min, respectively. System MR power capacity is neglected (0 MW);
- Case F: nominal ramp rates (Table 5.10), nominal system MR power capacity (600 MW) and minimum operating power restriction is disabled for all generating units;
- Case G: minimum operating power capacity is disabled, ramp rates and MR power capacity have the same assumptions of Case B (data from Table 5.12).

Table 5.12 – Updates on generating units flexibility parameters (ramp rates and MR capacity).

Unit size (MW)	Ramp rate (MW/min)	Must-run (MW)
50	50	-
76	-	50 (Bus 2)
100	20	50 (Bus 7)
155	20	50 (Bus 15), 100 (Bus 23) and 100 (Bus 16)
197	20	100 (Bus 13)
350	20	-
400	20	150 (Bus 18)

Source: own.

The assessment of those seven cases is carried out by analyzing conventional generation shedding (GSE and GSF) and waste of intermittent generation (WIGE and WIGF) indices. Thus, the evaluation is conducted in terms of DOR requirements. Figure 5.10 displays conventional generation shedding indices and Figure 5.11 exposes the outcomes related to waste of intermittent generation.

The results show that generating units' operational parameters (ramp rates and minimum operating power) have a direct influence on system capacity in reducing its total generation amount to meet the load. Additionally, the spatial location of generating units selected to fulfill MR power requirement and the total (systemic) MR affects on system's ability on maintaining power balance ($G = L$).

Figure 5.10 – GSE and GSF for simulations case of IEEE-RTS 79 HW varying the generating units flexibility parameters.

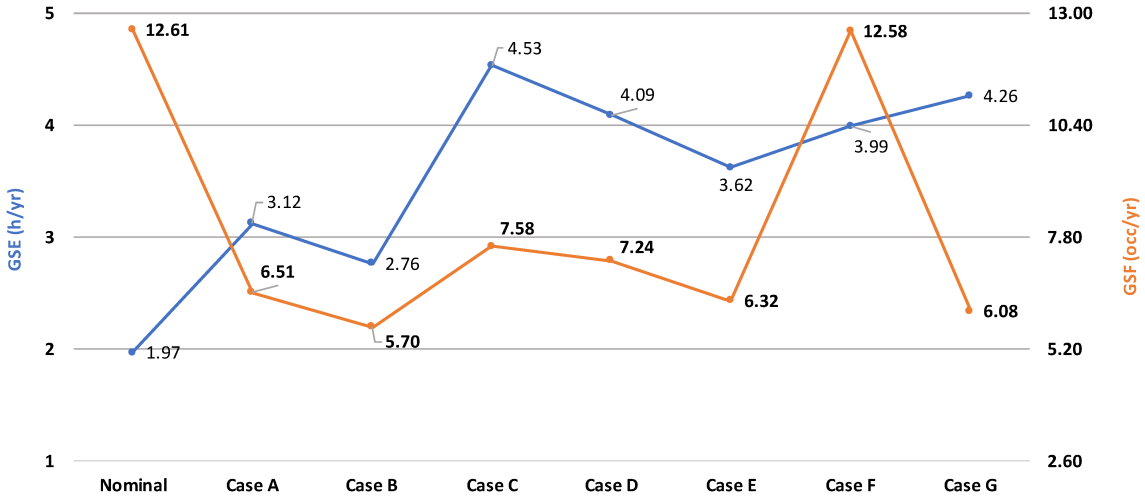

Source: own.

Figure 5.11 – WIGE and WIGF for simulations case of IEEE-RTS 79 HW varying the generating units flexibility parameters.

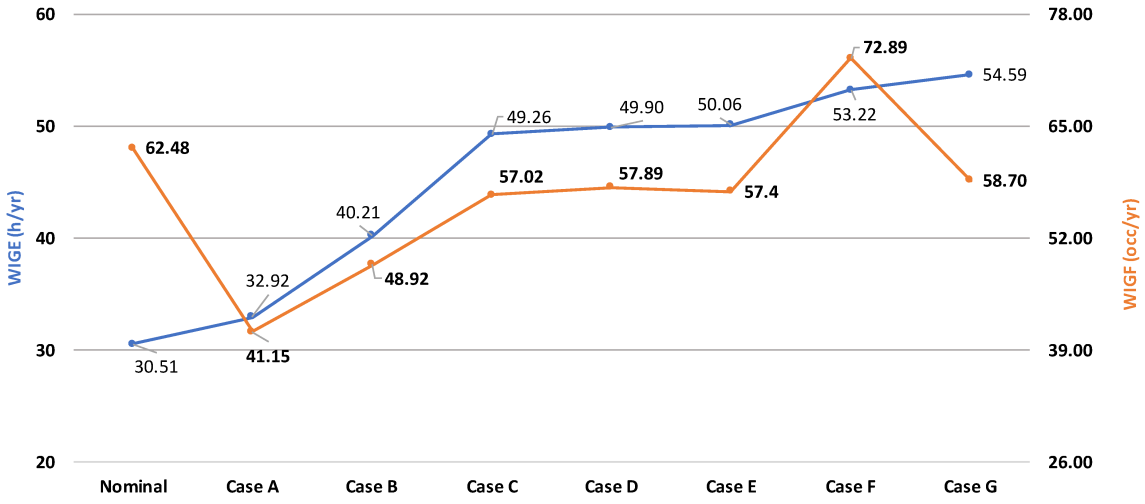

Source: own.

The evaluation of simulation cases posed on Figures 5.10 and 5.11 can be executed on a non-sequential manner. Cross assessments, selecting specific cases, can be performed. As an example, nominal case and case A assessment shows that faster ramp rates, technological characteristics applied for some generating units on case A, provide less frequency of conventional generation shedding (GSF) and waste of intermittent generation (WIGF) as well. However, the expectation of both events is augmented.

Another interesting situation can be observed when cases E and F are analyzed together. Case F has lower ramp rates and higher MR power capacity than case E. On

the other hand, case F has no restrictions connected with minimum operating power. So, case F presents, on average, two times more conventional generating shedding frequency with a higher expectation as well (GSF and GSE). A similar situation is identified when the waste of intermittent generation is analyzed (WIGF and WIGE).

In a general perspective, the indices estimates of cases A, B, C, D, E, and G show that rapid ramp rates bring benefits for system response in short periods. Case F and nominal case make use of nominal ramp rates and as consequence have the highest number of events that required conventional generation shedding, both with roughly 12.60 occ/yr (GSF).

Therefore, generating units minimum operating power, MR power capacity, and ramp rates are factors that affect directly system performance. The assessment of this group of cases yields important insights related to power system flexibility. It is important to emphasize that some practices featured in cases A to G may jeopardize the operational security of the system. In situations that $G > L$, the downward reserve is necessary to meet the load and preserve power balance, to fulfill this operational action generating units' internal parameters must be respected regarding each power plant type.

The evaluations using generating units' flexibility parameters are tentatives to be closer to security assessments. The control action of generating units is not represented in this thesis.

5.3.4 IEEE-RTS 79 HW with transmission flexibility

To vary the power capacity of the transmission lines, providing operational flexibility for the transmission network and at the same time respecting the conductor maximum allowable temperature, the analysis uses an annual hourly series for the wind speed (m/s), wind direction (°), ambient temperature (°C) and solar irradiance (W/m). A variation in weather conditions is generated over the IEEE-RTS in order to assess distinct weather regions. Additional data regarding specific weather conditions for each transmission line of the IEEE-RTS 79 HW are posed in Table F.1, in Appendix F. Table F.1 shows two types of conductors utilized in the simulation, one type of conductor for each system voltage level. There are three historical series for each weather parameter, representing three distinct historical years. At the beginning of each year of the simulation, one series for each weather parameter is sampled.

The conductor maximum temperature is a feature that relies on safety criteria and the physical condition of the conductor. It is related also to respecting the clearance-to-ground distance of the critical span (weakest span) of the line. Generally, typical values for the conductor design temperature are assumed to be between 65°C and 90°C. As exposed and addressed in section 5.1.2, each transmission line has a specific weather condition relying on the weather series obtained for three cities with

distinct meteorological conditions, namely, Florianópolis (Brazil), Saskatoon (Canada) and Porto (Portugal).

The simulation of the IEEE-RTS 79 HW with transmission system flexibility is performed considering the operating reserve assessment with the same criteria described in section 5.3.2. Also, the same short- and long-term load uncertainties are considered. Table 5.13 presents the estimates of the reliability indices considering three distinct T_c^{max}.

Table 5.13 – Adequacy indices for the IEEE-RTS 79 HW with transmission system flexibility per T_c^{max}.

Indice	**80℃, 90℃ and 100℃**
LOLE (h/yr)	20.86
EENS (MWh/yr)	2,479.47
LOLF (occ/yr)	20.52
LOLD (h/occ)	1.02

Source: own.

The analysis of Table 5.13 yields that the variation of the T_c^{max} has not presented a direct impact on the performance of the system in terms of reliability. Nonetheless, the transmission utilization factor (TUF) varies accordingly to the T_c^{max} considered. The annual average of transmission capacity, which is related to TUF, is an interesting parameter to be evaluated in this sense. The transmission line that connects buses 101 and 102, for instance, has an annual average capacity of 377 MVA with T_c^{max} equal to 80℃ and a capacity of 421 MVA with T_c^{max} equal to 100℃, reflecting an increase of 12% in line capacity. The conductor's maximum temperature is a predominant factor that needs to be evaluated in system planning and operation because it can change the system's point of operation. Also, a short-term conductor's maximum temperature can be utilized in emergencies to meet the load.

In a comparison with the results exposed in Table 5.9, the transmission system flexibility improves the performance of the system. The EENS index, for instance, is reduced approximately 7%, from 2671.54 MWh/yr to 2479.47 MWh/yr, mainly through decreasing the failures caused by transmission system limits violation. The main reason for that is the dynamic rating application.

5.3.4.1 Stressed transmission system case

To congest the transmission system of the IEEE-RTS 79 HW, the generation capacity and load are multiplied by 2, enforcing a high utilization factor of the transmission system. Table 5.14 shows the adequacy indices for this case with a static rating and with the transmission system flexibility (DLR). The operating reserve requirements have been also duplicated. The T_c^{max} is assumed equal to 80℃.

Table 5.14 – IEEE-RTS 79 HW adequacy indices: operating reserve needs with a stressed transmission system.

Indice	No flexibility (SLR)	Flexibility (DLR)
LOLE (h/yr)	4596.97	859.47
EENS (MWh/yr)	473,156.72	45,247.18
LOLF (occ/yr)	622.85	443.8
LOLD (h/occ)	7.38	1.94

Source: own.

The operating reserve analysis brings with them some operational constraints to the composite system assessment. The generation which is scheduled more frequently to meet the load in economic dispatch may be positioned in not strategic points of IEEE-RTS 79 HW, thus congesting the transmission system easily. In the case of the simulation involving SLR, the most of failures are occasioned due to transmission system congestion. To highlight the impact of DLR into the reliability assessment, the EENS index may be classified by failure type as exposed in Table 5.15.

Table 5.15 – EENS system index - contributions from G, T, and G&T.

IEEE-RTS 79 HW	G	T	G&T
No flexibility	1,356.15	467,006.58	4,793.95
Flexibility (DLR)	3,641.69	41,431.57	173.92

Source: own.

It is noted that, when DLR is considered, the share of EENS estimate occasioned only by transmission system failures, is roughly 10 times lower than the case study without DLR, reducing the LOLF due to transmission system failures as well. Fewer restrictions of power transmission capacity are encountered when DLR is implemented. The effects of use DLR are highlighted when transmission lines have a high utilization factor.

More insights about the impressions of DLR on the simulations can be observed assessing the loading of the transmission lines, as exposed in Table 5.16. It presents the TUF for the nominal and stressed transmission system cases. A monthly average for August is considered for both cases. Transmission line 23, which connects buses 116 to 117, is selected to illustrate the analysis.

Table 5.16 – Average transmission utilization factor - line 23.

IEEE-RTS 79 HW	TUF (%)	TUF (%) - DLR
Nominal system	64.08	32.95
Stressed system	90.00	59.30

Source: own.

The outcomes show that for both simulation cases the TUF is reduced with DLR

application, as expected. The DLR provides, on average, a higher capacity than the SLR, decreasing, for both cases, around 30% of TUF for this specific transmission line.

5.3.5 IEEE-RTS 79 HW with transmission and generation flexibility

The last group of simulations using IEEE-RTS 79 HW encompasses the combination of generating units' flexibility and transmission system flexibility via power plants' operational parameters and dynamic capacity estimation, respectively. Some simulation cases, established in section 5.3.3, are utilized in the analysis developed in this section. Other criteria already determined on previous simulations are maintained the same, such as (a) the three hydropower plants with pumping capacity; and (b) up and down operating reserve needs.

The assessment of down operating reserve indices is performed considering four study cases. Simulation results are shown in Table 5.17.

Table 5.17 – System flexibility analysis considering generation and transmission flexibility.

Indice	Nominal	Case A	Case C	Case G
GSE (h/yr)	1.59	3.00	3.27	3.90
GSF (occ/yr)	9.85	6.06	6.12	5.72
WIGE (h/yr)	32.28	33.21	48.00	54.74
WIGF (occ/yr)	62.44	41.53	55.78	58.82

Source: own.

Looking at the results presented in section 5.3.3, for the nominal case, it is observed that transmission system flexibility leads the system to less generation shedding states. The lack of down reserve flexibility is less frequent when DLR is considered as an operational action to improve flexibility. For instance, GSF is reduced by 21.89%, from 12.61 occ/yr to 9.85 occ/yr. This result can be justified by higher transmission power capacities generally provided by DLR, i.e., transmission bottlenecks limiting generating units point of operation are rarer to be encountered.

Results exposed in Table 5.17 shows that the frequency of conventional generation shedding and waste of intermittent generation is reduced from nominal case to case A. Focusing on case C, it is noted that transmission system flexibility brings some advantages to system performance related to capacity on responding to down operating reserve needs, reducing expectation and frequency of conventional generation shedding events. Evaluating Figure 5.10 and Table 5.17, reductions of 27.81% and 20.05% can be identified on GSE and GSF estimates, respectively.

Therefore, the DLR can be classified as an operational action that provides flexibility to power systems. It can reduce the number of events that might experience transmission capacity limit violation and aiding to find a feasible system point of operation after contingencies or sudden generation/load variations, for instance.

5.3.6 IEEE-RTS GMLC 2019

This section is concerned with assessing an updated IEEE-RTS configuration, named IEEE-RTS GMLC 2019. Firstly, the analyses consider the static and operating reserve perspectives. The reliability test system has been positioned in the Southwestern United States region, covering an area extending roughly from Los Angeles to Las Vegas. This IEEE-RTS update aims to introduce some congestion via the changes documented in Barrows et al. (2020) and described in section 5.2.1. The operating reserve requirements are established based on the same criteria used for other test systems (ONS, 2018). The reserve requirements are:

- Primary reserve = 28.5 MW;
- Up secondary reserve = 114 MW;
- Down secondary reserve = 71.25 MW;

The simulations are carried out considering only 1 region (area), assuming the data presented in RTS-GMLC (2018) and Barrows et al. (2020). Initially, in the first case simulated, wind power, solar photovoltaic, concentrating solar power, and storage technologies are not considered. The hydro variability follows the same monthly proportional values of IEEE-RTS 79 HW. Generating units and transmission lines' stochastic behaviors are assumed in the simulation. The estimates of the reliability indices are presented in Table 5.18, ensuring a coefficient of variation of 5% for the SMCS.

Table 5.18 – Adequacy indices for composite system evaluation of the IEEE-RTS GMLC 2019.

Indice	Static reserve	Operating reserve
LOLE (h/yr)	2.16	55.49
EENS (MWh/yr)	209.95	2,264.34
LOLF (occ/yr)	0.92	37.23
LOLD (h/occ)	2.36	1.49

Source: own.

The adequacy indices, from Table 5.18, in terms of static reserve assessment, depend on the equipment availabilities, capacity fluctuations and load uncertainties. However, operating reserve assessment depends not only on the conditions previously mentioned, but also on operational parameters of the generating units (e.g., start-up times), prespecified primary and secondary reserves criterion, and operation strategies (dispatching functions, must-run units, etc.) (LEITE DA SILVA; SALES, et al., 2010).

In the operating reserve assessment, the congestion observed for this new IEEE test system configuration, in some situations, may limit the incremental generation capacity of some synchronized generating units due to transmission capacity violations. In a comparison with the results presented for IEEE-RTS 79 HW, exposed in Table

5.9, the LOLE of IEEE-RTS GMLC 2019 configuration is roughly four times higher. The analysis of the expected energy not supplied (EENS) index by failure type provides that 1,626.70 MWh/yr (71.84%) of 2,264.34 MWh/yr are originated from transmission system failures, indicating that the enforced bottlenecks imposed by this configuration are really impacting the system performance.

In this sense, the following evaluation is performed regarding DLR application based on weather patterns experienced in the Southwestern United States. The objective is to assess the impact of DR on a system that has been designed with the idea to cause transmission system congestion. The weather data from Los Angeles have been considered for DLR calculations (JRC-PVGIS, 2020; JAGER; ANDREAS, 1996). Lines of 138 kV are assumed to be built with a Drake conductor and lines of 230 kV with a Bluejay conductor, similar to the assumptions considered for other IEEE-RTS configurations. The estimates of the adequacy indices for this case are presented in Table 5.19.

Table 5.19 – Composite system reliability evaluation of the IEEE-RTS GMLC 2019 considering DLR.

Indice	**Static reserve**	**Operating reserve**
LOLE (h/yr)	0.98	10.66
EENS (MWh/yr)	107.31	884.62
LOLF (occ/yr)	0.40	11.86
LOLD (h/occ)	2.43	0.90

Source: own.

The conductor maximum allowable temperature is settled as 80 ℃. It is possible to perceive that the DLR has a positive contribution on system performance since the simulation considering the DLR application experiences less failure states due to the higher capacity of the transmission lines. For instance, LOLE estimate decreases from 55.49 h/yr to 10.66 h/yr, when DLR is applied in the operating reserve assessment, representing a reduction of about 80%. The static reserve assessment, in its turn, reveals that the LOLD estimate remains roughly the same in comparison with the scenario without DLR, however, LOLE is reduced by approximately 55%.

The failure contribution share occasioned by the transmission system is reduced considerably related to the case without DLR (lines with fixed limits). System failures induced only due to transmission system bottlenecks are responsible for 257.95 MWh/yr of total load shedding, representing 29.16% of the EENS index.

To illustrate the discussion, Figure 5.12 exhibits the DLR and SLR of transmission line 1 that connects bus 101 to bus 102. This line has a static rating of 175 MVA.

As can be noted, higher capacities are encountered in months of winter. However, lower transmission capacities are found in summer months, generally, due to the higher ambient temperature, a factor that increases the heat gain and jeopardizes the

Figure 5.12 – Monthly average transmission capacity of line 1.

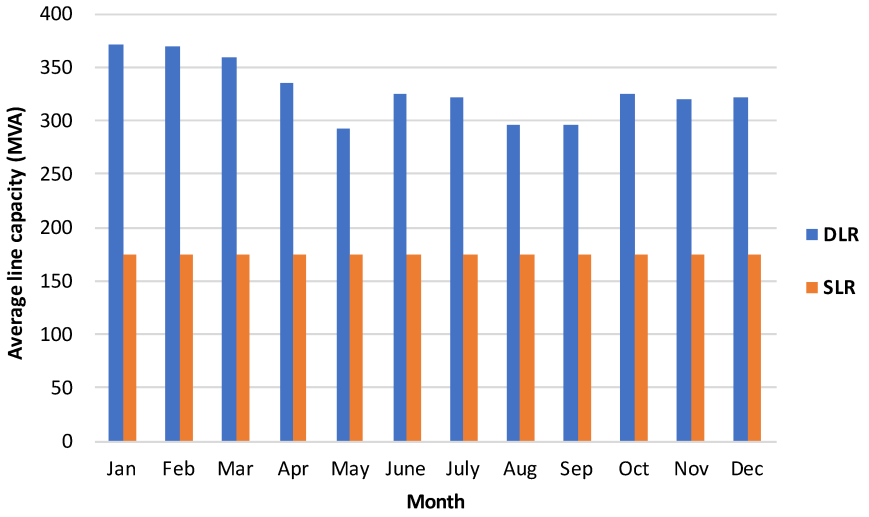

Source: own.

convective cooling, imposing to the conductor a lower electric current to maintain the heat balance.

5.3.6.1 Study cases considering generating units flexibility parameters

To complete the analysis perspective of this new IEEE-RTS configuration, two simulations are performed to assess the generation operational flexibility, taking into account the data provided in RTS-GMLC (2018). Table 5.20 presents the operational parameters, technology, and unit size for the generating units of these simulation cases. Also, the system MR capacity value is settled as 650 MW and only hot starts of generating units have been considered. DLR has been considered in both simulation cases.

Table 5.20 – Flexibility parameters for the IEEE-RTS GMLC 2019 configuration.

Unit size (MW)	Technology	Minimum down time (h)	Ramp rate (MW/min)	Min. power (MW)
12	Oil/Steam	2.0	1.0	5.0
20	Oil/CT	1.0	3.0	8.0
50	Hydro	-	50.0	-
55	Gas/CT	2.2	3.7	22.0
76	Coal/Steam	4.0	2.0	30.0
100	Oil/Steam	8.0	7.0	30.0
155	Coal/Steam	8.0	3.0	62.0
350	Coal/Steam	48.0	4.0	140.0
355	Gas/CC	4.5	4.14	170.0
400	Nuclear	48.0	20.0	396.0

Source: own.

It is emphasized that for this first study case, all power plants are dispatchable, vRES are not considered, and generating units operational parameters obtained from

RTS-GMLC (2018) are distinct from the ones utilized on IEEE-RTS 79 HW configuration.

DOR reserve indices estimated are presented on Table 5.21. For this first case, as no renewable intermittent generating units are integrated into the system, WIGE and WIGF are null and every downward reserve requirement needs to be attended by conventional generating units, indicating that, on average, the system experiences 102.36 occ/yr of generating units shut down.

Table 5.21 – System flexibility analysis considering generation and transmission flexibility.

Indice	Nominal Case	Case with vRES
GSE (h/yr)	90.14	1.85
GSF (occ/yr)	102.36	20.76
WIGE (h/yr)	-	67.69
WIGF (occ/yr)	-	137.23

Source: own.

The representation applied to characterize the operational actions of the generation fleet eliminates the hypothesis that all scheduled generating units can respond instantaneously to any increase or decrease in load level. In a real-time operation, a generating unit must respect ramp rates, MinDT, MinUT, minimum technical power, must run values, and so on.

For the second case, a modification is performed to highlight the impact of intermittent generation source penetration on real-world power systems. It consists of replacing all conventional additional generating units described in Table A.3 by wind and solar photovoltaic power plants, aiming at verifying the impact on the flexibility of the generation system. This substitution brings with them power fluctuations of these intermittent sources and a reduction of the capacity of the system on responding to sudden changes to meet the load since controllable units are replaced by non-dispatchable units. Hourly historical series with capacity factors are utilized to represent wind and solar power variability.

In order to evaluate the system performance properly, the operating reserve requirements need to be updated due to wind and solar generating units integration. The reserve needs are (ONS, 2018):

- Primary reserve = 28.5 MW;
- Up secondary reserve = 151.2 MW;
- Down secondary reserve = 108.45 MW;

The solar photovoltaic panels are added to buses 1, 7, and 15, and wind power farms are added to buses 15 and 23. It is assumed that for buses 15 and 23, 160 MW

is added instead of 155 MW because each wind farm is considered to have 80 wind turbines of 2 MW each. The total generation capacity is 3638 MW, an increase of 10 MW in comparison with the original test system configuration.

The results for this second case simulation are presented in Table 5.21. It is concluded that 610 MW of conventional generation replacement, which is controllable and provides flexibility, by 620 MW of solar and wind power plants gives profits for the system in terms of conventional generation shedding. However, the waste of intermittent renewable generation is required.

The outcomes show that the actual massive integration of vRES needs to be assessed carefully to verify the real impact on the system performance regarding the overall generation fleet. In some situations, the study of electromechanical and electromagnetic transitory phenomena is required for a more precise assessment of the power system operating condition. The impact on system operation cost is also another issue that needs to be evaluated for a more complete analysis of the system performance.

5.4 MULTI-AREA SYSTEMS RELIABILITY ASSESSMENT

Besides single area evaluations, this thesis presents evaluations over multi-area operation of power systems. The proposed approach can model operational procedures and market agreements between electrical areas. Three different supporting strategies are evaluated in terms of system performance to establish a market agreement that benefits the multi-area system. Representations 02 (R02) and 03 (R03) are utilized to study the performance of the IEEE-RTS 96 HW and Iberian Peninsula power system, which is composed of two electric areas: Portugal and Spain.

Similar to the previous simulations encompassing single-area systems, maintenance actions in transmission lines, interconnections, and generators are not considered in the following simulations.

5.4.1 IEEE-RTS 96 HW

To study the performance of the IEEE-RTS 96 HW, simulations considering the two multi-area representations (R02 and R03) are carried out. The simulations are based on four study cases:

- Study case 1: IEEE-RTS 96 HW multi-area operation.
- Study case 2: IEEE-RTS 96 HW multi-area operation with operational flexibility in interconnections (tie-lines).
- Study case 3: IEEE-RTS 96 HW multi-area operation with operational flexibility in interconnections and transmission networks.

- Study case 4: IEEE-RTS 96 HW multi-area operation with operational flexibility in generation, main transmission network, and interconnections.

Each study case has its particularities and the objective is to assess the influence of distinct operational flexibility issues. For study case 1, the adequacy indices are computed using the three market strategies for the multi-area operation and the two representations. The operating reserve requirements are distinct for each electric area because each one has a different total generation capacity installed, as exposed in Table A.2. Analogously of the single area studies, the criteria used to calculate the reserve needs of each area are based on ONS (2018). Therefore, the criteria for Area A are the same as Area C and Area B has a lower requirement of the secondary operating reserve due to its different wind power capacity, as follows.

- Area A and Area C: primary reserve equals 28.5 MW and secondary reserve equals 146 MW.
- Area B: primary reserve equals 28.5 MW and secondary reserve equals 141.48 MW.

Table 5.22 presents the indices for both representations and for each multi-area operation strategy.

Table 5.22 – IEEE-RTS 96 HW without operational flexibility aspects.

Indice	**Market**		**Assistance**		**Hybrid**	
	R02	R03	R02	R03	R02	R03
LOLE (h/yr)	0.34	0.44	0.90	9.44	1.05	4.25
EENS (MWh/yr)	51.96	50.57	130.54	328.02	81.72	173.78
LOLF (occ/yr)	0.22	0.32	0.52	3.20	1.53	3.45
LOLD (h/occ)	1.53	1.39	1.71	2.95	0.68	1.23

*R02: multi-area single bus with interconnections and R03: multi-area with transmission network of the main system.
Source: own.

It is noticed that the reliability indices are connected with the multi-area operation strategy. Besides, the outcomes emphasize the influence of system representation, mainly for assistance and hybrid strategies, which corroborates the relevance of concerns about the modeling applied in reliability studies.

Focusing on the assistance-based strategy for multi-area operation, the R03 shows that the power flow analysis and the meshed grid impact directly on the reliability indices. The global LOLF, for instance, increases from 0.52 occ/yr to 3.20 occ/yr, mainly due to the consideration of the transmission network of the main system what affects the energy balance of the system. This strategy has the worst reliability indices due to its main principles that assume as premises that each area has its unit commitment (individual basis) and no-load-loss sharing is imposed. Each system tries to meet its

load and reserve requirements, and if necessary, tries to cover the deficit through import action whether there is available capacity to export in neighboring systems (areas).

For the market-based strategy, where commercial exchanges between areas are evidenced by prioritizing the dispatch of the lower cost generating units, the level of representation of the multi-area system seems to not affect directly on the reliability indices. The unit commitment is carried out on a unified basis, therefore, generating units from any area can be committed to meet the load and reserve requirements of other areas.

In terms of reliability indices, the results indicate that the market-based strategy leads to a better performance of the multi-area system operation. However, some definitions need to be deeply studied, such as the establishment of the priority list of supported areas for situations in which there is a need for load shedding.

The second set of simulations, study case 2, is performed assuming that the flexibility of the power capacity is only applied in the interconnections between areas. The weather conditions are selected hypothetically for each interconnection line and those specifications are exposed in Table F.2. The estimates of the adequacy indices are presented in Table 5.23.

Table 5.23 – IEEE-RTS 96 HW with flexibility in interconnections.

Indice	**Market**		**Assistance**		**Hybrid**	
	R02	R03	R02	R03	R02	R03
LOLE (h/yr)	0.26	0.32	0.90	9.40	0.98	3.46
EENS (MWh/yr)	45.19	44.81	130.48	327.45	75.46	159.67
LOLF (occ/yr)	0.17	0.20	0.52	3.17	1.50	2.82
LOLD (h/occ)	1.52	1.61	1.71	2.97	0.66	1.23

*R02: multi-area single bus with interconnections and R03: multi-area with transmission network of the main system..
Source: own.

The results show that the varying power capacity of interchanges is not a direct restriction for the generation to meet the demand of this multi-area test system, either on R02 or R03. The failure states are more connected with generation capacity problems and restrictions on the transmission network of the main area.

To complement the analysis, still considering the operating reserve requirements, study case 3 is simulated considering that the DR is extended to the transmission network of the main system. The aim is to verify the effects of DR on tie lines and transmission network of the main system (principal area), covering all the lines of the IEEE-RTS 96 HW configuration. The estimates of the adequacy indices are presented in Table 5.24. The simulations are realized by using R03 only, which is the level of representation that permits the implementation of DLR in interconnections and transmission network of the main system.

The addition of DLR on the transmission network of the main area provides

Table 5.24 – IEEE-RTS 96 HW with flexibility in interconnections and transmission network.

Indice	Market	Assistance	Hybrid
LOLE (h/yr)	0.26	0.88	0.98
EENS (MWh/yr)	41.78	121.21	72.33
LOLF (occ/yr)	0.17	0.51	1.49
LOLD (h/occ)	1.51	1.72	0.66

Source: own.

an improvement on system global reliability. The EENS, for instance, is reduced 7%, 63%, and 54% for market-, assistance-, and hybrid-based strategies, respectively, in comparison with outcomes presented in Table 5.23. Figure 5.13 exhibits the LOLE index in an illustrative and summarizing form for the three previous study cases and every multi-area operation strategy.

Figure 5.13 – Comparison among different multi-area operation strategies and lines operational flexibility.

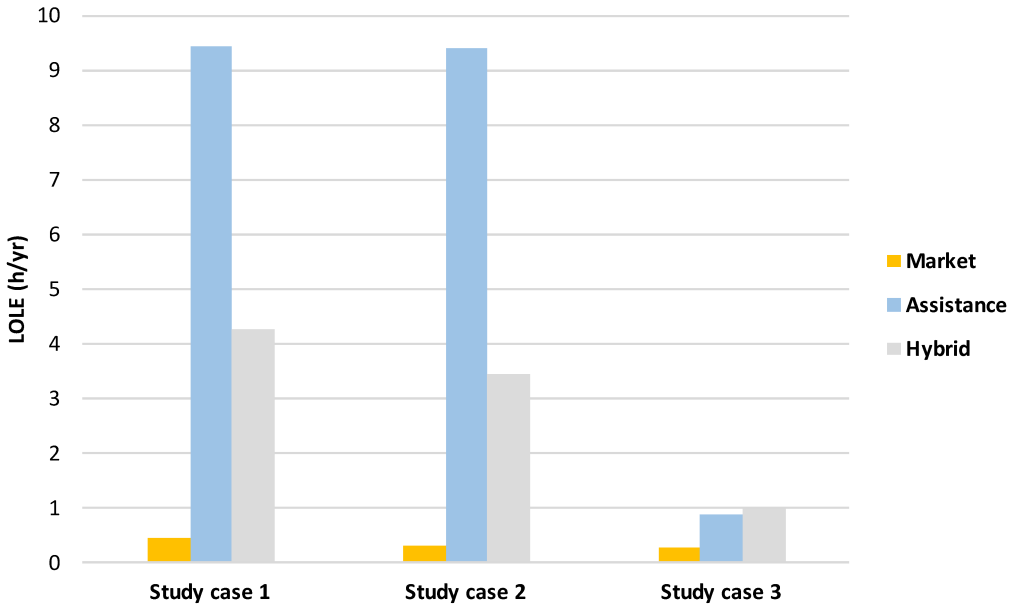

Source: own.

Analyzing Figure 5.13, it is possible to conclude that the assistance-based strategy to operate multi-area systems is the worst in terms of loss of load expectation. On the other hand, the market-based strategy is the best choice to be applied for a multi-area market agreement. This strategy is concerned with the well-being of the three areas that compose this multi-area test system since the unit commitment is carried out on a unified basis (generating units from any area can be committed to meet the load and reserve requirements of other areas). Also, the DLR may improve the performance of the system, bringing evident benefits. It is capable to reduce the estimate of the indices, mainly when its application is extended to the transmission network of the main

system. The advantages inherent in transmission lines with variable power capacity (operational flexibility) are more noticeable in assistance and hybrid-based strategies.

The last assessment is devoted to studying the impact of generating units' operational parameters together with dynamic line ratings. Study case 4 considers the multi-area operation with generation and transmission flexibility aspects. The simulations have criteria to represent the operational flexibility of generating units, transmission networks, and interchanges (tie lines).

The generating units operational parameters from nominal case, presented on section 5.3.3 (Table 5.10), are assumed for each electrical area. The estimates of DOR indices are exhibited on Table 5.25. They try to highlight the effects on system capacity in reducing its total generation to meet load induced by the restrictions provoked by generating units' operational parameters, such as upward or downward ramp rates, start-up times, MinDT, and so on.

Table 5.25 – IEEE-RTS 96 HW with flexibility in generation and transmission systems.

Indice	**Market**	**Assistance**	**Hybrid**
GSE (h/yr)	0.38	4.34	1.67
GSF (occ/yr)	30.12	168.60	8.40
WIGE (h/yr)	2.47	38.28	102.22
WIGF (occ/yr)	170.94	446.20	210.80

Source: own.

It is noticed, from Table 5.25, the influence of multi-area operation strategy onto down operating reserve performance. For example, a market-based strategy has the lowest GSE index (0.38 h/yr). The hybrid strategy presents the lowest value of the GSF index (8.40 occ/yr). Regarding vRES, the expectation and frequency of waste of intermittent renewable energy (WIGE and WIGF) are the lowest when the market-based strategy is adopted. Therefore, the worst performance scenario for DOR indices is observed with the assistance-based strategy, and the best scenario is envisioned with a market-based strategy. This latter strategy permits that reserve requirements can be covered by any electrical area, enhancing multi-area system flexibility.

The outcomes show the relevance of considering such reserve aspects and strategies in power system planning activities. The assumption that since a generating unit is committed to meet load in a small time frame (operating reserve), independently of its ramp rate, start-up time, MinUT or MinDT, is unrealistic from the operation point of view. These restrictions need to be handle with on real-time operation of power systems and they can lead to loss of load ($G < L$) and/or lack of flexibility to reduce generation capacity ($G > L$).

5.4.2 Iberian Peninsula power system: real application of transmission system flexibility

The Portugal power system is connected with the Spanish grid through nine interchange lines. The interconnections are spread out over the border between Portugal and Spain. The details related to each interchange line are presented in Table B.3 (Annex B). Some study cases are simulated in order to yield insights about the Portugal - Spain interconnected power system, devoting to assess the reliability of the multi-area system in distinct perspectives, such as:

- Case 1: reliability evaluation of Iberian Peninsula power system (R02);
- Case 2: reliability evaluation of Iberian Peninsula power system (R02) considering the interchanges with dynamic rating;

The operating reserve requirements are defined weekly. These values have been provided by REN. The short- and long-term load uncertainty parameters are assumed as the same utilized on the test systems simulations, 2% and 1%, respectively. The pumping capacity of both areas is enabled for all cases and the hydro generating capacity follows the energetic-based approach presented in section 2.9.5.

Simulations without transmission line flexibility consider that the lines have power capacity fixed by winter weather conditions (REN, 2018), where the ambient temperature is assumed to be 15℃.

Devising to analyze the utilization of DLR systems on Portugal - Spain interconnections, three annual hourly series for wind speed, wind direction, irradiance, and ambient temperature are used to estimate the dynamic ampacity of the nine interconnections (Table B.3). The interchange lines are inside six macro-regions that have been identified on the Iberian Peninsula's geographical map. The macro regions have been determined based on busbars of Portugal power system, they are: Alto Lindoso, Lagoaça, Falagueira, Alqueva, Pocinho and Tavira (JRC-PVGIS, 2020).

Table 5.26 presents the estimates of global and per area reliability indices combining results of simulation cases 1 (SLR) and 2 (DLR). Both cases consider operating reserve requirements and Representation 02 (R02). The impact of the strategy used to guide the multi-area operation is assessed through the market, assistance, and hybrid-based strategies.

Assessing Table 5.26, it is observed that the existing agreements between the TSO reflect on distinct reliability performance for each area. The market-based strategy for multi-area operation conducts a uniform sharing of the risk of failures since both areas have the same level of supporting priority and the unit commitment process is carried out on a unified basis. On the other hand, an assistance-based strategy contributes to reducing the global risk of failure. The Portugal power system, especially,

Table 5.26 – Iberian Peninsula reliability evaluation using R02 and three strategies for multi-area operation.

Indice	**Market based strategy with SLR**			**Market based strategy with DLR**		
	Global	Portugal	Spain	Global	Portugal	Spain
LOLE (h/yr)	26.05	26.00	25.79	26.01	25.96	25.75
EENS (MWh/yr)	11368.22	5719.29	5648.85	11366.91	5718.58	5648.26
LOLF (occ/yr)	24.94	24.86	24.72	24.91	24.83	24.69
Indice	**Assist. based strategy with SLR**			**Assist. based strategy with DLR**		
	Global	Portugal	Spain	Global	Portugal	Spain
LOLE (h/yr)	18.62	1.46	18.37	18.62	1.46	18.37
EENS (MWh/yr)	8170.85	229.80	7941.05	8170.85	229.80	7941.05
LOLF (occ/yr)	18.25	1.49	18.03	18.25	1.49	18.03
Indice	**Hybrid based strategy with SLR**			**Hybrid based strategy with DLR**		
	Global	Portugal	Spain	Global	Portugal	Spain
LOLE (h/yr)	56.56	37.88	21.11	56.53	37.85	21.11
EENS (MWh/yr)	16673.93	7786.24	8887.68	16664.12	7776.51	8887.60
LOLF (occ/yr)	52.08	35.08	19.68	52.04	35.03	19.68

Source: own.

presents a reduction in EENS from 5719.29 MWh/yr to 229.80 MWh/yr, representing a decrease of 96%, comparing the market and assistance-based strategies. The Spain power system, in its turn, has an increase of 44% on the amount of energy not supplied during a year, despite the reduction on LOLE from 25.79 h/yr to 18.37 h/yr. Therefore, the period of failure duration has been reduced, however, the magnitude of the loss of load events has been higher for the Spain power system.

From a global perspective point of view, the market-based strategy presents the best performance in terms of reliability for the Iberian Peninsula power system and the hybrid-based strategy has the highest risk of loss of load. Meanwhile, the analysis of the assistance-based strategy reveals that most failure events occur due to Spain's power system bottlenecks. This remark is possible to be interpreted by the results provided by the market-based strategy simulation, where Portugal's power system assumes part of the risk of failure from Spain.

Even though the reliability indices remain the same on study cases 1 and 2, independently of the multi-area operation strategy assumed, the transmission capacity of the interchanges is directly affected by the DR considered on the simulation. For instance, the interchange Alqueva - Brovales has an annual average of 1638 MVA of static capacity, however, when DLR is assumed this capacity grows to 2383 MVA, representing an increase of 45%. The most of failure events are occasioned by generation failures, explaining the results presented by the adequacy indices of Table 5.26. The improvement in interchange line capacity has not led the multi-area system to higher performance.

Figure 5.14 illustrates a comparison among monthly average transmission capacity calculated using the dynamic rating methodology and the thermal limits for each

season described in REN (2018). The analysis is carried out for Pocinho - Saucelle interconnection.

Figure 5.14 – Monthly average transmission capacity of Pocinho - Saucelle interconnection.

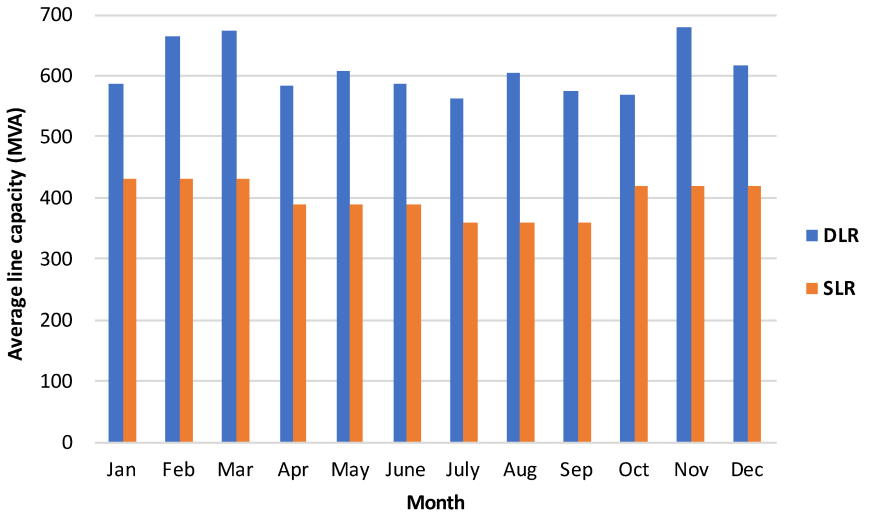

Source: own.

The analysis of Figure 5.14 implies that the DLR provides, on average, a higher capacity than the static rating for each month of the year. Namely, in November, the contribution is highlighted, the dynamic ampacity provides a transmission capacity of 680 MVA, on average. This value is 62.68% higher than the static rating for that month (418 MVA). It is noted that every month has a distinct behavior on the dynamic rating because of this total dependency on wind speed, wind direction, ambient temperature, and solar irradiance. The evaluation of the results, in general, shows that the interconnections present capacities, on average, higher than the static ratings during the year. Actually, on the simulation approach considering DLR, a dynamic transmission capacity is attributed for each simulation hour what on average represents a higher capacity than the static rating provided.

To complement the analysis of these real cases, a static reserve capacity assessment for the Iberian Peninsula power system has been performed. The results are not presented directly in this thesis because they may lead to unrealistic remarks about the multi-area system's reliability. In these simulations, assuming R02, the multi-area system operation has not presented failure states on this kind of approach. The Iberian Peninsula system has a total generation capacity of 119.36 GW and a total peak load of 48.4 GW. In fact, the probability of the multi-area operation experiences failure states is low assuming a static reserve assessment since the generation capacity is more than two times higher than the load value.

6 FINAL REMARKS

In power systems, a considerable fraction of doctoral theses contributions is directed to performance analysis. Due to the peculiar characteristic of the large implements and components of the power systems, the field of models and simulations is very required for the elaboration of studies and conception of advance in this research area. However, this thesis inaugurates a new vision related to contributions at the doctoral level to the power systems area.

The author of this thesis has been part of a multidisciplinary team in a research project that sought to implement new technologies at the service of power systems. The objectives of the project are merged, in large part, with the objectives of this thesis. In this sense, the technological contributions achieved in the scope of this project grant the proposition of new models and new solutions for the field of power systems analysis.

Following the digitization path, the transformation and/or conversion of traditional components of power systems, such as insulators, into active elements linked to smart grids with granular observation capacity of electrical, mechanical, and thermal variables, tends to be a route of work for the coming years, transforming power systems into systems with greater resilience and flexibility, as proposed by the author in the introduction of this work (see Figure 1.2). Inserting capacities into key components of the power system will allow a smooth transition from passive to active systems, improving the system's responsiveness in steady-state and during transients.

Bearing in mind that framework, this thesis promotes a scientific and technological basis to address the power system transition, which has been occurring since the beginning of the 21st century. Therefore, the main outcomes can be divided into three distinct perspectives: (a) proposition of a methodology to assess technological advances; (b) technological author contributions related to R&D project (segment II); and (c) scientific author contributions (segment III), which are connected with new models and probabilistic methods for power system analysis.

6.1 TECHNOLOGICAL ADVANCES IDENTIFICATION

In order to identify the technological advances reached in this thesis, a methodology based on the definition of maturity levels is utilized to measure and classify the technological contributions achieved during the thesis elaboration. The methodology proposed is based on TRL concept, which defines nine technological maturity levels, from 1 to 9, where level 1 represents the first step of the innovation chain, reporting and observing the basic principles of the future prototype, and level 9 is the highest rating, indicating that the technological device can be used on large scale in operating environments (see Figure 3.1). Therefore, the proposed methodology is applied to position the developments of the author of this thesis under the technological perspective.

6.2 TECHNOLOGICAL CONTRIBUTIONS

Technological contributions promoted by the author takes into account the TECCON II research project results. Those contributions are consolidated based on TRL of each development (see sections 3.2 and 3.3), where the main tasks performed by the author to materialize the TECCON MS installation in an operating environment (TRL 7) have been presented, such as:

- Optical circuit update: replacement of optical couplers, power adjustments, and establishment of an adequate level of power at photodetectors input;
- FBG strain and temperature sensors operation using OESPU: calibration;
- Electric current sensor operation using OESPU: calibration;
- TECCON Application Programming Interface: modifications in web application and software update;
- Installation of TECCON MS on a 230 kV transmission line: positioning and encapsulating of all units.

Hence, the TRL of the research project has migrated from level 4 to level 7 due to the technological contributions. Additionally, as discussed in the state of the art (chapter 2), different companies produce different equipment for DR data collection, where the monitoring system can have distinct required measurements and proposed approaches for ampacity calculations. In this sense, Table 6.1 shows a comparative framework about the main characteristics and functions of the TECCON MS and other existing real-time monitoring systems for evaluation of the overhead line conditions.

Table 6.1 – Comparison between different real-time monitoring systems.

Monitoring system name	Weather forecast	Conductor temperature evaluation	Tension monitoring	Line sag measurement	Clearance-to-ground measurement	Optical sensors application
TECCON MS	x	x	x			x
CAT-1™	x	x	x			
Power Donut®		x		x		
SONAR					x	
EMO		x				
TLM		x			x	
Ampacimon				x		
Sagometer	x	x	x			
SAGSEC				x		x

Source: adapted from Morozovska and Hilber (2017).

Therefore, as can be noted by analyzing Table 6.1, TECCON MS presents common characteristics when compared to other existing real-time monitoring systems,

however, one of the advantages of it is the number of variables monitored and the optical principles used in measurements. Namely, TECCON MS utilizes optical sensors to monitor line conditions, and is capable to provide data from distinct measurements (temperature, mechanical tension, weather conditions) in order to estimate DLR, offering some redundancy of information. It can be viewed as an alternative for the overhead lines monitoring systems market.

6.3 SCIENTIFIC CONTRIBUTIONS

As the renewable energetic potential increases worldwide, mainly pushed by solar and wind power sources, there is a need to maximize transmission grid capacities in order to drain the electricity generation to the large points of consumption. Whereas the location and construction of solar and wind generation facilities are relatively easy, it is becoming increasingly difficult to construct new transmission lines. Therefore, electric power authorities around the world are looking for new ways to maximize existing power lines capacities.

The proposed DLR-based technology method explores the idea of a transmission line rating may be variable and dynamic, instead of static, depending upon the actual weather conditions. It has been applied to assess the impact of considering the capacity of the transmission line as a time-dependent variable in the composite system adequacy performance. Reliability measures are used to quantify the risk based on the use of DLR as a planning alternative. As the thermal rating of a transmission line depends on its maximum design temperature, and the overhead cable temperature varies as a function of line current and meteorological conditions, the capacity of the transmission line will vary according to these variables. Thus, DLR technology method is able to change the system performance depending on the environment where the transmission line is located.

In this context, DLR technology appears as an incremental planning solution that can be safely included in the list of possible alternatives to maximize or reinforce transmission grid capacity, being an option to connect new generation plants and to meet future load in a secure manner, providing flexibility for implementing operative strategies in order to drain electricity generation to the large centers.

6.4 FUTURE RESEARCHES

The author expects that future theses also approach technological and scientific contributions. This kind of thesis allows the experience of contact with technologies that are endowing the power system with intelligence and the validation (representation) of some applications of those technologies in the field of simulations and power systems analysis. Therefore, the future works that may come up from this thesis results can be

divided into technological and scientific perspectives. Some ideas are pointed out as follows.

- Future works on a technological perspective:
  - Implementing TECCON MS on a 525 kV transmission line: enables the proliferation of active insulators in 230 kV and 525 kV transmission lines, enabling the dynamic ampacity and employing other benefits from a more systemic point of view;
  - To measure electrical current, via optical sensoring, of high voltage bundled conductors, i.e., more than one conductor per phase: in 525 kV transmission lines, bundled conductors measurement may be necessary due to the line design (geometry);
  - Implementation of new optical sensors to monitor other transmission lines information: conductor vibration monitoring, for instance, can avoid/reduce conductor fatigue and provide additional information for sag and clearance-to-ground estimations, which may reduce the number of failures and utility discounts.
- Future works on a scientific perspective:
  - Assessing the correlation between wind power generation and dynamic transmission system capacity: during the windy periods, the power line cooling effect and the wind power capacity are increased, enabling wind energy integration and reducing eventual transmission system bottlenecks;
  - Reliability of DLR systems: to set failure and repair rates for each monitoring system, promoting situations which the SLR can be considered since the monitoring system that enables the DLR is repairing;
  - Adding uncertainties associated with weather data historical series (wind speed and direction, ambient temperature and irradiance): to improve the dynamic ampacity forecasting, considering uncertainties into historical observation;
  - Proposal of a methodology to select the most critical lines in terms of power conveying: to evaluate which line is a bottleneck for system operation, assessing the benefits provided by dynamic ampacity implementation in those specific lines;
  - Improvements on operational flexibility parameters: a security analysis can be carried out to assess the system response due to sudden changes in load and generation. Generating units modeling can be improved in terms

of control and frequency excursion aspects. Frequency and voltage stability could be analyzed;

- To evaluate South and Southeast Brazilian Subsystem reliability considering the real DLR implementation on 230 kV Lages - Abdon Batista transmission line: reliability performance assessment of the Brazilian Interconnected system considering the transmission line dynamic ampacity. It can be extended to other transmission lines;
- Proposing improvements on thermal rating calculations of overhead lines: models depending on the type of the conductor and real-time monitoring, aiming to provide a more accurate representation.

REFERENCES

AGGARWAL, R.K et al. An overview of the condition monitoring of overhead lines. **Electric Power Systems Research**, v. 53, n. 1, p. 15–22, 2000. ISSN 0378-7796. DOI: https://doi.org/10.1016/S0378-7796(99)00037-1.

ALLIL, R. C. S. B.; WERNECK, M. M. Optical High-Voltage Sensor Based on Fiber Bragg Grating and PZT Piezoelectric Ceramics. **IEEE Transactions on Instrumentation and Measurement**, v. 60, p. 2118–2125, 2011.

AMPACIMON. **Datasheet Ampacimon - Innovative solution for Dynamic Line Rating**. [S.l.: s.n.], 2019. Last accessed 21 April 2019. Disponível em: http://www.ampacimon.com/wp-content/uploads/2015/09/datasheet-Ampacimon.pdf.

ASTM INTERNATIONAL. **ASTM Standard E8/E8M - 15a: Standard Tests Methods for Tension Testing of Metallic Materials**. [S.l.: s.n.], 2015. Accessed in: 06.09.2018.

BARROWS, C. et al. The IEEE Reliability Test System: A Proposed 2019 Update. **IEEE Transactions on Power Systems**, v. 35, n. 1, p. 119–127, 2020.

BILLINTON, R.; ALLAN, R. N. **Reliability Evaluation of Engineering Systems**. 2. ed. [S.l.]: Springer US, 1992. ISBN 9781461577287.

BILLINTON, R.; ALLAN, R. N. **Reliability Evaluation of Power Systems**. New York: Plenum Press, 1996. ISBN 9781489918628.

BILLINTON, R.; LI, W. **Reliability Assessment of Electric Power Systems Using Monte Carlo Methods**. [S.l.]: Springer US, 1994. ISBN 9781489913463.

BILLINTON, R.; SATISH, J. Predictive assessment of bulk-system-reliability performance indices. **IEEE Proceedings - Generation, Transmission and Distribution**, v. 141, n. 5, p. 466–472, Sept. 1994. DOI: 10.1049/ip-gtd:19941219.

BLACK, C.; CHISHOLM, W. Key Considerations for the Selection of Dynamic Thermal Line Rating Systems. **Power Delivery, IEEE Transactions on**, v. 30, p. 2154–2162, Oct. 2015. DOI: 10.1109/TPWRD.2014.2376275.

BOHNERT, K. et al. Fiber-Optic Current and Voltage Sensors for High-Voltage Substations. In: IN Proceedings of the 16th International Conference on Optical Fiber Sensors. [S.l.: s.n.], 2003. P. 752–754.

BOLACELL, G. S.; DA ROSA, M. A. Composite Power System Reliability Assessment Considering Transmission Line Flexibility. In: 2020 International Conference on Probabilistic Methods Applied to Power Systems (PMAPS). [S.l.: s.n.], 2020. P. 1–6. DOI: 10.1109/PMAPS47429.2020.9183505.

BRAZILIAN ELECTRICITY REGULATORY AGENCY - ANEEL. **Auction Notice N°001/2005, Annex 6F, Section F, 230 kV Transmission Line, in Portuguese, Barra Grande - Lages - Rio do Sul**. [S.l.], 2005.

BRAZILIAN ELECTRICITY REGULATORY AGENCY - ANEEL. **Normative Resolution N°191, December 12, 2005, in Portuguese**. [S.l.], 2005.

BRAZILIAN ELECTRICITY REGULATORY AGENCY - ANEEL. **Normative Resolution N°729, June 28, 2016, in Portuguese**. [S.l.], 2016.

BRAZILIAN ENERGY TRANSMISSION COMPANIES (TBE). **Project TECCON I Final Report, in Portuguese**. Santos, Dec. 2013.

BRAZILIAN NATIONAL STANDARDS ORGANIZATION - ABNT. **Polymeric insulators for indoor and outdoor use with nominal voltage greater than 1000 V - design tests**. [S.l.], 2018.

BROWN, F. A. **Apparatus and method of monitoring a power transmission line**. [S.l.]: US Patent 6,229,451 B1, May 2001.

CARVALHO, J. et al. Long-Period Gratings Dynamic Interrogation With Modulated Fiber Bragg Gratings and Optical Amplification. **IEEE Sensors Journal**, v. 12, p. 179–183, Jan. 2012. DOI: 10.1109/JSEN.2011.2128305.

CARVALHO, L. M. **Advances on the Sequential Monte Carlo Reliability Assessment of Generation-Transmission Systems using Cross-Entropy and Population-based Methods**. 2013. PhD thesis – Faculty of Engineering of University of Porto, Porto, Portugal.

CARVALHO, L. M. et al. Probabilistic Analysis for Maximizing the Grid Integration of Wind Power Generation. **IEEE Transactions on Power Systems**, v. 27, n. 4, p. 2323–2331, Nov. 2012. ISSN 0885-8950. DOI: 10.1109/TPWRS.2012.2207411.

CATARINENSE TRANSMISSION SYSTEM INC. - STC. **Project Report - 230 kV Transmission Line, in Portuguese, Barra Grande - Lages - Rio do Sul**. [S.l.], Mar. 2006.

CESPEDES, R. et al. Evolution of power to smart energy systems. In: 2010 IEEE/PES Transmission and Distribution Conference and Exposition: Latin America (T D-LA). [S.l.: s.n.], 2010. P. 616–621. DOI: 10.1109/TDC-LA.2010.5762946.

CHESINI, G. **Special optical fibers for sensoring, in Portuguese**. 2018. PhD thesis – State University of Campinas, Campinas, Brasil.

CHRISTIE, R.; DABBAGCHI, I. **Power Systems Test Case Archive**. [S.l.: s.n.], 1993. $https://labs.ece.uw.edu/pstca/rts/pg_tcarts.htm$. Accessed in: 07.14.2020.

CIGRE. Guide for Thermal Rating Calculations of Overhead Lines, Dec. 2014.

COSTA, A. S.; SALGADO, R. **Grid configurator, in Portuguese**. Florianópolis, Brazil: [s.n.], 2002. $http://www.labspot.ufsc.br/\ simoes/assp/assp8.pdf$. Last Accessed in October 2018.

CRUZAT, C.; KOPSIDAS, K. 2019 IEEE Milan PowerTech - Reliability Evaluation of ICT Used on Dynamic Line Rating for Power System Flexibility. In. DOI: 10.1109/PTC.2019.8810609.

DA ROSA, M. A. et al. Impact evaluation of the network geometric model on power quality indices using probabilistic techniques. In: 2016 International Conference on Probabilistic Methods Applied to Power Systems (PMAPS). [S.l.: s.n.], 2016. P. 1–8. DOI: 10.1109/PMAPS.2016.7764215.

DAY, G.; DEETER, M.; ROSE, A. Faraday Effect Sensors: A Review of Recent Progress. In.

ENTSO-E. **Dynamic Line Rating for overhead lines - V6**. [S.l.: s.n.], 2015. $https://www.entsoe.eu/Documents$. Accessed in: 08.29.2019.

EPRI. **Video Sagometer Application Guide**. Palo Alto: [s.n.], Sept. 2001. Last accessed 22 April 2019. Disponível em: http://lindsey-usa.com/wp-content/uploads/2017/03/11F-001-TLM-March-2017.pdf.

EPRI. **Electric Power System Flexibility: Challenges and Opportunities**. [S.l.], Feb. 2016.

EUROPEAN COMMISSION JOINT RESEARCH CENTRE. **Photovoltaic Geographical Information System (PVGIS)**. [S.l.: s.n.], 2020. $https://re.jrc.ec.europa.eu/pvg_tools/en/tools.html$. Accessed in: 08.21.2019.

FERNANDES, S. W. **State estimator and gross errors analysis applied to real-time ampacity monitoring systems, in Portuguese**. 2018. MA thesis – Federal University of Santa Catarina, Florianópolis, Brazil.

FERNANDES, S. W.; DA ROSA, M. A.; ISSICABA, D. A robust dynamic line rating monitoring system through state estimation and bad data analysis. **Electric Power Systems Research**, v. 189, p. 106648, 2020. ISSN 0378-7796. DOI: https://doi.org/10.1016/j.epsr.2020.106648.

FERNANDEZ, E. et al. Dynamic line rating systems for wind power integration. In: IEEE Power and Energy Society Conference and Exposition in Africa: Intelligent Grid Integration of Renewable Energy Resources (PowerAfrica). Africa: [s.n.], July 2012. P. 1–7. DOI: 10.1109/PowerAfrica.2012.6498618.

FERNANDEZ, E. et al. Review of dynamic line rating systems for wind power integration. **Renewable and Sustainable Energy Reviews**, v. 53, p. 80–92, 2016. ISSN 1364-0321. DOI: https://doi.org/10.1016/j.rser.2015.07.149.

FERREIRA, T. V. et al. Laboratory Tests of a Composite Insulator Instrumented with Optical Fiber Sensors. In: NÉMETH, B. (Ed.). **Proceedings of the 21st International Symposium on High Voltage Engineering**. Cham: Springer International Publishing, 2020. P. 483–491.

FLORKOWSKI, M.; LI, J. Condition Monitoring and Diagnostics. **IEEE Transactions on Dielectrics and Electrical Insulation**, v. 27, n. 6, p. 1769–1769, 2020. DOI: 10.1109/TDEI.2020.009340.

FRACAROLLI, J. P. V. et al. Development and field trial of a FBG-based magnetic sensor for large hydrogenerators. In: UDD, E.; PICKRELL, G.; DU, H. H. (Eds.). **Fiber Optic Sensors and Applications XIII**. [S.l.]: SPIE, 2016. International Society for Optics and Photonics, p. 159–164. DOI: 10.1117/12.2223919.

GILL INSTRUMENTS. **User manual for compact weather weather station**. [S.l.], 2019. Last accessed in April 2019. Disponível em: http://gillinstruments.com/products/anemometer/maximet-compact-weather-stations.html.

GONZALEZ-SALAZAR, M. A.; KIRSTEN, T.; PRCHLIK, L. Review of the operational flexibility and emissions of gas- and coal-fired power plants in a future with growing renewables. **Renewable and Sustainable Energy Reviews**, v. 82, p. 1497–1513, 2018. ISSN 1364-0321. DOI: https://doi.org/10.1016/j.rser.2017.05.278.

GRAINGER, J. J.; STEVENSON JR., W. D. **Power System Analysis**. [S.l.]: McGraw-Hill, Inc., 1994.

GREENWOOD, D. M.; TAYLOR, P. C. Investigating the Impact of Real-Time Thermal Ratings on Power Network Reliability. **IEEE Transactions on Power Systems**, v. 29, n. 5, p. 2460–2468, 2014.

GRIGG, C. et al. The IEEE Reliability Test System-1996. A report prepared by the Reliability Test System Task Force of the Application of Probability Methods Subcommittee. **IEEE Transactions on Power Systems**, v. 14, n. 3, p. 1010–1020, Aug. 1999. ISSN 0885-8950. DOI: 10.1109/59.780914.

HAJEFOROSH, F.; BOLLEN, M.; ABRAHAMSSON, L. Dynamic Line Rating Operational Planning: Issues and Challenges. In: 25TH International Conference on Electricity Distribution (CIRED). [S.l.: s.n.], June 2019. P. 1–5.

HAJEFOROSH, S.; BOLLEN, M. H. J. Transmission Line Overloading Analysis Using Probabilistic Dynamic Line Rating. In: 2020 International Conference on Probabilistic

Methods Applied to Power Systems (PMAPS). [S.l.: s.n.], 2020. P. 1–6. DOI: 10.1109/PMAPS47429.2020.9183550.

HARINGA, G. E.; JORDAN, G. A.; GARVER, L. L. Application of Monte Carlo simulation to multi-area reliability evaluations. **IEEE Computer Applications in Power**, v. 4, n. 1, p. 21–25, Jan. 1991. ISSN 1558-4151. DOI: 10.1109/67.65031.

HATZIARGYRIOU, N. et al. Definition and Classification of Power System Stability – Revisited & Extended. **IEEE Transactions on Power Systems**, v. 36, n. 4, p. 3271–3281, 2021. DOI: 10.1109/TPWRS.2020.3041774.

HILL, K. O.; MELTZ, G. Fiber Bragg grating technology fundamentals and overview. **Journal of Lightwave Technology**, v. 15, n. 8, p. 1263–1276, Aug. 1997. ISSN 1558-2213. DOI: 10.1109/50.618320.

HILL, K.O.; FUJII, Y., et al. Photosensitivity in optical fiber waveguides: Application to reflection filter fabrication. **Applied Physics Letters**, v. 32, n. 10, p. 647, May 1978. DOI: 10.1063/1.89881.

HOTATE, K.; THAI, B. T.; SAIDA, T. Comparison between flint glass fiber and twisted/bent single-mode fiber as a Faraday element in an interferometric fiber optic current sensor. In: CULSHAW, B.; JONES, J. D. C. (Eds.). **European Workshop on Optical Fibre Sensors**. [S.l.]: SPIE, 1998. International Society for Optics and Photonics, p. 233–237. DOI: 10.1117/12.309681.

HULD, T.; MÜLLER, R.; GAMBARDELLA, A. A new solar radiation database for estimating PV performance in Europe and Africa. **Solar Energy**, v. 86, n. 6, p. 1803–1815, 2012. ISSN 0038-092X. DOI: https://doi.org/10.1016/j.solener.2012.03.006.

IEC. **IEC 61850: Communication networks and systems in substations**. [S.l.], 2001.

IEEE. **IEEE 738: Standard for Calculating the Current-Temperature Relationship of Bare Overhead Conductors**. [S.l.], Dec. 2013. P. 1–72.

IEEE RTS TASK FORCE OF APM SUBCOMMITTEE. IEEE Reliability Test System. **IEEE Transactions on Power Apparatus and Systems**, PAS-98, n. 6, p. 2047–2054, Nov. 1979. ISSN 0018-9510. DOI: 10.1109/TPAS.1979.319398.

INESC P&D BRASIL. **Project TECCON II Final Report**. [S.l.], Nov. 2020.

IRENA. **Planning for the Renewable Future: Long-term modelling and tools to expand variable renewable power in emerging economies**. Abu Dhabi: International Renewable Energy Agency, 2017.

JAGER, D.; ANDREAS, A. **Measurement and Instrumentation Data Center (MIDC)**. Boulder, Colorado: NREL National Wind Technology Center (NWTC), 1996.

JORGE, P. A. **Optical sensors for electric current measurement in high voltage, in Portuguese**. 2001. MA thesis – University of Porto, Porto, Portugal.

KERSEY, A. D. et al. Fiber grating sensors. **Journal of Lightwave Technology**, v. 15, n. 8, p. 1442–1463, Aug. 1997. ISSN 1558-2213. DOI: 10.1109/50.618377.

LEITE DA SILVA, A. M.; MANSO, L.; SALES, W., et al. Application of Monte Carlo simulation to generating system well-being analysis considering renewable sources. **European Transactions on Electrical Power**, v. 17, p. 387–400, July 2007. DOI: 10.1002/etep.157.

LEITE DA SILVA, A. M.; MANSO, L. A. F.; FLÁVIO, S. A., et al. Composite Reliability Assessment of Power Systems with Large Penetration of Renewable Sources. In: **Reliability and Risk Evaluation of Wind Integrated Power Systems**. Ed. by R. Billinton, R. Karki and A. K. Verma. India: Springer India, 2013. P. 107–128. ISBN 978-81-322-0987-4. DOI: 10.1007/978-81-322-0987-4_8.

LEITE DA SILVA, A. M.; MANSO, L. A. F., et al. Pseudo-chronological simulation for composite reliability analysis with time varying loads. **IEEE Transactions on Power Systems**, v. 15, n. 1, p. 73–80, Feb. 2000. DOI: 10.1109/59.852103.

LEITE DA SILVA, A. M.; MELO, A.C.G.; CUNHA, S.H.F. Frequency and duration method for reliability evaluation of large-scale hydrothermal generating systems. English. **IEE Proceedings C (Generation, Transmission and Distribution)**, v. 138, 94–102(8), 1 Jan. 1991. ISSN 0143-7046.

LEITE DA SILVA, A. M.; PEREZ A., G., et al. Loss of load costs in generating capacity reliability evaluation. **Electric Power Systems Research**, v. 41, n. 2, p. 109–116, 1997. ISSN 0378-7796. DOI: https://doi.org/10.1016/S0378-7796(96)01182-0.

LEITE DA SILVA, A. M.; RESENDE, L. C. D., et al. Well-being analysis for composite generation and transmission systems based on pattern recognition techniques. **IET Generation, Transmission Distribution**, v. 2, n. 2, p. 202–208, Mar. 2008. ISSN 1751-8687. DOI: 10.1049/iet-gtd:20070109.

LEITE DA SILVA, A. M.; SALES, W. S., et al. Long-Term Probabilistic Evaluation of Operating Reserve Requirements With Renewable Sources. **IEEE Transactions on Power Systems**, v. 25, n. 1, p. 106–116, Feb. 2010. ISSN 0885-8950. DOI: 10.1109/TPWRS.2009.2036706.

LINDSEY MANUFACTURING CO. **TLM Conductor Monitoring, Real Time Transmission Line Conductor Monitor**. [S.l.: s.n.], 2019. Last accessed 21 April

2019. Disponível em: http://lindsey-usa.com/wp-content/uploads/2017/03/11F-001-TLM-March-2017.pdf.

LUMBRERAS, S. et al. Introduction: The Key Role of the Transmission Network. In: **Transmission Expansion Planning: The Network Challenges of the Energy Transition**. Ed. by S. Lumbreras, H. Abdi and A. Ramos. [S.l.]: Springer International Publishing, 2021. ISBN 978-3-030-49428-5. DOI: 10.1007/978-3-030-49428-5.

LUYCKX, G. et al. Three-dimensional strain and temperature monitoring of composite laminates. eng. **INSIGHT**, British Inst. Non-Destructive Testing, v. 49, n. 1, p. 10–16, 2007. ISSN 1354-2575.

MALIK, O.P. Evolution of Power Systems into Smarter Networks. **Journal of Control, Automation and Electrical Systems**, v. 24, Apr. 2013. DOI: 10.1007/s40313-013-0005-6.

MASSAUD, A. G.; SCHILLING, M. T.; HERNANDEZ, J. P. Electricity restriction costs. **IEE Proceedings - Generation, Transmission and Distribution**, v. 141, n. 4, p. 299–304, July 1994. DOI: 10.1049/ip-gtd:19949998.

MATOS, M. et al. Probabilistic evaluation of reserve requirements of generating systems with renewable power sources: The Portuguese and Spanish cases. **International Journal of Electrical Power & Energy Systems**, v. 31, n. 9, p. 562–569, 2009. ISSN 0142-0615. DOI: https://doi.org/10.1016/j.ijepes.2009.03.031.

MEDEIROS, S. **Optical current transformers: technical and technological feasibility analysis, in Portuguese**. [S.l.: s.n.], 2016. Undergraduate Thesis.

MELLO, J. C. O.; PEREIRA, M. V. F.; LEITE DA SILVA, A. M. Evaluation of reliability worth in composite systems based on pseudo-sequential Monte Carlo simulation. **IEEE Transactions on Power Systems**, v. 9, n. 3, p. 1318–1326, Aug. 1994. DOI: 10.1109/59.336134.

MELLO, J.C.O.; PEREIRA, M.V.F.; SILVA, A. M. Leite da, et al. Application of chronological load modeling in composite reliability worth evaluation. **Electric Power Systems Research**, v. 40, n. 3, p. 167–174, 1997. ISSN 0378-7796. DOI: https://doi.org/10.1016/S0378-7796(96)01150-9.

MICCA. **EMO - Easy Monitoring Overhead Lines**. [S.l.: s.n.], 2019. Last accessed 21 April 2019. Disponível em: https://www.micca.at/products-services/11-sensors-on-the-line.

MIRANDA, S. T. **Introducing the flexibility concept in the long-term operating reserve assessment, in Portuguese**. 2020. MA thesis – Federal University of Santa Catarina, Florianópolis, Brazil.

MONTICELLI, A.J. **Load flow in electric power grids, in Portuguese**. [S.l.]: E. Blucher, 1983.

MORGAN, V. T. The current-carrying capacity of bare overhead conductors. **Electrical Engineering Transactions**, EE4, p. 63–72, 1968.

MORGAN, V. T. The heat transfer from bare stranded conductors by natural and forced convection in air. **International Journal of Heat and Mass Transfer**, v. 16, n. 11, p. 2023–2034, 1973. ISSN 0017-9310. DOI: https://doi.org/10.1016/0017-9310(73)90105-1.

MORGAN, V. T. The thermal rating of overhead-line conductors Part I. The steady-state thermal model. **Electric Power Systems Research**, v. 5, n. 2, p. 119–139, 1982. ISSN 0378-7796. DOI: https://doi.org/10.1016/0378-7796(82)90033-5.

MORGAN, V. T. **Thermal behaviour of electrical conductors: steady, dynamic, and fault-current ratings**. [S.l.]: Research Studies Press, 1991. ISBN 9780863801198.

MOROZOVSKA, K.; HILBER, P. Study of the Monitoring Systems for Dynamic Line Rating. **Energy Procedia**, v. 105, p. 2557–2562, 2017. 8th International Conference on Applied Energy, ICAE2016, 8-11 October 2016, Beijing, China. ISSN 1876-6102. DOI: https://doi.org/10.1016/j.egypro.2017.03.735.

MOROZOVSKA, K.; NAIM, W., et al. A framework for application of dynamic line rating to aluminum conductor steel reinforced cables based on mechanical strength and durability. **International Journal of Electrical Power & Energy Systems**, v. 116, p. 105491, 2020. ISSN 0142-0615. DOI: https://doi.org/10.1016/j.ijepes.2019.105491.

MUTULE, A. et al. Overhead line weak point mechanical analysis based on Markov chain method. In: 2016 International Conference on Probabilistic Methods Applied to Power Systems (PMAPS). [S.l.: s.n.], 2016. P. 1–5.

NAGARAJAN, R. **Composite system based multi-area reliability evaluation**. 2009. MA thesis – Texas A&M University, College Station, USA.

NASA. **Technology Readiness Level**. [S.l.: s.n.], 2019. Last accessed 12.03.2019. Disponível em: https://www.nasa.gov/directorates/heo/scan/engineering/technology/txt_accordion1.html.

NASCIMENTO, C. A. M.; BRITO, J. M. C., et al. The state of the art for increased overhead line ampacity utilizing new technologies and statistical criteria. In: 2004 IEEE/PES Transmision and Distribution Conference and Exposition: Latin America. [S.l.: s.n.], Nov. 2004. P. 464–469. DOI: 10.1109/TDC.2004.1432424.

NASCIMENTO, C. A. M.; GIUDICE, E. B., et al. Application of real-time monitoring technologies to improve overhead lines capacity, in Portuguese. **Procel/ANEEL**, v. 98, p. 99, 2001. Disponível em: http://www.cgti.org.br/publicacoes/.

NASCIMENTO, I. M. **Optical fiber sensors technology for supervision, control and protection of high power systems**. 2016. PhD thesis – University of Porto, Porto, Portugal.

NASCIMENTO, I.M.; BAPTISTA, J.M., et al. Passive interferometric interrogation of a magnetic field sensor using an erbium doped fiber optic laser with magnetostrictive transducer. **Sensors and Actuators A: Physical**, v. 235, p. 227–233, 2015. ISSN 0924-4247. DOI: https://doi.org/10.1016/j.sna.2015.10.021.

NIEWCZAS, P. et al. Magnetic crosstalk compensation for an optical current transducer. **Instrumentation and Measurement, IEEE Transactions on**, v. 50, p. 1071–1075, Nov. 2001. DOI: 10.1109/19.963160.

ONS, Brazilian ISO. **Grid procedures: Sub-module 10.6 - Generation control, in Portuguese**. [S.l.: s.n.], 2018. Accessed in: 04.20.2020.

PERCIANTE, C. D.; FERRARI, J. A. Magnetic Crosstalk Minimization in Optical Current Sensors. **IEEE Transactions on Instrumentation and Measurement**, v. 57, n. 10, p. 2304–2308, Oct. 2008. ISSN 1557-9662. DOI: 10.1109/TIM.2008.919913.

PEREIRA, M. V. F.; BALU, N. J. Composite generation/transmission reliability evaluation. **Proceedings of the IEEE**, v. 80, n. 4, p. 470–491, Apr. 1992. DOI: 10.1109/5.135372.

PINTO, A. A. Z.; GARCIA, J. R. Assessment of the Impact of Dynamic Line Rating on Reliability Indices of Level I Systems. **Recent Advances in Electrical & Electronic Engineering**, v. 12, n. 4, p. 286–297, 2019. ISSN 2352-0965/2352-0973. DOI: 10.2174/2352096511666180531103420.

REN, Portugal ISO. **National Transmission Grid Characterization for Grid Connections Effects, in Portuguese**. [S.l.: s.n.], 2018. Accessed in: Nov. 21, 2020. Disponível em: https://www.centrodeinformacao.ren.pt/PT/publicacoes/CaracterizacaoRNT/Caracteriza%C3%A7%C3%A3o%5C%20da%5C%20RNT%5C%2031-12-2017.pdf/.

RIBEIRO, A. B. L. et al. Optical Fiber Sensor Technology in Portugal. **Fiber and Integrated Optics**, Taylor & Francis, v. 24, n. 3-4, p. 171–199, 2005. DOI: 10.1080/01468030590922722.

ROCHA, O. A. et al. Dynamic rating assists cost-effective expansion of wind farms by utilizing the hidden capacity of transformers. **International Journal of Electrical**

Power & Energy Systems, v. 123, p. 106188, Dec. 2020. DOI: 10.1016/j.ijepes.2020.106188.

ROSOLEM, J. Power-Over-Fiber Applications for Telecommunications and for Electric Utilities. **InTech**, June 2017. DOI: 10.5772/68088.

RTS-GMLC. **Reliability Test System - Grid Modernization Laboratory Consortium**. [S.l.: s.n.], 2018. $https://github.com/GridMod/RTS-GMLC$. Accessed in: 05.02.2020.

SCHRÖDER, A. et al. **Current and Prospective Costs of Electricity Generation until 2050**. [S.l.: s.n.], 2013.

SEPPA, T. O. A practical approach for increasing the thermal capabilities of transmission lines. **IEEE Transactions on Power Delivery**, v. 8, n. 3, p. 1536–1550, July 1993. DOI: 10.1109/61.252680.

SEPPA, T. O. Increasing transmission capacity by real time monitoring. In: 2002 IEEE Power Engineering Society Winter Meeting Conference Proceedings. [S.l.: s.n.], Jan. 2002. 1208–1211 vol.2. DOI: 10.1109/PESW.2002.985201.

SILVA, R. M. et al. Optical Current Sensors for High Power Systems: A Review. **Applied Sciences**, v. 2, n. 3, p. 602–628, 2012. ISSN 2076-3417. DOI: 10.3390/app2030602.

SILVERSTEIN, A.; FOLLUM, J. **High-Resolution, Time-Synchronized Grid Monitoring Devices**. [S.l.], Mar. 2020. P. 1–48.

SINGH, C.; LAGO-GONZALEZ, A. Improved algorithms for multi-area reliability evaluation using the decomposition-simulation approach. **IEEE Transactions on Power Systems**, v. 4, n. 1, p. 321–328, Feb. 1989. ISSN 1558-0679. DOI: 10.1109/59.32495.

SOROUDI, A.; AMRAEE, T. Decision making under uncertainty in energy systems: State of the art. **Renewable and Sustainable Energy Reviews**, v. 28, p. 376–384, 2013. ISSN 1364-0321. DOI: https://doi.org/10.1016/j.rser.2013.08.039.

TEH, J. **Analysis of Dynamic Thermal Rating System of Transmission Lines**. 2016. PhD thesis – Faculty of Engineering and Physical Sciences of University of Manchester, Manchester, England.

TEH, J.; COTTON, I. Reliability Impact of Dynamic Thermal Rating System in Wind Power Integrated Network. **IEEE Transactions on Reliability**, v. 65, n. 2, p. 1081–1089, 2016.

TÓMASSON, E.; SÖDER, L. Multi-area power system reliability evaluation by application of copula theory. In: 2016 IEEE Power and Energy Society General Meeting (PESGM). [S.l.: s.n.], July 2016. P. 1–5. DOI: 10.1109/PESGM.2016.7741943.

ULBIG, A. **Operational Flexibility in Electric Power Systems**. 2014. PhD thesis – ETH Zurich, Zurich, Switzerland.

US CANADA POWER SYSTEM OUTAGE TASK FORCE. **Final Report on the August 14, 2013 Blackout in the United States and Canada: Causes and Recommendations**. [S.l.: s.n.], 2004. Accessed in: 09.23.2020.

USI. **CAT-1 Dynamic Line Rating System**. [S.l.: s.n.], 2019. Last accessed 21 April 2019. Disponível em: http://www.usi-power.com/cat-1-dynamic-line-rating-system/.

USI. **Power Donut® Line Monitor**. [S.l.: s.n.], 2019. Last accessed 21 April 2019. Disponível em: http://www.usi-power.com/power-donut-line-monitor/.

VIEIRA, P. et al. Long-term Static and Operational Reserves Assessment Considering Operating and Market Agreements Representation to Multi-Area Systems. **Energies**, v. 13, n. 6, 2020. ISSN 1996-1073. DOI: 10.3390/en13061455.

VIEIRA, P. C. C. **Reliability Evaluation of Multi-Area Power Systems: Representations, Models, and Simulation Methodology, in Portuguese**. 2020. PhD thesis – Federal University of Santa Catarina, Florianópolis, Brazil.

WALLNERSTRÖM, C. J. et al. Potential of dynamic rating in Sweden. In: 2014 International Conference on Probabilistic Methods Applied to Power Systems, PMAPS 2014 - Conference Proceedings. [S.l.: s.n.], July 2014. DOI: 10.1109/PMAPS.2014.6960605.

WERNECK, M. M. et al. A Guide to Fiber Bragg Grating Sensors. In: CUADRADO-LABORDE, C. (Ed.). **Current Trends in Short- and Long-period Fiber Gratings**. Rijeka: IntechOpen, 2013. chap. 1. DOI: 10.5772/54682.

WILLIAMS, P. A. et al. Temperature dependence of the Verdet constant in several diamagnetic glasses. **Appl. Opt.**, OSA, v. 30, n. 10, p. 1176–1178, Apr. 1991. DOI: 10.1364/AO.30.001176.

WOOD, A. J.; WOLLENBERG, B. F.; SHEBLÉ, G. B. **Power Generation, Operation, and Control**. 03. ed. [S.l.]: John Wiley & Sons, Inc., 2014.

APPENDIX A – CONDUCTOR THERMAL BEHAVIOR

The conductor temperature is a function of conductor material properties, conductor diameter, conductor surface condition, weather conditions, and conductor electrical current (CIGRE, 2014; IEEE, 2013). The conductor thermal behavior is modeled using a set of mathematical equations based on CIGRE (2014).

Considering that all parameters remain constant over time, the conductor can be considered in a steady-state condition with both current and temperature constants. Hence, in this situation, the heat gain, which is mainly supplied by Joule effect (P_j) and solar radiation (P_s) is equal to the heat loss (dissipated), which is primarily by convection (P_c) and radiation (P_r) to the surrounding atmosphere. Besides, secondary sources of heating by Corona losses (P_i) and magnetic core losses in steel core conductors (P_m) and intermittent heat loss by evaporation (P_w) can be considered in the thermal balance (CIGRE, 2014).

This relation indicates that the heat gain (W/m) must be equal to heat loss (W/m), as exposed in (A.1):

$$P_j + P_s + P_m + P_i = P_c + P_r + P_w \tag{A.1}$$

It is highlighted that the heating by Corona effect is more significant in situations with high humidity and high wind speed. Although, as at these conditions the cooling effects are more relevant, the Corona effect heating is often neglected. Similarly, evaporative cooling is often not considered in thermal ratings due to its uncommon occurrence (entire line wet) over all the line extension and the difficulty of assessment (MORGAN, 1968). The following simplification gives the general equation for conductor heat balance:

$$P_j + P_s = P_c + P_r \tag{A.2}$$

where the magnetic heating can be included in the Joule heating term by increasing the effective conductor resistance. Figure A.1 illustrates the conductor thermal balance (CIGRE, 2014).

As weather conditions and load current vary during the time, the conductor is not always in thermal equilibrium, but in ongoing changing, where the heat gain is not equal to heat loss. Therefore, the heat stored in the conductor is equal to heat gain minus heat loss.

Methods based on the conductor thermal behavior monitoring are needed to carry out more accurate and consistent analyzes in operation real-time situations. These methods can avoid possible violations of conductor-ground safety distance and conductor damaging due to high temperatures. The conductor temperature variations may

Figure A.1 – Overhead conductor thermal balance.

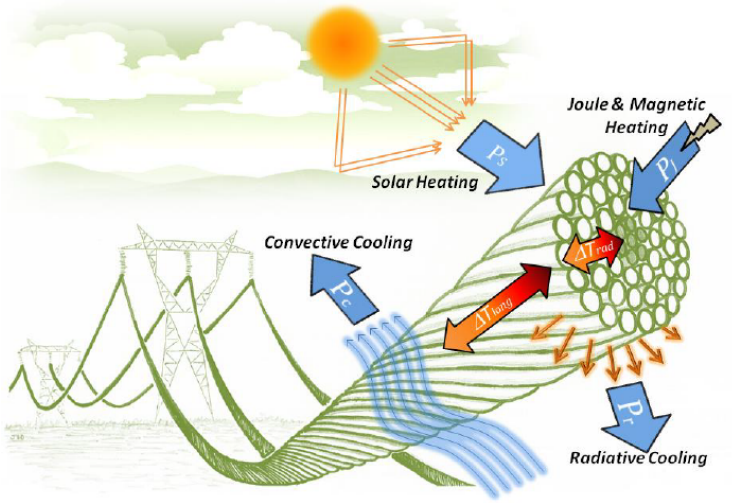

Source: adapted from CIGRE (2014).

be represented by the transient conductor temperature relation (non-steady-state heat balance), as in (A.3), (CIGRE, 2014):

$$\frac{dT_{avg}}{dt} = \frac{1}{mC_p}\left(P_j + P_s - P_c - P_r\right) \tag{A.3}$$

where mC_p is the total heat capacity of conductor, in $J/(m-°C)$, and T_{avg} is the average temperature of aluminum strand layers $(°C)$. The mathematical equations required to compute P_j, P_s, P_c and P_r are presented next.

A.1 HEAT GAIN MATHEMATICAL FORMULATION

The Joule effect is computed using (A.4):

$$P_j = I^2 R(T_{avg}) \tag{A.4}$$

where I is the electrical current, in (A) and the ac resistance of conductor (Ω/m) at temperature T_{avg} (average temperature), defined as $R(T_{avg})$, is computed by interpolation (A.5):

$$R(T_{avg}) = \frac{R(T_{high}) - R(T_{low})}{T_{high} - T_{low}}\left(T_{avg} - T_{low}\right) + R(T_{low}) \tag{A.5}$$

where T_{high} and T_{low} are the high and low average conductor temperatures for which AC resistance is specified, respectively. The resistance values used already include the frequency-dependent "skin-effect".

In the model, there is also the rate of solar heat gain, $P_s\,(W/m)$, which is equal to (CIGRE, 2014):

$$P_s = \alpha_S I_T D \tag{A.6}$$

where α_S is the solar absorptivity, usually from around 0.20 to 0.91, D is the conductor outside diameter, in (mm), and I_T is the global radiation intensity. Devices for measuring global radiation intensity may be used for line monitoring systems providing measurements estimated values. The I_T is a combination of the direct solar radiation on a surface normal to the sun's beam (I_B), the diffuse sky radiation to a horizontal surface (I_d), and the incident radiation reflected from the ground or albedo, F, as described in (A.7).

$$I_T = I_{B(y)} \left(\sin(\eta) + \frac{\pi}{2} F \sin(H_S) \right) + I_d \left(1 + \frac{\pi}{2} F \right) \tag{A.7}$$

The direct (beam) solar radiation intensity at sea level, $(I_{B(0)})$, is (A.8):

$$I_{B(0)} = N_S \left(\frac{1280 \sin(H_S)}{\sin(H_S) + 0.314} \right) \tag{A.8}$$

where N_S is a clearness ratio, having the value of 1.0 for the standard atmosphere. The direct beam radiation (I_B) increases with increasing height above sea level, y, according to the following equation (A.9).

$$I_{B(y)} = I_{B(0)} \left[1 + 1.4 \times 10^{-4} y \left(\frac{1367}{I_{B(0)}} - 1 \right) \right] \tag{A.9}$$

H_S is the solar altitude, given by (A.10):

$$H_S = \arcsin \left(\sin(\phi) \sin(\delta_S) + \cos(\phi) \cos(\delta_S) \cos(Z) \right) \tag{A.10}$$

ϕ is the latitude, Z is the hour angle of the sun $= 15(12 - Time)$, in degrees, with $Time$ given in hours, from 0 to 24 and δ_S is the declination of the sun that can be defined as the angle between the equator and a line drawn from the centre of the earth to the centre of the sun:

$$\delta_S = 23.3 \sin \left[\frac{2\pi(284 + N^*)}{365} \right] \tag{A.11}$$

N^* is the day of year, 1st January = 1, for instance. I_d is the diffuse solar radiation intensity, in (W/m^2). There is a correlation between direct radiation I_B and diffuse radiation I_d, as clouds cause both a reduction in I_B and and increase in I_d. It can be computed, for all skies, using (A.12):

$$I_d = (430.5 - 0.3288 I_B) \sin(H_S) \tag{A.12}$$

η is the angle of solar beam with respect to the axis of the conductor. This angle is given by (A.13):

$$\eta = \arccos\left[\cos(H_S)\cos(\gamma_S - \gamma_c)\right] \tag{A.13}$$

where γ_c is the azimuth of the conductor and γ_S is the azimuth of the sun (A.14):

$$\gamma_S = \arcsin\left[\frac{\cos(H_S)\sin(Z)}{\cos(H_S)}\right] \tag{A.14}$$

A.2 HEAT LOSS MATHEMATICAL FORMULATION

The heat loss due to convection is almost always the most important factor for the transmission line conductors cooling, even with no winds. The P_c used in the conductor thermal behavior should be the highest value among forced and natural convection where the difference is presented in a function of Nusselt number. The convective heat loss can be expressed as a function of the dimensionless Nusselt number (Nu) as follows (A.15):

$$P_c = \pi\lambda_f(T_S - T_a)Nu \tag{A.15}$$

where λ_f is the thermal conductivity of the air (W/km) at T_f, the temperature of the film of air in contact with the surface, and T_S and T_a are the temperature of the conductor surface and the air respectively. For film temperatures up to 300 $^{\circ}C$ the thermal conductivity of the air (λ_f) can be expressed as (A.16):

$$\lambda_f = 2.368 \times 10^{-2} + 7.23 \times 10^{-5}T_f - 2.763 \times 10^{-8}T_f^2 \tag{A.16}$$

where the film temperature (T_f) is assumed to be $T_f = 0.5(T_S + T_a)$.

Depending on the situation (forced or natural convection), different correlations have been proposed to obtain Nu. For forced convection, perpendicular flow, there is a correlation between the Nu and Reynolds number (Re):

$$Re = \frac{VD}{\upsilon_f} \tag{A.17}$$

where V (m/s) is the wind speed, D (m) is the diameter of the conductor and υ_f is the kinematic viscosity of the air at the film temperature which depends on the elevation of the conductor above sea level and can be expressed as $\upsilon_f = \mu_f/\gamma$, being μ_f the dynamic viscosity of the air at film temperature and γ the density of the air at the elevation of the conductor. The dynamic viscosity is computed using (A.18).

$$\mu_f = (17.239 + 4.635 \times 10^{-2}T_f - 2.03 \times 10^{-5}T_f^2)10^{-6} \tag{A.18}$$

The density of air at given film temperature and elevation can be expressed as (A.19):

$$\gamma = \frac{1.293 - 1.525 \times 10^{-4} y + 6.379 \times 10{-}9y^2}{1 + 0.0036 T_f} \tag{A.19}$$

Among the correlations proposed in the literature, it is used the following equation given by Morgan (1973).

$$Nu_{90} = BRe^n \tag{A.20}$$

where the coefficients B and n are given in Table A.1. They depend on the Reynolds number and the roughness (R_s) of the surface of the conductor, which is computed using (A.21):

$$R_s = \frac{d}{2(D-d)} \tag{A.21}$$

where d is the diameter of the wires in the outermost layer and D is the overall diameter.

Table A.1 – Coefficients for calculating forced convective heat transfer.

$R_s \leq 0.05$			$R_s > 0.05$		
Re	B	n	Re	B	n
100 - 2,650	0.641	0.471	100 - 2,650	0.641	0.471
2,650 - 50,000	0.178	0.633	2,650 - 50,000	0.048	0.800

Source: adapted from CIGRE (2014).

The above equations are only valid for an airflow perpendicular to the conductor, with an angle of attack (δ) equal to $90°$. In other words, δ is the angle between the wind and line direction. The following equations proposed by Morgan (1968, 1991) are used, being valid to stranded conductors and $Re < 4,000$.

$$\frac{Nu_\delta}{Nu_{90}} = 0.42 + 0.68(\sin(\delta))^{1.08}; with\, \delta \leq 24° \tag{A.22}$$

$$\frac{Nu_\delta}{Nu_{90}} = 0.42 + 0.58(\sin(\delta))^{0.90}; with\, \delta > 24° \tag{A.23}$$

In the case of natural convection (zero wind speed), it has been found from different studies that the Nusselt number (Nu_{nat}) is related to the Grashof (Gr) and Prandtl numbers (Pr), that can be calculated using (A.24) and (A.25), respectively:

$$Gr = \frac{D^3(T_s - T_a)g}{(T_f + 273)v_f^2} \tag{A.24}$$

$$Pr = \frac{c_f \mu_f}{\lambda_f} \tag{A.25}$$

From Gr and Pr it is possible to compute (Nu_{nat}), as follows.

$$Nu_{nat} = A(GrPr)^m \tag{A.26}$$

Values of the coefficients A and m, based on hundreds of experimental measurements, for various ranges of $GrPr$, are exposed in Table A.2 (MORGAN, 1982).

Table A.2 – Coefficients for calculating natural convective heat transfer.

Range of $GrPr$		A	m
from	to		
10^{-1}	10^{2}	1.02	0.148
10^{2}	10^{4}	0.850	0.188
10^{4}	10^{7}	0.480	0.250
10^{7}	10^{12}	0.125	0.333

Source: adapted from CIGRE (2014).

Inclination of a conductor to the horizontal (β) reduces the natural convective heat loss. The ratio $\frac{Nu_\beta}{Nu_0}$, for stranded conductors (MORGAN, 1991), can be computed using (A.27):

$$\frac{Nu_\beta}{Nu_0} = 1 - 1.76 \times 10^{-6}\beta^{2.5}; with\, \beta < 80° \tag{A.27}$$

The radiated heat loss from a conductor is the total radiative energy transmitted from its surface. It is composed of the heat radiated to the ground and surroundings and the heat radiated directly to the sky. Applying the Stefan-Boltzmann law, the heat loss from the conductor due to radiation can be expressed as (A.28):

$$\begin{aligned} P_r = \pi D\sigma_B F_{c-g}\epsilon_s \left[(T_s+273)^4 - (T_g+273)^4\right] + \\ \pi D\sigma_B F_{c-sky}\epsilon_s \left[(T_s+273)^4 - (T_{sky}+273)^4\right] \end{aligned} \tag{A.28}$$

where σ_B is the Stefan-Boltzmann constant, ϵ_s is the emissivity of the conductor surface, T_g is the temperature of the ground beneath the conductor, T_{sky} is the temperature of the sky above the conductor, F_{c-g} is the fraction of radiated energy from the conductor that reaches the ground and surroundings, and F_{c-sky} is the fraction of radiated energy from the conductor that goes to the sky.

It is considered that T_g and T_{sky} are equal to the ambient temperature and the summation of F_{c-g} and F_{c-sky} is the total radiated energy leaving the conductor surface, which is equal to one. So, the radiative cooling effect can be computed using (A.29).

$$P_r = \pi D\sigma_B\epsilon_s \left[(T_s+273)^4 - (T_a+273)^4\right] \tag{A.29}$$

According to CIGRE (2014), it is recommended, that for weathered conductors, an emissivity value of 0.8 or 0.9 to be used.

APPENDIX B – SEQUENTIAL MONTE CARLO SIMULATION

In the SMCS, there is a chronological representation, the states of the components are sequentially sampled simulating the chronology of the stochastic process of system operation through the assessment of synthetic sequences of system states. It is created a power system “life story” where the system components state residence duration is obtained by the probability distributions, associated with Mean Time to Failure (MTTF) and Mean Time to Repair (MTTR) of each component system (BILLINTON; LI, 1994; CARVALHO, 2013).

Figure B.1 exposes a basic synthetic series of system components states using as an example a simple composite system adequacy study in which a thermal generation unit supply a load through a unique transmission circuit. It is noted that the system is in a state of success when at least the transmission line and the generation unit are operating (up state). Conversely, between the period 7 and 8 of the graph, there is an interesting interval in which the load increases significantly, and two hypotheses may happen causing a failure state: it becomes higher than the generation capacity and/or the transmission line operative limits are exceeded, both making the generation system not capable of supplying the demand (CARVALHO, 2013).

Figure B.1 – Simplified representation of a sequence of events over a period of time.

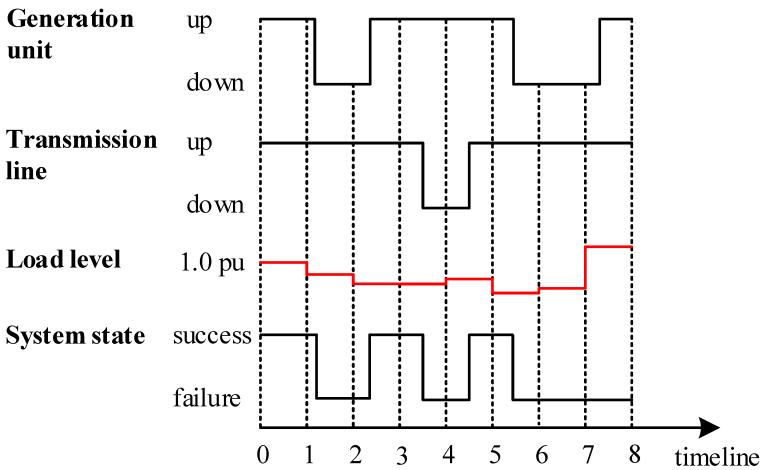

Source: own.

Figure B.1 also demonstrates that the state transition between different load levels is made in fixed time step whereas the duration of the states of the generating unit and the transmission line are not fixed and totally dependent of underlying probability distributions. Like non-sequential MCS, an alternative to estimate the expected value of reliability indices is given as follow (CARVALHO, 2013):

$$\tilde{E}[H(x)] = \frac{1}{NY} \sum_{i=1}^{NY} H\left(\{x_n\}_{n=1}^{S_i}\right) \tag{B.1}$$

where NY represents the number of periods simulated, and $\{x_n\}_{n=1}^{S_i} = \{x_1, ..., x_{Si}\}$, $S_i \in \mathbf{N}$, is the synthetic sequence of system states x over the period i. Namely, the test function H of the index LOLP, which is evaluated at the end of each simulated period T, typically a year or 8760 h, can be defined as:

$$H_{LOLP}\left(\{x_n\}_{n=1}^{S_i}\right) = \frac{1}{T}\sum_{n=1}^{S_i} d(x_n) \times H_{LOLP}(x_n) \tag{B.2}$$

where x_n is the n-th state of the sequence, T is the duration of the synthetically simulated period, $d(x_n)$ is the state duration residence in x_n and $H_{LOLP}(x_n)$ is the outcome of the following equation (B.3) taking x_n as argument.

$$H_{LOLP}(x_i) = \begin{cases} 1, & \text{if } x_i \in X_{failure} \\ 0, & \text{if } x_i \in X_{success} \end{cases} \tag{B.3}$$

The following test function can be used for the EPNS index:

$$H_{EPNS}\left(\{x_n\}_{n=1}^{S_i}\right) = \frac{1}{T}\sum_{n=1}^{S_i} d(x_n) \times H_{EPNS}(x_n) \tag{B.4}$$

where $H_{EPNS}(x_n)$ is the outcome of (B.5) taking x_n as argument.

$$H_{EPNS}(x_i) = \begin{cases} \Delta P_i, & \text{if } x_i \in X_{failure} \\ 0, & \text{if } x_i \in X_{success} \end{cases} \tag{B.5}$$

On the contrary of non-sequential MCS, the frequency and duration indices calculations are very easy to do, the detection of load curtailment is made only by following the sequential simulation of the system as:

$$H_{LOLF}\left(\{x_n\}_{n=1}^{S_i}\right) = \sum_{n=2}^{S_i} h(x_n, x_{n-1}) \tag{B.6}$$

where

$$h(x_n, x_{n-1}) = \begin{cases} 1, & \text{if } x_n \in X_{failure} \text{ and } x_{n-1} \in X_{success} \\ 0, & \text{otherwise} \end{cases} \tag{B.7}$$

Sequential and non-sequential MCS have peculiar characteristics when it is analyzed the simulation steps of both methods: states selection, reliability indices calculation, simulation step evolution, for instance, depend on each method. However, similarities appear in the state evaluation step (adequacy analysis), where corrective measures may be applied to solve the problem (CARVALHO, 2013).

APPENDIX C – TECCON I OVERVIEW

TECCON I project had as principal motivation the development of new systems based on optical sensors to monitor and optimize high voltage electric energy systems. Optical fiber technology has been chosen due to its versatility, electromagnetic interference immunity, low weight, and capacity for remote and real-time monitoring of many relevant quantities for the electric sector.

The research project has proposed to develop sensors to measure, in real-time, conductor temperature, catenary state, and electric current. In addition, systems to interrogate the sensors and software to acquire and interpret the data have been developed. The goal has been providing new tools to the operator allowing estimate the real load condition of transmission lines in real-time (TBE, 2013).

The research project has achieved TRL 4, i.e., the optical sensors have been validated in the laboratory environment. Table C.1 highlights the TRL of TECCON I research project and shows that the author has no contributions related to this development.

Table C.1 – TRL and contributions related to TECCON I research project.

TRL	Level 4
Contributions	No direct contributions. The author has not participated of this research project.

Source: own.

APPENDIX D – TECCON II OVERVIEW

TECCON II has started in November 2015 as a continuation of TECCON I research project. The challenge proposed has been to elevate the TRL from rating 4 to 7. To accomplish that, a real-time monitoring system, robust enough, has been developed to be installed in a high voltage transmission line of the South Subsystem of the Brazilian Interconnected System.

Several challenges have needed to be overcome to build a real-time transmission line monitoring system, such as processing optical/analogic signals from sensor arrangements, ensuring a continuous and reliable energy supply, and establishing a robust communication system to send the local information to the substation where the line operator has the front end information. These systems should be installed remotely on a specific span of the transmission line, usually, critical spans, and the location of the components on the tower must be chosen precisely to avoid electromagnetic interference and vandalism.

The monitoring system, named TECCON MS, is based on a polymeric insulator that serves as an interface between optical fiber sensors and the transmission line. TECCON MS provides information about the electrical current, mechanical tension, conductor temperature, and weather variables (wind direction and speed, pressure, humidity, precipitation, dew point, and ambient temperature). The weather variables are measured using a meteorological station (GILL, 2019).

FBG sensors are applied to strain and conductor temperature measuring. Two kinds of optical sensors are employed for electrical current measurement. An ambient temperature and strain sensors are placed on a central rod of the anchorage conductor piece. It is noticed that the ambient temperature is also measured by one FBG sensor, besides the weather station measurement, in order to compensate the FBG wavelength displacement caused by the temperature on the strain sensor measurement, aiming an accurate measure of the conductor strain.

The TECCON MS entire solution for line CM application is shown in Figure D.1 and it can be split into 5 parts (units): (1) high voltage insulator; (2) sensors unit; (3) OESPU; (4) energy supplying; and (5) real-time CM unit. The first conception and specifications of each unit are described briefly in the next sections.

D.1 HIGH VOLTAGE INSULATOR UNIT

To provide a paradigm change and acquire the information at transmission line intermediate points, the proposed polymeric (composite) insulator works as an active grid component, intending to change the insulator role paradigm. The proposal is to embed part of the measurement solution in the insulator. Project requirements imply a polymeric insulator, mainly due to the need for an optical fiber passing through the

Figure D.1 – Representation of TECCON MS entire solution.

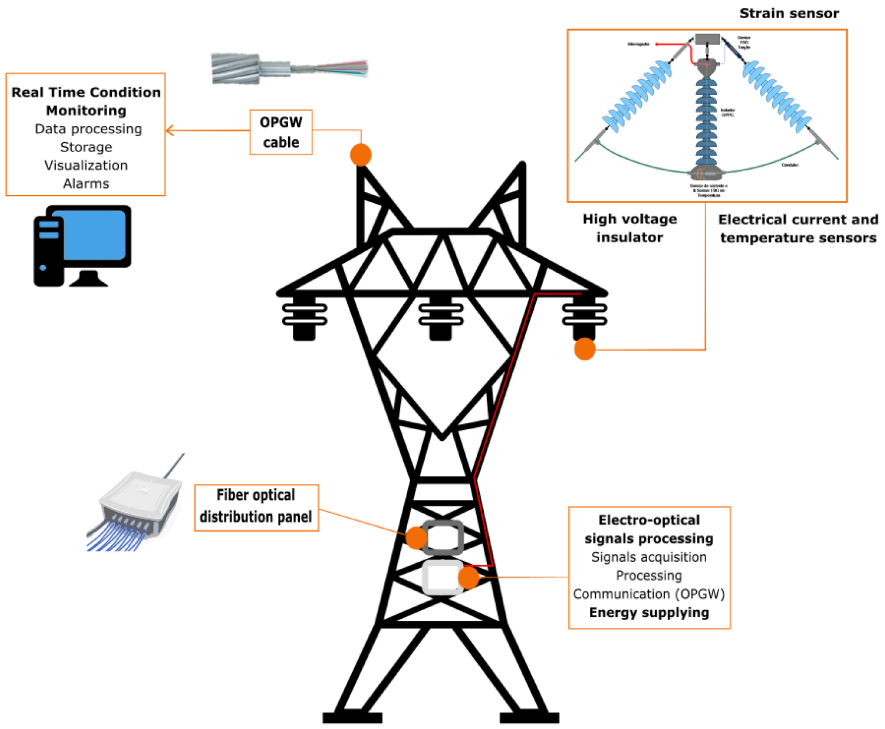

Source: own.

insulator core. Notice that the insulator should be filled with silicone gel to avoid any water infiltration. Conductor current and temperature sensors are placed on a sensor housing mounted on the bottom of the insulator, as shown in Figure D.2.

Figure D.2 – Design of TECCON high voltage polymeric optical fiber insulator.

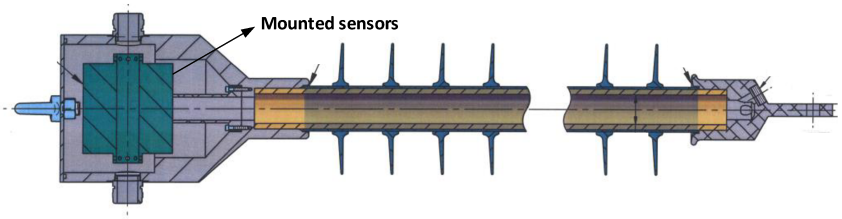

Source: own.

Moreover, deformation is measured on the central rod of the anchorage piece. The insulator with the fiber sensors is designed to be placed, firstly, on the auxiliary insulator string (jumper insulator) at an anchorage tower and, as consequence, the tower must have a fiber optics splicing box for communication. The transmission line needs an OPGW for data transmission to the AMC.

The new insulator responds perfectly to the usual functions of an insulator (ABNT, 2018), i.e., it has been exhaustively tested on relevant ambient with the most adverse conditions (rain, dust, fog) to evaluate the mechanical and electrical insulation capability (FERREIRA et al., 2020).

D.1.1 High voltage tests with the insulator

In order to ensure the safety and reliability of the developed prototype, and consequently, of the power system that will receive the equipment, several electrical and mechanical tests (and pre-stressing procedures) have been conducted. Most of these tests are described in Brazilian and European standards: dielectric strength; steep-front impulse voltage test; DC inclined-plane tracking and erosion test; partial discharges tests; 1000 hours salt-fog test; impulse voltage tests; flammability test; dimensional check; interfaces adhesion strength test; tests on interfaces and connections of end fittings; assembled core load-time tests; galvanizing test; visual examination.

In addition to the standardized tests, compatibility tests have been also carried out. The purpose of these additional tests is to verify the operation of the entire TECCON assembly, allowing the detection of eventual improvement points between components. Furthermore, in the electrical compatibility tests, current and voltage impulse applications have been performed during the data acquisition process, allowing to verify the consistency of the data acquisition during fast (transitory) events, as well as the behavior of the electronic components during these events.

D.2 SENSORS UNIT

The sensors unit encompasses the apparatus towards measuring electrical current, deformation, and temperature measurements in real-time, utilizing optical fiber sensors which, in general, are immune to electromagnetic interference. The set of sensors includes a meteorological station that provides wind speed and direction, ambient temperature, and other data to a server responsible for data processing. Electrical current and conductor temperature are measured directly at the conductor of the transmission line (on an auxiliary polymeric insulator string) whereas a mechanical strain is acquired at the conductor anchorage piece, where the deformation of this piece is measured using a weldable FBG sensor.

Two configurations of optical current sensors subjected to the Faraday effect are used for real-time current measuring, allowing the DLR applications: a bulk optical sensor, called μTECCON, and an all-fiber sensor, named Hi-Bi TECCON.

D.3 OPTO-ELECTRONIC SIGNALS PROCESSING UNIT

This unit is the brain of the remote monitoring system. It is responsible for getting information from the optical sensors and the weather station. It is composed of three major parts: analog signal conditioning circuits, digital module, and power supply circuits. The PCB developed, shown in Figure D.3, is assigned to control the optical light source, to provide different voltage levels for the weather station and media converter, and receive (photodetectors output) and treat transductors response.

Figure D.3 – TECCON MS scheme representation highlighting features of each unit.

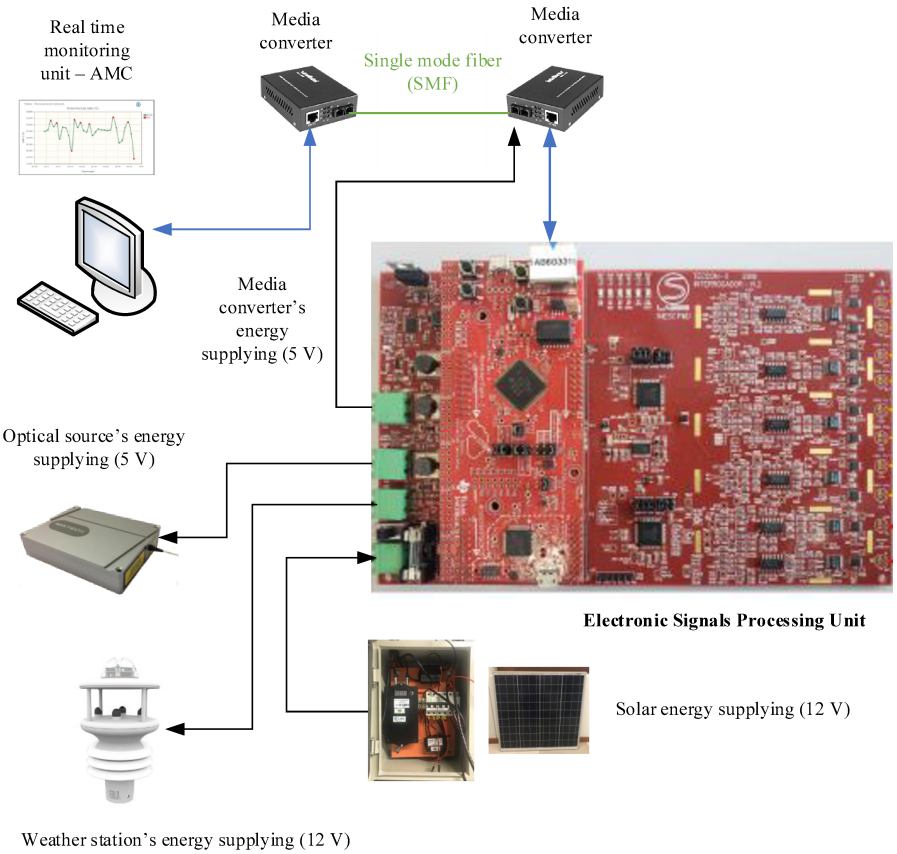

Source: own.

Sensors' information is acquired locally in the tower structure and signals need to be processed, digitized, and transmitted by an Ethernet/optical link. Regarding the project specifications, an Erbium Doped Fiber Amplifier (EDFA), spontaneous emission, with wavelength centered at 1550 nm, is used as an optical source. Infrared region optical sources provide the minimum optical loss through the fiber (0.3 dB/km), i.e., the attenuation of the fiber is much less than other wavelengths (ultraviolet and visible regions, for instance). The OESPU is accommodated in a customized enclosure that can hold multiple mounting plates inside of it with an International Protection Marking (IP) 67, where there is a heat dissipation control and immunity to electromagnetic interference.

D.4 ENERGY SUPPLYING

Photovoltaic panels and a storage system (lithium-ion battery) with load controller make up the energy supplying unit, as shown in Figure D.4.

It must serve the load (10 W) continuously, 24 h per day. The load of the system is composed of the weather station, the OESPU (with its photodetectors, optical source), and one optical fiber media converter (communication system). The energy supplying

Figure D.4 – General setup of the supplying system prototype.

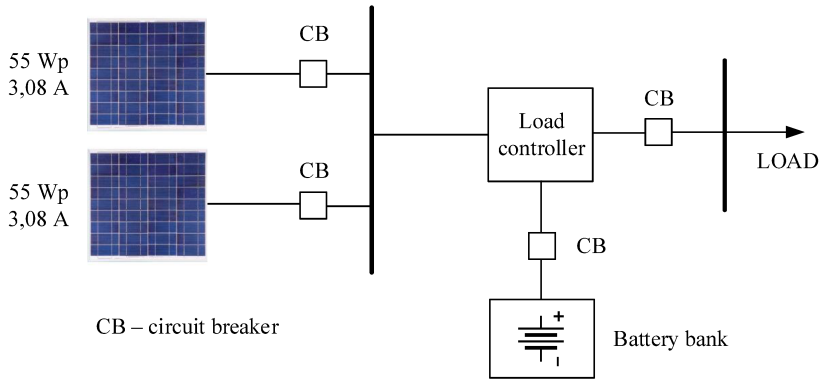

Source: own.

system can be projected for the autonomy of one to five days, depending on the project requirements. A battery, a Maximum Power Point Tracking (MPPT) load controller, and circuit breakers are packed in a case with IP 66, similarly to the enclosure of the OESPU.

D.5 REAL-TIME CONDITION MONITORING UNIT

The fifth unit is composed of the communication channel and supervisory control made in the AMC. The communication system implements a data transmission system by OPGW, which is the ground or guard cable on transmission lines. Every line information achieved on optical sensors is transported up to the control center in the substation. Information acquired on the OESPU is encapsulated in Sampled Values (SV) messages up to the first media converter to transform the electric signal into an optical signal.

A Fiber Optical Distribution Panel (FODP) or generally referred to as splicing box receives the fiber termination to connect with the OPGW in order to transmit the message until the next media converter located at the substation, transforming the optical in the electric signal before the information arrives at the server (AMC). International Electrotechnical Commission (IEC) 61850 standard is applied as communication protocol and the communication system (located on the tower) has a power consumption of 2 W (IEC, 2001).

The web application has been developed to provide several functionalities for the user, such as monitoring electrical current, wind speed and direction, the temperature of the cable, ambient temperature, cable mechanical tension, and other weather information. All these data allow identifying possible deteriorations (corrosion), overheating, and the real-time ampacity level of the transmission line, as already mentioned. Real-time measurements, statistic signal data, fault detection, and conductor CM are some of the web application functionalities. Furthermore, the AMC has a state estimator which

rejects gross errors and calculates in real-time the heat balance on the transmission line, i.e., performs the DLR aiming to determine the line condition in terms of load level.

APPENDIX E – TECCON MONITORING SYSTEM PRACTICAL RESULTS

Figure E.1 – Conductor temperature behavior during February 2, 2021.

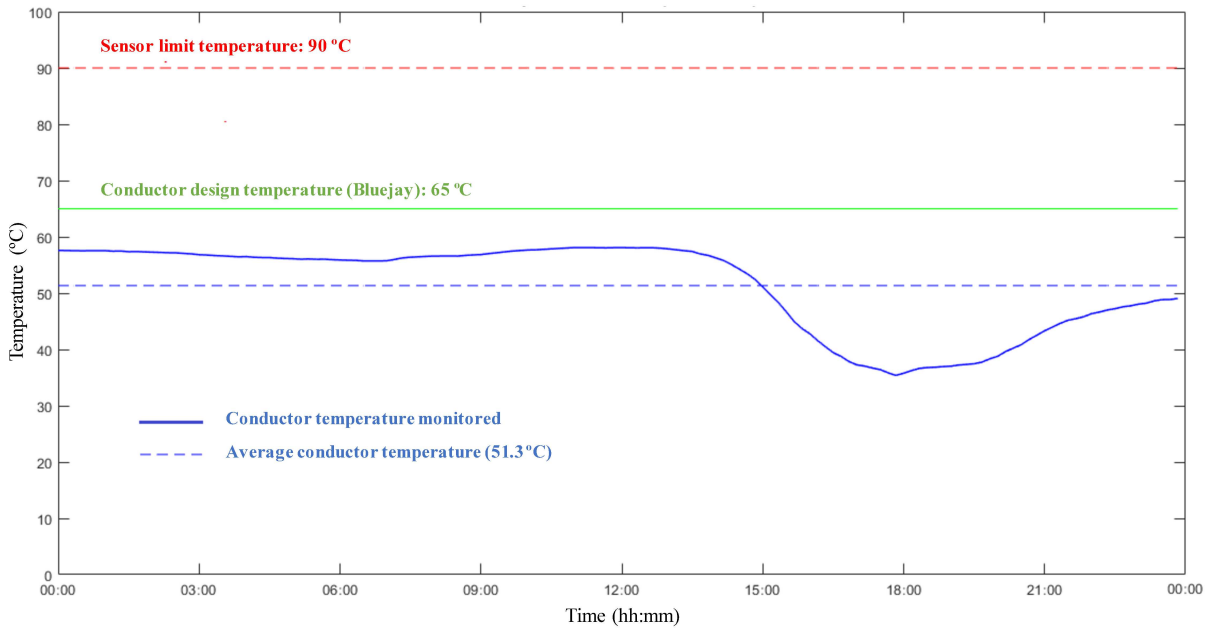

Source: own.

Figure E.2 – Mechanical traction behavior during February 2, 2021.

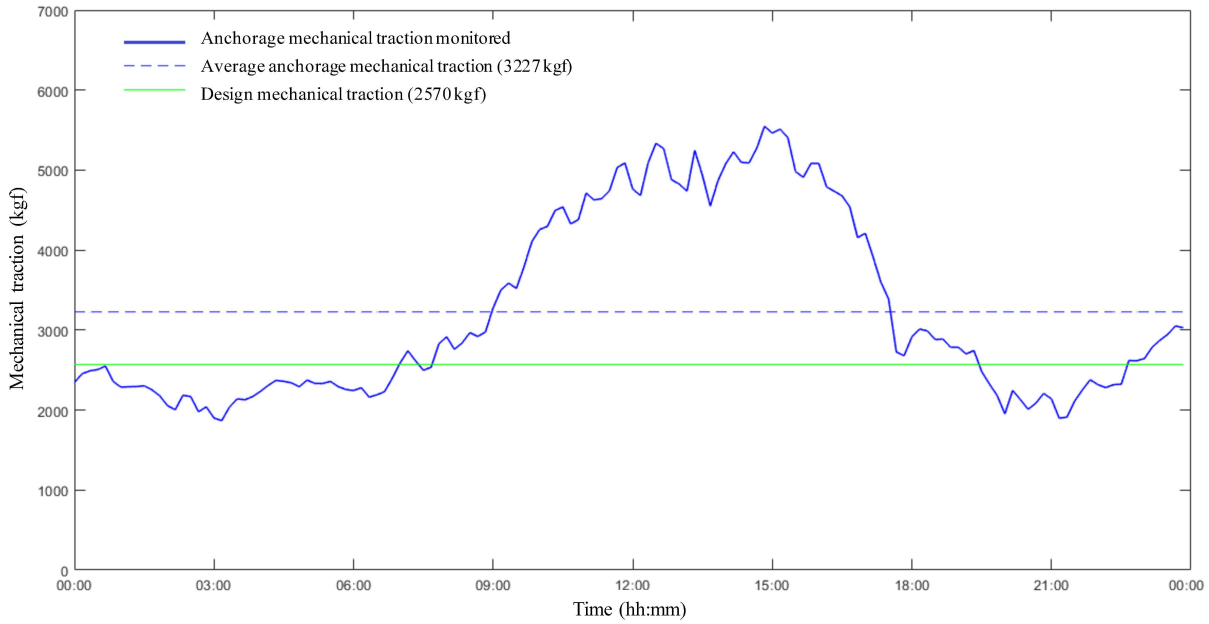

Source: own.

Figure E.3 – Conductor electrical current variation during February 2, 2021.

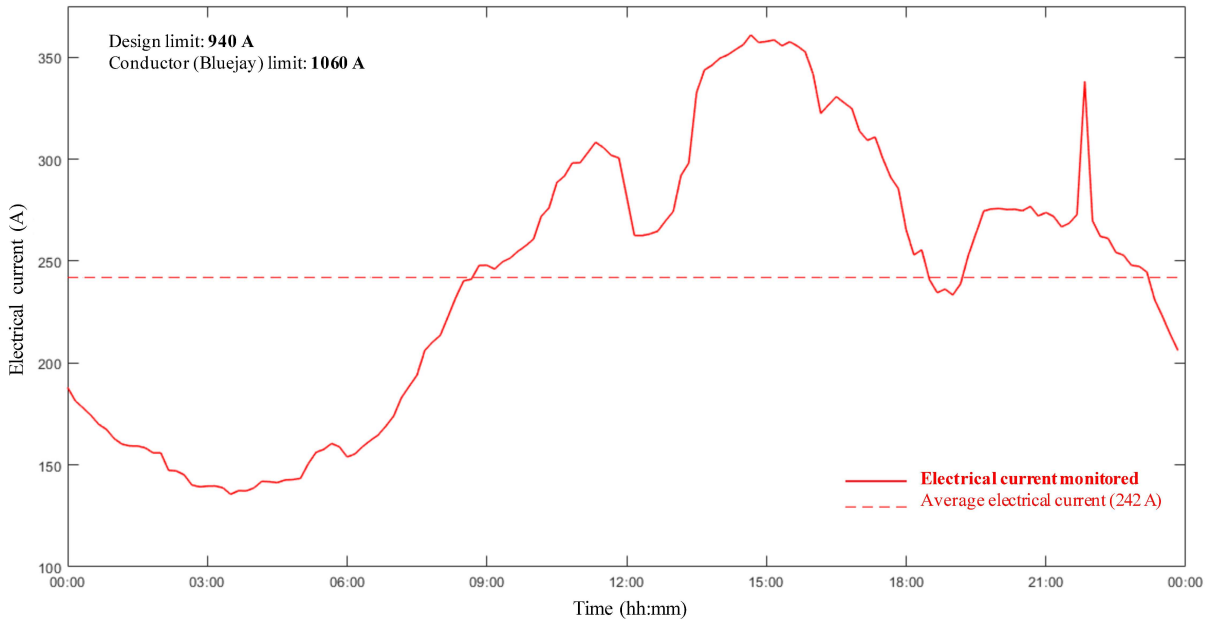

Source: own.

Figure E.4 – Mechanical stress and ambient temperature variation on February 5, 2021.

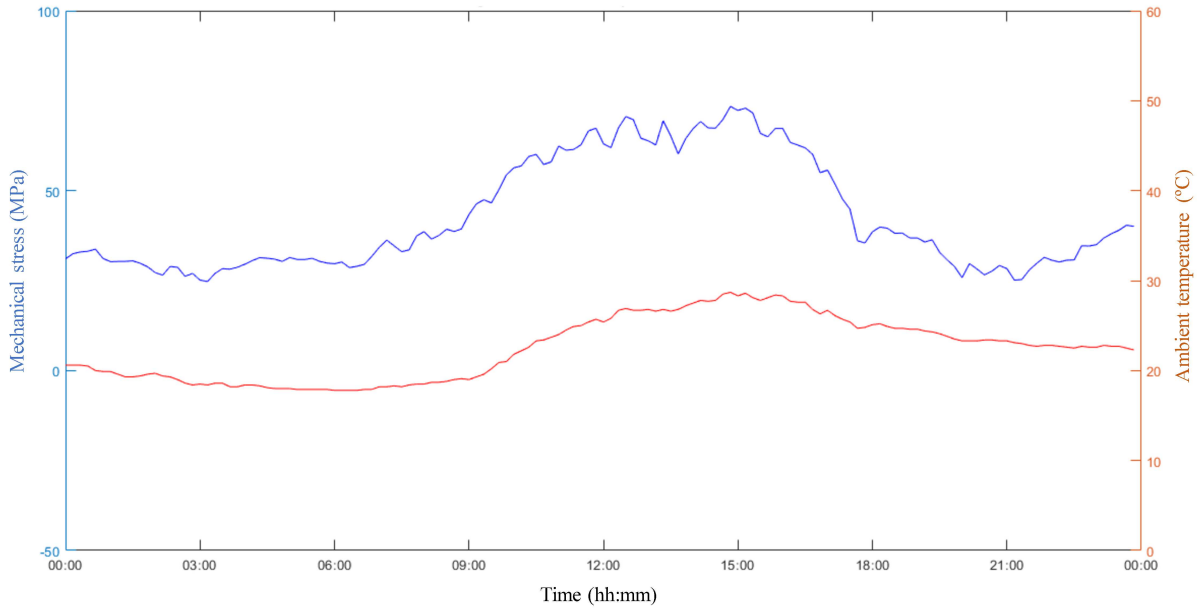

Source: own.

Figure E.5 – Mechanical stress and wind speed variation on February 5, 2021.

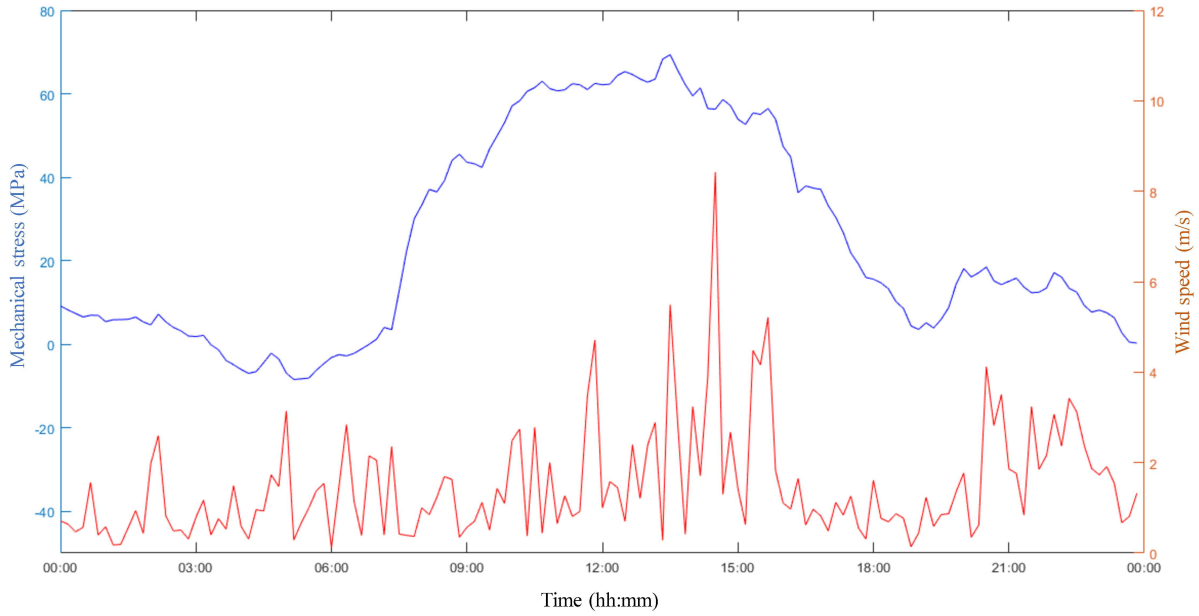

Source: own.

Figure E.6 – Electrical current and ambient temperature variation on February 2, 2021.

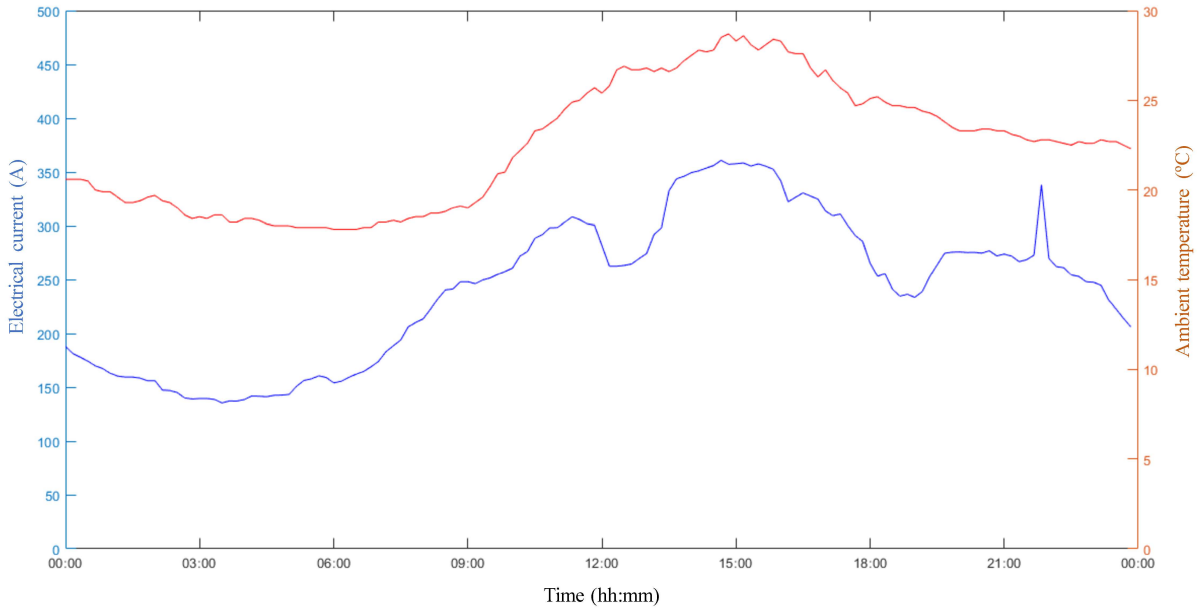

Source: own.

APPENDIX F – ADDITIONAL TRANSMISSION SYSTEM DATA FOR THE IEEE TEST SYSTEMS

Table F.1 – Additional data for the IEEE-RTS 79.

Transmission line	Conductor	Weather region
1-7	Drake	Porto
8-10	Drake	Saskatoon
11-12	Drake	Florianópolis
13-24	Bluejay	Florianópolis
25-31	Bluejay	Saskatoon
32-33	Bluejay	Porto

Source: own.

Table F.2 – Additional data for the IEEE-RTS 96 HW.

Interconnection	Conductor	Weather region
AB-1	Drake	Porto
AB-2	Bluejay	Saskatoon
AB-3	Bluejay	Florianópolis
CB-1	Bluejay	Florianópolis
CA-1	Bluejay	Saskatoon

Source: own.

APPENDIX G – PATENTS

The TECCON II research project has originated five distinct patents related to its developments. The author is positioned as an inventor in the conception of two patents that are connected with the technological contributions of this Ph.D. thesis, namely:

- Patent 01: *Sensor compacto de corrente elétrica e temperatura baseado em fibras ópticas* (Compact sensor of electrical current and temperature based on optical fibers). Process number: BR 10 2020 025220 8. Inventors: Carlos Avelino de Jesus Gouveia, Ana Margarida Rodrigues Pinto, Milton José Cinelli, Mauro Augusto da Rosa, Gabriel Santos Bolacell, and Pedro Alberto da Silva Jorge;
- Patent 02: *Sistema de Avaliação Dinâmica de Linhas Óptico* (Optical DLR System). Process number: BR 10 2020 025230 5. Inventors: Diego Issicaba, Vladimiro Henrique Barrosa Pinto de Miranda, Mauro Augusto da Rosa, Gabriel Santos Bolacell, Samir Walker Fernandes, Pedro Alberto da Silva Jorge, and Claudomiro de Souza de Sales Junior.

APPENDIX H – LIST OF PUBLICATIONS: DIRECT CONNECTION WITH THE THESIS

Publications in Peer Reviewed Journals

Due to the innovative nature of the research project that this Ph.D. thesis is inserted, a careful planning of publications has been followed with the aim of not compromising the registration of patents. Thus, three articles have been proposed and are under evaluation:

- M. Rosa, G. Bolacell, E. C. Junior, J. Pissolato, E. Guedes, T. Vilela, G. Lira, E. Neto, A. Klautau, H. D. Monego, L. Lira, I. Sousa, L. Passos, H. Pereira, M. J. Cinelli, A. Pinto, C. M. B. Cordeiro, P. A. S. Jorge, C. Gouveia, D. Issicaba, C. Sales, R. Piedade, S. Lima, A. Rocco, and V. Miranda. Instrumented Composite Insulator for Transmission Line Condition Monitoring. The paper is accepted for submission, the full article has been submitted to IEEE Electrical Insulation Magazine.
- G. S. Bolacell, M. A. da Rosa and A. M. Leite da Silva. Dynamic Line Rating Technology as Alternative for Transmission System Expansion Planning. Article submitted to Power Systems Computation Conference (PSCC) 2022: if accepted will be included in a special issue of the journal Electric Power Systems Research (EPSR).
- G. S. Bolacell and M. A. da Rosa. Power System Flexibility Aspects in a Long-Term Reliability Evaluation. Article in preparation for submission to IEEE Transactions on Power Systems.

Publications in Peer Reviewed Conferences

- G. S. Bolacell and M. A. da Rosa. Composite Power System Reliability Assessment Considering Transmission Line Flexibility. In: 2020 International Conference on Probabilistic Methods Applied to Power Systems (PMAPS). 2020.
- M. J. Cinelli, G. S. Bolacell, C. M. B. Cordeiro, H. Freitas, M. Rosa. All-optical electrical conductor characterization using a Fiber Bragg Grating. In: XXXIX CBrAVIC 2018.
- T. V. Ferreira, F. L. M. Andrade, G. R. S. Lira, E. G. Costa, G. S. Bolacell, J. P. Filho, C. M. B. Cordeiro, E. T. Wanderley Neto, M. J. Cinelli, M. A. Rosa and E. L. Carvalho Junior. Laboratory Tests of a Composite Insulator Instrumented with Optical Sensors. In: Proceedings of the 21st International Symposium on High Voltage Engineering - ISH 2019.

APPENDIX I – LIST OF PUBLICATIONS: INDIRECT CONNECTION WITH THE THESIS

Publications in Peer Reviewed Journals

- G. S. Bolacell, L. F. Venturini, M. A. da Rosa, and D. Issicaba. Evaluating short circuit indices in an integrated assessment of distribution system adequacy and power quality. Electric Power Systems Research, vol. 2020.

Publications in Peer Reviewed Book Chapters

- L. F. Venturini, G. S. Bolacell, L. M. Carvalho, M. A. da Rosa, and D. Issicaba. Reliability Analysis of Active Distribution Systems. Practical Aspects of Active Distribution Networks, Springer. The book chapter is approved and is going to be published in 2021.

Publications in Peer Reviewed Conferences

- G. S. Bolacell, L. F. Venturini, and M. A. da Rosa. Distribution System Reliability Evaluation Considering Power Quality Effects. In: 2018 International Conference on Probabilistic Methods Applied to Power Systems (PMAPS).
- G. S. Bolacell, D. Calado, L. F. Venturini, D. Issicaba, and M. A. da Rosa. Distribution System Planning Considering Power Quality, Loadability and Economic Aspects. In: 2020 International Conference on Probabilistic Methods Applied to Power Systems (PMAPS).

ANNEX A – IEEE TEST SYSTEMS DATA

Table A.1 – Interconnections between areas of the IEEE-RTS 96

Interconnection	From	To	Capacity (MVA)
AB-1	Area A	Area B	175
AB-2	Area A	Area B	500
AB-3	Area A	Area B	500
CB-1	Area C	Area B	500
CA-1	Area C	Area A	500

Source: own.

Table A.2 – Generation capacity of the three areas of IEEE-RTS 96 HW.

Technology	Capacity (MW)	Number of units		
		Area A	Area B	Area C
Thermal	12	5	5	5
	20	4	4	4
	76	4	4	4
	100	3	3	3
	155	4	4	4
	197	3	3	3
	350	1	1	0
	400	2	2	2
Hydro	50	6	6	6
Wind	2	267	229	267

Source: own.

Table A.3 – Additional generation added in each region (area) of IEEE-RTS GMLC 2019.

Bus	Gen. capacity (MW)
1	100
7	100
15	100
15	155
23	155

Source: adapted from RTS-GMLC (2018).

Table A.4 – Changing on load buses of IEEE-RTS GMLC 2019.

Bus	**Load (MW): RTS 79**	**Load (MW): RTS GMLC 2019**
13	265	745
14	194	80
15	317	132
19	181	75
20	128	53

Source: adapted from RTS-GMLC (2018).

ANNEX B – IBERIAN PENINSULA POWER SYSTEM DATA

Table B.1 – Portugal generation system.

Technology	Centers	Units	Capacity (MW)	Share %
Hydro	82	82	6,363.10	32.23
Thermal	16	16	5,585.10	28.47
Wind	47	2507	4,911.50	25.03
Mini hydro	22	22	613.60	3.13
Alternative (biomass and solar)	75	75	2,187.10	11.15

Source: own.

Table B.2 – Spanish generation system.

Technology	Centers	Units	Capacity (MW)	Share %
Hydric	20	20	14,648.40	14.69
Thermal	95	95	42,057.02	42.17
Wind	115	11,500	22,900.00	22.96
Mini hydric	5	210	1,918.11	1.99
Alternative (biomass and solar)	30	1,216	13,720.00	13.76

Source: own.

Table B.4 presents the data to estimate the DLR in analyses using the Iberian Peninsula power system. On the estimation of the dynamic rating, the solar absorptivity and emissivity of the conductor are assumed to be equal to 0.8 for all type of conductors.

Table B.3 – Interconnections between Portugal and Spain.

Interconnection	ID	Voltage level (kV)	From	To	Capacity (MVA)
1	AV_BLB	400	Portugal (Alqueva)	Spain (Brovales)	1640
2	TVR_PGM	400	Portugal (Tavira)	Spain (Puebla de Guzmán)	1386
3	XCA_AL11	400	Portugal (Alto Lindoso)	Spain (Cartelle)	1660
4	XCA_AL11	400	Portugal (Alto Lindoso)	Spain (Cartelle)	1660
5	XAL_LA11	400	Portugal (Lagoaça)	Spain (Aldeadávila)	1706
6	XCE_FR11	400	Portugal (Falagueira)	Spain (Cedillo)	1386
7	XAL_PN21	220	Portugal (Pocinho)	Spain (Aldeadávila)	435
8	XSA_PN21	220	Portugal (Pocinho)	Spain (Saucelle)	430
9	XAL_PN21	220	Portugal (Pocinho)	Spain (Aldeadávila)	435

Source: own.

Table B.4 – Conductors characteristics.

Data	Bear	Zambeze	Zebra	Rail
Conductor outside diameter (mm)	23.45	31.80	28.62	29.59
Core diameter (mm)	10.05	6.96	9.54	7.41
Outer strand diameter (mm)	3.35	4.14	3.18	3.70
Conductor dc resistance at 20°C (Ω/km)	0.1093	0.0510	0.0674	0.0596
Conductor ac resistance at 75°C (Ω/km)	0.1332	0.0623	0.0821	0.0728
Static rating (A)	650	610	860	920

Source: own.